RESEARCH REPORT 987-9

ASPHALT OVERLAY DESIGN METHODS FOR RIGID PAVEMENTS CONSIDERING RUTTING, REFLECTION CRACKING, AND FATIGUE CRACKING

Yoon-Ho Cho, Chiu Liu, Terry Dossey, and B. F. McCullough

CENTER FOR TRANSPORTATION RESEARCH
BUREAU OF ENGINEERING RESEARCH
THE UNIVERSITY OF TEXAS AT AUSTIN

OCTOBER 1998

Technical Report Documentation Page

1. Report No.	2. Government Accession No.	3. Recipient's Catalog No.
TX-98/987-9		
4. Title and Subtitle ASPHALT OVERLAY DESIGN METHODS FOR RIGID PAVEMENTS CONSIDERING RUTTING, REFLECTION CRACKING, AND FATIGUE CRACKING		5. Report Date October 1998 6. Performing Organization Code
7. Author(s) Yoon-Ho Cho, Chiu Liu, Terry Dossey, and B. F. McCullough		8. Performing Organization Report No. 987-9
9. Performing Organization Name and Address Center for Transportation Research The University of Texas at Austin 3208 Red River, Suite 200 Austin, TX 78705-2650		10. Work Unit No. (TRAIS) 11. Contract or Grant No. Project 7-987
12. Sponsoring Agency Name and Address Texas Department of Transportation Research and Technology Transfer Section/Construction Division P.O. Box 5080 Austin, TX 78763-5080		13. Type of Report and Period Covered Research Report (9/96-8/97) 14. Sponsoring Agency Code
15. Supplementary Notes Project conducted in cooperation with the Texas Department of Transportation.		

16. Abstract

The overall objectives of this study were (1) to provide basic performance evaluation of asphalt overlays on rigid pavements and (2) to provide a design tool for supporting a long-range rehabilitation plan for the US 59 corridor in the Lufkin District. A factorial overlay method was applied to several test sections with the objective of preventing recurrent problems such as reflective cracking. Data collection was carried out before, during, and after the construction of the test sections under a carefully designed monitoring program. In addition, weigh-in-motion (WIM) devices were installed at the test sites to collect traffic-related information as well as pavement surface and ambient temperature. The performance at the initial stage of the overlay was evaluated based on the following information: (1) detailed traffic information such as axle weights and lateral displacement; (2) distress conditions on different overlays; and (3) effects of previous pavement conditions and overlay recipes on overall performance of the pavements.

Mechanistic models were developed using a finite element method (FEM) in a multipurposed program (ABAQUS). The objective of this FEM modeling effort was to establish a reasonable structural design scheme for the overlays on flexible bases for protecting the pavement from both reflective cracking and rutting development.

Finally, design equations were developed by using a fractional factorial design. An analysis of variance (ANOVA) was performed to identify significant factors, and a design equation was developed using regression analysis. To minimize costs, an asphalt overlay design method using linear programming was proposed.

17. Key Words	18. Distribution Statement		
Pavement rehabilitation, weigh-in-motion (WIM) systems, traffic reports, Lufkin District, US 59	No restrictions. This document is available to the public through the National Technical Information Service, Springfield, Virginia 22161.		
19. Security Classif. (of report) Unclassified	20. Security Classif. (of this page) Unclassified	21. No. of pages 204	22. Price

Form DOT F 1700.7 (8-72) Reproduction of completed page authorized

ASPHALT OVERLAY DESIGN METHODS FOR RIGID PAVEMENTS CONSIDERING RUTTING, REFLECTION CRACKING, AND FATIGUE CRACKING

by

Yoon-Ho Cho,

Chiu Liu,

Terry Dossey,

and

B. Frank McCullough

Research Report Number 987-9

Research Project 7-987

A Long-Range Plan for the Rehabilitation of US 59 in the Lufkin District

Conducted for the

TEXAS DEPARTMENT OF TRANSPORTATION

by the

CENTER FOR TRANSPORTATION RESEARCH

Bureau of Engineering Research

THE UNIVERSITY OF TEXAS AT AUSTIN

October 1998

ACKNOWLEDGEMENTS

The researchers acknowledge the expert assistance provided by the Texas Department of Transportation project director, Mr. E. Starnator (Lufkin District).

Prepared in cooperation with the Texas Department of Transportation.

DISCLAIMERS

The contents of this report reflect the views of the authors, who are responsible for the facts and the accuracy of the data presented herein. The contents do not necessarily reflect the official views or policies of the Texas Department of Transportation. This report does not constitute a standard, specification, or regulation.

There was no invention or discovery conceived or first actually reduced to practice in the course of or under this contract, including any art, method, process, machine, manufacture, design or composition of matter, or any new and useful improvement thereof, or any variety of plant, which is or may be patentable under the patent laws of the United States of America or any foreign country.

NOT INTENDED FOR CONSTRUCTION,
BIDDING, OR PERMIT PURPOSES

B. Frank McCullough, P.E. (Texas No. 19914)
Research Supervisor

TABLE OF CONTENTS

CHAPTER 1. INTRODUCTION

An asphalt concrete pavement (ACP) overlay over a rigid pavement represents a viable rehabilitation strategy. It can provide good serviceability at an initial construction cost that is substantially less than that of a rigid overlay rehabilitation. In addition, ACP overlays require less construction time, which can reduce user costs during construction. However, it may not be the most economical solution for long-term rehabilitation. Because of their relatively short service life, ACP overlays may require maintenance sooner than rigid overlays. And one of the more critical distresses that effectively determine the life span of the structure is reflection cracking. This report investigates alternative strategies that seek to prevent reflection cracking on ACP overlays.

BACKGROUND

The objective of Project 7-987 was to prepare a long-term rehabilitation plan for Highway US 59 in the Lufkin District. The US 59 corridor is one of the most heavily used highways in Texas and represents an important link between Houston, Texas, and the U.S. Midwest. Since its construction in the 1940s, this highway has received several overlays to improve ride quality. Different types of distress have developed on the ACP surface as a result of heavy traffic and environmental impacts. In order to reduce the maintenance cost of US 59, and to provide for an economical long-term rehabilitation strategy, Project 987 researchers built fourteen test sections along US 59; these sections employed various types of rehabilitation recipes (see CTR Reports 987-1 and 987-3) so as to observe the performance of the sections in terms of the surface distress development in the overlays. The most practical and economical solution for rehabilitating the highway will be recommended based on empirical observations and proposed mechanistic models.

STUDY OBJECTIVES

The objectives of this report are (1) to present performance information relating to each rehabilitation method, (2) to identify some ACP overlay methods that can prevent reflection cracking, and (3) to provide an immediate design tool for developing a long-range rehabilitation plan not only for the Lufkin District, but for other highways in Texas as well.

The recommendations included in this report are based on combined empirical and mechanistic research results. Rutting, fatigue cracking, and reflection cracking are considered separately in the analysis and are combined to identify the optimal design thickness. Regressed equations were developed to estimate pavement behavior under traffic loading and temperature-induced stress within pavements.

RESEARCH SCOPE

The first step was to obtain performance information from the field. Test sections were built to observe pavement performance under actual field conditions (i.e., traffic loading and changing climate). Various designs and construction solutions were applied to prevent reflective cracking. A weigh-in-motion (WIM) device was installed to collect traffic-related information, including weight per axle, speed, and lateral position. Pavement temperature information was also collected at the WIM site. Field data collections were performed before the overlay construction, during construction, and after overlay construction under a carefully designed monitoring program. Structural factors, including cross sections, core, deflection, and stiffness, were estimated using known backcalculation procedures. Roughness was measured using the international roughness index (IRI); condition surveys for cracking and rutting were also performed.

In the second stage, a mechanistic model that predicts pavement behavior under traffic and temperature variance was suggested. Mechanistic models were developed based on the finite element method (FEM) using the multipurpose program ABAQUS. Solutions obtained from three different FEM models were compared with available classical solutions. Plane strain, axisymmetric modeling, and three-dimensional (3-D) modeling were initially considered for this composite pavement structure. Owing to the time and effort involved in using a 3-D model, a two-dimensional modeling was applied. Sensitivity analysis was performed to identify significant factors that directly affect pavement behavior. Pavement behavior under traffic loading was observed by employing the linear and nonlinear elastic axisymmetric models. The possible causes of the distress appearing on the test sections can be explored by applying the mechanistic model. In addition, a 3-D model was incorporated to determine the effect of tandem-axle versus single-axle loads on an ACC overlay pavement structure. Thermal stress could be estimated by the plane strain model. To estimate the temperature effect on the pavement structure, a temperature prediction model was developed, and its solution was calibrated with temperature measurements.

Finally, design equations were developed based on the mechanical modeling and statistical work known as *fractional factorial design.* We also undertook 243 runs of FEM analysis per model using fractional factorial design. The analysis of variance (ANOVA) test was performed to identify significant factors that affect pavement performance; a design equation was also developed by regression analysis, with the regressed design equation then calibrated by the field results. To verify the suggested design method, a sample pavement design program was generated using linear programming technique.

REPORT ORGANIZATION

Chapter 2 presents the characteristics of pavement overlays and of overlay design systems, with performance and overlay design methods also addressed. We are not going to repeat the cost estimation of the overlays, WIM information, and the FWD measurement, which has been presented in previous reports (CTR Reports 987-3–987-6).

The mechanistic development of the pavement design model is described in Chapters 3 through 5. In Chapter 6, conclusions of this study are drawn and the initial results of the FEM feasibility study are reported. Chapter 3 describes the results obtained from a sensitivity analysis from the mechanistic model under the traffic loading. As a topic for further research, the inelastic material parameter was introduced into the model and compared with results obtained from the linear elastic analysis. Furthermore, the 3-D model was adapted to show the tandem axle load effect on the pavement structure. In Chapter 4, the development of both the temperature distribution model and the sensitivity analysis for thermally induced stresses is investigated. The thermal stress prediction model was also developed using the plane strain models (the results, however, have not been calibrated with field observations). The significant reduction of thermal stress obtained by inserting a flexible base interlayer is also shown in Chapter 4. In Chapter 5, the development of a mechanistic design model is explored. Fractional factorial results are presented in detail and a design equation developed through regression analysis is given.

CHAPTER 2. PAVEMENT OVERLAY STRATIGIES

This chapter briefly reviews three approaches to predicting pavement performance. In addition, it reports on research efforts undertaken to predict the occurrence of the three dominant distresses affecting asphalt overlays (i.e., rutting, reflection cracking, and fatigue cracking).

FACTORS CONSIDERED IN OVERLAY DESIGN

Overlay design depends strongly on the physical condition of the existing pavement. For example, the overlay design method using the remaining-life approach requires previous traffic loading to determine the remaining life of the existing pavement. Furthermore, careful consideration in choosing the overlay type and construction method in terms of financial and user delay cost is necessary. Accordingly, an asphalt overlay is often selected as a rehabilitation method because of its rapid construction completion potential. And given that the overlay is constructed on the existing pavement, the structural properties of both the existing layer and the sublayers must be taken into account.

An asphalt concrete (AC) overlay on an existing rigid pavement has a different failure mechanism than does an AC overlay on a flexible pavement. In the case of AC overlays on portland cement concrete (PCC), reflection cracking is the primary pavement distress. Many methods have been applied to prevent reflection cracking, such as using thicker AC layers, inserting a modified AC binder, inserting stress relief interlayers, rubberizing the existing PCC, and so on (Sherman et al. 1982). Whatever the application, it has been determined that the selection of the actual recipe does affect pavement performance (Cho et al. 1994).

The thickness of the new AC overlay depends on the thickness of the existing pavement and the condition of the existing pavement (AASHTO *Design Guide* 1986; Seed et al. 1981). The life span of an overlay depends on the following factors and their interactions: (1) the traffic and environmental loading; (2) the temperature and moisture changes in the overlaid pavement structure; (3) the rutting on the AC overlay owing to the softening of asphalt materials in summer (Echman 1987); and (4) reflection cracking on an ACC overlay on rigid pavement that mainly takes place in winter (Cho and McCullough 1994). To deal with these problems, the Asphalt Institute suggests increasing the AC thickness on the longer slab length with a high temperature differential (AI 1983).

PREDICTION OF PAVEMENT PERFORMANCE

Pavement overlay design can be classified into three categories. The first category, shown in Figure 2.1, is the empirical design method. The AASHTO Interim Guide Design Method (1972), Asphalt Institute design method (AI 1982), and CALTRANS's flexible overlay design method (CALTRANS 1972) are empirical.

The second category is a mechanistic design method that uses theory to predict stress, strain, and distress for pavements, although a complete theoretical model that simulates pavement structure is not available (Lytton et al. 1993).

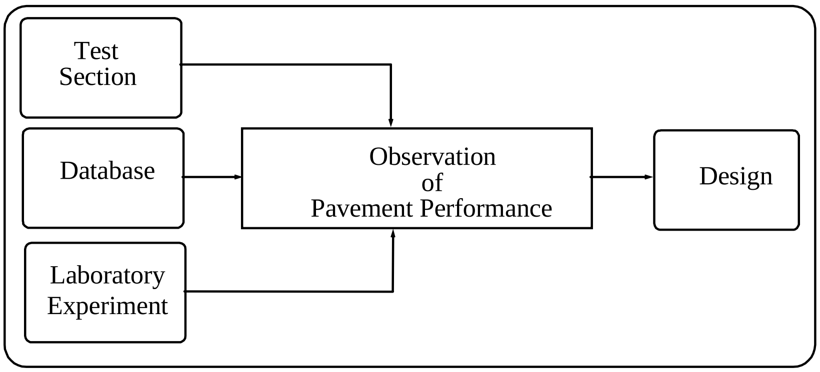

Figure 2.1. Concept of empirical design method

The third approach is to combine the theoretical modeling with empirical observations; that is, to compare and calibrate the prediction for stress/strain for a given pavement structure with empirical observations from either the lab or field. Thus, it may reduce the possible error of extrapolation. For example, the current AASHTO *Pavement Design Method* (AASHTO 1986) and the TBCO method (Lundy 1991) have adopted this approach.

EXISTING PERFORMANCE PREDICTION METHODS

The AC overlay on US 59 in Lufkin, Texas, has exhibited reflection cracking and rutting on the pavement surface of both existing pavements (Cho and McCullough 1995). Typical fatigue cracking is also apparent on the specific section that has a flexible base layer between the AC and PCC layers. It can be assumed that these three types of distress represent the dominant asphalt overlay failing. (The models for distress prediction methods are discussed in the following sections.)

Rutting is a permanent deformation that develops along the wheelpath on the pavement. Rutting prediction methods have progressed from simple empirical methods to inelastic structural analysis models. The limiting of maximum strain or stress on the subgrade was a basic concept of the first design chart presented by the Shell Oil Company (Seed 1962). In addition, other design methods using the subgrade strain criteria have been proposed to control rut depth (Dorman and Metcalf 1965; Majizadeh et al. 1978). Monismith suggested a rut depth prediction model to estimate rut depth by the soil layer through compressive strain when a 10 mm maximum rut depth criterion was used (Monismith and McLean 1971).

$$\varepsilon = a\,(N_f)^{b} \tag{2.1}$$

where

ε = compressive strain on the top of subgrade,

Nf = rut depth life under compressive strain (ESAL), and

a, b = coefficient of curve fitting (a = 0.01055505, b = -2.00832×10^{-1} for Monismith; a = 0.01054846, b = -2.23676×10^{-1} for Dorman and Metcalf).

While the static layered theory has been applied to estimate rutting (Romain 1972; Heukelom et al. 1967), this type of quasi-elastic approach neglects the dynamic interaction between pavement and traffic loading. Another approach involves considering the viscoelastic properties of the pavement structure by performing lab creep tests (Rauhut 1975). These two approaches were incorporated by Eckmann (Eckmann 1987). In addition, a fully mechanistic approach has been attempted using inelastic analysis (Goacolou 1987; White 1993). Furthermore, rutting prediction models are statistically generated based on field or laboratory experience.

Reflection cracking may lead to such failures as spalling and pumping by permitting water to enter the subgrade. It can cause early pavement failure and decrease the serviceable life of the overlay (Sherman 1982). Reflection cracking, generally, occurs on an AC overlay on rigid pavement. In addition, temperature variations can increase tensile stress or strain in the interface between the underlying layer and the overlay (Harvey et al. 1977; Alberto et al. 1983). McCullough et al. suggested an analytical procedure for the design of an AC overlay on PCC to prevent reflection cracking. The vertical movement induced by traffic loading and which causes shear strain was calculated on PCC pavement using load transfer efficiency based on deflection measurements.

Ramsamooj et al. explained the methodology for crack development in overlay pavement under repeated traffic loadings based on the Paris crack growth theory (Ramsamooj et al. 1972; Ramsamooj 1973). The opening mode (mode I) and the in-plane sliding mode of crack propagation are considered in the following equation:

$$dc/dN = A_1\,(\Delta K_1)^{4} + A_2\,(\Delta K_2)^{4} \tag{2.2}$$

where

c = crack length,

N = number of cycles,

A1, A1 = materials property, and

$k1, k2$ = stress-intensity factors for the mode 1 and 2.

Other research by Luther et al. identified what occurs on the overlaid AC pavement under traffic only (Luther et al. 1976). Based on laboratory work and on two traffic loading conditions, symmetric and nonsymmetric loading, these authors showed that the stress intensity factor *K1* for the opening mode was negative. Ponniah et al. investigated temperature-related reflection cracking on asphalt overlays (Ponniah et al. 1987). The example of practical implementation of fracture mechanics in pavement overlay was researched by Jayawickrama and Lytton (Jayawickrama and Lytton 1987). Employing Paris law to estimate the rate of crack propagation in asphalt concrete, they suggested the following design equation:

$$N_i^* = f(N_{dt}, N_{db}, N_{ds}) \tag{2.3}$$

where

N_i^* = observed number of days of pavement failure at i damage level,

N_{dt} = expected number of days of pavement failure due to temperature movement,

N_{db} = expected number of days of pavement failure due to bending mode, and

N_{ds} = expected number of days of pavement failure owing to shear mode. Furthermore, regressional approach based on the historical database has been used to derive the following equation (Darter et al. 1989):

CRACK = f (ESAL, AGE, freezing index, existing pavement type and crack)

Fatigue theory relating to repetitive traffic loading—one of the main pavement failure mechanisms—has also been applied. The concept of fatigue and damage in PCC was described by McCullough (McCullough et al. 1973). Fatigue life can be defined by the number of traffic loadings on a given pavement structure. Almost all researchers have suggested rigid pavement overlay design methods are based on fatigue life (von Metzinger 1991; Monismith 1970; Kennedy 1975; Kennedy 1976). These researchers generally calculated tensile stress at the bottom of asphalt layers by various theories and predicted long-term performance using an established fatigue equation.

For the FHWA/Texas design method, the following equation was used to match specified failure criteria and traffic:

$$N_f = 46000\,(f/\sigma)^3 \tag{2.4}$$

where

N_f = number of 18-kip ESALs,

f = flexural strength of the concrete in psi*, and

σ = governing stress in the concrete in psi* (*1 psi = 6.89 kPa).

Various fatigue equations have been suggested (Kennedy 1983) based on either initial tensile strain, stress, or stress-strength ratio, depending on aggregate type and temperature, which can be observed in the AC layer. For example:

$$Nf = 1.56 * 10^8 (1/\sigma)^{3.73}, \quad (R^2 = 0.72, S = 0.43, \text{at } 75°F) \tag{2.5}$$

$$Nf = 9.38 * 10^{-8} (1/\varepsilon_{mix})^{2.76}, \quad (R^2 = 0.70, Se = 0.44) \tag{2.6}$$

where

N_f = number of 18-kip ESALs,

σ = tensile stress in ACC, and

ε_{mix} = initial strain in ACC.

The AC field experience showed that the fatigue equation derived from only laboratory results did not meet the performance on pavement. Freeme et al. (1982) suggested the use of a shift factor, such as $N_{f\ field} = c * N_{f\ lab}$, to compensate for the difference between laboratory and field conditions. Bowen included the penetration of an AC binder in the basic fatigue equation for recycled asphalt concrete (Brown 1987). AASHTO road test and field results predict up to 10% of the fatigue cracking in the wheelpath area, as shown in Equation (2.7) (Monismith et al. 1985). The complex modulus replaced the resilient modulus in a study improving the asphalt mix design by TxDOT (Mahboub et al. 1988).

$$\text{Log } N_f = 15.497 - 3.291 \log(\varepsilon_t) - 0.854 \log(E^*/1000) \tag{2.7}$$

where

N_f = number of cycles to failure (18-kip ESALs),

ε_t = repeated tensile strain (in/in * 10 -6), and

E^* = complex modulus of ACC (psi).

PAVEMENT RESPONSE AND THEORIES

Pavement behavior under traffic loading has been a primary concern of pavement engineers. The plate theory and the layered theory (Westergaard 1926; Yoder 1972) for pavement response have been widely used. The finite element method (FEM) has been widely used subsequently in computer packages, such as ILLI-Slab and ILLI-Pave (WA-RD

65.1, 1983). Recently, 3-D FEM software programs, including ABAQUS and ADINA, have been available for research. In this report, the FEM method will be applied to estimate the stress and strain in a pavement structure.

Material characterization is a determination of model parameters by a given constitutive equation. This quasi-elastic approach is an approximation obtained from the test that was performed so as to replicate as closely as possible the actual stress level, moisture, and temperature conditions in the field. The viscoelastic parameters of an AC binder, and the inelastic stress strain of a concrete sample can be determined in lab tests. The performance-based design approach performed by SHRP might be an example of efforts to connect the material testing and mechanistic theory into the pavement design (Lytton 1993).

SUMMARY

This chapter reported the results of a review of the literature pertaining to pavement overlay performance prediction. The next step is to define pavement overlay performance and pavement failure criteria. The characteristics of pavement overlays, factors affecting overlay performance, and methodologies used in estimating performance and their implementation in pavement design were reviewed. The historical performance prediction models concerning asphalt overlays were also discussed. All such information indicates that asphalt pavement overlay design methods must be capable of taking into account the three basic types of pavement distress, namely, rutting, reflection cracking, and fatigue cracking.

CHAPTER 3. SENSITIVITY ANALYSIS UNDER TRAFFIC LOADING

The project test section installed on US 59 basically demonstrated that the asphalt overlay with interlayer, including the flexible layer, stress relief layer, and existing asphalt pavement layer, has achieved its function of preventing (to an extent) reflection cracking on rigid pavements. While rutting has not been a serious problem so far, some test sections show rut depths greater than those of others sections. R3, a sandwich type of structure (i.e., a flexible base layer placed between the overlay AC and the existing jointed concrete pavement or JCP), serves as an example of a section demonstrating, more so than others, minimum reflection cracking and rapid rutting development. The success of this construction recipe (R3) relies mainly on the quality of the flexible base layer: Its Young's modulus is relatively lower than that of both the JCP (at the bottom) and the AC layer (on top); also, the flexible base layer is squeezed by traffic if the AC layer or the layer itself is not sufficiently thick. The question is: How does the thickness of the flexible base layer affect its performance?

These questions can be answered by constructing, as resources permit, other test sections. Another way to answer these questions is to apply mechanistic models that can evaluate the stress and strain responses of a pavement structure. Quasi-elastic analysis, which has been generally adopted in pavement design, has relatively simple input parameters, such as resilient modulus and Poisson's ratio. The present research concentrates primarily on elastic analysis. We next apply an FEM (finite element method) to model traffic loads from their dynamic and static aspects.

PAVEMENT STRUCTURE AND MATERIAL PROPERTIES

Similar to the pavement structure constructed on test section R3, the sample pavement has 76.2 mm (3 in.) of ACC and 203.2 mm (8 in.) of flexible base, with 203.2 mm (8 in.) of JCP. The material properties are shown in Table 8.1. The inelastic material parameters were derived mainly from previous research on sensitivity analysis (Zaghloul and White 1993; and Zaghloul and White et al. 1994). The material properties were listed for future analysis. The traffic wheel load was initially fixed at 40 kN (9,000 lb), corresponding to the standard single-axle load in the AASHTO *Design Guide.* The static analysis with linear elastic material properties was initially performed; its results will be compared with results obtained from both dynamic analysis and inelastic analysis.

PAVEMENT BEHAVIOR

The deflection basin of a given pavement structure under the 40-kN (9,000-lb) static loading is shown in Figure 3.1. The maximum deflection was about 0.387 mm (15.5 mil) and its SCI was about 0.25 mm (10 mil). The larger SCI could be used to explain the possibility of a rutting problem (Cho et al. in CTR Report 987-4). No large radial displacement was observed. The stress distribution by depth is shown in Figure 3.2. The horizontal stress distribution (S11) in the asphalt layer had a different distribution for an ACC overlay without a flexible interlayer. The composite pavement structure without the flexible interlayer had only horizontal compression stress in the ACC layer (Cho 1996); the maximum tensile stress occurred at the bottom of the asphalt layer. This might help to explain the fatigue cracking that appeared in one area of Section R3. The PCC layer had similar stress distribution with plate theory under traffic wheel loading, such as compression in the top and tension in the bottom. The hoop stress (S33) was shown to have the same magnitude stress as the horizontal stress. The vertical stress distribution (S22) shows that the compressive stress on the subgrade was reduced significantly. However, the compressive stress on the flexible base was relatively higher; this explains the rutting problem in the flexible base layer observed in the test section.

Table 3.1. Material properties used in the analysis

Layer	Material	Parameter	Value
Overlay	Hot Mix Asphalt Concrete	Modulus of elasticity (psi)	350,000
		Poisson's Ratio	0.35
		Damping coefficient	5 %
		Density (pcf)	150
Interlayer	Flexible base	Modulus of elasticity (psi)	25000
		Poisson's Ratio	0.4
		Angle of Internal Friction	30,35,40
		Cohesion (psi)	1.5, 25
		Yield Stress (psi)	see Table 8.12
		Damping Coefficient	5%
		Density (pcf)	140
Existing Layer	Portland Concrete Cement	Modulus of elasticity (psi)	4,000,000
		Poisson's Ratio	0.15
		Density (pcf)	150
Subgrade	Silty sand	Modulus of elasticity (psi)	15000
		Poisson's Ratio	0.4
		Angle of Internal Friction	30, 35, 40
		Cohesion (psi)	1.5, 25
		Yield Stress (psi)	see Table 8.12
		Damping Coefficient	5 %
		Density (pcf)	130

1 psi = 6.897 kPa
1 pcf = 16.01 kg/m^3

Hereafter, based on these observations, deflection basin and horizontal tensile stresses will primary be used to show sensitivity to the given factor.

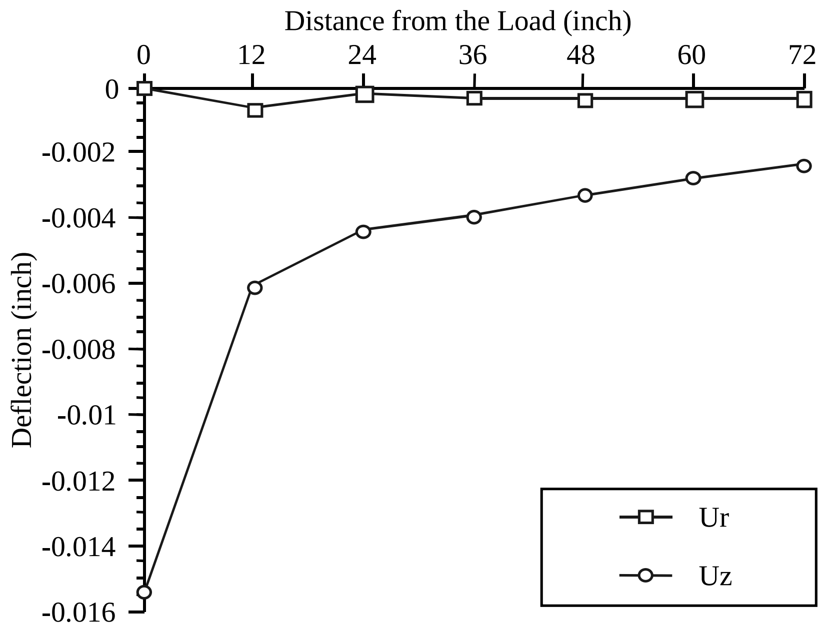

Figure 3.1. Displacement under 40 kN (9,000 lb) by static analysis (1 in. = 25.4 mm)

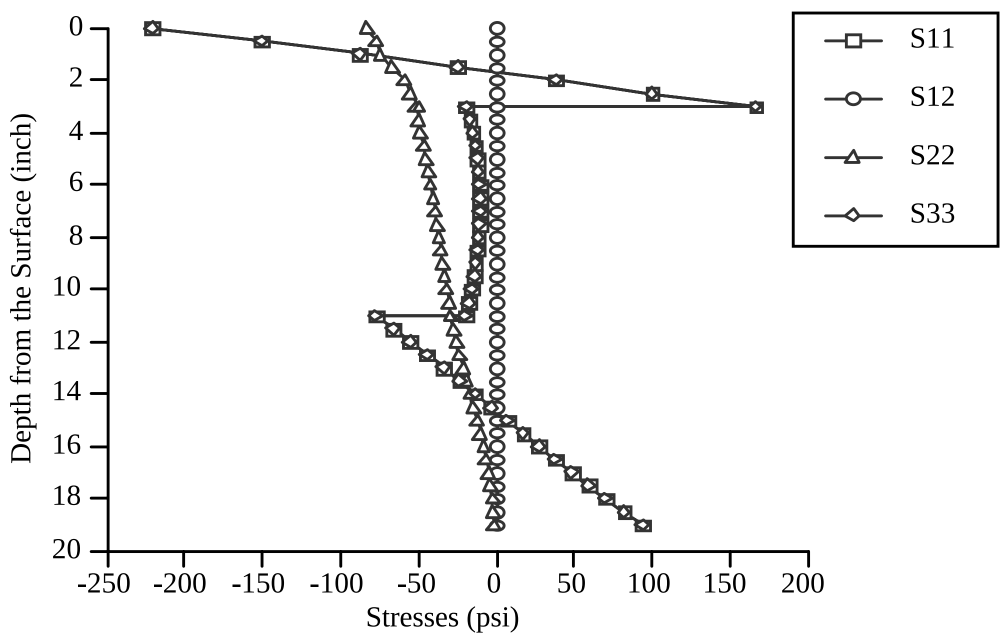

Figure 3.2. Stress distribution under 40 kN (9,000 lb) static analysis. (1 in. = 25.4 mm, 1 psi = 6.897 kPa)

SENSITIVITY ANALYSIS TO THE TRAFFIC WEIGHT

The vertical deflection basins under different traffic loadings are shown in Figure 3.3. As the traffic wheel loads increase, both maximum deflection and SCI increase. For example, the 93.5 kN (21,000 lb) single wheel load induces 0.75 mm (30 mil) of SCI, or about 3 times the value caused by the 40 kN (9,000 lb) single wheel load. Assuming there is a correlation between SCI and rutting, the rutting could be more severe when a heavier wheel load is applied to the pavement. We found that the deflection at all measured points increases as the traffic loading increases.

The horizontal stress distribution in the pavement structure is also shown in Figure 3.4. Still, the maximum tensile stress occurs in the asphalt layer for all wheel loads. The stress in the ACC layer increases from about 689.4 kPa (100 psi) to 2,757.6 kPa (400 psi) when the wheel load is increased from 27.2 kN (6 kip) to 93.5 kN (21 kip). The PCC layer also experiences increased tensile stresses, though the maximum stress produced by the heaviest loading is less than 1,723.5 kPa (250 psi) below its tensile strength.

The vertical stress distribution along the depth right below the wheel loading is shown in Figure 3.5. The higher compressive stress appears on the top of the flexible layer as the traffic load increases, which could lead to the development of rutting in the flexible layer. For example, compressive stress in the top of the flexible layer is about 344.7 kPa (50 psi) under the standard single wheel loading, while it increases to 827.3 kPa (120 psi) under the heaviest single wheel loading. However, compressive stress at the top of the subgrade is close to 0 for all different loads. This implies that the rutting possibility on the subgrade layer is negligible for this type of pavement.

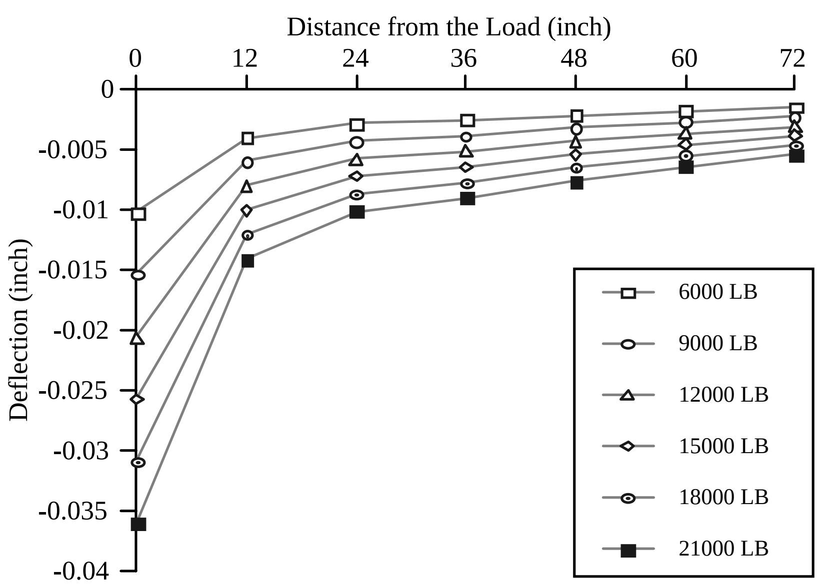

Figure 3.3. Deflection variation under different loading (1 in. = 25.4 mm, 1 lb = 4.45 N)

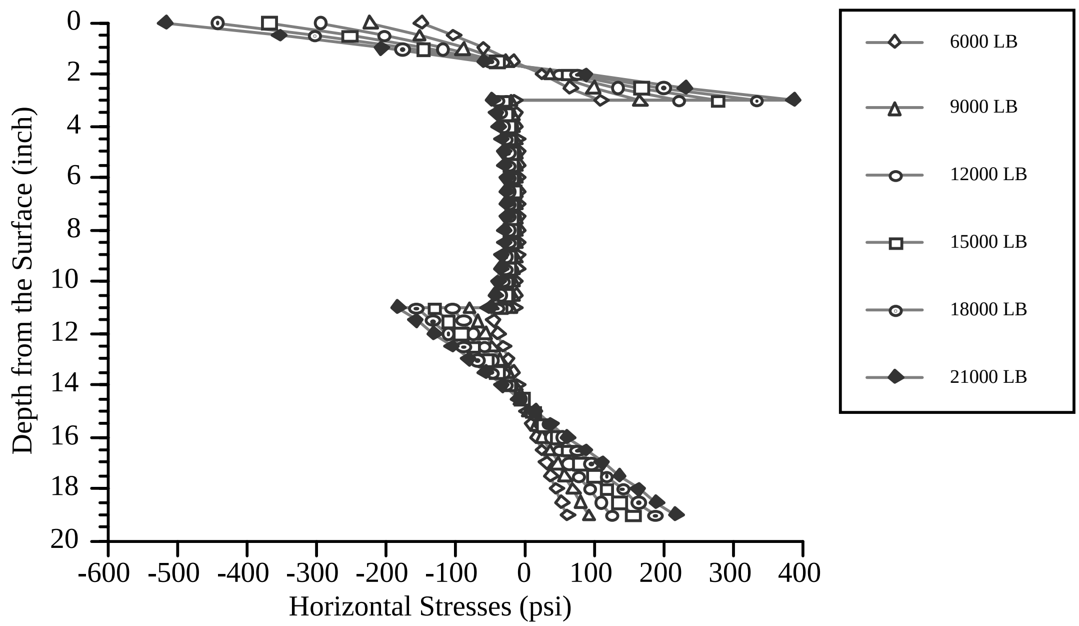

Figure 3.4. Horizontal stress distribution under different loading (1 in. = 25.4 mm, 1 psi = 6.897 kPa, 1 lb = 4.45 N)

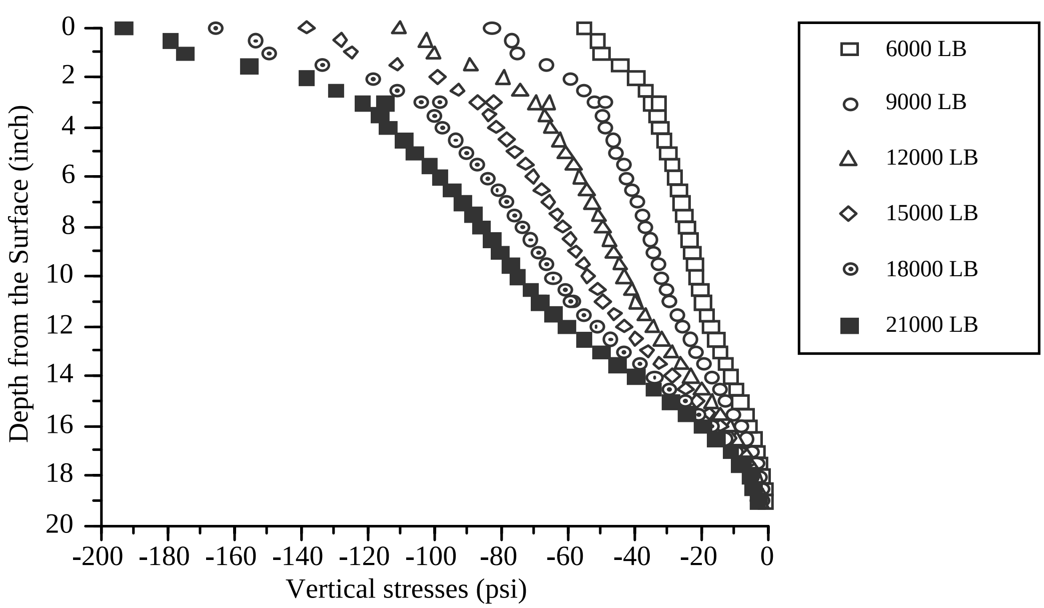

Figure 3.5. Vertical stress distribution under different loading (1 in. = 25.4 mm, 1 psi = 6.897 kPa, 1 lb = 4.45 N)

SENSITIVITY ANALYSIS FOR THE INTERLAYER

In this section, we describe the sensitivity of the pavement behavior by varying the thickness and the stiffness of the flexible interlayer. This sensitivity analysis can provide information useful in understanding test section performance and in designing strategies for this type of overlay.

Thickness of the Interlayer

Suggesting a way to reduce traffic-related distress throughout the stress analysis is important insofar as the interlayer is an effective buffer in preventing reflection cracking. In Figure 3.6, pavement surface deflection is shown against the thickness of the interlayer.

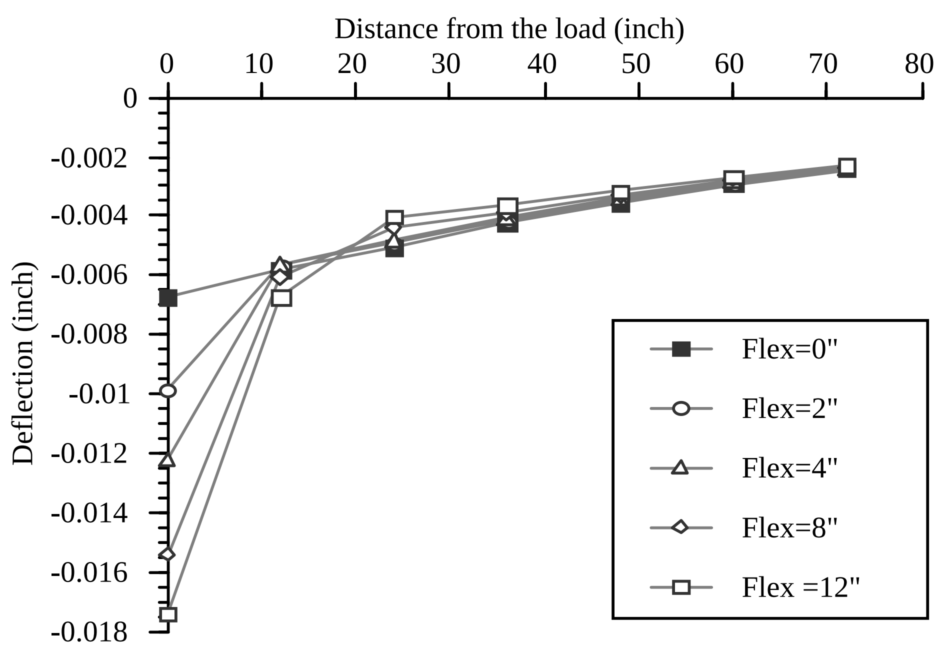

Figure 3.6. Comparison of deflection by the thickness of interlayer (1 in. = 25.4 mm)

First, there is a large difference in SCI between the pavement without an interlayer and the pavement with an interlayer. The pavement without the interlayer shows relatively small SCI values, while the pavement with the interlayer changed its SCI from 0.1 mm to 0.25 mm (4 to 10 mil) depending on the interlayer thickness. Second, the magnitude of the deflection beyond 0.304 m (1 ft) away from the loading source is almost the same no matter how thick the interlayer.

The stress distribution in the PCC and ACC layer vis-à-vis the thickness of the interlayer was also examined. The stress in the asphalt layer changes from compression to tension when a flexible base is inserted in the interface, as shown in Figure 3.7. The compression stress at the bottom of the ACC layer without a flexible base is 44.7 kPa (50 psi), while the ACC with 304.8 mm (12 in.) of the interlayer is about 1,240.9 kPa (180 psi) of tensile stress. For a 50.8 mm (2-in.) flexible base, the tensile stress at the bottom of the ACC layer is about 413.6 kPa (60 psi). This means that there is no way to avoid load-induced distress in the ACC overlay when a flexible base is inserted. However, the vertical stress in the ACC layer decreases as the thickness of the flexible base layer increases, as shown in Figure 3.8. The insertion of 50.8 mm (2 in.) of flexible layer does not greatly affect the vertical compressive stress, but adding an interlayer of 304 mm can lead to a 60% drop in compressive stress. This implies that the compressive stress on the top of the flexible base layer decreases with the increasing thickness of the flexible base layer.

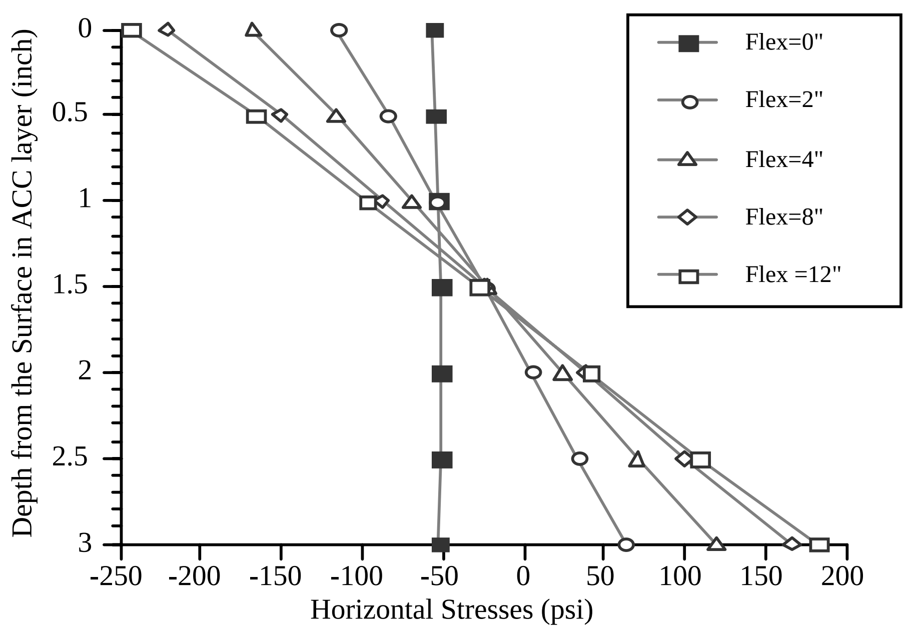

Figure 3.7. Horizontal stress distribution in ACC layer under the different thickness of interlayer (1 in. = 25.4 mm, 1 psi = 6.897 kPa)

Figure 3.9 shows the horizontal stress variation in the concrete layer as related to the thickness of the interlayer. The maximum tensile stress in the bottom of the PCC layer decreases from 896 kPa (130 psi) to 524 kPa (76 psi) as the thickness of the interlayer increases. The tensile stress in the PCC is reduced by about 70% using a thickness of 304.8 mm (12 in.) for the interlayer, compared with the AC overlay with no interlayer. This shows that thin, flexible interlayers do not reduce tensile stress in the PCC layer. For example, 50.8

mm (2 in.) of flexible base layer did not decrease the horizontal tensile stress in the PCC layer. The vertical stress distribution in the PCC layer is shown in Figure 3.10. It shows that the vertical stress changes dramatically as the interlayer thickness varies. The maximum vertical stress is about 551 kPa (80 psi) without the interlayer, while only 124 kPa (18 psi) is observed for an ACC overlay with 305 mm (12 in.) of interlayer.

Considering the higher compressive strength of the pavement material, insertion of a flexible base interlayer does not improve the performance of pavement under traffic loading. Rather, it might have a negative effect, taking into account the tensile stress in the ACC layer under the traffic loads. Therefore, the flexible base should be as thin as possible to prevent fatigue cracking in the ACC layer.

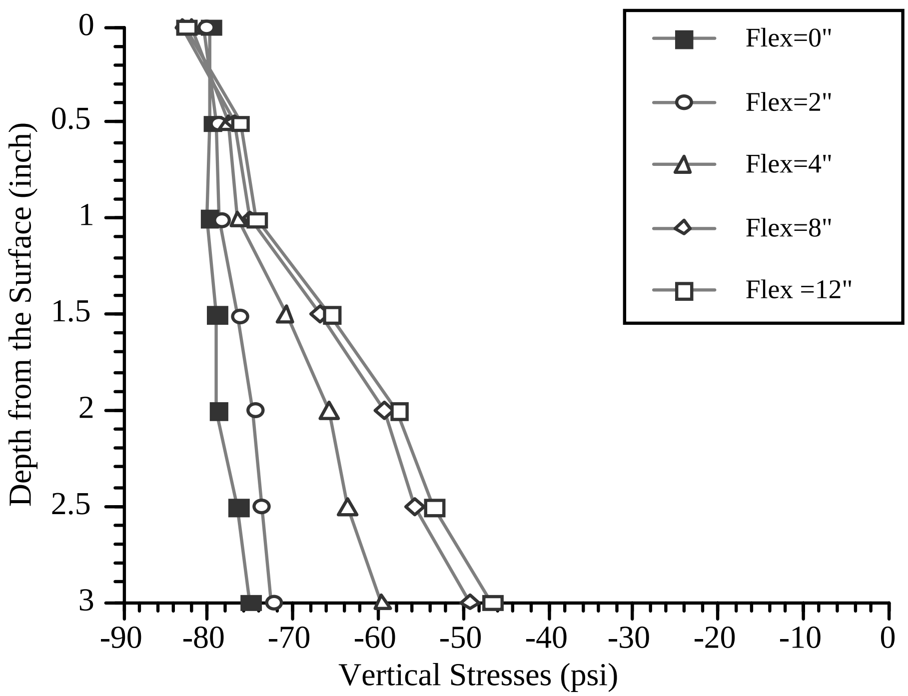

Figure 3.8. Vertical stress distribution in ACC layer under different interlayer thicknesses (1 in. = 25.4 mm, 1 psi = 6.897 kPa)

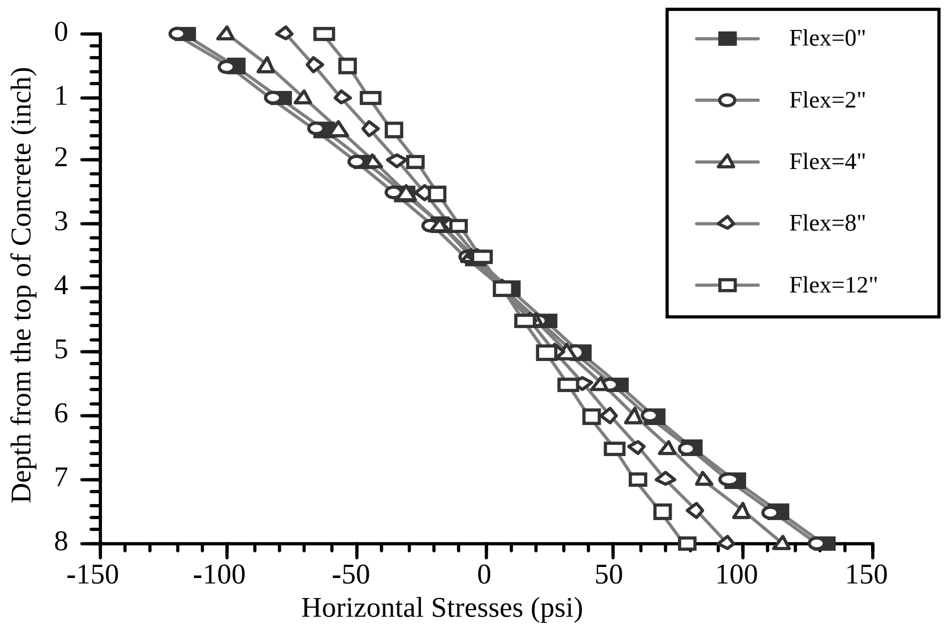

Figure 3.9. The horizontal stress distribution in the PC layer by different thicknesses of interlayer (1 in. = 25.4 mm, 1 psi = 6.897 kPa)

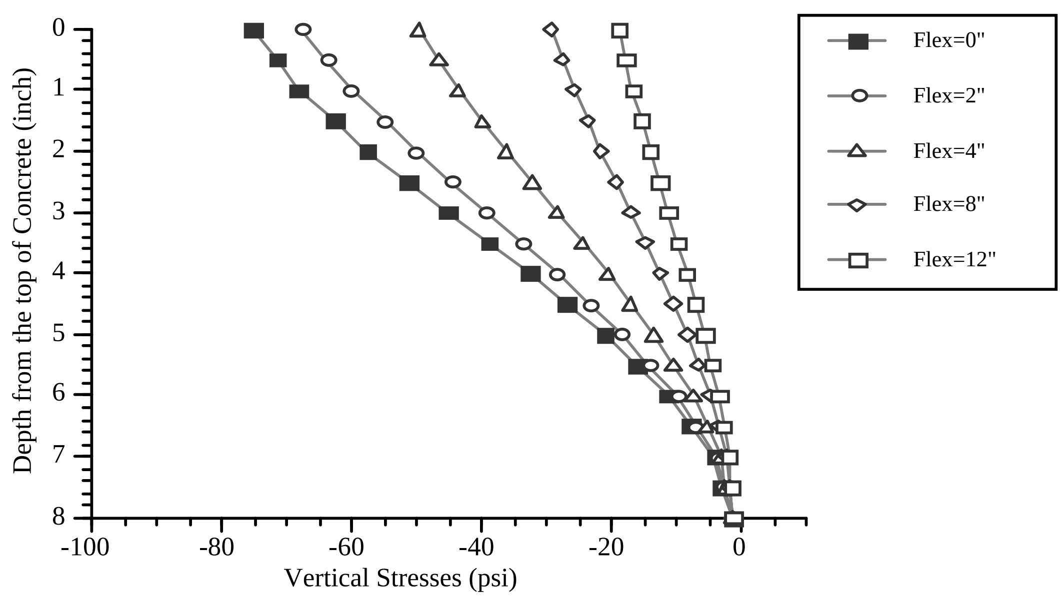

Figure 3.10. The vertical stress distribution in the PC layer by different thicknesses of interlayer (1 in. = 25.4 mm, 1 psi = 6.897 kPa)

The Effect of Stiffness of the Interlayer

The stiffness of the interlayer can significantly influence stress distribution in the pavement structure. Observations of the sensitivity of deflection and horizontal stress are made by changing the stiffness of the interlayer under standard traffic and basic pavement geometry. The interlayer could be a flexible base, stress relief layer, or asphalt-combined material layer, as observed from the Test Sections. Then, the modulus of elasticity of the flexible layer is varied from 172.4 MPa (25,000 psi) to 344.7 MPa (50,000 psi) (Adrianus et al. 1985). The stiffness for the bituminous material used for the interlayer was allowed to range from 551.5 MPa (80 ksi) to 1,034 MPa (150 ksi). For the four different levels of stiffness chosen (shown in Figure 3.11), the deflection variation resulting from a change of stiffness shows that both the maximum deflection and SCI decrease significantly as the stiffness increases. The decrease of SCI is in the range from 0.1 mm (4 mil) for the stiffest interlayer, to 0.225 mm (9 mil) for the material having the least stiffness. Beyond 0.6 m (2 ft) from the loading plate, the interlayer stiffness has little effect on the deflection of the pavement surface. The deflection calculation shows that a stiffer interlayer can reduce the possibility of rutting.

The horizontal stress distribution in a pavement structure is shown in Figure 3.12. The tendency of decreasing tensile stresses in the ACC layer is noticeable. The horizontal stress in the asphalt layer can be reduced to less than 68.9 kPa (10 psi) with the insertion of a stiffer interlayer. The tensile stress of the PCC layer, however, is almost the same regardless of the stiffness of the interlayer. This means that a stiffer interlayer can prevent the early failure of the asphalt layer without causing a negative effect on the PCC layer under traffic loading. The vertical stress distribution throughout the whole structure is shown in Figure 3.13. The stiffer material rapidly reduces the vertical stress in both the ACC and the interlayer, while the same stress remains in the PCC layer.

In summary, introducing a stiffer interlayer can decrease the horizontal tensile stress in the ACC layer as well as the vertical compressive stress. It can be inferred that insertion of a stiffer interlayer may reduce the rutting problem as well as the fatigue cracking on pavement surfaces. This is confirmed by the field results observed for test sections R4, R5, R6 and R0, which have different types of stiffer interlayers between the ACC overlay and the PCC.

Sensitivity Analysis for the Other Layers

This section discusses the sensitivity analysis used to examine the effects of varying the parameters of the layers other than the interlayer. The variation of thickness and stiffness of both layers, ACC and PCC, for example, can change pavement behavior and response, as explained below.

Thickness Effect

In order to observe the effect of the interlayer, the three other layers in the previous sensitivity analysis are set at constant thicknesses. It is necessary to determine which layer had the deciding effect on the pavement behavior for the constant thickness of interlayer. The deflection and horizontal stress are also selected to explain the variation of pavement behavior under traffic loading.

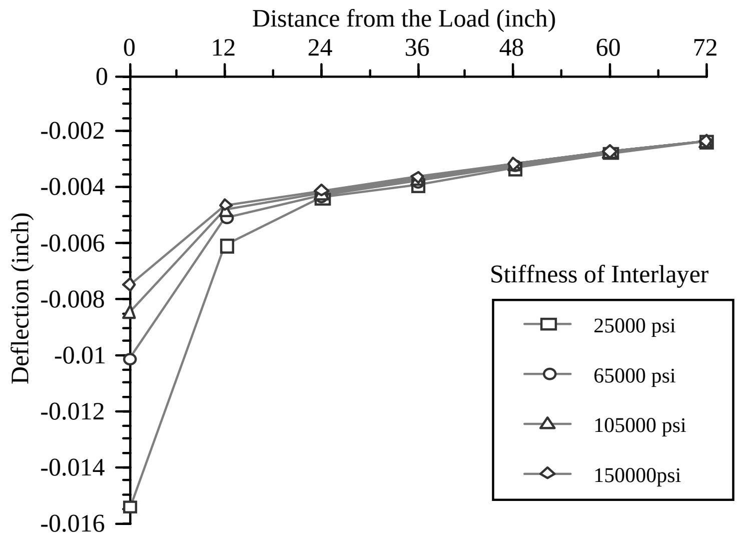

Figure 3.11. Comparison of deflection by the stiffness of interlayer (1 in. = 25.4 mm, 1 psi = 6.897 kPa)

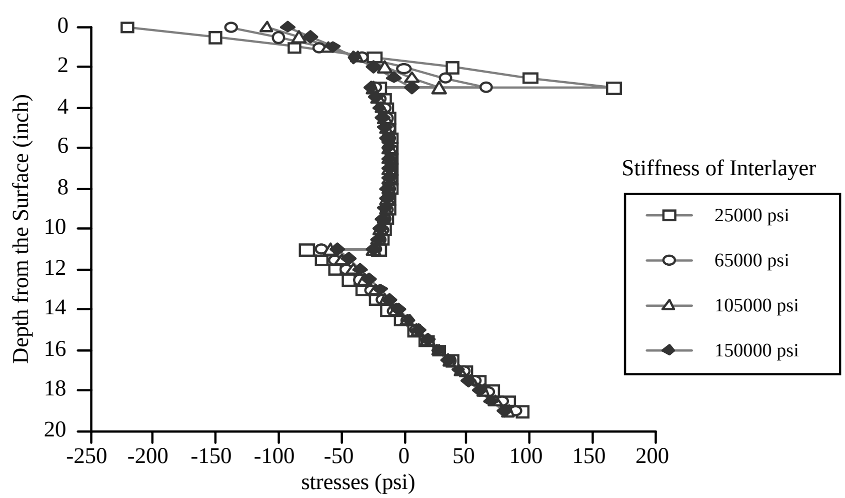

Figure 3.12. Different horizontal stress distribution by the stiffness variation of interlayer (1 in. = 25.4 mm, 1 psi = 6.897 kPa)

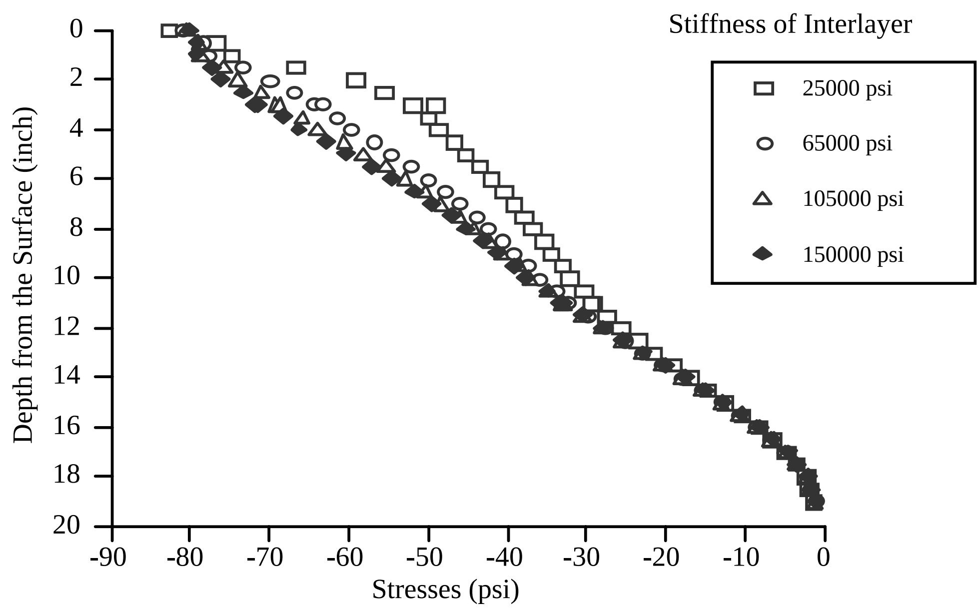

Figure 3.13. Different vertical stress distribution by the stiffness variation of interlayer (1 in. = 25.4 mm, 1 psi = 6.897 kPa)

ACC layer: The thickness of the ACC layer was changed from 76.2 mm (3 in.) to 228.6 mm (9 in.), which represents a practical ACC overlay thickness. A thin ACC layer, for example, 50.8 mm (2 in.), was excluded from this analysis even though it has been used on urban streets. As shown in Figure 3.14, the maximum deflection decreased noticeably as the surface thickness increased. For example, the maximum deflection decreased about 50% with the addition of 152 mm (6 in.) of ACC overlay. The SCI also noticeably decreases as the surface thickness increases.

The horizontal stress distribution in both the interlayer and the PCC layers is shown in Figure 3.15. The horizontal compressive stress in the flexible interlayer decreases close to zero because of the increasing thickness of the surface layer. The tensile stress in the PCC layer also decreased about 30% with the addition of the ACC layer. Thus, the thicker ACC overlay protects the existing PCC layer from further deteriorations by reducing the tensile stress in the PCC pavement. Furthermore, the tensile stress at the bottom of the ACC layer decreases to some extent with increasing thickness.

Table 3.2 shows the extreme values of stresses in all layers, including the ACC layer. It shows that the tensile stress in the ACC layer decreases noticeably (about 40%) when the ACC layer thickness is increased. The tensile stress decreases from about 654 kPa (95 psi) to 517 kPa (75 psi) and to 413.6 kPa (60 psi) by adding a 7.62-cm (3-in.) asphalt layer, respectively.

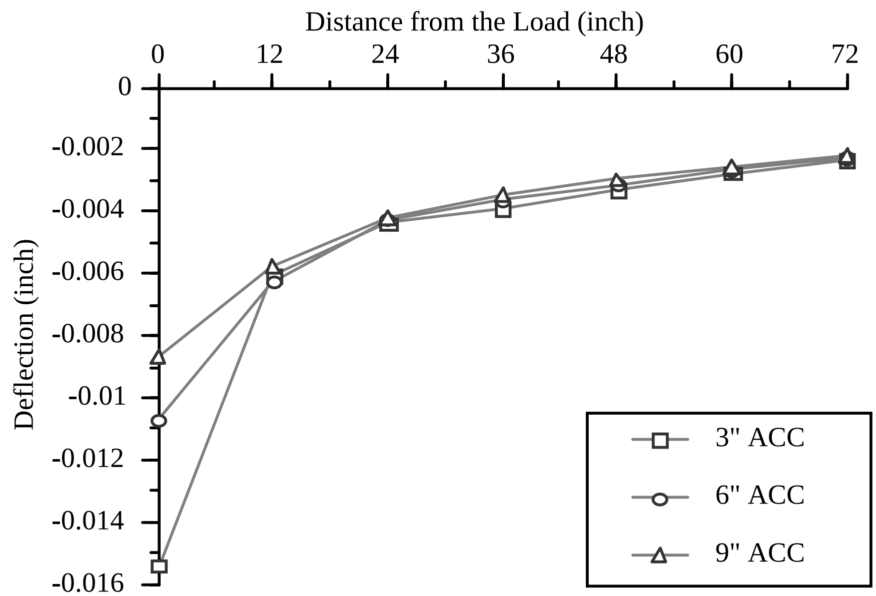

Figure 3.14. Comparison of deflection by changing thickness of interlayer (1 in. = 25.4 mm, 1 psi = 6.897 kPa)

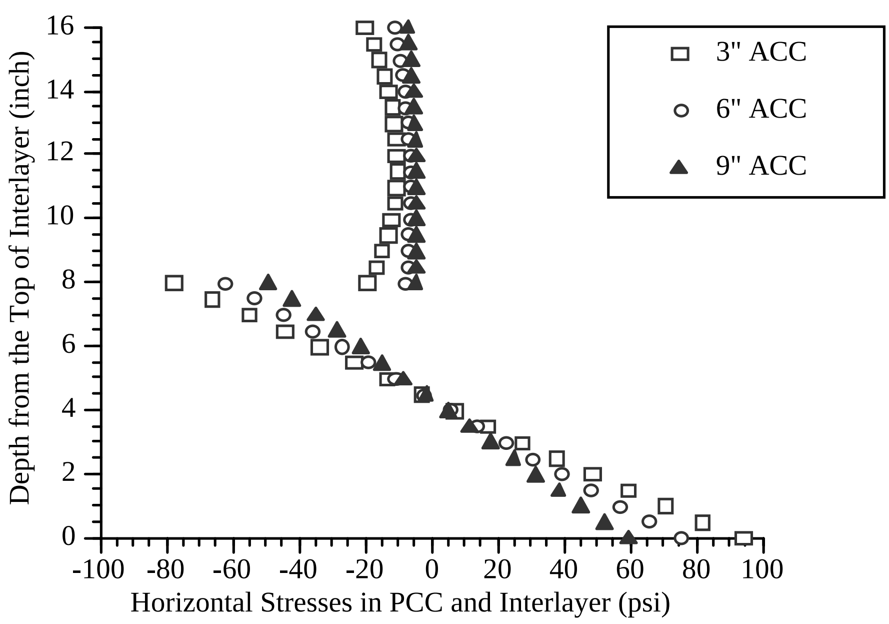

Figure 3.15. Different horizontal stress distribution by the thickness of ACC layer (1 in. = 25.4 mm, 1 psi = 6.897 kPa)

The effect of increasing the overlay thickness is shown in the vertical stress distribution. The vertical compressive stress at the top of the flexible base—about 206.8 kPa (30 psi) for 76.2 mm (3 in.) of the ACC layer—decreases to 68.9 kPa (10 psi) when the thickness of the AC overlay increases to 228.6 mm (9 in.). By adding an extra 76.2-mm (3-in.) ACC overlay, the vertical stress can be reduced to approximately 103 kPa (15 psi). We found a maximum compressive stress reduction in the PCC layer from 344.7 kPa (50 psi) for 76.2 mm (3 in.) to 103 kPa (15 psi) for a 228.6 mm (9 in.) ACC overlay. Thus, it can be concluded that a thicker ACC layer can have a significant impact on the interlaid pavement system, such that the fatigue life of both the PCC and ACC layers would increase and the rutting problem of flexible interlayers would be reduced.

Table 3.2. Maximum and minimum stress (psi) by changing the ACC thickness

	Thickness of ACC	Horizontal Stress - max.	Horizontal Stress - min.	Vertical - Stress max.	Vertical - Stress min.
ACC	3 "	93.7	-77.9	-1.4	-29.4
	6 "	74.8	-62.4	-1.2	-16.1
	9 "	59.6	-49.1	-1.1	-10.2
FB	3 "	-10.7	-20.3	-29.5	-52.1
	6 "	-6.6	-11.3	-16.0	-25.7
	9 "	-4.4	-7.2	-10.1	-15.3
PCC	3 "	166.7	-221.0	-49.2	-82.8
	6 "	102.3	-140.8	-23.5	-81.2
	9 "	62.8	-106.0	-14.1	-80.3

1 in. = 25.4 mm, 1 psi = 6.897 Kpa, FB = Flexible Base

PCC layer: Five PCC layer thicknesses were used to investigate the effect of the thickness of the PCC layer on the asphalt overlay with flexible base. JCP with 15.24 cm (6 in.) in thickness was excluded from the analysis owing to its infrequent application in Texas. The deflection variation shown in Figure 3.16 indicates that, while the surface deflection does not change, the magnitude of overall deflection increases as the PCC layer becomes thinner. As expected, the SCI remains the same throughout the range of thicknesses. This means that increasing the thickness of the PCC layer does not control the deformation of the surface layer in this system. Figure 3.17 shows the horizontal stress distribution in the ACC layer as well as in the interlayer; the stress in the surface layer on top of the 203-mm (8-in.) PCC layer is nearly equivalent to the tensile stress of the 406-mm (16-in.) PCC layer. Of course, stress within the PCC layer varies by varying its thickness, as shown in Figure 3.18.

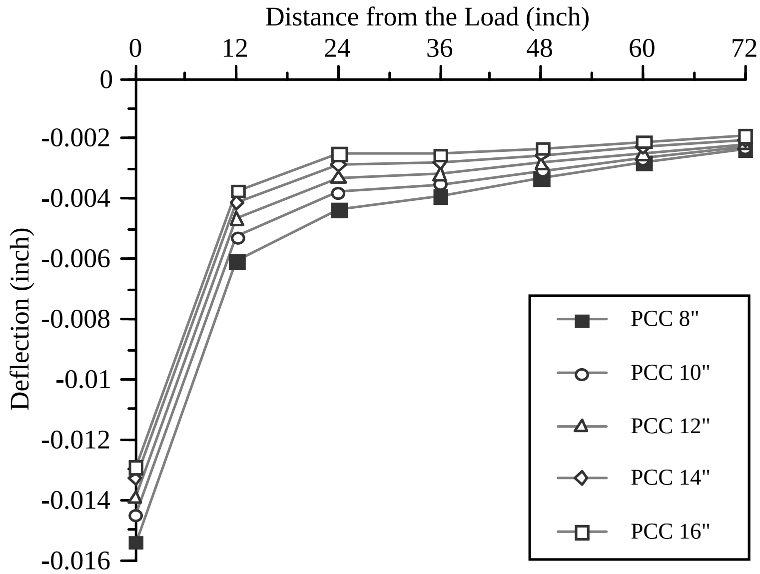

Figure 3.16. Comparison of deflection by changing thickness of PCC layer (1 in. = 25.4 mm)

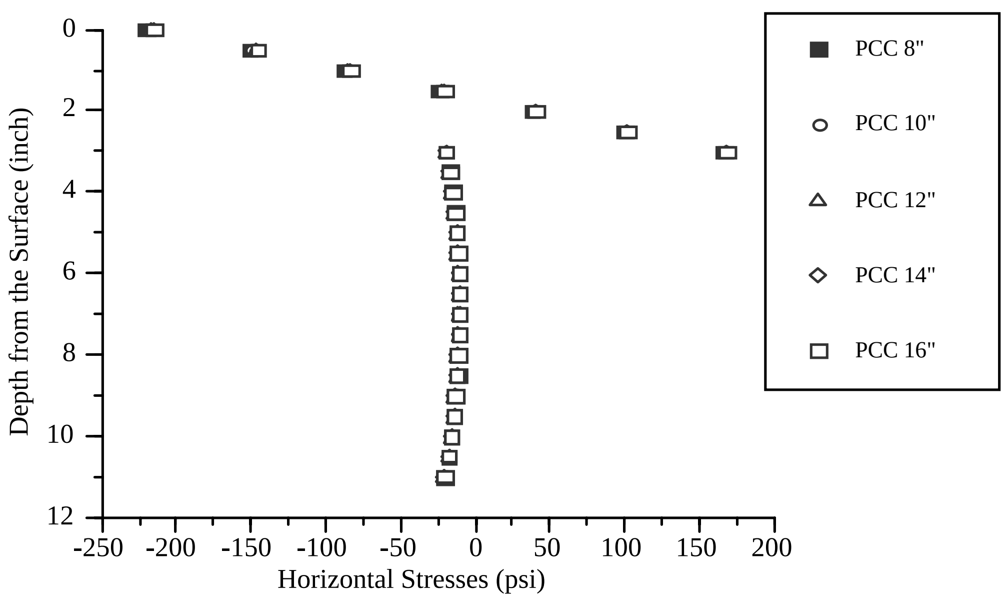

Figure 3.17. Different horizontal stress distributions in both ACC and flexible layer by PCC layer thickness variations (1 in. = 25.4 mm, 1 psi = 6.897 kPa)

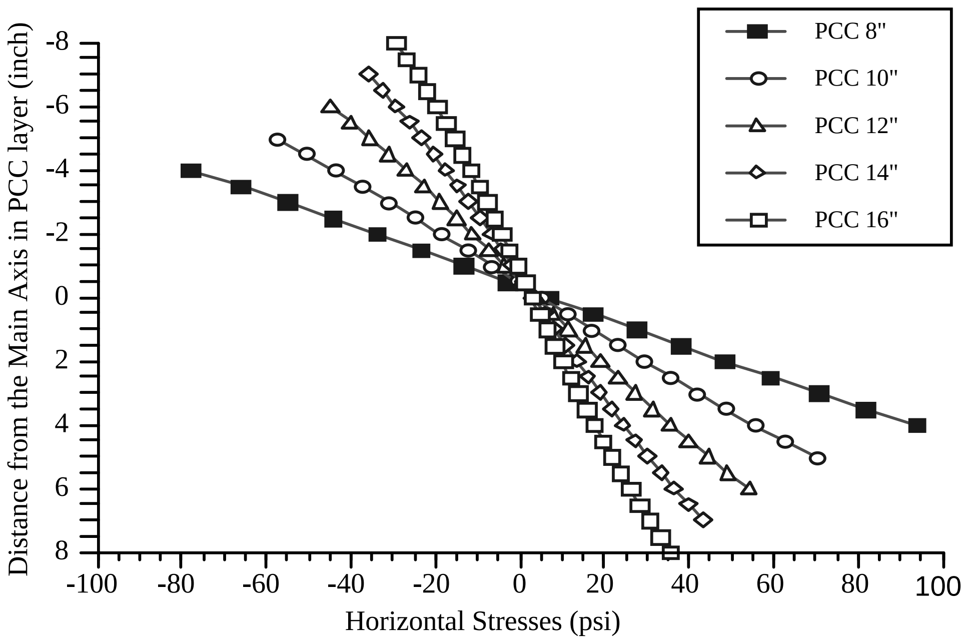

Figure 3.18. Different horizontal stress distributions in the PCC layer by varying the thickness of PCC layer (1 in. = 25.4 mm, 1 psi = 6.897 kPa)

The Stiffness Effect of the Other Layers

The effect of layer stiffness on pavement structure response depends on the cross-sectional geometric design of the structure. It is not feasible to consider all the possibilities in this initial analysis: Accordingly, the approach adopted here is to change the stiffness of one layer and compare the results with those obtained from some known pavement structures. The following observations can vary with different combinations of design factors. This is explained using the following fractional factorial design scheme.

ACC layer: The stiffness of asphalt changes with temperature. It is known that AC stiffness is high in winter and low in summer. Thus, the severity of pavement damage caused by traffic loading is not the same throughout a year. The damage may be assessed by seeking the pavement response to traffic loads in different seasons using different values of ACP stiffness, e.g., selecting the minimum 1,034 MPa (150 ksi) in summer and the maximum 6,894 MPa (1,000 ksi) in winter. Two different stiffnesses lying between the minimum and the maximum are included in the analysis, with the results shown in Figure 3.19. The maximum deflection increases as the stiffness of the ACC layer decreases. However, the values of the deflections at the other positions remain almost the same as those shown in the sensitivity study on the thickness of the ACC layer. This suggests that the maximum deflection under traffic loading strongly depends on the stiffness of the surface layer, and that the magnitude of the SCI decreases with increasing stiffness, implying that the rate of rutting varies according to the season.

The horizontal stress in the PCC and flexible interlayer changes little by increasing the stiffness of the ACC layer; these results are shown in Figure 3.20. However, the tensile stress in the ACC layer shows a sharp increase, from about 483 kPa (70 psi) to 2,068 kPa (300 psi). Thus, the stiffer ACC mix is not an effective alternative for this type of structure. In cases of higher tensile stress, the stress in the ACP layer might exceed the yield stress of the material, resulting in tensile failure in winter (though the strength of the layer would increase as a result of the temperature drop). Thus, this pavement structure may not serve as a good rehabilitation recipe in areas where the temperature variation in a year or in a season is extreme.

PCC layer: The modulus of the existing PCC layer, which ranging typically from 20,682 MPa to 34,470 MPa (3 to 5 million psi), does not vary dramatically when its composition, external environment, traffic loading history, or other factors change, As shown in Figure 3.21, the variation of deflection variation caused by changing the stiffness of the PCC layer is not as significant as the variation caused by changing the stiffness of the ACC layer. A small difference is observed in the maximum deflection.

The horizontal stress distribution by depth shows that the stiffness variation in the PCC layer does not much affect the stress in the ACC layer, as shown in Figure 3.22. The tensile stress difference in the ACC layer is less than 68.9 kPa (10 psi) within the modulus range of the PCC layer. Only the stress in the PCC layer changes. However, for a modulus beyond 34,470 MPa (5 million psi), little change of stress in either the ACC or the PCC layer is observed.

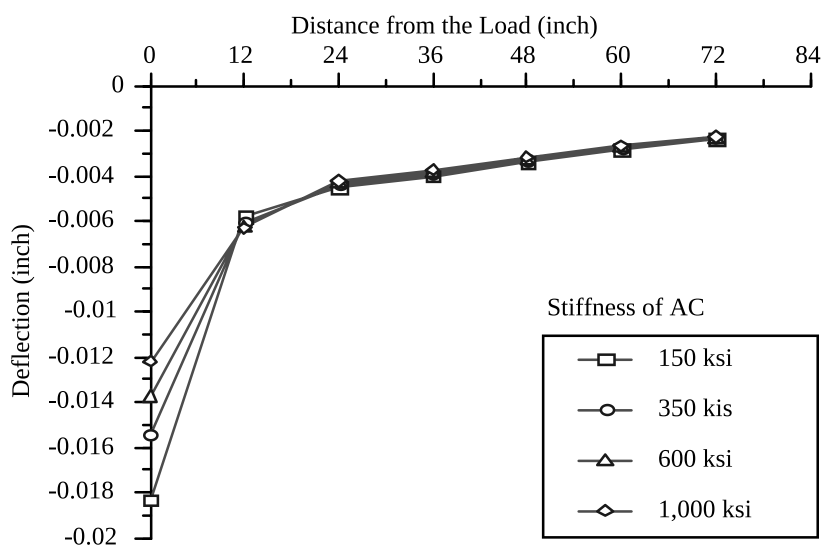

Figure 3.19. Different deflection basins by changing the stiffness of ACC layer (1 in. = 25.4 mm)

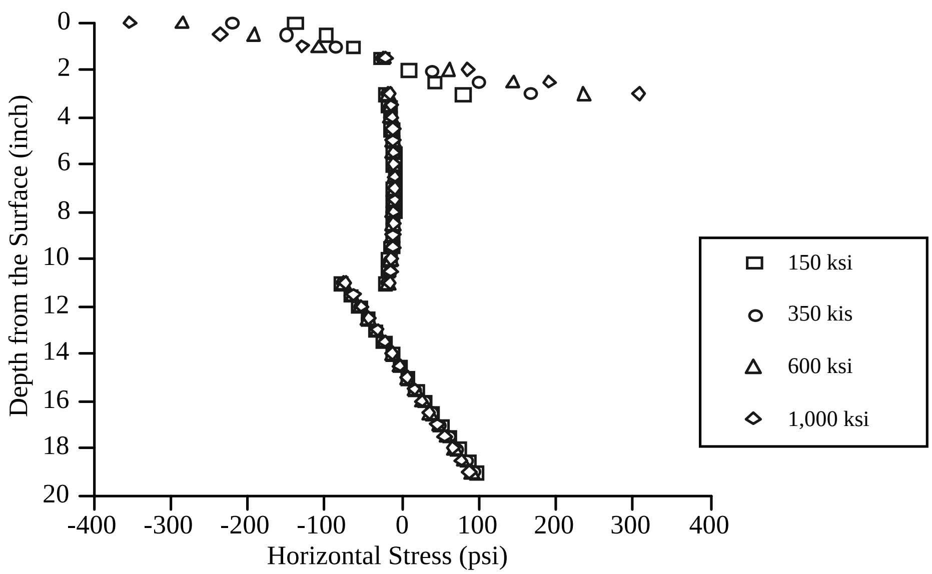

Figure 3.20. Different horizontal stress distributions by stiffness variation of ACC layer (1 in. = 25.4 mm, 1 psi = 6.897 kPa)

In summary, changing the stiffness of the PCC layer does not affect the behavior of the surface layer as long as the stiffness of the PCC layer is kept within engineering range; that is, higher than 6,894 MPa (1 million psi) for an average PCC. Thus, we conclude that both the stiffness and the thickness of the PCC layer are not the important factors to consider when selecting an AC overlay design.

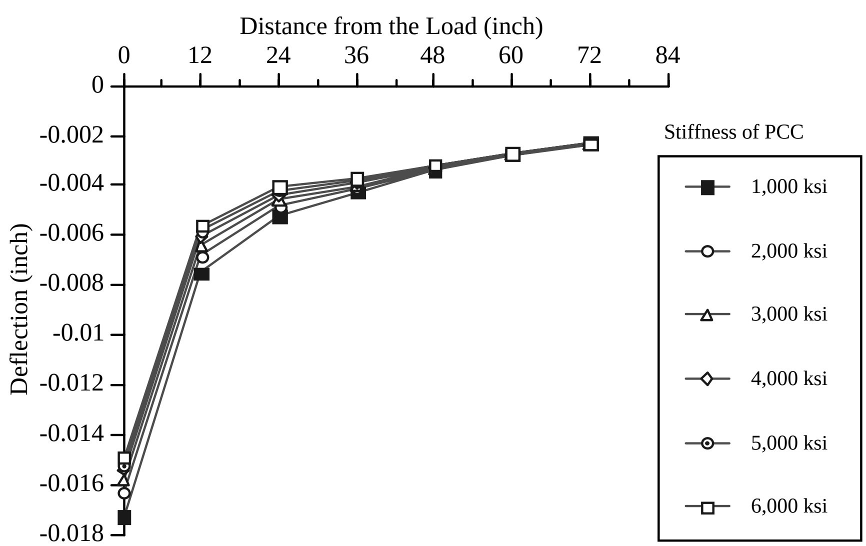

Figure 3.21. Different deflection basins by changing the stiffness of PCC layer (1 in. = 25.4 mm)

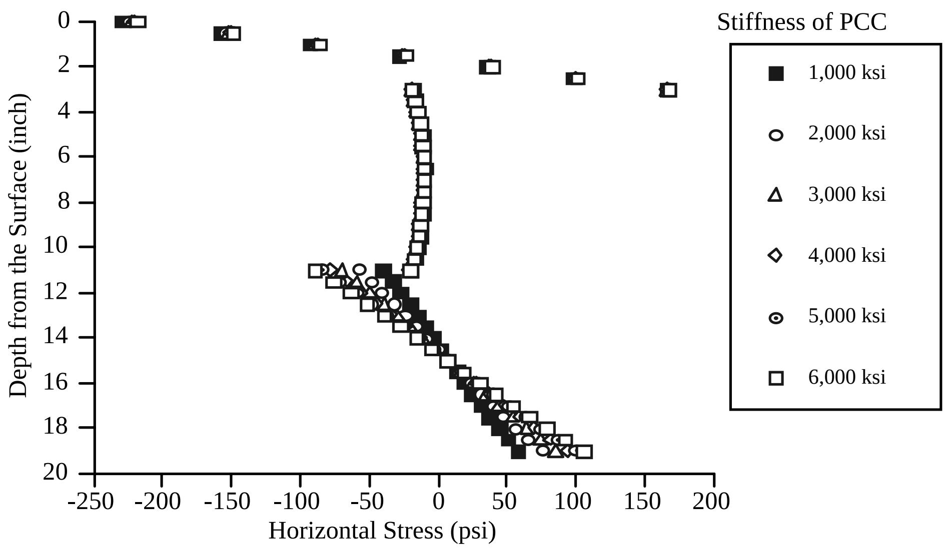

Figure 3.22. Different horizontal stresses by changing the stiffness of PCC layer (1 in. = 25.4 mm, 1 psi = 6.897 kPa)

The roadbed material–soil: The resilient modulus of the subgrade, or the roadbed material, has been considered an important factor in many design methods. The AASHTO design method introduces the resilient modulus of soil in determining the thickness of ACC or PCC layers. However, consideration of the stiffness of the subgrade layer for rehabilitation purposes may not be as important as it is in the design of a new pavement.

In Figure 3.23, the deflection basin is shown against the stiffness of the soil foundation. The maximum deflection is strongly related to the stiffness of the soil layer, although the SCI does not change. The deflection basins supported by a 103.5-MPa (15,000-psi) subgrade are larger than those supported by the soilbed of higher moduli. This implies that a weak soil layer may affect the overlay design.

In Figure 8.24, the horizontal stress in different layers is shown against the stiffness of soil layer. It indicates that the horizontal stress in the ACC layer as well as the interlayer are not affected by the strength of the soil layer. However, the stress condition in the PCC layer is reduced from about 792 kPa (115 psi) to 482 kPa (70 psi) as the stiffness of the soilbed increases. In addition, the trend of the vertical stresses remains the same. That is, the vertical stress difference in the two surface layers on top of the PCC is not significant. The vertical stress for a weak subgrade is 4 ksi and is vanishing for a strong subgrade. Thus, it may be necessary to increase the overlay thickness to protect the existing PCC layer. In cases where both the PCC layer and the roadbed soil are too flexible and fragile to support traffic loading, strengthening the subgrade is necessary.

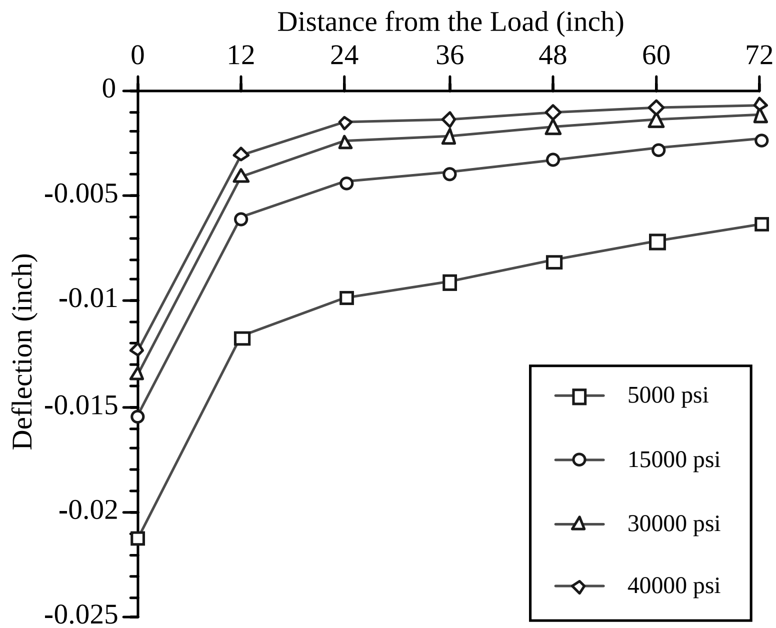

Figure 3.23. Different deflection basins by changing the stiffness of subgrade soil (1 in. = 25.4 mm)

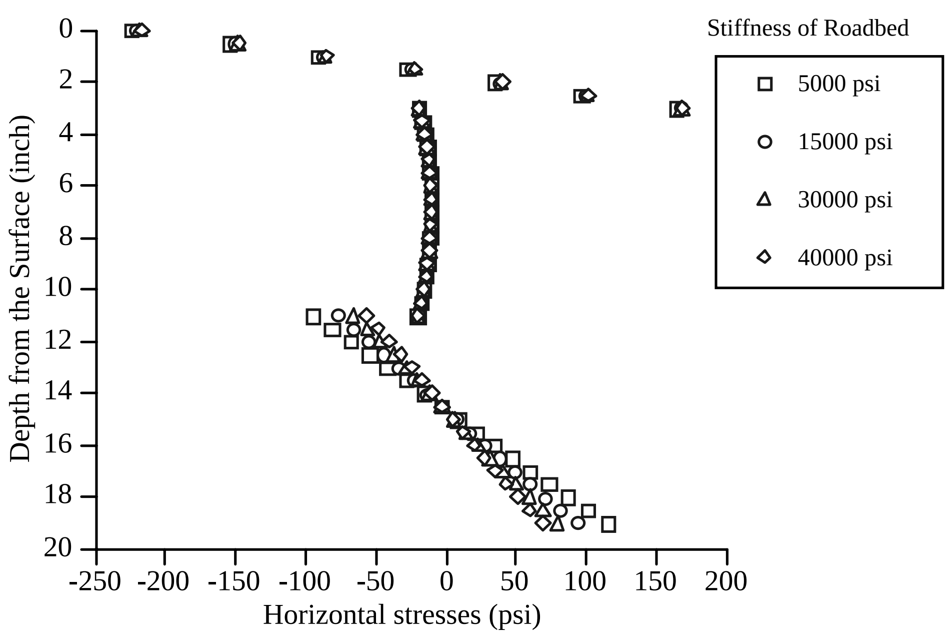

Figure 3.24. Different horizontal stress by changing the stiffness of subgrade soil (1 in. = 25.4 mm, 1 psi = 6.897 kPa)

CONCLUSION OF SENSITIVITY ANALYSIS OF INTERLAYER UNDER STATIC ANALYSIS

The above sensitivity analysis for the interlayered asphalt overlay pavement can be combined, as shown in Figures 3.25 and 3.26. The maximum deflection and SCI are first assumed to be important performance indicators associated with a rehabilitated structure. As shown in Figure 3.25, the traffic loading was much more significant than the two attribute groups—thickness and stiffness. As traffic loading increases, the width of possible ranges of deflection increases 3 times the range of deflection in other situations. The thickness and stiffness of the interlayer and the stiffness of the soil layer also greatly shifted the maximum deflection. However, the stiffness and thickness of the PC layer does not influence maximum deflection in this type of structure. Unlike the maximum deflection, the stiffness of the soil layer does not have a significant effect on SCI. From the numerical results, we found that neither the PCC layer thickness nor the stiffness represents a primary factor controlling SCI.

The possible maximum and minimum ranges of horizontal stress in previous sensitivity analyses are shown in Figure 3.26. Traffic loading is still the main factor inducing stress in both the ACC layer and in the flexible base layer. However, the thickness and stiffness of the ACC layer can significantly change the stress response in the ACC layer. The interlayer may be a main control attribute describing the tensile stress of the ACC layer but not the PCC layer. Also, the stiffness and thickness of the PCC layer do not appear to affect the physical response of the ACC layer. Further experimentation is needed to identify the major factors that influence stress response of the flexible interlayer. A partial factorial analysis that may identify the main factors is presented next.

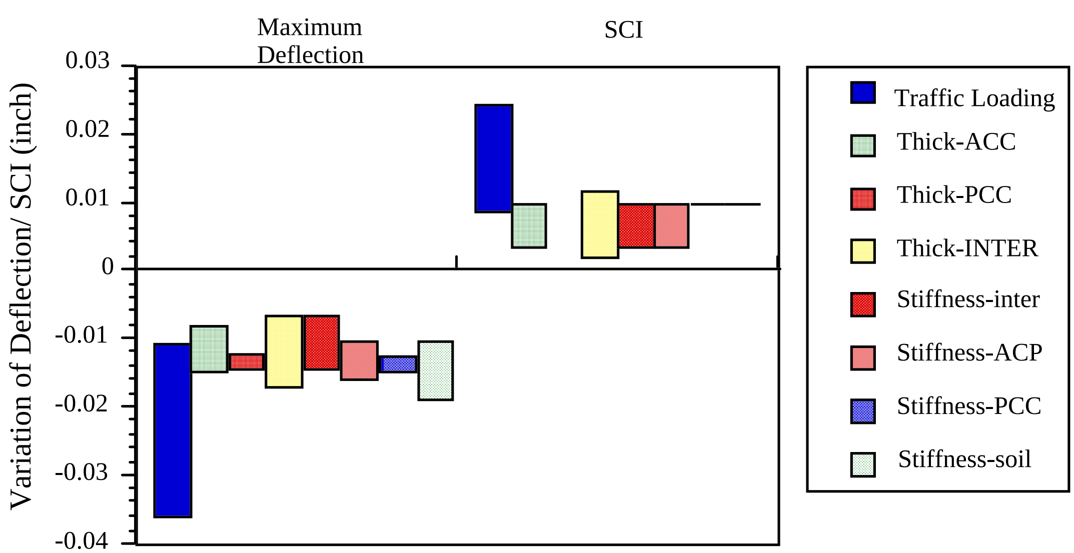

Figure 3.25. Deflection and SCI variation by factor analysis (1 in. = 25.4 mm)

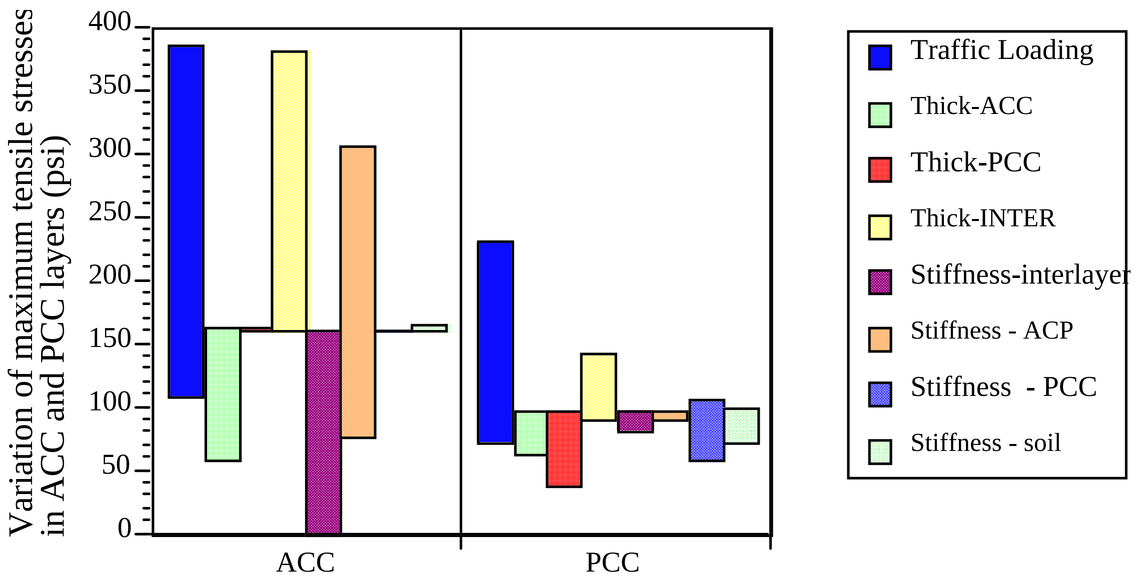

Figure 3.26. Horizontal stress variation in both ACC and PCC layer by factor analysis (1 psi = 6.897 kPa)

DYNAMIC EFFECT

Traffic loading on the pavement is actually dynamic, not static. The pavement response will differ when considering the mass effect of the structure in the analysis. The response of the ACC layer changes with the contact time of the traffic load; that is, the shorter the contact time, the stiffer the ACC appears to be. Thus, a dynamic analysis should be considered with ACC visco-elastic propriety. To be consistent with the above analysis, the loading effect is considered using the same linear elastic material properties, with the visco-elastic material property taken into account later. It is assumed that the load pressure is calculated by dividing the load by the loading area in the dynamic analysis. First, the falling weight deflectometer (FWD) loading simulation is introduced to observe the overall effect of the dynamic analysis on this type of structure. Then, four speeds—1, 32, 64, and 96 kph (1, 20, 40, and 60 mph)—are selected to identify the effect of traffic speed on the response of pavements.

LOADING HISTORY FUNCTION

The loading history of the FWD can be modeled using the two functions shown in Figure 3.27 (even though the actual FWD loading history is neither a triangular type nor a truncated sawtooth function). The second amplitude function is simplified to simulate actual amplitude function for the FWD. Generally, the triangular function is adapted if a vehicle speed is less than 32 kph (20 mph) and a truncated sawtooth function is chosen for a vehicle whose speed exceeds 32 kph (20 mph).

FWD load function (AF2)	A triangular load function	A truncated sawtooth load function (AF1)
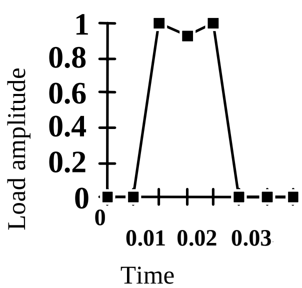	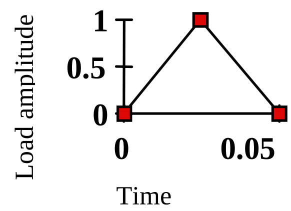	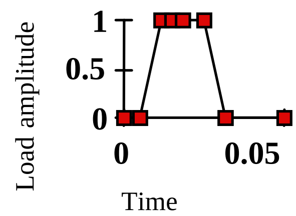

Figure 3.27. The modeling approaches of traffic loading in time

In Figure 3.28, the deflection pattern is shown employing the triangular loading function; in Figure 3.29, the deflection pattern is shown using the second load amplitude function. The peak deflection occurred almost at the same time as the peak load for the triangular function. However, under the second amplitude function, the deflection shows a continuously increasing tendency up until 50 msec. The peak deflection does not appear right after the unloading; instead, it lags behind loading.

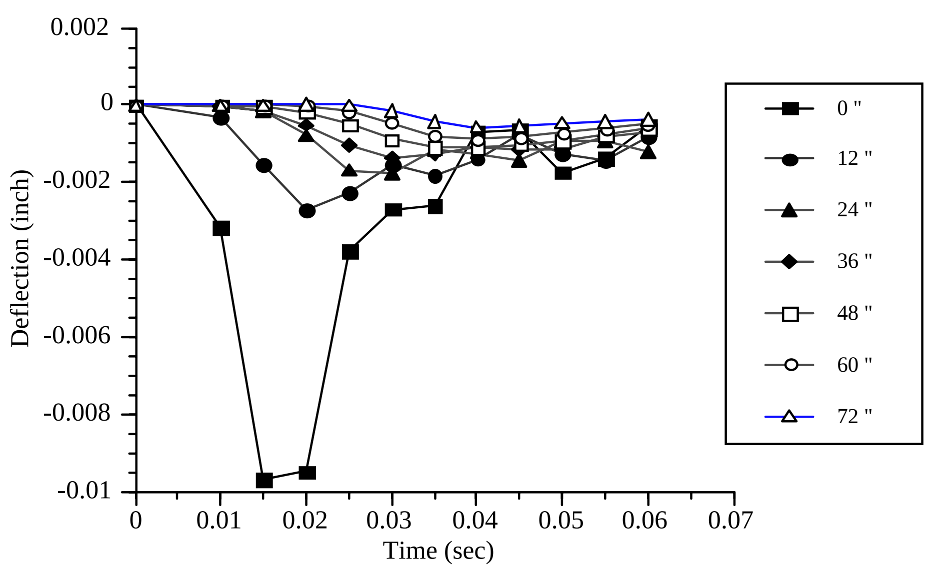

Figure 3.28. The deflection under the triangular loading function (Load-Tri) (1 in. = 25.4 mm)

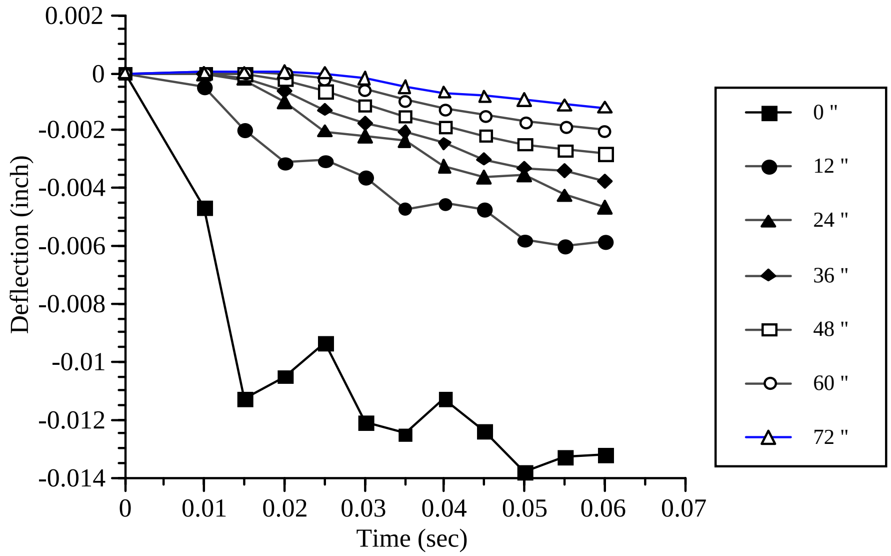

Figure 3.29. The deflection under a truncated sawtooth loading function (AF1) (1 in. = 25.4 mm)

The deflection at the peak for the three given amplitude functions was compared with deflection under the static analysis. As shown in Figure 3.30, the maximum deflection under the truncated sawtooth loading function (Load-AF1) is well matched with the result using the real amplitude function (Load-AF2) and with the results obtained from the static analysis; observe also that the triangular loading function is the least maximum deflection among the three loading functions.

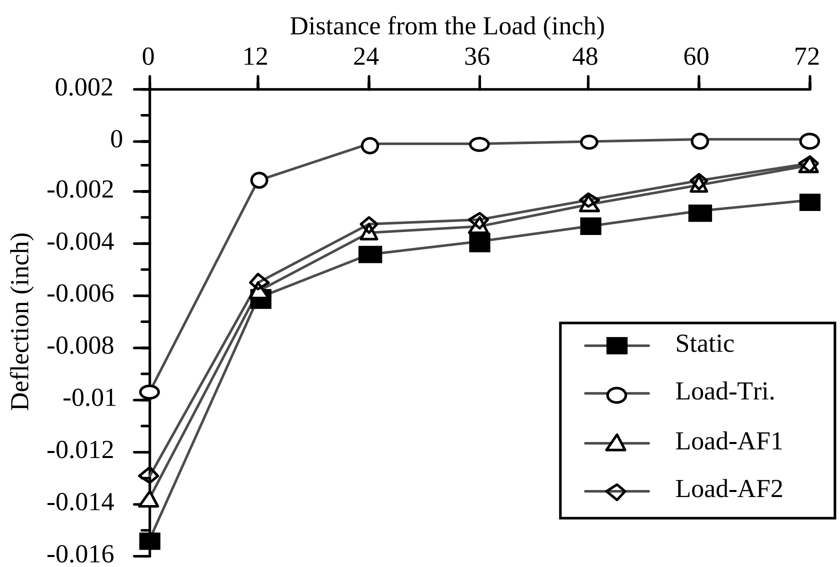

Figure 3.30. Comparison of deflection from dynamic and static analysis (1 in. = 25.4 mm)

This observation matched that documented by Ko-young, who found that (1) the maximum deflection from the static analysis is well matched with dynamic analysis in the linear elastic analysis near the loading plate and (2) some variance between them was shown far from the loading plate (Ko-young Shao 1985).

The maximum horizontal stress by time in the three layers under the dynamic load is shown in Figure 3.31. Unlike with the static analysis, the state of stress of each layer as a function of time differs; and the surface layer arrived at its maximum stress first, followed by the interlayer as the wave propagated in the pavement. The stress in both ACC and PCC is higher for the truncated sawtooth amplitude function in the dynamic analysis than that for the triangular amplitude function. In Figure 3.32, the horizontal stress distribution by depth for both amplitude functions is compared with static stress distribution. The truncated amplitude function induces higher tensile stress in the AC layer and lower stress in the PCC layer. Unlike with static loading, the interface layer develops tensile stresses at the top of the layer in the dynamic analysis.

In summary, the deflections calculated using dynamic analysis and static analysis are almost the same; but a higher peak stress is found in the ACC layer in the dynamic analysis for fast-moving conditions. Lower deflection and stress are observed when using the triangular amplitude function (other than the truncated sawtooth function); moreover, the stress response of the pavement shows little time lag to the dynamic triangular loading.

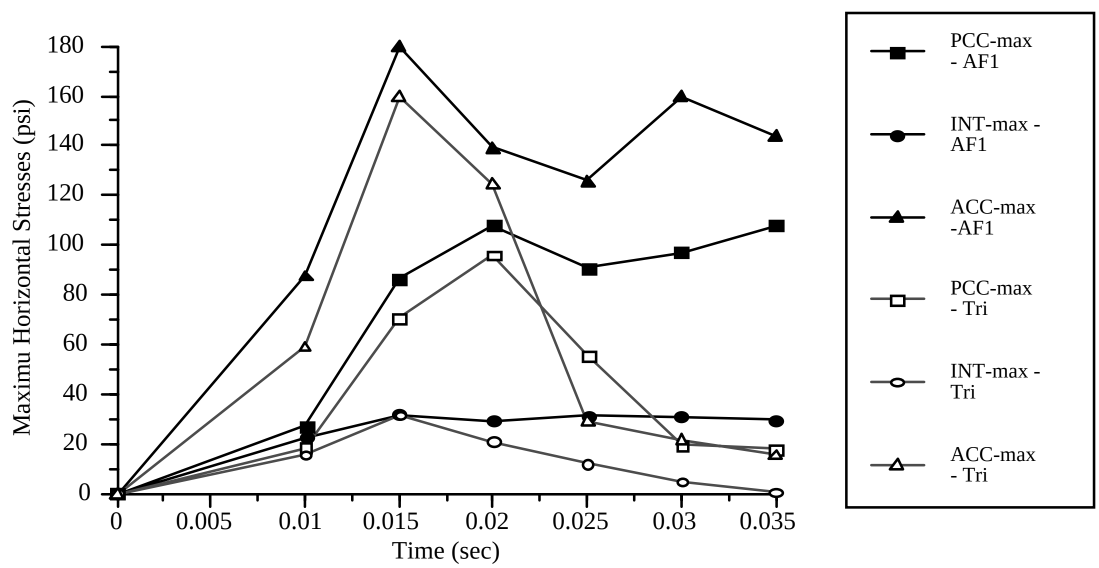

Figure 3.31. The horizontal stress variation in the pavement by time under the dynamic analysis (1 in. = 25.4 mm, 1 psi = 6.897 kPa)

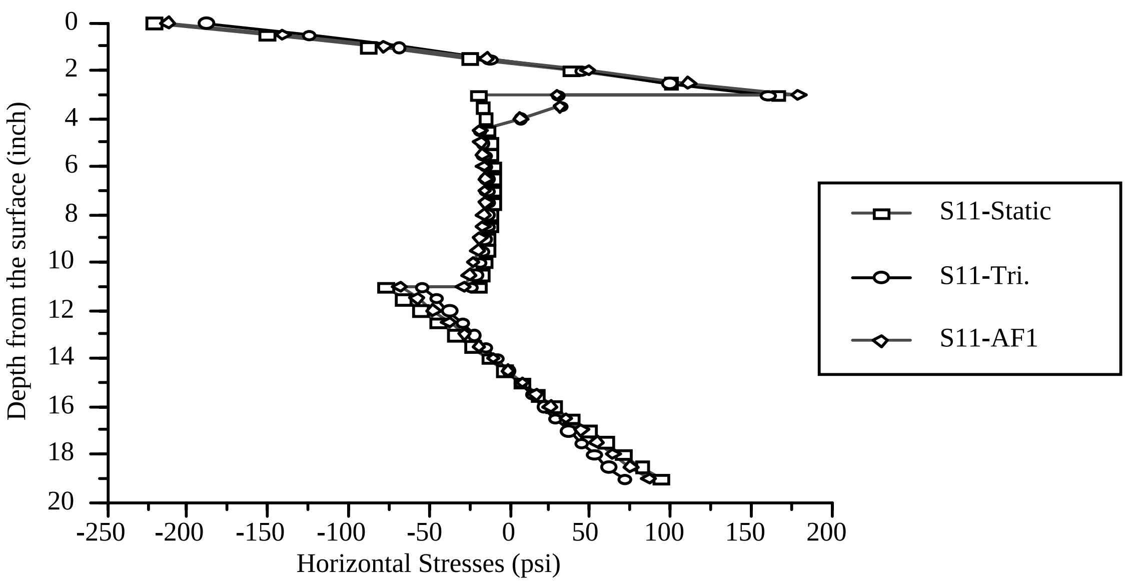

Figure 3.32. Comparison of the static analysis and dynamic analysis by horizontal stress (1 in. = 25.4 mm, 1 psi = 6.897 kPa)

DAMPING EFFECT

The damping effect on the material is shown in Figure 3.33 by comparing the deflection and stress with and without damping in the pavement layer. Five percent material damping is assumed in our analysis (Zaghloul and White 1994). The deflection of the two models had the same pattern and same values under the truncated sawtooth load function. The horizontal stress distribution as a function of time, illustrated in Figure 3.34, shows the damping effect in the pavement layers. The damping changes the phase lag but not the stress magnitude. In a moving traffic analysis for an in situ pavement, the damping effect may act as a critical factor. The damping parameter does not appear to be insignificant for the single-loading condition. However, it can be worthwhile to investigate the actual moving wheel loads.

SPEED EFFECT

Based on a linear elastic analysis, the speed effect on the pavement was studied using maximum deflections and horizontal stresses at four different vehicle speeds. The triangular amplitude function was arbitrarily chosen. The peak deflection as a function of speed is shown in Figure 3.35. Deflection in the dynamic analysis is far less than that found in the static analysis at high speed. However, the stress caused at the higher speed is far greater than that at a lower speed, as shown in Table 3.3.

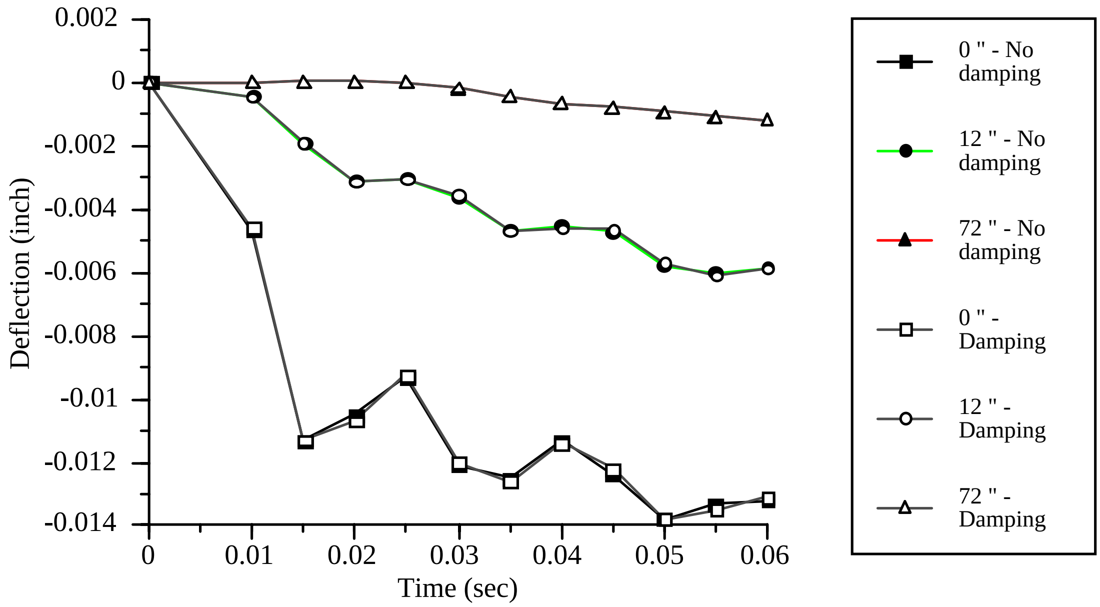

Figure 3.33. Deflection comparison between damping and nondamping models (1 in. = 25.4 mm)

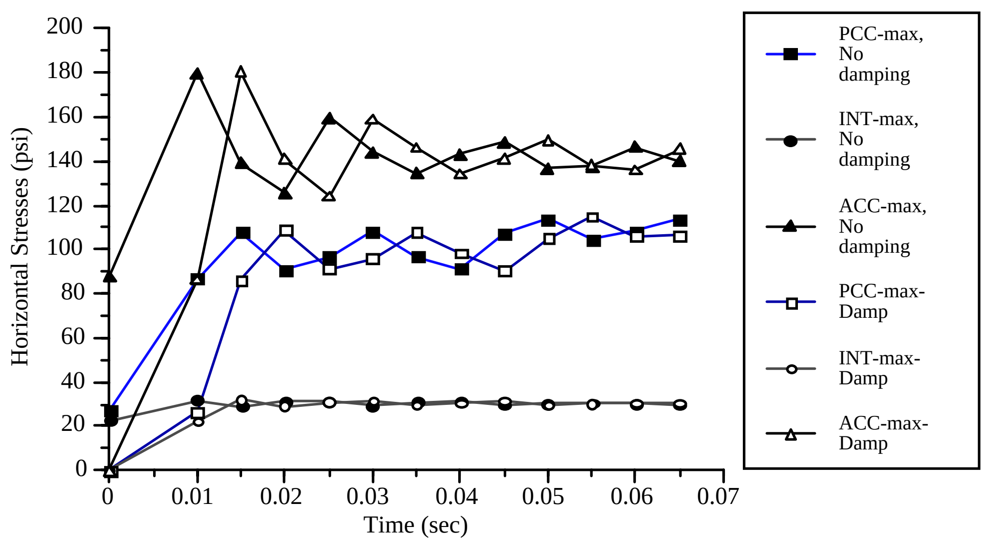

Figure 3.34. Stress comparison between damping and nondamping models (1 in. = 25.4 mm)

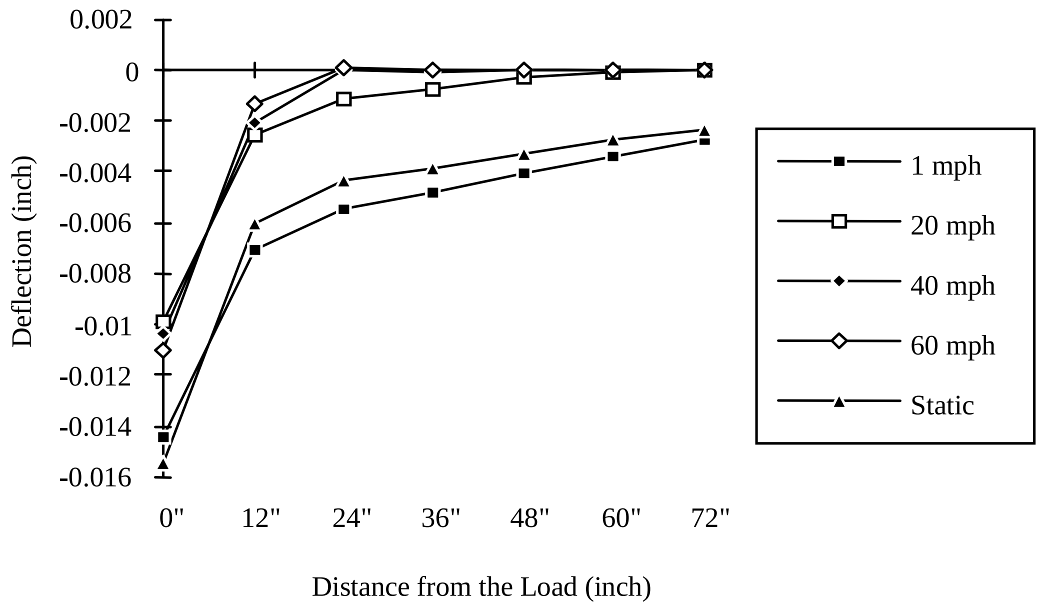

Figure 3.35. Deflection variation by the different speed (1 in. = 25.4 mm, 1 mph = 1.61 km/h)

The tensile stress in the ACC layer is about 12% higher than that in the static analysis at the 96 km/hr (60 mph) and 20% less at the lower speed. However, the tensile stress in the PCC layer decreases with increasing speed. The results obtained from the static analysis agree with those obtained from dynamic analysis at 48 km/h speed vehicle loading. Interestingly, the tensile stress at the top of the interlayer determined from the dynamic analysis, shown in Table 3.3, is far above the result obtained from static analysis.

Table 3.3. Maximum stress difference between various speed (unit = psi)

Speed	Maximum Horizontal Tensile in AC	Minimum Horizontal Tensile in PC	Maximum Vertical Tension in interlayer	Maximum Vertical Compression in interlayer
1 MPH	137.60	100.50	28.68	-46.84
20 MPH	138.80	91.02	22.84	-42.23
40 MPH	158.90	87.19	20.40	-47.81
60 MPH	184.40	73.79	13.40	-49.52
Static	166.70	93.75	0.00	-19.80

1 mph = 1.61 kph, 1 psi = 6.897 kPa

TANDEM AXLE AND SINGLE AXLE EFFECT ON THE ACC OVERLAY WITH INTERLAYER PAVEMENT

The damage caused by five-axle truck traffic contributes about 90% of the total damage to the pavement (Cho and McCullough 1995). A five-axle truck generally consists of one single axle followed by two tandem axles. The pavement response under tandem-axles and single axles may yield different stresses in the pavement. A three-dimensional model can be applied to take into account the axle load patterns in order to generate a proper design strategy. The current truck wheel spacing and total weight information can be found in the information collected by the weigh in motion (WIM) device installed in the control section for Project 987. The tire pressure and contact area under a given loading are approximated based on previous CTR findings.

TIRE PRESSURE AND CONTACT AREA

Tire pressure and contact area are related to inflation pressures under a wheel load. The most common tire sizes observed in Wisconsin were 11R24.5 and 11R22.5 (DeCabooter 1988). The maximum reported inflation was 1,034 kPa (150 psi). A survey of truck tire pressures conducted in Arkansas also found that the average inflation pressure was 724 kPa (105 psi), with pressures in excess of 828 kPa (120 psi) not being uncommon (Elliott. et al. 1991). In Illinois, the average inflation pressure was 669 kPa (97 psi), with a high of 896 kPa (130 psi) and a low of 358 kPa (52 psi) (Hansen et al. 1989). In Texas, radials were the most common tire type, occurring twice as often as bias tires (Hansen et al. 1989). Hansen reported that the most popular truck tires in use today in Texas were: 11R24.5 load range G (LR G); radial 11R22.5 LR-G; bias 10.00-20 LR-F; and bias 11.00-22.5 LR-F. A tire identified as 11R 24.5 R-G represents a tire that is 28 cm (11 in.) wide and has a 29 kN (6,430 lb) maximum load, as recommended by the manufacturer. As reported in previous sensitivity analyses, the tire pressure and wheel load relationship has been considered linearly with the contact area, based on membrane theory, which assumes that the contact pressure at each point is equal to the membrane’s inflation pressure if the inflated membrane lacks any bending stiffness and is in contact with a flat surface (Hansen 1989). However, that may lead to inaccurate results because the contact pressure was not the same as the inflation pressure owing to the stiffness of the sidewall. For example, Van Vuuren suggested a relationship between the tire inflation pressure and maximum contact pressure quantitatively (Van Vuuren 1974):

$$q = 0.349\,p + 315 \text{ (for 18 kN tire load)} \tag{3.1}$$

$$q = 0.279\,p + 258 \text{ (for 12.6 kN tire load)} \tag{3.2}$$

where

p = tire inflation pressure (kPa), and

q = contact pressure (kPa).

To permit comparisons, the CTR study chose two popular tire types, the 11R24.5 LR-G radial tire and the super single 18-22.5 LR-H bias tire, and tested them using three loading ranges with two inflation tire pressures. The contact area and maximum contact area under normal stress are measured with specially designed test equipment. The results obtained for the radial and bias tire are reported in Tables 3.4 and 3.5 (Hansen et al. 1989). The maximum normal contact pressure and contact area tend to increase as inflation pressure and wheel load increase, but the contact pressure becomes more uniform under the constant inflation tire pressure. Figures 3.36 and 3.37 show a relationship between the contact area and wheel load. A simple curve-fitting equation is derived based on these results.

Table 3.4. Radial 11R24.5 tire experimental results (Hansen et al. 1989)

Inflation Pressure (psi)	Wheel Load (lb.)	Max. Contact Pressure (psi)	Maximum Location	Mode (psi)	Contact Area (inch ^{2})
90	5000	136	Tread center	78	68.2
	6000	121	Tread center	76	77.1
	7000	139	Tread center	74	88.4
105	5000	110	Tread center	76	66.0
	6000	124	Tread center	78	76.1
	7000	133	Tread center	84	82.5

1 in. = 25.4 mm, 1 lb = 4.45 N, 1 psi = 6.897 kPa

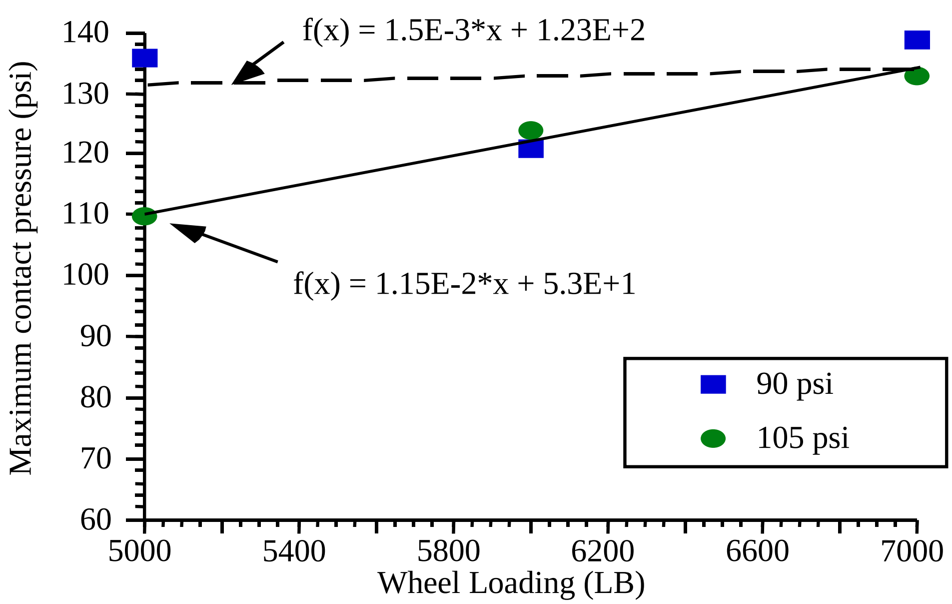

Figure 3.36. Maximum contact pressure variation under wheel loading and inflation pressure by 11R 24.5 radial tire (1 lb = 4.45 N, 1 psi = 6.897 kPa)

Table 3.5. Bias 18-22.5 tire experimental results (Hansen et al. 1989)

Inflation Pressure (psi)	Wheel Load (lb.)	Max. Contact Pressure (psi)	Maximum Location	Mode (psi)	Contact Area (inch ^{2})
85	8000	340	Tread center	82	75.6
	10000	391	Tread center	91	99.9
	12000	249	Tread center	58	114.9
100	8000	316	Tread center	58	74.4
	10000	342	Tread center	66	87.7
	12000	238	Tread center	94	112.0

1 in. = 25.4 mm, 1 lb = 4.45 N, 1 psi = 6.897 kPa

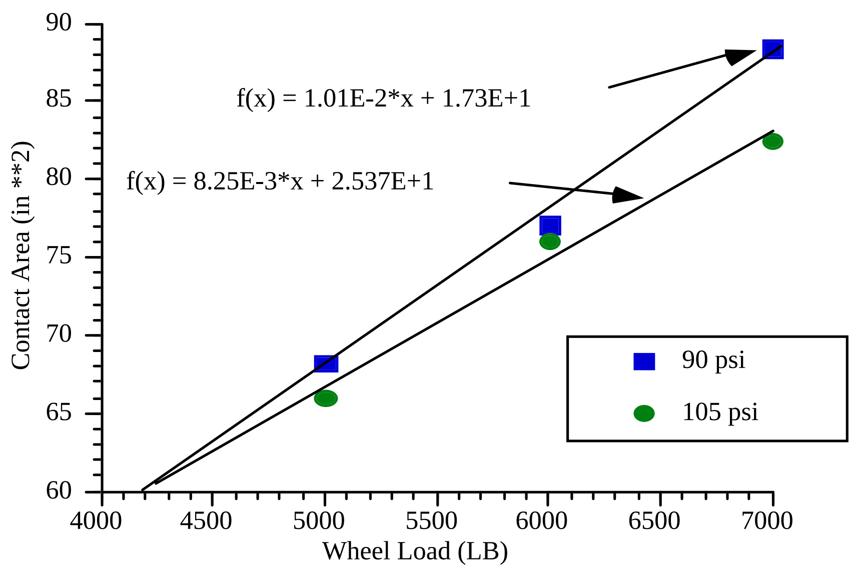

Figure 3.37. Contact area variation under wheel load and inflation pressure (psi) by bias 18-22.5 tire (1 in. = 25.4 mm, 1 lb = 4.45 N, 1 psi = 6.897 kPa)

In addition to normal pressure perpendicular to the contact surface, the shear component, tangential to the contact surface, is applied to the surface of the pavement. Bonse et al. showed that the horizontal shear stress is mostly affected by speed, not inflation pressure (Bonse et al. 1959). With a tire inflation pressure of 193 kPa (28 psi) for a car and 483 kPa (70 psi) for a truck, Bonse et al. found that the longitudinal shear stress was 75.8 kPa (11 psi) for a car and 151.7 kPa (22 psi) for a truck at constant speed. However, this was increased to 276 kPa (40 psi) during acceleration or deceleration.

WHEEL LOAD DISTRIBUTION

Figure 3.38 represents the growth truck weight of a 3-S2 vehicle. The mean weight of the 3-S2 truck was estimated to be 260 kN (58,000 lb). The extreme value of truck traffic loading was reported to be 445 kN (105,000 lb) (Walton 1978). The truck traffic loading is also measured from the test section installed on US 59. A total of 800 3-S2 vehicle samples were chosen from the database, and axle weight and spacing information were recorded. First, Table 3.6 summarizes the axial spacing information for the five-axle vehicles. The mean axial spacing between the first and second axles was 4.86 m (16.17 ft) for the first lane and 5.17 m (16.71 ft) for the second lane. The spacing between the second and third wheels is1.4 m (4.70 ft) and 1.39 m (4.57 ft), respectively; the spacing between the third and fourth measured 10.1 m (33.27 ft) and 10.2 m (33.43 ft). All the information suggests that most truck traffic passing the test section meets the layout of the 3-S2 truck given by the specifications.

Table 3.6. Wheel spacing for 3-S2 vehicles on the test section (unit = in.)

Lane	spacing	axle 1-2	axle 2-3	axle 3-4	axle 4-5
Right (1st Lane)	Mean	16.17	4.70	33.37	4.30
	Std	3.03	1.83	4.24	0.65
	COV	18.76	38.98	12.70	15.12
Left (2nd Lane)	Mean	16.71	4.57	33.43	4.37
	Std	3.00	0.15	3.26	0.74
	COV	17.95	3.23	9.75	16.84

1 in. = 25.4 mm

Figure 3.38 shows growth vehicle weight (GVW) distribution on Texas interstate highways (Walton 1983). The weight distribution of the 3S-2 truck was also measured as shown in Table 3.7 and3.8 for both lanes. The average wheel weight does not exceed the specified total weight of 151 kN (34,000 lb), as shown in Figure 3.39. The figure also shows that the front tandem axle carried more weight than the following tandem axle.

The cumulative frequency distribution of each wheel weight is shown in Figures 3.40 and 3.41. The single axle did not exceed the weight specification of 53.4 kN (12,000 lb), while the percentage of the traffic loading exceeding the specified limits was about 2%. The 90% of the weight of the tandem axles is in the range from 130.8 kN (29,400 lb) to 143 kN (32,120 lb). However, maximum weight of the total tandem axle load is above 178 kN (40,000 lb).

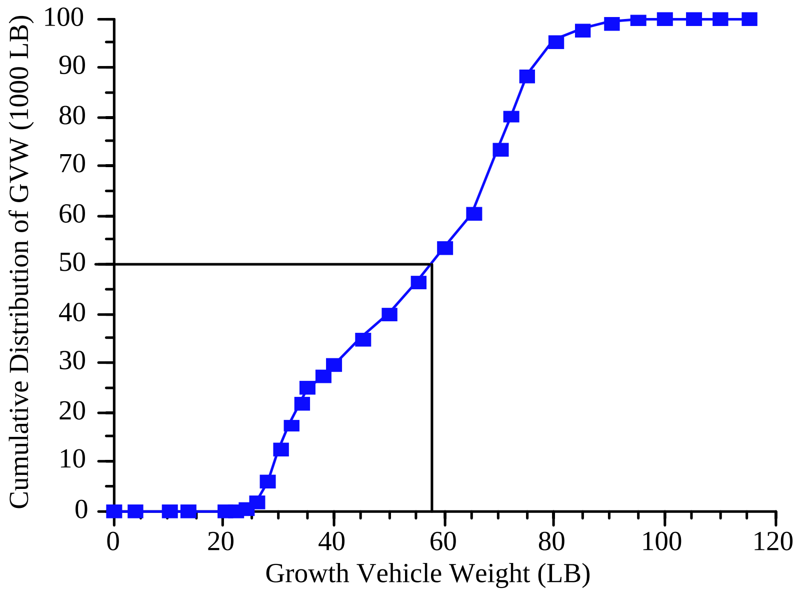

Figure 3.38. Growth vehicle weight (GVW) (1 lb = 4.45 N)

Table 3.7. Wheel weight information for 3-S2 vehicles on the test section—Right lane (unit = 1,000 lb)

		wheel 1	wheel 2	wheel 3	wheel 4	wheel 5
Left	Mean	5.00	6.02	6.11	5.41	5.72
	Std	0.67	1.87	1.95	2.05	2.13
	COV	13.33	31.02	31.95	37.99	37.30
	Max.	8.00	10.70	10.80	10.50	10.50
Right	Mean	4.87	5.99	5.59	5.33	5.45
	Std	0.67	1.91	1.85	1.99	2.11
	COV	13.83	31.85	33.15	37.36	38.63
	Max.	8.60	10.20	10.10	9.80	10.60

1 lb = 4.45 N

Table 3.8. Wheel weight information for 3-S2 vehicles on the test section—Left lane (unit = 1,000 lb)

Wheel path		weight 1	weight 2	weight 3	weight 4	weight 5
Left	Mean	5.15	5.63	5.28	5.32	4.67
	Std	0.62	1.93	1.82	2.29	2.02
	COV	12.00	34.37	34.40	43.05	43.27
	Max.	6.40	10.0	9.30	10.20	8.90
Right	Mean	4.55	5.87	5.83	5.42	5.38
	Std	0.71	1.72	1.82	2.11	2.28
	COV	15.64	29.28	31.27	38.87	42.37
	Max.	5.70	9.60	9.20	10.60	10.10

1 lb = 4.45 N

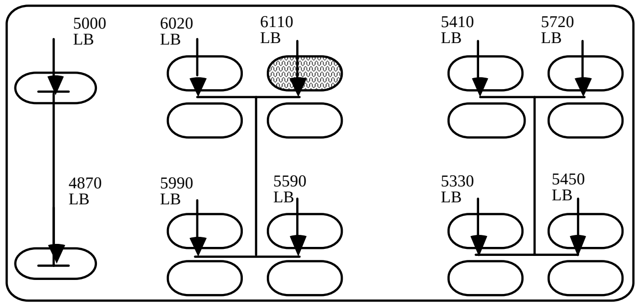

Figure 3.39. Mean weight distribution of 3-S2 truck at right lane in field (1 lb = 4.45 N)

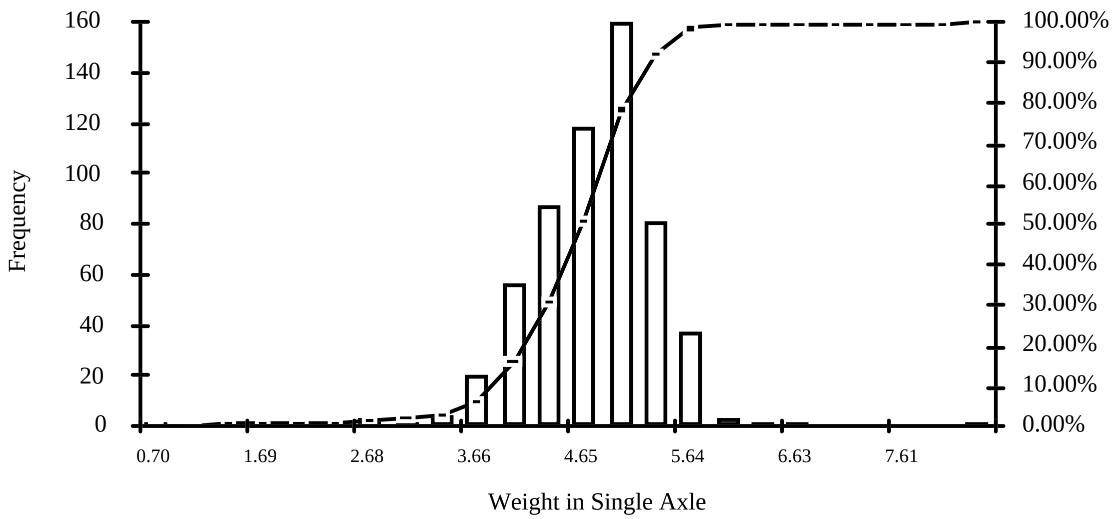

Figure 3.40. Histogram of weight in single axle in 3S2 truck (1,000 lb) (1 lb = 4.45 N)

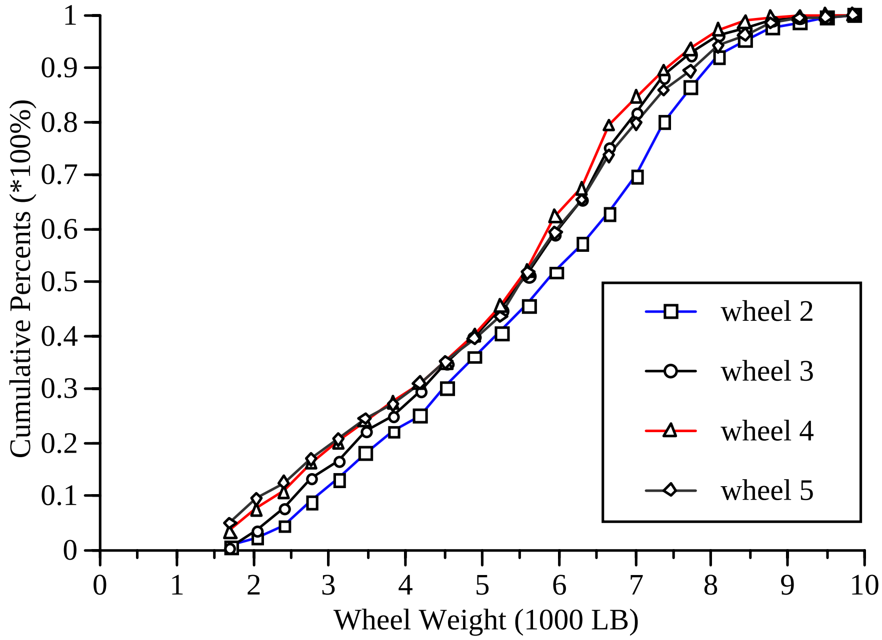

Figure 3.41. Histogram of weight in tandem axle in 3S2 truck (1,000 lb) (1 lb = 4.45 N)

MECHANISTIC ANALYSIS

In this analysis we consider a pavement consisting of a 76.2 mm (3 in.) thick ACC top layer, a 203.2 mm (8 in.) thick flexible interlayer, and a 203.2 mm thick (8 in.) PCC layer. The stiffness of the ACC layer is the same as that used in the previous sensitivity analysis. The following sensitivity analysis was conducted to investigate the tandem axle effect on the pavement structure. First, the result obtained from tandem axle loading is compared with that obtained from the single axle loading. Then, the results for edge loading is compared with that for interior loading to examine the effect of loading position on the response of the AC overlay structure.

Single Axle and Tandem Axle Load

Introducing the tandem axle to decrease the damage under the heavier truck was considered by comparing the maximum deflection and stresses with the ideal single axle wheel under the same weight. Using WIM data, we selected three traffic loads: 107 kN (24,000 lb), 178 kN (40,000 lb), and 249 kN (56,000 lb). In this study, the average value of the tandem dual tire loading, 26.7 kN (6,000 lb), corresponded to a 107 kN total tandem axle weight; the maximum 44.5 kN (10,000 lb) corresponded to 178 kN (40,0000 lb); and the 31 kN (7,000 lb) single wheel load, corresponded to the 249 kN (56,000 lb) tandem axle load.

The model configuration for the FEM is shown in Figures 3.42 and 3.43. For the single axles, a quarter pavement slab was modeled. The tire contact area was fixed to the same area for the single wheel load; the tire contact pressure was changed according to the traffic loading.

For the tandem axle, the tire inflation pressure was assumed to be 723.8 kPa (105 psi). The contact areas were found to be 0.0322 m^2 (50 square^2) for 3,000 lb, and 0.0532 m^2 (82.5 in.^{2}) and 0.0438 m^2 (68 in.^{2}) for 5,000 lb and 7000 lb, respectively. Even though the maximum estimated contact pressure for 3,000 lb is 603 kPa (87.5 psi), the maximum normal contact pressure was 723 kPa (105 psi) for 13.7 kN (3,000 lb). Also, the 758.3 kPa (110 psi) normal contact pressure was found for a 22.3 kN (5,000 lb) load, and 916.9 kPa (133 psi) for the 31.2 kN (7,000 lb) load, respectively. In the FEM, the detailed axle and tire arrangements for the tandem axles are taken from the Texas-MLS design manual and from WIM wheel spacing information. The dimension of tire contact area was calculated by an equivalent area concept used to make PCA design methods, as shown in Figure 3.43 (Huang 1993). Then, the detail mesh was generated based on the mesh.

First, Figures 3.44 and 3.45 show deflection variations under tandem axles under different weights. Two different deflection bowls show that the width of dual tires affects pavement response significantly, especially under the heavier loading. The maximum deflection appears at the lower right tire, not at the center of the dual tire.

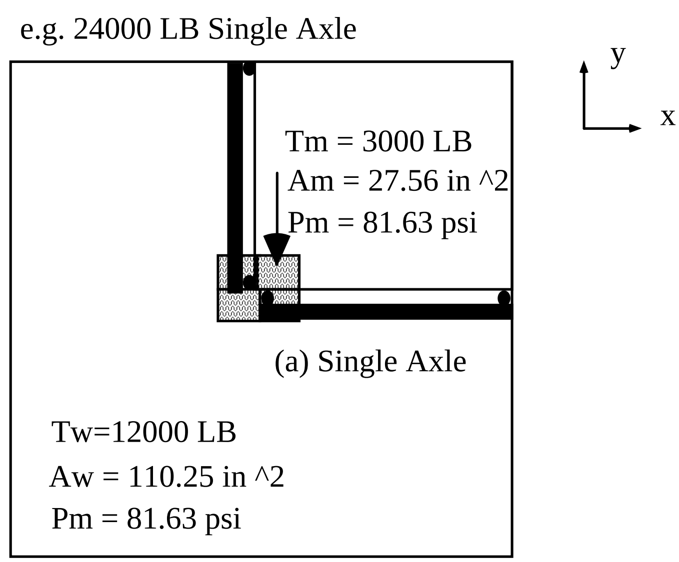

Figure 3.42. FEM modeling for single and tandem axle (1 in. = 25.4 mm, 1 lb = 4.45 N, 1 psi = 6.897 kPa)

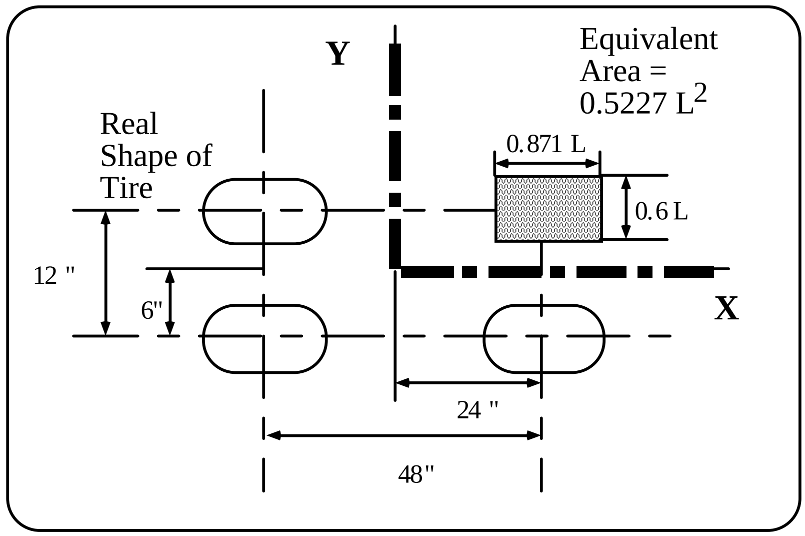

Figure 3.43. Tire arrangement and configuration of tandem axle and FEM (1 in. = 25.4 mm)

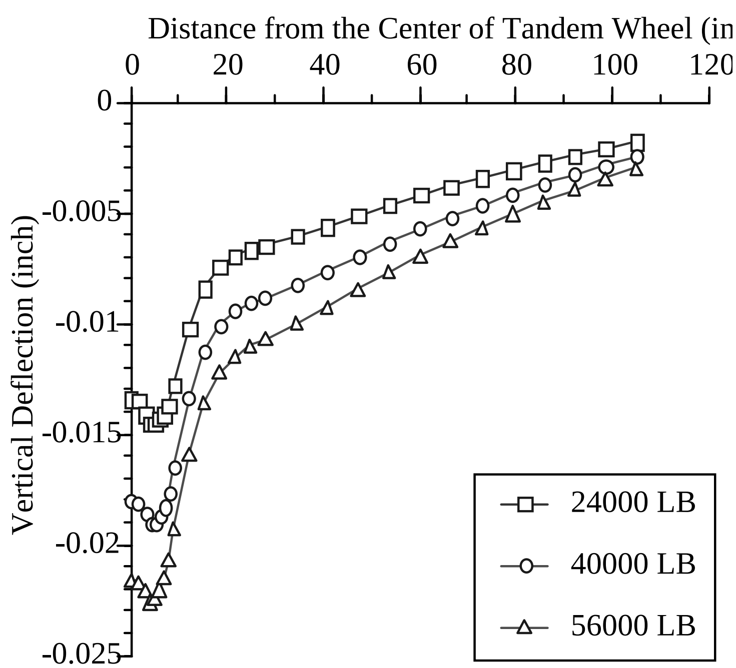

Figure 3.44. The deflection of transverse direction (Y) under tandem axle loading (1 in. = 25.4 mm, 1 lb = 4.45 N)

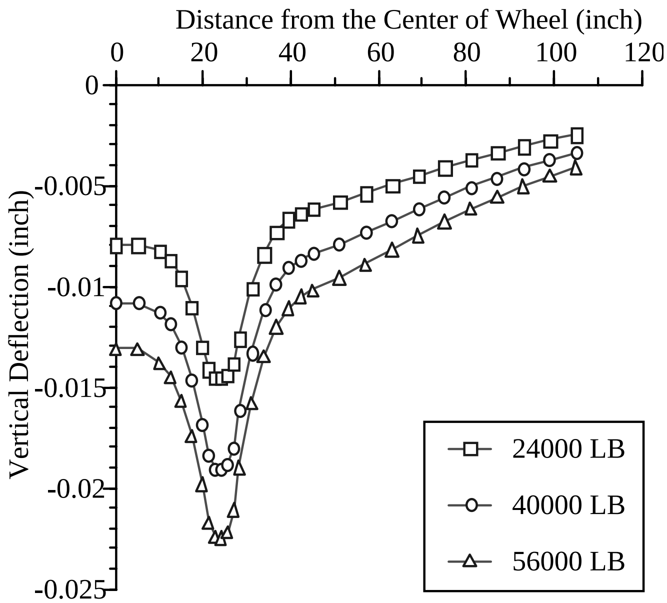

Figure 3.45. The deflection of longitudinal direction (X) under tandem axle (1 in. = 25.4 mm, 1 lb = 4.45 N)

Both horizontal stress distributions in the PCC layer and the ACC layer are shown in Figures 3.46 and 3.47. Traditionally, the center of the tandem axle load is considered as a maximum point of stress, rather than the point directly under the wheel. However, the maximum horizontal stress on both layers appears right below the tire load, as shown in Figure 3.46. As also shown in the figure, the horizontal stress in the ACC increases continuously, so that the maximum stress appears at the center of the tire.

The deflection of the single and that of the tandem axles agree at 107 kN (24,000 lb) loading; but a large difference in deflection is observed at 178 kN (40,000 lb) and 249 kN (56,000 lb) axle loads, as it is shown in Figure 3.48. The tandem axle presented about 50% less deflection than the single axle at 249 kN (56,000 lb) of traffic loading. This clearly shows that a tandem axle configuration can distribute load better on the pavement and induces less stress than a single axle does.

There is a significant difference in the maximum horizontal stresses induced in the PCC layer between the single axle and the tandem axle configuration, as shown in Figure 3.49. The maximum horizontal stress in the ACC layer doesn't change when the magnitude of traffic loading under the tandem axle load varies, but it increases due to heavier traffic weight in the single axle. However, the horizontal stress in the PCC layer increases with increasing traffic loads for both types of loading.

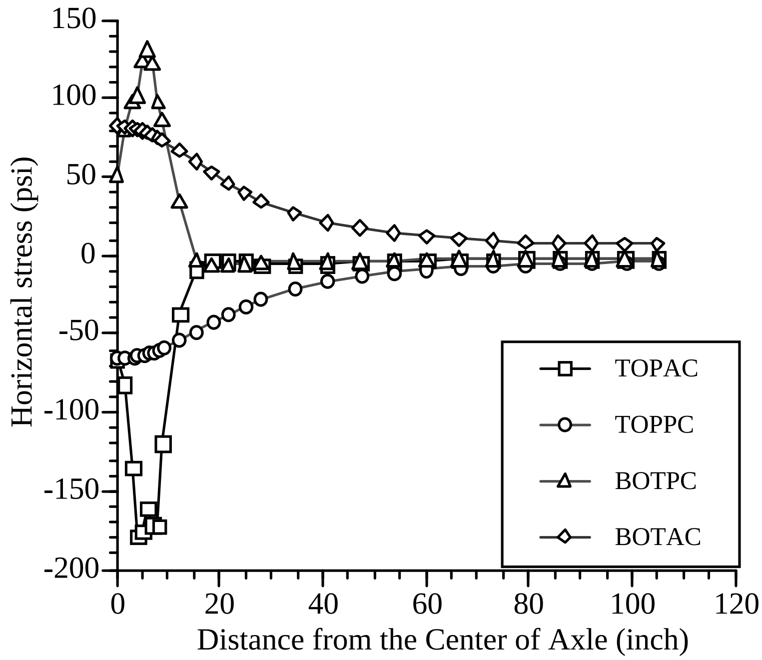

Figure 3.46. The horizontal stress of transverse direction (Y) under 40,000 lb axle loading (1 in. = 25.4 mm, 1 psi = 6.897 kPa)

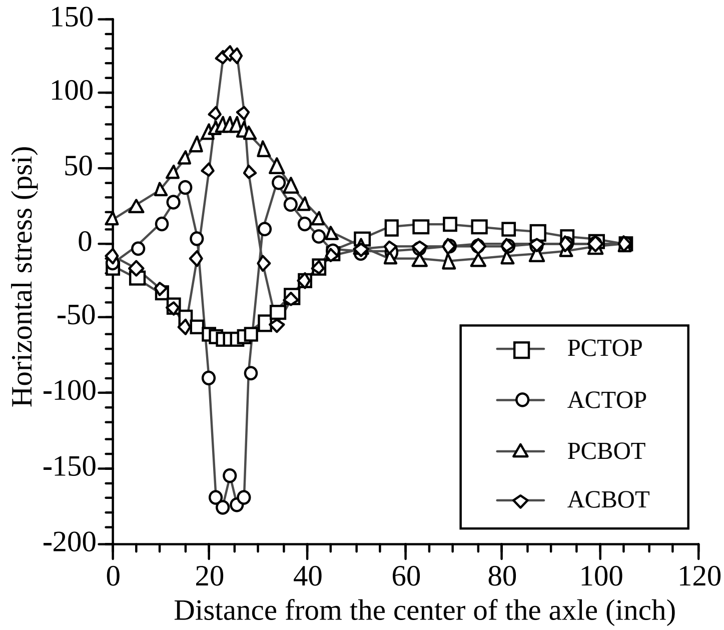

Figure 3.47. The horizontal stress of longitudinal direction (X) under 40,000 lb axle loading (1 in. = 25.4 mm, 1 psi = 6.897 kPa)

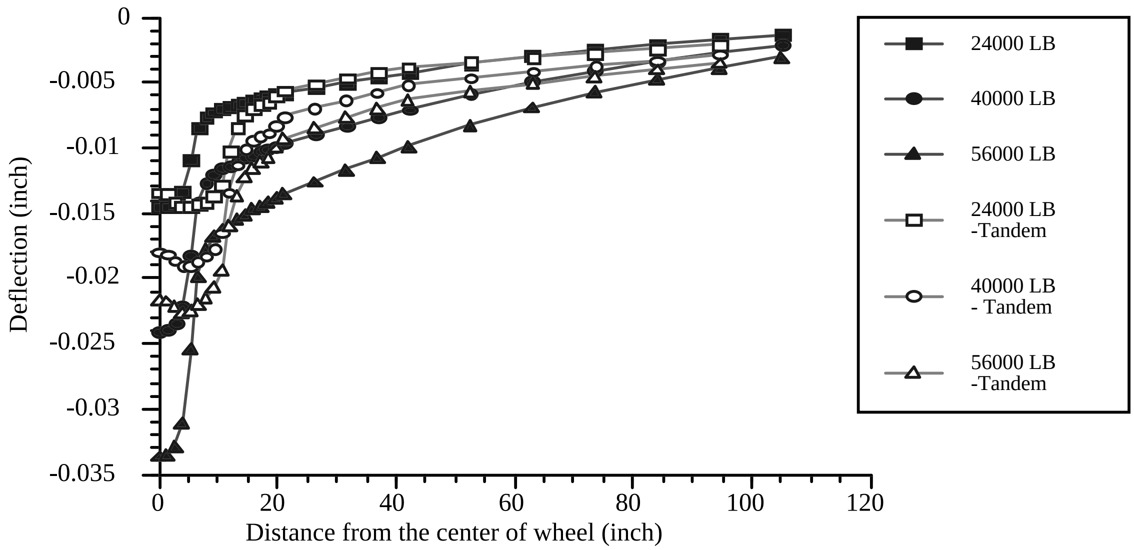

Figure 3.48. Comparison of deflection between single and tandem axle (1 in. = 25.4 mm, 1 lb = 4.45 N)

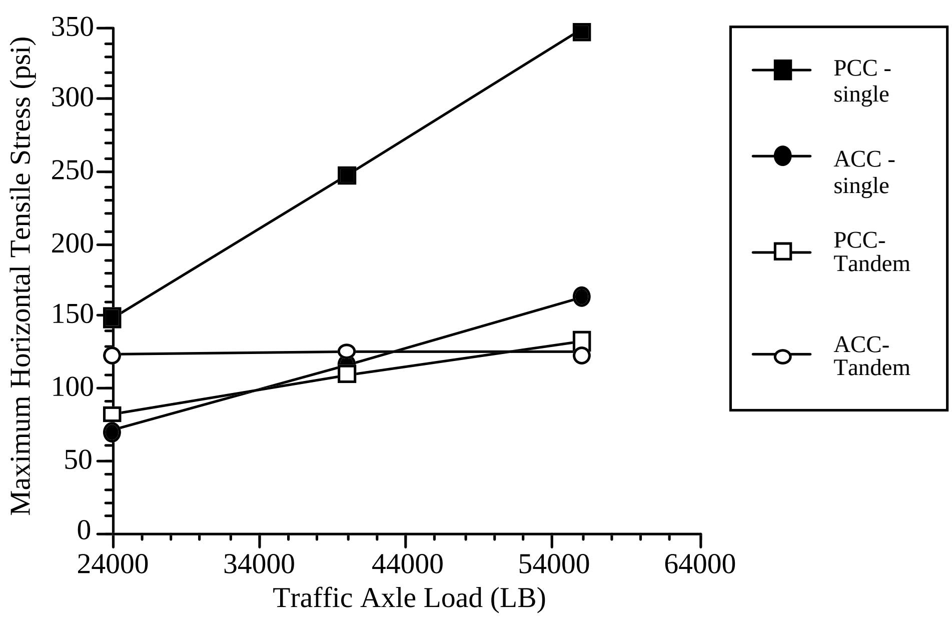

Figure 3.49. Comparison of horizontal stress between single and tandem axle (1 lb = 4.45 N, 1 psi = 6.897 kPa)

The other difference is the stress reduction in the PCC layer owing to the tandem axle. For example, the maximum horizontal stress in the PCC layer under 107 kN (24,000 lb) axle loading induced by the single axle is about 1,034 kPa (150 psi), while it is 551.2 kPa (80 psi) for the tandem axle. As the loading is increased, the horizontal stress caused by the single axle increases dramatically up to 250% for both ACC and PCC layers.

Interlayer Effect under the Tandem Axle

The thickness of the interlayer was decreased to zero to observe the effect of interlayer thickness in the overlay structure under tandem axle loading. Table 3.9 shows that the tensile stress in the AC layer decreases with decreasing interlayer thickness. The stress in the ACC layer changes from tensile to compressive stress when the interlayer is not present. Table 3.9 shows that (1) a thicker interlayer with low stiffness induces greater tensile stress at the bottom of the ACC layer, as shown in Figure 3.50; and (2) the wheel load induces slightly different horizontal stresses in the ACC layer when a thick interlayer is present and causes relatively larger horizontal stresses when a thin interlayer is present. The horizontal stress in the PCC layer decreases with increasing interlayer thickness. This finding suggests that the interlayer might protect the PCC layer from further failure.

Table 3.9. Pavement overlay behavior under different interlayer thicknesses

	Interlayer thickness	8"	6"	2"	0"
	Axle Load				
ACC -S11	24000 lb	123.8	112.3	60.4	-46.8
	40000 lb	126.2	111.3	48.6	-56.9
	56000 lb	124.1	106.7	37.5	-61.7
PCC -S11	24000 lb	82.5	87.2	105.4	121.6
	40000 lb	110.8	117.3	140.4	162.2
	56000 lb	133.0	140.9	167.4	198.2
Def.	24000 lb	-1.45E-02	-1.36E-02	-1.13E-02	-1.07E-02
	40000 lb	-1.90E-02	-1.78E-02	-1.48E-02	-1.44E-02
	56000 lb	-2.26E-02	-2.11E-02	-1.76E-02	-1.78E-02

1 in. = 25.4 mm, 1 lb = 4.45 N

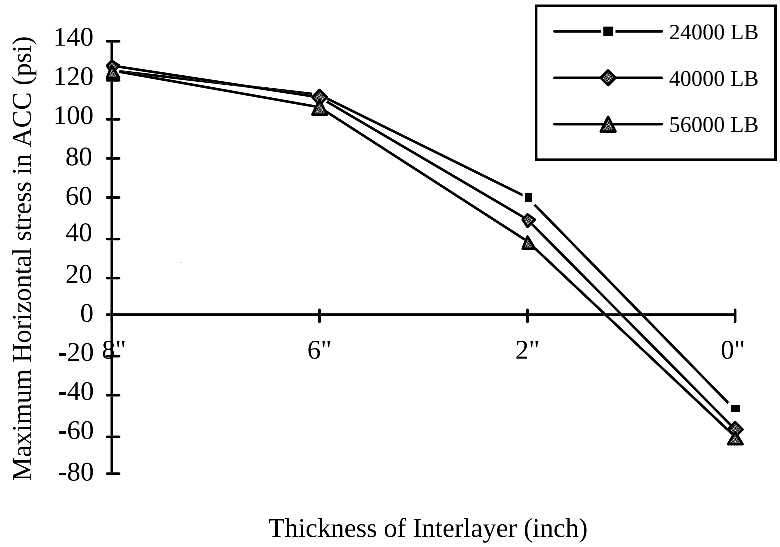

Figure 3.50. The horizontal tensile stress variation by varying the thickness of interlayer (1 lb = 4.45 N, 1 psi = 6.897 kPa)

The effect of stiffness in the interlayer was examined for a 178-kN (40,000-lb) tandem axle loading by varying the thickness of the interlayer; the results are as shown in Table 3.10. The deflection and tensile stress in the PCC layer show little variation when the stiffness of the interlayer is changed; but the tensile stress in the ACC layer is affected by the variation of the interlayer modulus. Figure 3.51 shows how variations in the thickness and the modulus of the interlayer can affect the compressive zone by moving the neutral axis upward. Thus, increasing the stiffness of the interlayer is a potential solution for preventing fatigue failure of the ACC layer.

Table 3.10. The variation of pavement behavior under the variation of thickness and stiffness under 40,000 lb tandem axle traffic load (1 in. = 25.4 mm, 1 psi = 6.897 kPa)

Thickness	stiffness	max. Def.	max. PCC	max. ACC
2"	25000 psi	-0.014812	140.4	48.5
	50000 psi	-1.37E-02	137.6	16.7
	100000 psi	-1.30E-02	133.1	-9.1
6"	25000 psi	-0.019048	110.8	126.2
	50000 psi	-1.49E-02	114.2	58.0
	100000 psi	-1.31E-02	108.9	18.9
8"	25000 psi	-0.017801	117.3	111.3
	50000 psi	-1.54E-02	103.7	66.6
	100000 psi	-1.31E-02	98.0	23.3

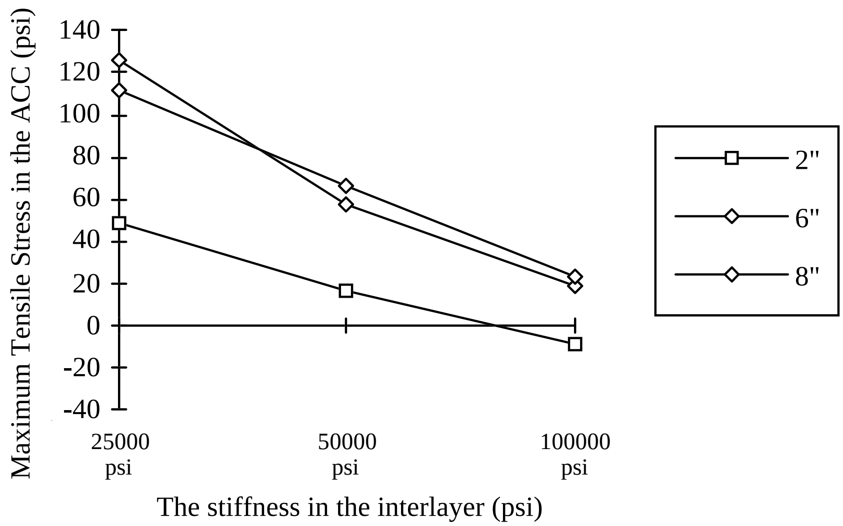

Figure 3.51. The variation of maximum tensile stress in the AC layer by changing the thickness and stiffness under 40,000 lb tandem axle load (1 in.=25.4 mm, 1 psi=6.897 kPa)

Edge and Interior Loading Condition

The tandem axle configuration and corner loading condition are excluded from the analysis because of limitation of computational resources. The pavement structure consists of a 101.6 mm (4 in.) ACP layer, a 203 mm (8 in.) interlayer, and a 203 mm (8 in.) PCC layer, as it is shown in figure 3.52. The edge loading may have both a larger value of deflection and stress, predicted by using plate theory for rigid pavements.

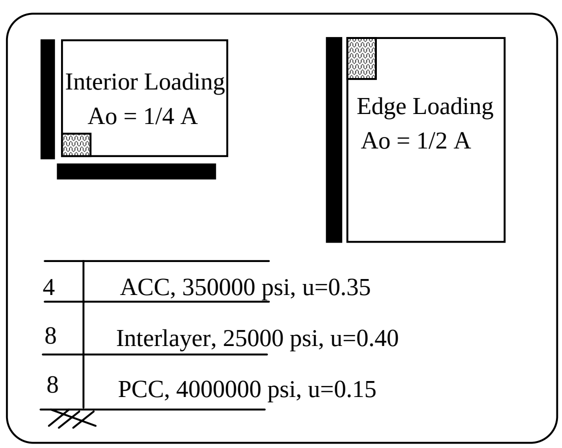

Figure 3.52. Model configuration of interior and edge loading for the mechanistic analysis (1 psi = 6.897 kPa)

The results are presented in Figure 3.53 and in Table 3.11. Both the maximum deflection and tensile stress under edge loading are twice as large as that induced under the interior loading. This analysis shows that the traffic loading position on the overlaid pavement is as important as it is for the rigid pavement, because the AC overlay is fundamentally applied on the discontinued rigid pavement where a joint or crack existed. Edge loading could be an important factor if the pavement has a relatively narrow width and no shoulders.

Table 3.11. Variation of pavement behavior under interior and edge loading

	Maximum Deflection		Tensile stress in PCC Layer	
Loading	Interior	Edge	Interior	Edge
18000	-5.69E-03	-1.43E-02	120.6	245.5
24000	-7.58E-03	-1.91E-02	160.9	327.3
30000	-9.52E-03	-2.40E-02	202.0	410.9
36000	-1.14E-02	-2.86E-02	241.3	491.0
42000	-1.33E-02	-3.34E-02	281.5	572.8

1 lb = 4.45 N

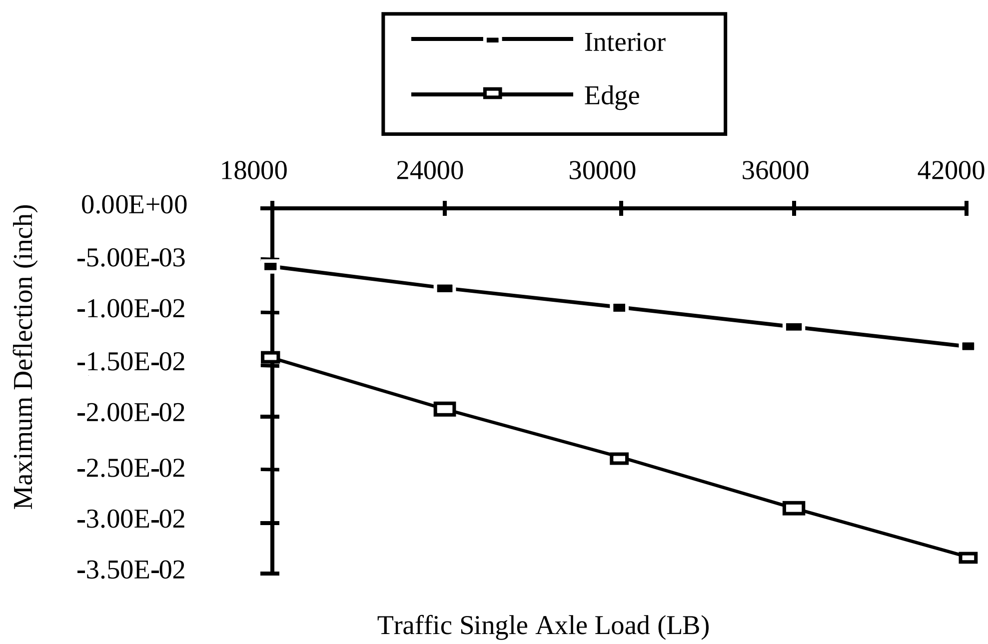

Figure 3.53. Variation of maximum deflection under different loading positions (1 in. = 25.4 mm, 1 lb = 4.45 N)

CHAPTER 4. TEMPERATURE EFFECT ON ASPHALT OVERLAYS ON JCP

We next investigate the effect of temperature on pavement. In this chapter we discuss two models related to thermal stress analysis: a temperature prediction model based on the heat transfer theory, and a thermal stress analysis model for pavement structures. We then correlate our numerical results with field performance data collected from the test sections for Project 987.

THREE COMPONENTS OF THERMAL STRESS

Temperature-induced thermal stresses are known to be one of the primary causes of reflection cracking in ACC overlays. Thermal stresses caused by temperature can be separated into three components (Choubane and Tia 1992): (1) Axial displacement is caused by horizontal movement of the slab owing to the temperature gradient, as shown in Figure 4.1; (2) the bending stress of pavement is induced by the vertical linear temperature differential; and (3) a nonlinear component, generated by the remaining component of temperature, is determined by subtracting the uniform and linear temperature from the total temperature differentials. The existing model for estimating thermal stress considers only warping or horizontal movement components for one-layer systems (Westergaard 1928; Won and McCullough 1991). Therefore, to model the response of a pavement reasonably, additional parameters characterizing pavement structures should be introduced to evaluate thermal stresses in the pavement under field conditions.

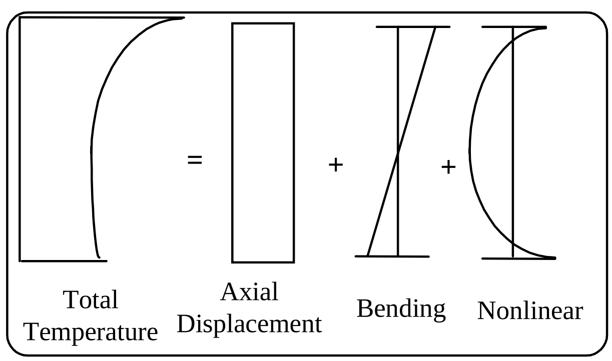

Figure 4.1. Three components of temperature distribution to thermal stress in the pavement

PREDICTION OF TEMPERATURE DISTRIBUTION IN PAVEMENTS

Estimating temperature as a function of depth in pavement structures is important for understanding pavement response. Below, we suggest a simple approach for estimating the pavement temperature as a function of depth using the finite difference method (FDM).

Barber's equation is the first effort to apply a basic heat equation to pavement structures in order to deduce temperature as a function of depth (Barber 1957). The maximum temperature on a pavement surface was assumed to be a function of solar radiation, wind velocity, and surface absorptivity. Instead of the thermal diffusion model, a regression equation was suggested by CTR to predict temperature in the rigid pavement based on the air temperature; this equation was able to predict temperature distributions that matched field observations (Shahin and McCullough 1972). Choubane and Tia suggested a quadratic form function of the thickness of a slab for predicting temperature distribution (Choubane and Tia 1992). Strategic Highway Research Program (SHRP) researchers used total heat energy flow surrounding the pavement structure to find a maximum temperature in the ACC layer (Kennedy and Solaimanian 1993). However, all such approaches have been applied for the temperature at the surface layer and not for a multilayer pavement structure. The ACC overlay on PCC pavement may have a different heat transfer pattern compared with rigid or flexible pavements. Thus, a temperature distribution model based on Barber's equation was developed to estimate maximum temperature in a pavement structure as a function of depth.

Pavement temperature was predicted based on Barber’s equation using mean air temperature and several parameters related to material heat diffusion (Barber 1957). A comparison of mean air temperature and effective temperatures is shown in Figure 4.2.

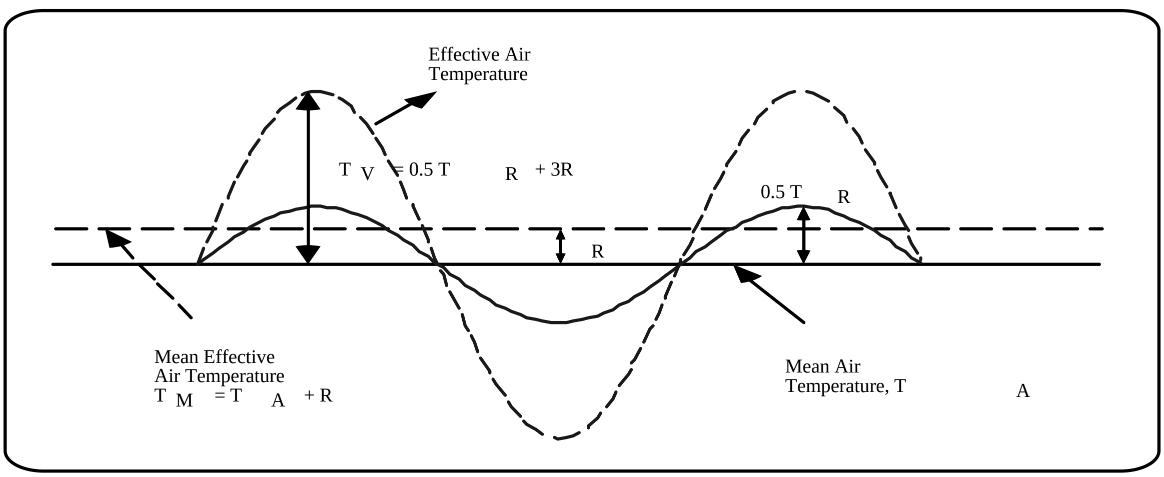

Figure 4.2. Comparison between air temperature and effective air temperature

Based on the differential equation of heat conduction in a homogenous isotropic solid, the following temperature prediction model (as a function of depth) was suggested (Barber 1957):

$$T = T_M + T_V \frac{He^{-xC}}{\sqrt{(H+C)^2 + C^2}} \sin(0.262t - xC - \arctan\frac{C}{C+H}) \tag{4.1}$$

where

T = temperature of mass,
T_M = mean effective air temperature,
T_V = maximum variation in temperature from effective mean,
t = time from beginning of cycle, hours (one cycle = 24 hours),
x = depth below surface, feet,
H = h/k,
h = surface coefficient, BTU per square foot per hour,
k = conductivity, BTU per square foot per hour,
c = diffusivity, square foot per hour = k/sw,
s = specific heat, BTU per pound,
w = density, pounds per cubic foot, and
C = 0.131/c.

The assumption made by Barber can be a problem in that an actual pavement is a multilayer system. Specific physical terms for heat transfer, such as conductivity, specific heat, and absorptivity, are dependent on the material through which the heat radiates. The pavement structure to be considered here is an asphalt overlay on a rigid pavement. It basically consists of a soil layer, a concrete layer, and an asphalt or an asphalt plus a flexible base layer. Thus, the following model is suggested to identify the temperature distribution in actual field situations.

Heat Transfer Model

Thermal conductivity relates to a material's capacity for transferring heat. Specific heat is the amount of heat required for a unit mass of material to increase its temperature by 1 degree. Then, diffusivity is defined by the ratio of conductivity and a value that is a multiple of density and specific heat. Thus, the basic equation of heat conduction in a homogenous isotropic is:

$$\frac{\partial T}{\partial t} = c\left(\frac{\partial^2 T}{\partial x^2} + \frac{\partial^2 T}{\partial y^2} + \frac{\partial^2 T}{\partial z^2}\right) \tag{4.2}$$

where

T = temperature of mass as a function of t, x, y, and z,
t = time,
x, y, z = directions in rectangular coordinate, and
c = diffusivity.

When the heat flow is assumed to be one dimensional, i.e., the temperature is a function of time *t* and space *x* only, equation (4.2) can be abbreviated:

$$\frac{\partial T}{\partial t} = c\left(\frac{\partial^2 T}{\partial x^2}\right) \tag{4.3}$$

The initial condition that time is equal to zero is assumed to follow the same temperature distribution of Barber's equation. Thus:

$$T_i^1 = T_M + T_V \frac{He^{-xC}}{\sqrt{(H+C)^2 + C^2}} \sin\left(-xC - \arctan\frac{C}{C+H}\right) \tag{4.4}$$

The boundary conditions of the governing partial differential equation are at three different positions in our pavement structure of interest. The surface of the pavement temperature is assumed to follow the same distribution of Barber's solution. When the heat is transferred to another medium, the energy loss is assumed to be negligible. In micro-mechanistic approaches, there may exist a loss of energy such that the heat distribution might differ. At the bottom of the pavement structure, it was assumed that the heat flow would be beyond a certain depth of the pavement; the depth here is assumed to be 1.82 m (6 ft).

Top layer boundary condition:

$$T_1^j = T_M + T_V \frac{H}{\sqrt{(H+C)^2 + C^2}} \sin\left(0.262t - \arctan\frac{C}{C+H}\right) \tag{4.5}$$

Intermediate condition between asphalt and concrete, concrete and soil:

$$T_{Tac}^j \rightarrow k_a \frac{\partial T}{\partial x} = k_b \frac{\partial T}{\partial x} \tag{4.6}$$

$$T_{Tpcc}^j \rightarrow k_b \frac{\partial T}{\partial x} = k_c \frac{\partial T}{\partial x} \tag{4.7}$$

where

K_a = conductivity of asphalt layer,

K_b = conductivity of concrete layer, and

K_c = conductivity of soil.

Bottom boundary:

$$T^{j}_{Tfin} \rightarrow \quad k_c \frac{\partial T}{\partial x} = 0 \tag{4.8}$$

The finite difference method (FDM) is employed to solve this boundary value problem. The FDM uses approximately differential increments in the temperature and space coordinator. Generally, the smaller the increment, the better the solution. The Crank-Nicolson method adopts the midpoint of time increments for difference approximation; and the second derivative of space can be represented as:

$$\frac{\partial^2 T}{\partial x^2} = \frac{1}{2}\left(\frac{T^{l}_{i+1} - 2T^{l}_{i} + T^{l}_{i-1}}{\Delta x^2} + \frac{T^{l+1}_{i+1} - 2T^{l+1}_{i} + T^{l+1}_{i-1}}{\Delta x^2}\right) \tag{4.9}$$

Because the Crank-Nicolson method is considered to have many advantages compared with other methods, it is employed to solve PDEs (3) and (4). The mathematical expression for generating a mesh (along with its FORTRAN program and output) is attached as Appendix A and B.

Calibration of Temperature Prediction Model

Pavement geometry and material properties, including unit weight (w), conductivity (k), and specific heat(s), are given in Figure 4.3. The pavement structure consists of a 30.04-m (10-in.) ACC and a 22.86-m (9-in.) PCC layer. The material properties of the ACC, as well as those of the PCC, are assumed to be the same as those used by Barber (1957). The possible magnitude of solar radiation is assumed to be 650 langleys per day for the summer and 250 langleys per day for the winter; the wind speed is set at 24.15 km (15 mph) for winter and 12.88 km (8 mph) for summer; the absorptivity of surface to solar radiation for black asphalt is known to be 0.95. Mean air temperature and range of maximum and minimum daily temperatures in the test sections are shown in Table 4.1.

Table 4.1. Weather information at the test section in Lufkin, Texas, in 1993

Date	*July 25, 1993*	*December 24, 1993*
Mean Air Temperature, °F	91.0°F	46.0°F
Air Temperature Range, °F	38.0°F (74-112°F)	32.0°F (32-64°F)
Mean Wind Speed (mph)	8.0	15.0
Solar Radiation (Langleys/Day)	650	250

°F= 9/5 °C+32

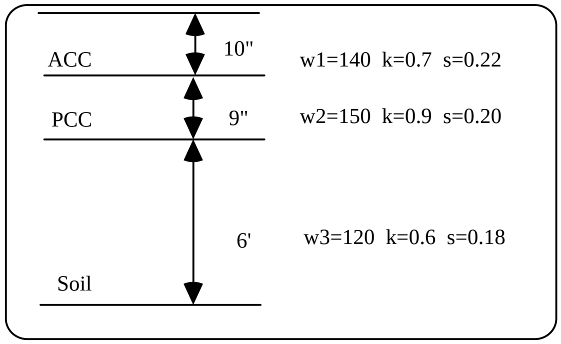

Figure 4.3. Geometry and material characteristics of example problem (1 in. 25.4 mm)

As shown in Figure 4.4, the purely theoretical result indicates that there is a large fluctuation in the amplitudes of temperature for both winter and summer. The measured maximum temperature on the site ranges from about 32.3°C (90°F) to 48.9°C (120°F), while 21.1°C (70°F) to 60°C (140°F) is estimated from the model for summer. This may be introduced by having a strong solar radiation contribution in Barber's equation. The solar radiation effect can be reduced based on previous research performed at CTR (Shahin and McCullough 1972). This requires a calibration process, such that the average contribution of the solar radiation to the effective air temperature (R) is reduced:

$$T_V = 0.5 * T_R + a R$$

where

a = constant to be calibrated. (a,=0,1,2,3)

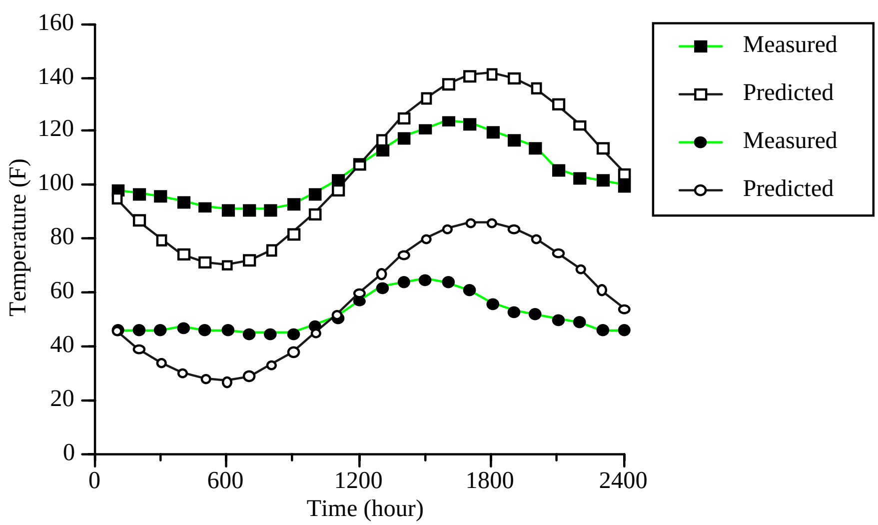

°F= 9/5 °C+32

Figure 4.4. Large difference between estimated and predicted temperature in the test section

As shown in Figure 4.5 and Figure 4.6, the coefficient for average contribution of the solar radiation to the effective air temperature (R) can range from 0 to 1; and it is zero in winter and 1 in summer. Choosing a coefficient a = 1 implies a more conservative approach for the minimum and maximum temperature prediction for both seasons; this approach can be used if an engineer does not know the temperature range.

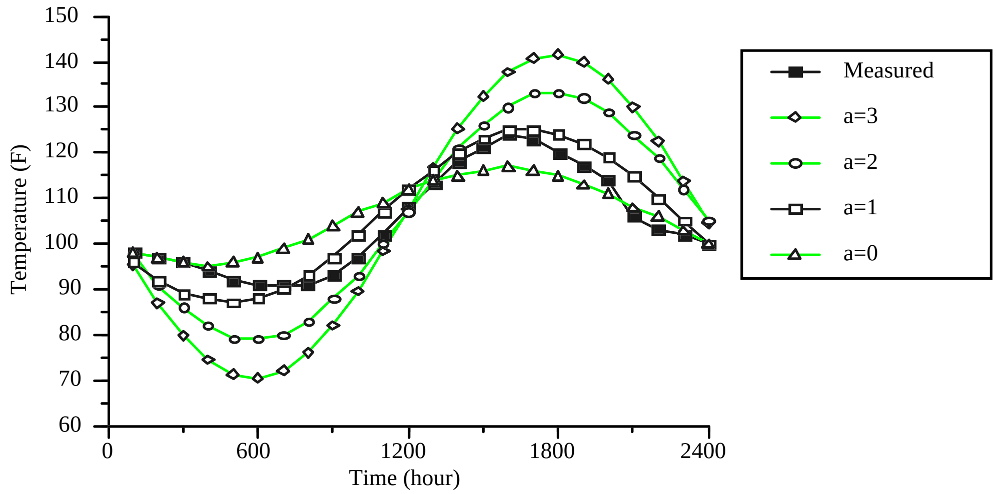

°F= 9/5°C+32

Figure 4.5. Calibration by the coefficient (a) of average contribution of the solar radiation to the effective air temperature (R) for summer condition

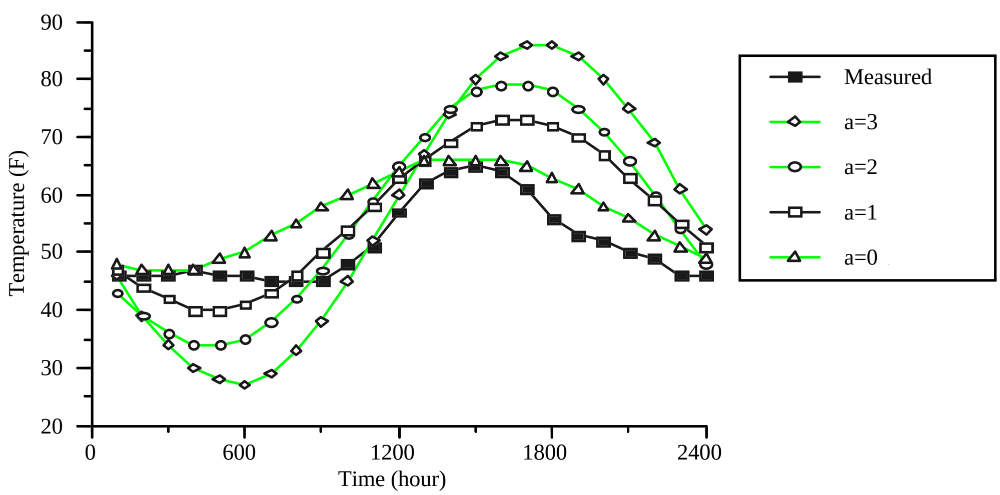

°F= 9/5 °C+32

Figure 4.6. Calibration by the coefficient (a) of average contribution of the solar radiation to the effective air temperature (R) for winter condition

Temperature Distribution in ACC and PCC Layer

The calibrated-model-generated temperature distributions shown in Figure 4.7 are based on weather information for December 23, 1993. The maximum surface temperature varied from 6.1C (43°F) to 20°C (68°F), while the temperature in the PCC layer ranged between 10°C (50°F) and 15.6°C (60°F). The temperature in the soil layer did not vary as much as did the temperature in the two upper layers. Unlike the ACC layer, the temperature variation in the PCC layer does not much fluctuate. Figure 4.8 shows the temperature variation at various depths and time (hours). The temperature variation at a layer near the surface clearly follows a sinusoidal function in time, though the soil layer responds differently.

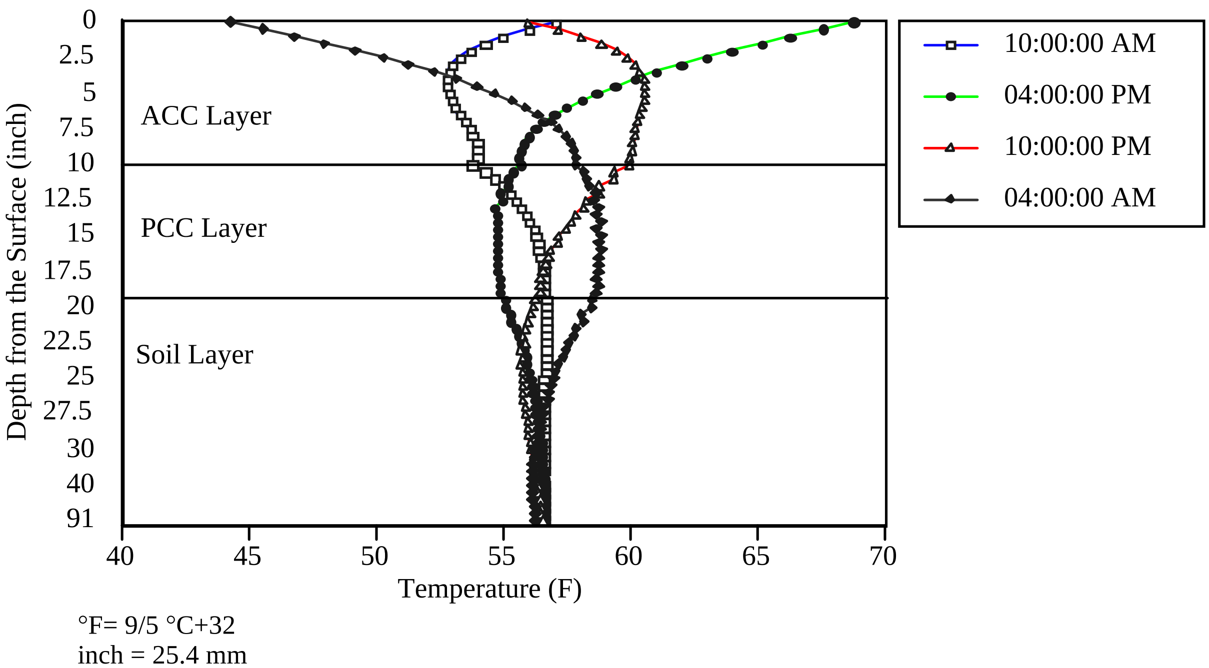

Figure 4.7. Generated temperature distribution by depth in composite pavement structure in winter

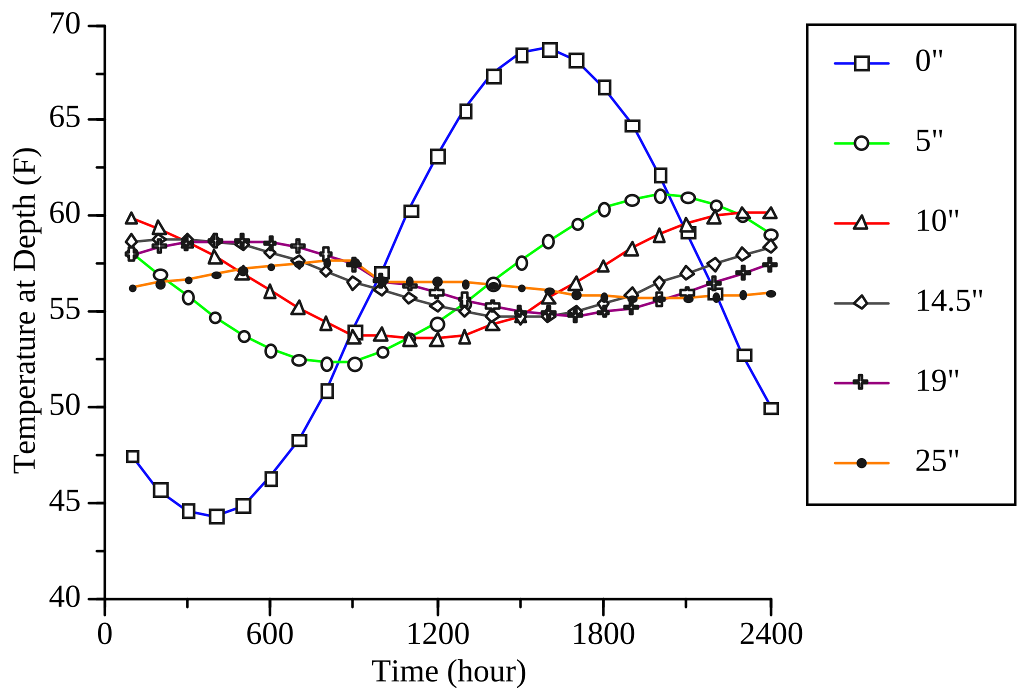

°F= 9/5 °C+32

Figure 4.8. Temperature distribution by time in composite pavement structure in winter

Temperature Distribution in Pavements with a Flexible Interlayer

The temperature was also predicted for the flexible interlayer section with a type of pavement similar to the one constructed in test section R3, which is also the main pavement structure for the mechanistic analysis under traffic loading presented in previous CTR reports (987-3 and 987-4). The geometry of the pavement structure consists of a 76.2-mm (3-in.) ACC layer, a 203.2-mm (8-in.) flexible layer, and a 203.2-mm (8-in.) PCC layer. The material properties for the flexible base layer are approximately the same as those of the soil. Figure 4.9 shows the estimated temperature distribution in a pavement having a flexible interlayer. During the winter, the surface temperature on the ACC layer ranges from 6.1°C (43°F) to 20°C (68°F). Owing to a thin ACC layer and a thick flexible base layer, the PCC layer had a temperature that fell into a wider range, from 8.9°C (48°F) to 18.3°C (65°F). Considering daily air temperature variations of 17.8°C (32°F), the temperature variation in the PCC layer is roughly one-half of the air temperature variation; but the variation in the ACC layer is about the same as that of the air temperature. The lowest temperature in the subgrade layer is found to be above 10°C (50°F), indicating that freeze/thaw is not a problem with this type of pavement.

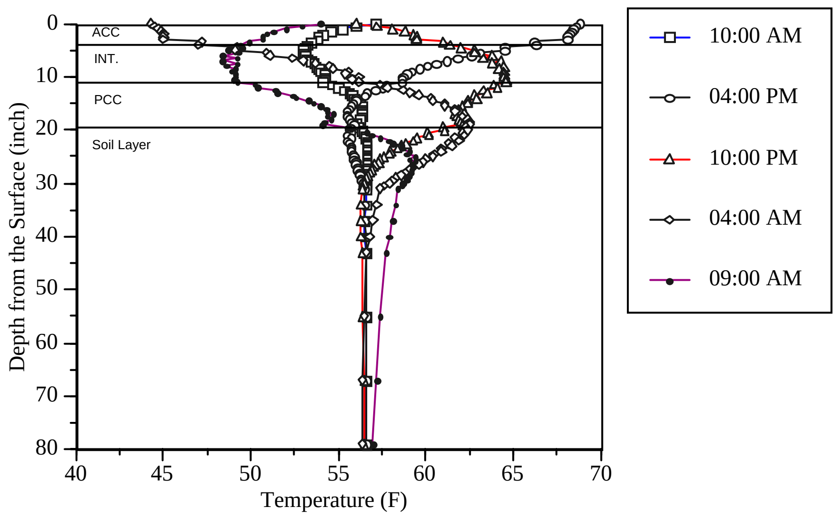

°F= 9/5 °C+32
inch = 25.4 mm

Figure 4.9. Temperature distribution by depth with flexible base in winter

The temperature distribution in the summer estimated by the model is presented in Figure 4.10. The temperature on the surface of the ACC layer goes up to 54.4°C (130°F), and the temperature in the PCC layer reached 48.9°C (120°F) at 4 p.m. The maximum air temperature recorded was 44.5°C (112°F). The high temperatures in the ACC layer reduce its stiffness, which might cause rutting in the ACC layer and in the subgrade layer in summer.

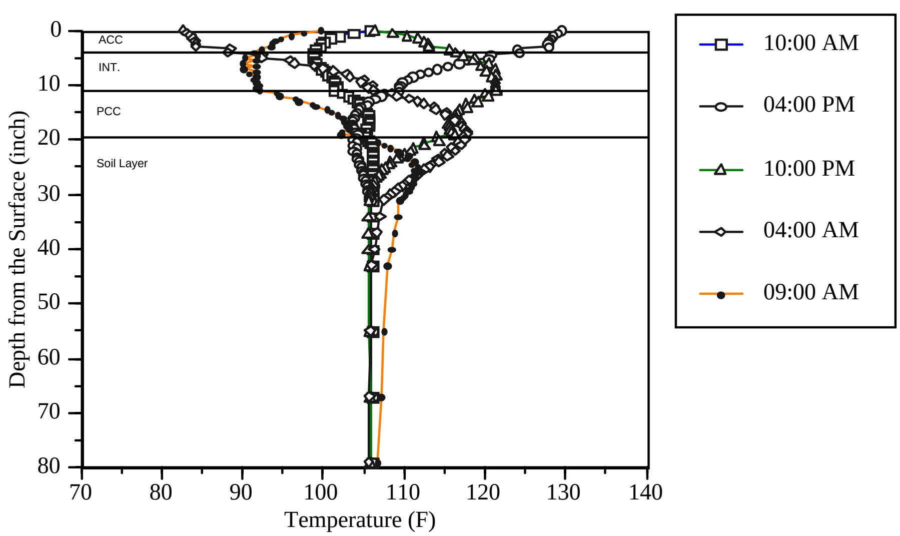

°F= 9/5 °C+32, inch = 25.4 mm

Figure 4.10. Temperature distribution by depth with flexible base in summer

In summary, the temperature prediction model was developed using a heat diffusion model. Once it was calibrated using the field measurements, the modified model generated a reasonable temperature distribution. Thus, this temperature prediction model can provide a pavement engineer with more accurate information relating to thermal stress and traffic-induced stresses in the summer as well as in the winter.

DEVELOPMENT OF A MECHANISTIC MODEL

After estimating temperature distributions in the pavement structure, the theoretical model to predict thermal stresses in the pavement structure was developed using the FEM. The model geometry, material properties, and its results are described below.

Model Geometry and Boundary Conditions

The two types of FEM used previously in this report considered (1) only warping stress in multilayer pavements caused by a linear temperature differential and (2) the frictional force between the PCC and subgrade caused by thermal movement. Because the length of a JCP slab is relatively short (e.g., 4.56–9.12 m, or 15–30 ft), the stress of frictional forces generated by horizontal movement was excluded from the analysis based on previous research that determined that shorter slabs were strongly related with warping and that longer slabs are more closely related to horizontal movement (Yoder and Witczak 1975). The friction force is included for comparison purposes only. As shown in Figure 4.9, the actual temperature distribution in the pavement structure is nonlinear as a function of depth. However, it can be approximated by a linear function. Maximum temperature differential is defined by the maximum temperature difference between the top of the ACC layer and the bottom of the PCC layer. Thus, the linear temperature distribution assumption is used for the sensitivity analysis as well as for the mechanistic design.

Model geometry and assumptions are shown in Figure 4.11. The type of pavement considered is the same as that used for the traffic loading analysis discussed previously. The basic pavement structure consists of a 76.2-mm (3-in.) ACC layer, a 203-mm (8-in.) flexible layer, and a 203-mm (8-in.) PCC layer. The soil layer is initially modeled by a linear spring element and then replaced by nontensional spring elements. The pavement is assumed to have no movement horizontally in the center of the composite slab, primarily because the existing JCP is separated by a discontinuity (i.e., a joint or crack). No restraint is applied in the end of the PCC slab. The ACC and flexible interlayer are horizontally constrained by the layer itself because it is assumed that there are no cracks present.

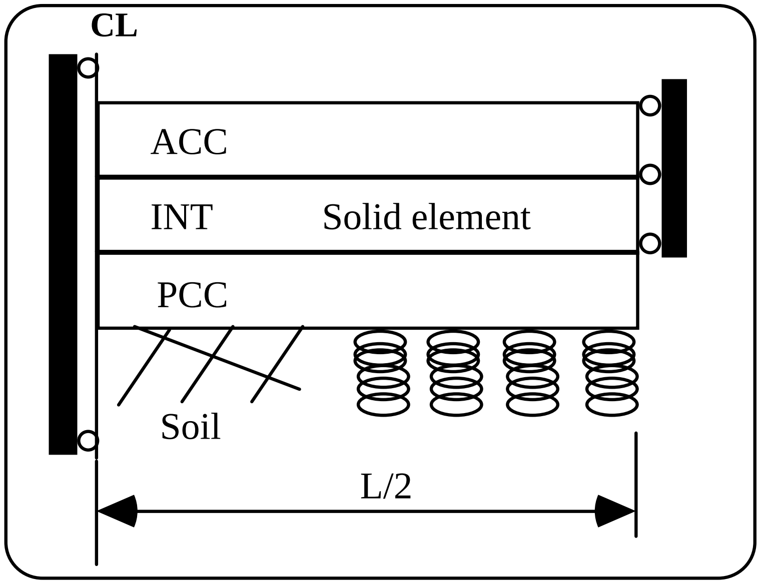

Figure 4.11. Basic FEM of asphalt overlay on the PCC

Material Properties

The material properties for the quasi-linear elastic analysis of the traffic loading were provided in Chapter 3. For the thermal stress analysis, the stiffness of the ACC is estimated to be 6,894 MPa (1,000 ksi), the interlayer is 172.4 MPa (25 ksi), and the PCC is 27,576 MPa (4,000 ksi). The subgrade reaction of the soil layer is estimated to be 21,305,900 kg/m^3 (770 pci) for Winkler's foundation model. The stiffness of the ACC is given a somewhat higher value because of the high stiffness at low temperature in winter.

The thermal coefficient of PCC is related to the coarse aggregate mixed in the concrete, given that the aggregate consists of about 75% of the total volume. The thermal coefficient of the aggregate has been known to have an almost linear relationship with the PCC thermal coefficient. For example, the coefficient of limestone-based concrete is less than that of siliceous river gravel . The aggregate effect on the coefficient ranged from 4.84 micro inch/inch/°F to 8.18 micro inch/inch/°F, depending on the aggregate used. The silica content of the aggregate is also found to have a strong effect on the coefficient of the PCC and can be predicted by this portion of chemical elements in the aggregate (Dossey and McCullough 1993). The thermal coefficient is known to be affected by the curing of concrete. Generally, air-cured concrete has a thermal coefficient larger than that for wet-cured concrete (Nevile 1981). Table 4.2 summarizes the thermal coefficients for PCCs having a typical aggregate type and curing method.

Table 4.2. Thermal coefficient of PCC as a function of aggregate and curing method (in./in./°F, Nevile 1981)

Aggregate	Air cured	Water cured	Air cured and wetted
Gravel	$7.3*10^{-6}$	$6.8*10^{-6}$	$6.5*10^{-6}$
Limestone	$4.1*10^{-6}$	$3.4*10^{-6}$	$3.3*10^{-6}$

in./in./°F= 9/5 * mm/mm/°C

The thermal coefficient of the ACC has been shown to have generally a higher value than that of PCC, even though the aggregate has almost the same portion of volume in the ACC; this is explained by the heat conductivity of the AC binder. For example, the Texas asphalt overlay design method suggests using 14.0 micro inch/inch/°F (Diaz et al. 1983). A recently completed SHRP project that collected ACC samples nationwide had the distribution shown in Figure 4.12.

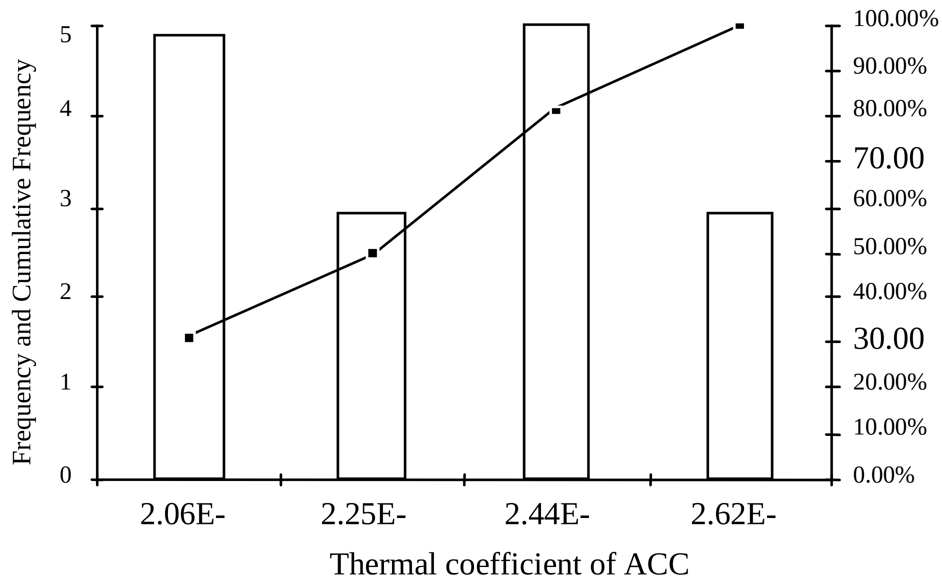

Figure 4.12. Distribution of thermal coefficient (m/m/°C) of ACC layer

As shown in Figure 4.12, ACC has a mean of 2.39E-05 mm/mm/°C (4.302 E-05 inch/inch/°F) and a 10% coefficient variation. The overall variation of coefficient in the ACC is lower than that of PCC.

The thermal coefficient of the flexible base is difficult to define since the size distribution and voids between aggregate particles make it difficult to estimate the coefficient of the layer. The thermal coefficient of the aggregate is investigated, but the coefficient of the flexible layer may not be the same as that of the aggregate itself. Considering the low stiffness and the relatively larger volume of air and soil, the thermal coefficient of the flexible layer may be negligible.

Based on literature reviews, the thermal coefficient of the ACC is initially fixed as $7.76 * 10^{-6}$ mm/mm/°C ($14 * 10^{-6}$ inch/inch/°F); the interlayer is at $3.3 * 10^{-7}$ mm/mm/°C ($6 * 10^{-7}$ in./in./°F), and the PCC layer is at $3.3 * 10^{-6}$ mm/mm/°C ($6 * 10^{-6}$ in./in./°F).

The mechanistic FE model considered in this study may not be as exact as classical mechanistic theory. Yet it is introduced to determine what factors significantly contribute to the development of reflection cracking. It is also applied to explain the observed performance of the test sections constructed on US 59 (Cho and McCullough 1994). Thus, an absolute value for stress and deflection cannot be calibrated from the following analysis for the actual pavement. Also, it may be impossible to estimate actual stress conditions because of the complexity of thermal stress analysis in the overlaid pavement. However, a trend identified by the FEM model can be applied for practical situations.

Thermal Stresses Owing to Warping Force on Winkler's Foundation

The basic pavement structure, as represented by Winkler's foundation, has an existing JCP layer, a flexible interlayer, and an ACC surface layer. The temperature differential is initially assumed as 16.7°C (30°F) through the depth, which may be larger than the differences measured in the field.

Figure 4.13 shows a different vertical displacement along the slab. In the figure, the "Temp1" condition is the night condition, when temperatures are low on the surface and high at the bottom of the JCP layer. The "Temp2" condition refers to the opposite distribution of temperature, such as high temperature on the surface and low temperatures at the bottom of the pavement. The warping forces caused by these temperature differentials cause the pavement structure to curl up and down. The nighttime temperature causes the pavement structure to curl up, while the daytime temperature yields the opposite trend for the deflection. The modeling also shows that the maximum deflection is a function of joint spacing. About 0.075 mm (3 mil) of deflection is observed for the shorter slab (3.04 m [10 ft] joint spacing), while twice the deflection is shown in the longer slab (6.08 m [20 ft] joint spacing). In addition, the short slab experiences monotonically increasing deflections, while the longer slab has a point of inflection that changes the slope of deflection along the surface.

Horizontal stress distribution in the center of the pavement as a function of depth is shown in Figure 4.14 for a pavement having 3.05-m (10-ft) joint spacing. In one case, here defined by Temp2, there is no tensile stress in the ACC layer, while in the other case, there is only tensile stress. This means the maximum tensile stress of the ACC layer occurs on the surface of the ACC layer at night. We also found that a 16.7°C (30°F) temperature differential led to higher tensile stress, about 2.275 MPa (330 psi), on the ACC layer. The high stress in the surface of the ACC layer may have been caused by the high stiffness of the ACC layer, 6,894 MPa (1,000 ksi), representing the ACC stiffness in winter. The results above indicate that the reflection cracking in the ACC layer may develop during winter nights.

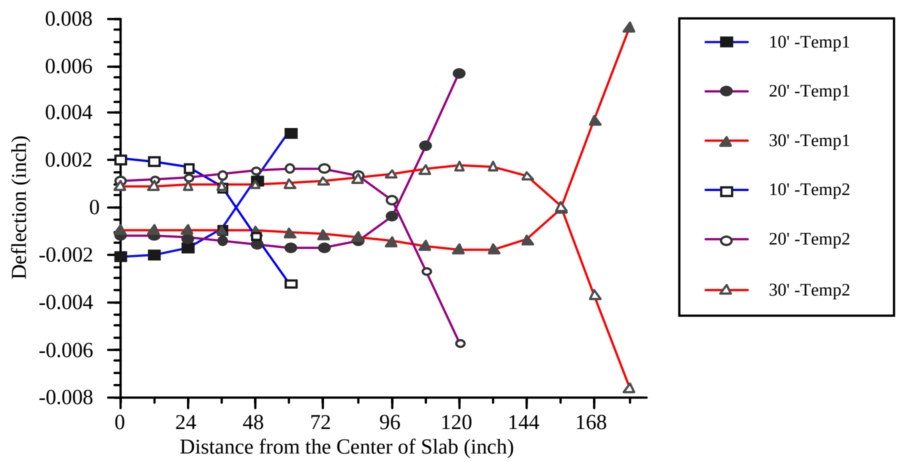

inch = 25.4 mm

Figure 4.13. Deflection variation by the warping force under two distinct temperature distributions

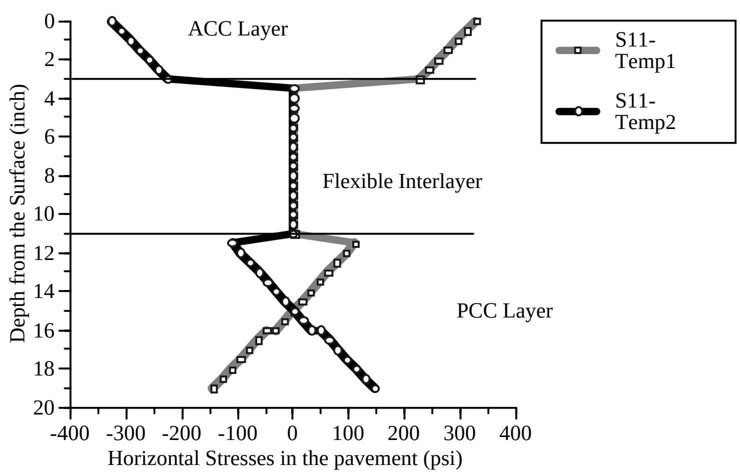

inch = 25.4 mm, psi = 6.897 kPa

Figure 4.14. Horizontal stresses distribution under different temperature distribution — 3.04 m (10 ft) joint spacing

The extreme values of horizontal stresses in the pavement as a function of slab length are shown in Table 4.13. The extreme stresses in the ACC layer occur at the discontinuity (i.e., at a crack or joint). Tensile stress on the PCC layer decreases as the slab length increases. As the length of the slab grows, the movement of the neutral axis in the slab decreases tensile stresses but increases the compressive stress within the PCC. However, the tensile stress in the PCC layer increases during the day as joint spacing or slab length increases.

Table 4.3. Horizontal stress distribution by warping force with slab length

Slab Length	*Extreme Value*	*Temp1*		*Temp2*	
		AC	*PCC*	*AC*	*PCC*
10 inch slab	Maximum	327.3	110.3	-155.6	144.8
	Minimum	226.5	-144.8	-388.3	-110.3
20 inch slab	Maximum	354.2	94.8	-82.5	215.9
	Minimum	248.6	-202.3	-389.8	-96.2
30 inch slab	Maximum	364.6	59.7	-15.3	301.9
	Minimum	260.1	-225.7	-381.6	-74.4

inch = 25.4 mm
psi = 6.897 kPa

However, for the ACC layer, nighttime temperature is critical in areas above joints or cracks on the PCC layer. No tensile stress is observed during the day. Considering the tensile stress in ACC layer only, the slab length, which is a function of joint spacing, does not much affect the stress in the ACC layer. In summary, the ACC layer experiences tension or compression only as a result of warping force. However, the tensile stress in the PCC layer is strongly related to the slab length. In designing the ACC layer, one must consider the critical nighttime temperature distribution.

Comparison of Winkler's Foundation and Solid Foundation

This section compares Winkler's foundation and a continuous, solid-element foundation. The stiffness of the soil layer is assumed to be 21,305,900 kg/m^3 (770 pci) for Winkler's foundation, and 103.4 MPa (15,000 psi) of resilient modulus for the solid foundation based on the AASHTO *Design Guide* (AASHTO 1986). The continuous, solid-element foundation depth was fixed at 2.4 m (8 ft).

The temperature differentials induced more deflections in the spring foundation than in the solid foundation model, as shown in Figure 4.15. The solid-element model shows less than 0.025 mm (1 mil) of deflection, while the spring element shows about 0.2 mm (8 mil) of deflection. This may mean that the formula given by the AASHTO guide to relate resilient modulus and soil subgrade reaction, the so-called *K* value, is not accurate for thermal loading (as is the case with traffic). However, *both* models may fail to show precise (field) pavement response because the predictions obtained from the two do not agree. The correct answer lies somewhere between the two predictions.

The extreme horizontal stresses exerted in both the ACC and PCC layers are shown in Table 4.4. The solid-element model results in compression in the PCC and tension in the ACC for the given temperature loading condition. The spring foundation results in larger tensile stresses in the ACC as well as in the PCC layer. The maximum tensile stress in the ACC layer for the solid foundation model yields one-third the tensile stress given by Winkler's foundation. These results suggest that thermal stresses are strongly dependent on the foundation modeling and that direct comparisons between the spring element and the solid element cannot be performed without field verification. Therefore, all sensitivity analyses hereafter will be based on Winkler's foundation model, since it is simple and widely used in rigid pavement design.

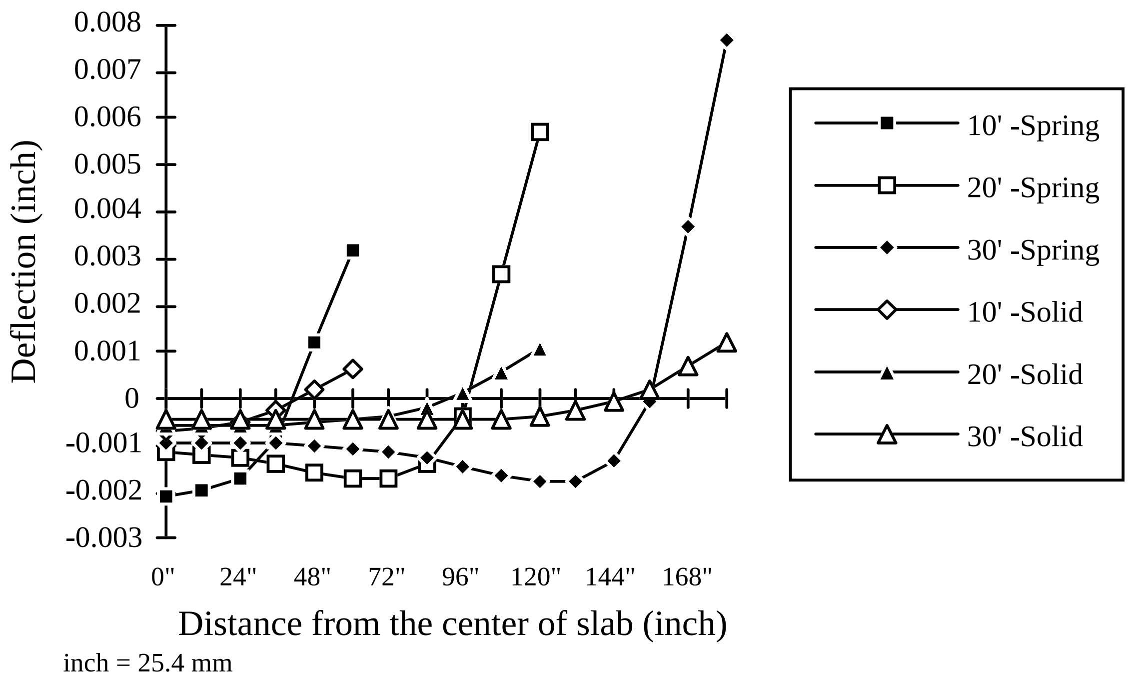

Figure 4.15. Deflection variation in the pavement structure by different foundation models

Table 4.4. Different maximum horizontal stresses caused by different foundation models (unit=psi)

Slab length		*Solid element*		*Spring element*	
		ACC	*PCC*	*ACC*	*PCC*
10 ft slab	Maximum	114.1	-27.8	327.3	110.3
	Minimum	81.5	-341.9	226.5	-144.8
20 ft slab	Maximum	115.9	-50.1	354.2	94.8
	Minimum	82.6	-382.6	248.6	-202.3
30 ft slab	Maximum	115.8	-61.8	364.6	59.7
	Minimum	82.4	-395.9	260.1	-225.7

inch = 25.4 mm, psi = 6.897 kPa

Gravity Force Effect

The classical Westergaard solution for the rigid pavement under traffic or thermal loading did not include gravity force in its closed-form solutions. Dead load induced by gravity force may change pavement behavior subjected to warping force. As shown in Figure 4.16, the deflection of a slab with/without gravity force differs slightly. The dead load acts against the curve so that the deflection basin with dead load tends to move downward; its effect can, however, be negligible in short slabs. The extreme horizontal stress values shown in Table 4.4 indicate that stress on all layers increases slightly when considering uniform load by gravity force in the analysis. For example, the stress in the ACC layer with gravity force is changed about 10%. The overall uniform load in the ACC layer become active as the slab become longer. The gravity force effect is also related to slab length, such that tensile stress in the PCC layer does not change at all in the shorter slab, while the longer slab experiences higher stresses when considering the gravity force. With the opposite temperature distribution (which causes the pavement to curl down), the gravity force effect on the deflection is clear. The maximum deflection is increased, as shown in Figure 4.17. About 1 mil of difference of deflection is observed between the two cases without changing the shape of deflection. However, it results in almost the same extreme value of horizontal stresses in both layers (unlike its behavior at nighttime), as shown in Table 4.5.

In summary, the gravity force can affect pavement behavior when a nighttime temperature distribution in the pavement is in effect. This effect is not as significant during the day as it is at night.

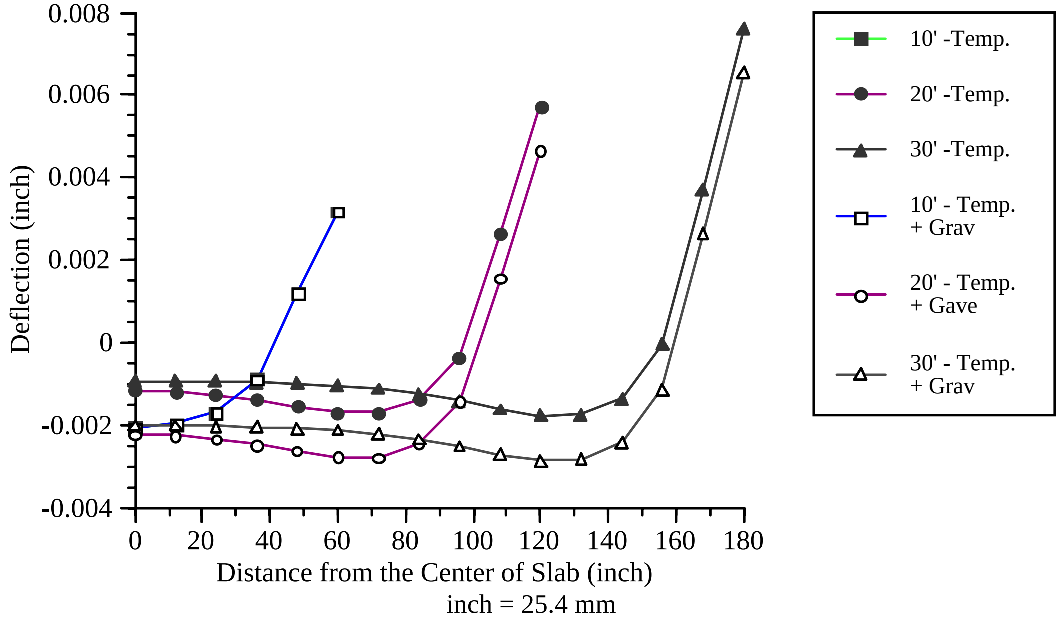

Figure 4.16. Weight effect of deflection under nighttime temperature

Table 4.5. Extreme values of horizontal stress distribution by including gravity force at nighttime (unit = psi)

	Tensile stress	*10 ft slab*		*20 ft slab*		*30 ft slab*	
		Max.	*Min.*	*Max.*	*Min.*	*Max.*	*Min.*
Temp.	AC	327.3	226.5	354.2	248.6	364.6	260.1
Temp. + Grav.	AC	388.3	155.6	389.9	82.25	381.8	15.0
Temp.	PCC	110.3	-144.8	94.8	-202.3	59.7	-225.7
Temp. + Grav.	PCC	110.3	-144.8	96.2	-215.6	74.5	-301.7

inch = 25.4 mm, foot = 0.304 mm, psi = 6.897 kPa

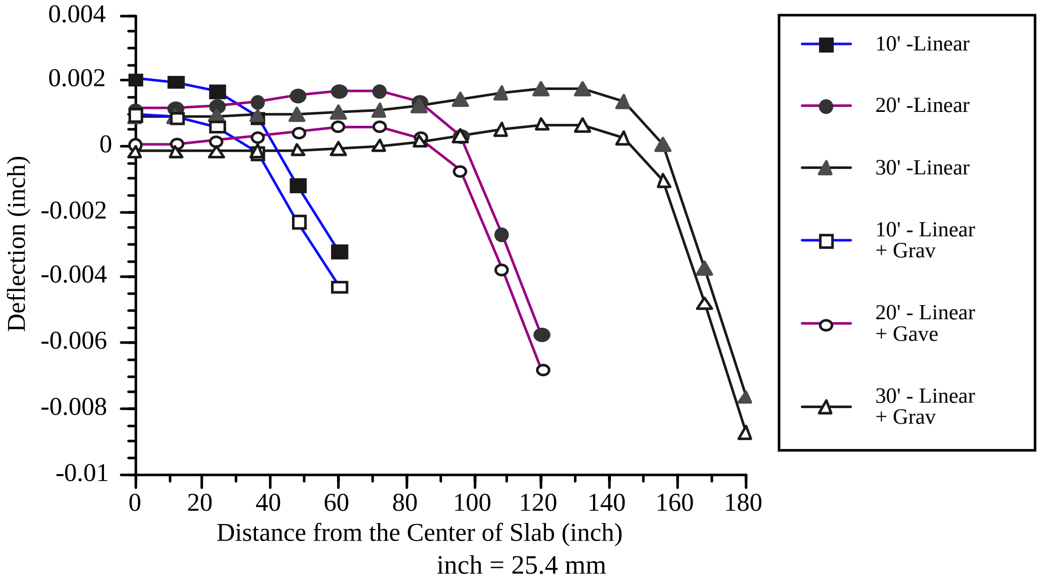

Figure 4.17. Weight effect of deflection under daytime temperature

Table 4.6. Extreme values of horizontal stress distribution by including gravity force under daytime (unit = psi)

	Tensile stress	*10 ft slab*		*20 ft slab*		*30 ft slab*	
		Max.	*Min.*	*Max.*	*Min.*	*Max.*	*Min.*
Temp.	AC	-155.6	-388.3	-82.53	-389.8	-15.31	-381.6
Temp. + Grav.	AC	-155.8	-388.2	-82.8	-389.6	-15.64	-381.5
Temp.	PCC	144.8	-110.3	215.9	-96.21	301.9	-74.42
Temp. + Grav.	PCC	143.7	-109.9	216.2	-96.23	302.1	-74.4

inch = 25.4 mm, foot = 0.304 m, psi = 6.897 kPa

NONLINEAR SPRING EFFECT

The soil layer without tensile stiffness can be incorporated into the FEM model using the nonlinear spring element. Comparisons of the deflection in linear (LS) and nonlinear (NLS) spring elements are shown in Figure 4.18. The deflection shape in the two cases is not affected, but maximum deflection of the nonlinear spring is increased for the long joint spacing. It may be reasonable to expect larger deflections at the end of the slab because of nontensile resistance in the spring.

The extreme value of the horizontal stress in each layer is shown in Table 4.7. Larger differences in horizontal stresses between linear and nonlinear springs were observed in the longer slab. The nonlinear spring has about 0.5 MPa (70 psi) in tensile stresses in the ACC layer — more than those from Winkler's foundation. The tensile stress of the ACC layer also increased as the slab length became longer in the nonlinear spring foundation. The PCC layer also experiences distinct tensile stresses for the two different foundations, though it is hard to define the special relationship between them.

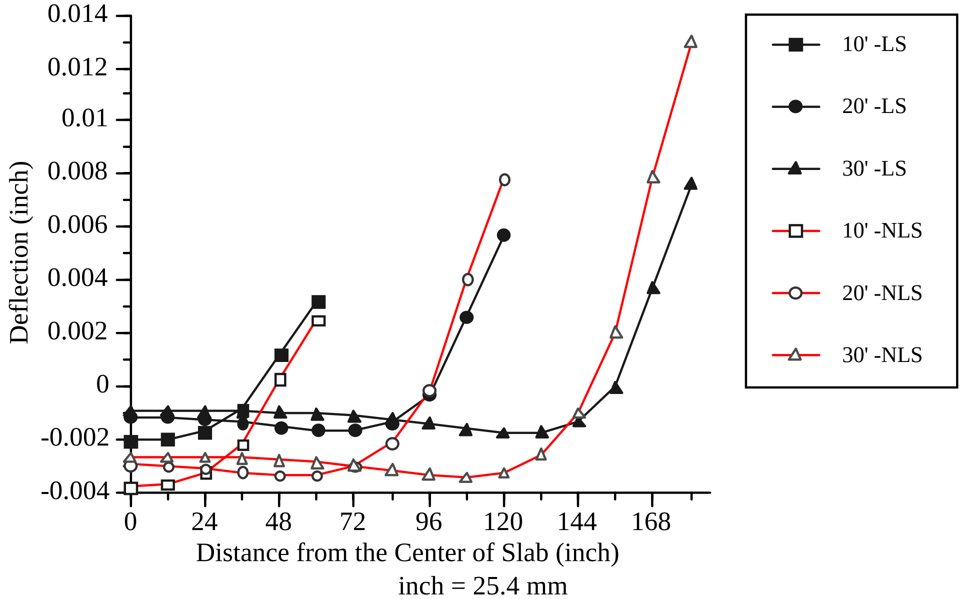

Figure 4.18. Nonlinear spring of deflection by nighttime temperature

In summary, a larger difference of horizontal stress between Winkler’s foundation model and a nonlinear spring model is observed in the ACC layer. As joint spacing increases, the stress in both layers changes slightly.

Table 4.7. Extreme values of horizontal stress distribution by nonlinear spring elements (unit = psi)

	10 ft slab		*20 ft slab*		*30 ft slab*	
	Maximum	*Minimum*	*Maximum*	*Minimum*	*Maximum*	*Minimum*
LS-AC	327.3	226.5	354.2	248.6	364.6	260.1
LS-PCC	110.3	-144.8	94.7	-202.3	59.65	-225.7
NLS-AC	397.3	152.8	420.2	75.6	433.5	2.7
NLS-PCC	102.5	-133.4	102.6	-199.9	78.75	-279.6

inch = 25.4 mm, foot = 0.304 m, psi = 6.897 kPa, LS: Linear spring; NLS: Nonlinear spring

On the basis of the above initial stage of our mechanical analysis, the asphalt overlay pavement structure was modeled as a nonlinear spring element having three layers in order to determine the most significant factor from all possible factors in the field. When calibrated by using field data, the models developed can also serve as a tool to select design thickness.

SENSITIVITY ANALYSIS

This section discusses the sensitivity of pavement response to changes of thickness and stiffness for all layers under thermal loadings. These results provide valuable information regarding test section performance and support design approaches for this type of overlay structure.

Basic Pavement Behavior

For the sensitivity analysis, thermal loading is considered the maximum temperature difference in the pavement structure with linear variation as a function of depth, which is generally chosen for the thermal stress analysis. The maximum thermal stress on both the ACC and PCC layers are compared, along with the deflection basins. The slab having a joint spacing of 4.56 m (15 ft) is selected as the basic pavement for the sensitivity analyses. The pavement behavior in two different temperature cases for two different foundations (linear and nonlinear spring foundations) is considered. The basic stiffness of the soil foundation is assumed to be 5,534,000 kg/m^3 (200 pci); other material stiffnesses, as well as thickness, are have the same values as those identified in section 4.3.

The nonlinear spring effect is remarkable in this low subgrade reaction, unlike the high subgrade reaction of soil shown in Figure 4.19. All deflection is down to about 0.05 mm (2 mil) without changing of shape for the nonlinear spring. However, as shown in Table 4.8, the horizontal stress variation under both temperatures shows almost no stress difference between two spring elements in both layers, unlike the relatively large difference seen with deflections. The overall stress contour is not significantly different between the two foundations. Table 4.8 also shows that the maximum tensile stress in the ACC layer occurs only at the Temp-1 condition, which has a low temperature at the top of the pavement and a high temperature at the bottom. Therefore, we consider night temperature only because of its significance to the overlay design.

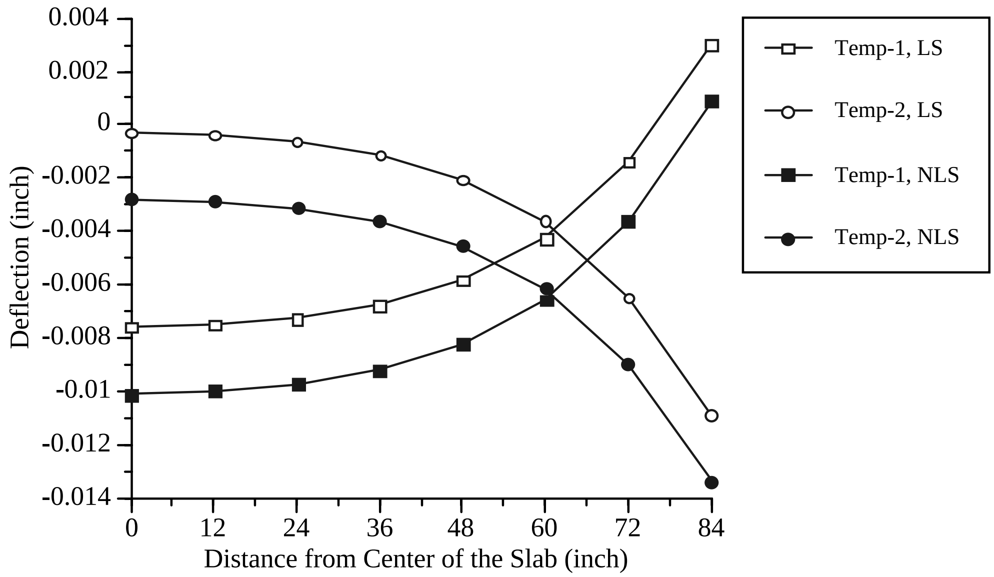

inch = 25.4 mm, foot = 0.304 m
LS: Linear spring (Winkler's foundation), NLS: Nonlinear spring

Figure 4.19. Deflection basin variation by the nonlinear spring

Table 4.8. Extreme value of horizontal stress by nonlinear spring foundation (unit = psi)

	Linear Spring		*Nonlinear Spring*	
	Temp-1	*Temp-2*	*Temp-1*	*Temp-2*
PCC-max.	101.6	154.1	100.9	154.1
PCC-min.	-156.4	-100.6	-154.5	-100.6
ACC-max.	424.2	-115.6	426.8	-115.6
ACC-min.	115.1	-423.8	114.6	-423.8

psi = 6.897 kPa

Effect of Maximum Temperature Difference

Maximum temperature differentials were varied to observe the temperature effect on the pavement response. The inputs were set at 16.7°C (30°F)/day, 27.8°C (50°F)/day, and 38.9°C (70°F)/day. The maximum daily temperature differential reported from the test section was 16.7°C (30°F)/day.

As the maximum temperature differentials increase, the radius of the curvature decreases and maximum deflection increases up to 0.5 mm (20 mil), as shown in Figure 4.20. The temperature effect shown in Figure 4.21 indicates that the horizontal stress increases in all layers when increasing the maximum temperature differentials.

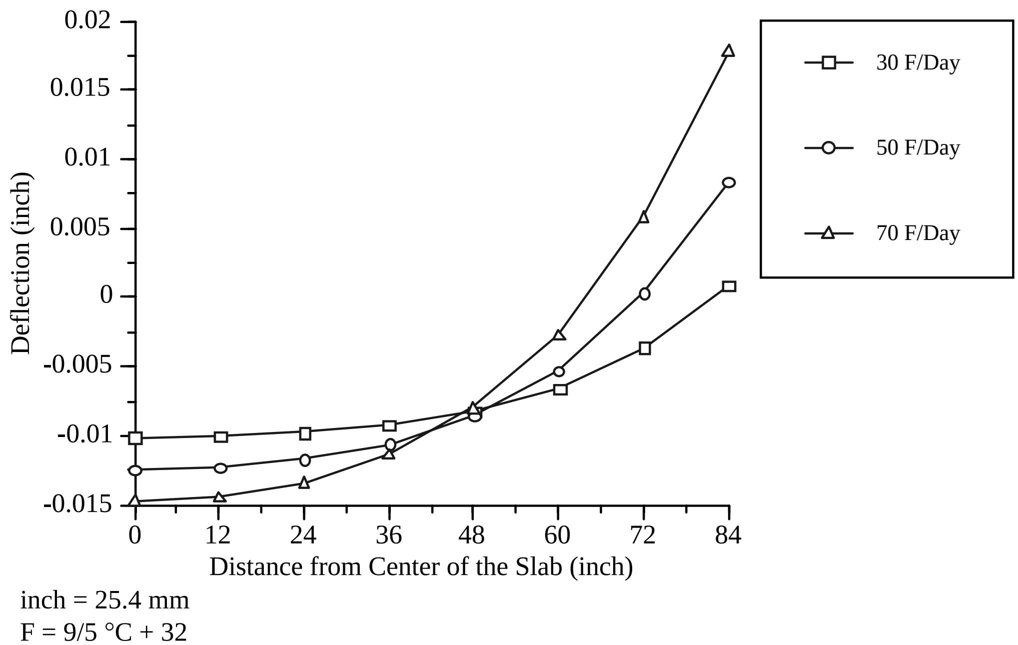

Figure 4.20. Deflection variation by different temperature differentials

This finding means that the likelihood of thermal cracking appearing on the surface of the ACC layer would increase even if the tensile strength of the ACC increases as the temperature decreases during the winter. The PCC layer also experiences increased tensile stresses up to 1.4 MPa (200 psi), a relatively lower stress compared with the tensile strength of the PCC. However, this may cause fatigue cracking, and the center of the slab may experience tensile fatigue cracking owing to thermal cyclic loading. In summary, maximum temperature differentials on the pavement structure are critical in the development of tensile stresses on the ACC overlay pavement.

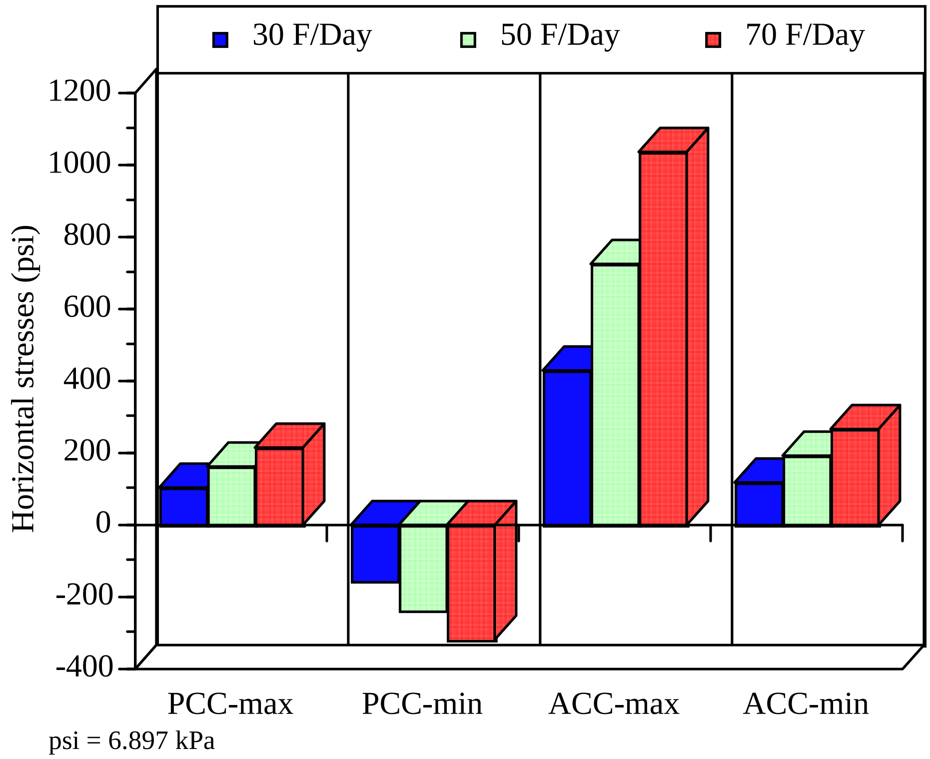

Figure 4.21. Horizontal stress variation by temperature differentials

Effect of the Flexible Interlayer

The flexible interlayer is inserted to prevent reflection cracking; its good performance in the field represents empirical proof of the desired function of the layer. The verification of the interlayer effect on pavement response is one of the main objectives of this research effort.

Three different thicknesses, ranging from 0 to 203 mm (0 to 8 in.), were chosen; their deflections are plotted in Figure 4.22. Deflection shape does not vary as a function of thickness of the interlayer — only the magnitude of the deflection changes. As the thickness of the interlayer increases, the deflections decrease. The extreme value of the horizontal stress given in Table 4.8 shows that the thermal stress in the PCC and ACC layers decreases as the interlayer thickness increases. For example, tensile stress on the ACC layer decreases from 5.2 MPa (760 psi) to 2.9 MPa (426 psi) as 203 mm (8 in.) of flexible interlayer are inserted.

However, the ratio of stress difference between flexible bases is not as significant as the ratio of stress difference between those with and without the interlayer. The thermal stress in the 101 mm (4 in.) of flexible layer increases less than 10% in the ACC layer, compared with 203 mm (8 in.) of flexible base. By contrast, the maximum thermal stress in the ACC layer without the interlayer reaches 5.2 MPa (760 psi), almost twice as high as the thermal stress in the case where an interlayer is included. The rapid increase of tensile stresses in the ACC layer without interlayer indicates efficiency of the flexible base layer in protecting the asphalt overlay from reflection cracking. Thermal stress in the PCC layer also decreases monotonically as the thickness of interlayer increases.

In summary, it can be said that the flexible interlayer significantly decreases tensile stresses in both the ACC and PCC layers under the same temperature differentials. In addition, the difference between 101 mm (4 in.) and 203 mm (8 in.) of flexible layer is not so significant; accordingly, a thinner flexible layer is suggested for future overlay designs, given that a thicker flexible base layer can cause fatigue cracking in the ACC layer, as well as rutting in the flexible layer itself, as indicated in field results.

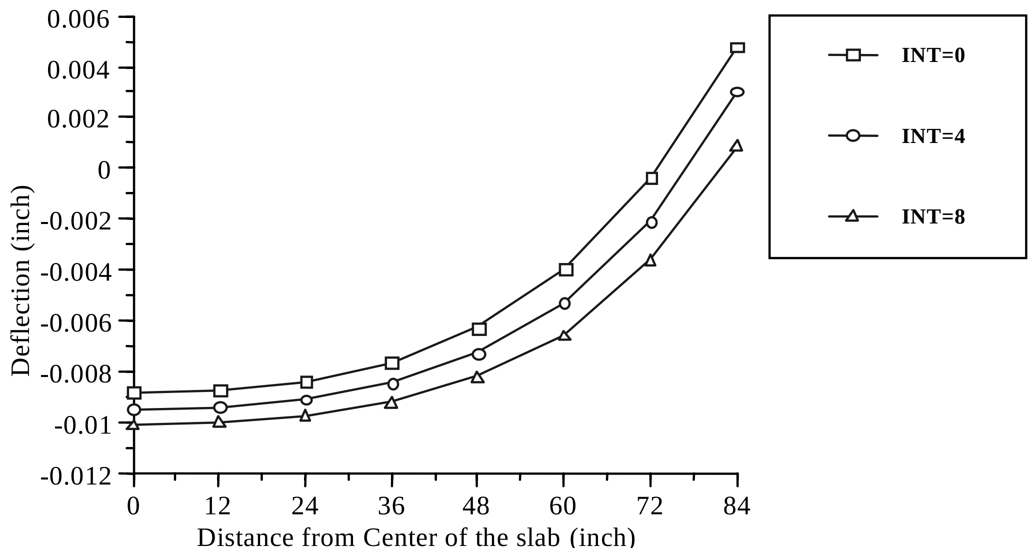

inch = 25.4 mm

Figure 4.22. Deflection basin variation by changing thickness of interlayer

Table 4.9. Extreme horizontal stress by different thickness of interlayer (unit = psi)

	PCC-max.	*PCC-min.*	*ACC-max.*	*ACC-min.*
Int. = 0"	248.1	-282.3	762.5	-323.8
Int. = 4"	149.2	-196.5	468.3	24.5
Int. = 8"	100.9	-154.5	426.8	114.6

inch = 25.4 mm, psi = 6.897 kPa

To observe the effect of both the stiffness and thickness of the interlayer simultaneously, two thicknesses and three different resilient moduli of flexible bases are selected, as shown in Figure 4.23. The stiffness of the interlayer changes the radius of curvature of the slab to a smaller value when the thickness of the interlayer is increased. This means that a stiffer interlayer can increase thermal stresses in both layers. It is also shown, through this mechanistic analysis effort, that the influence of the stiffness of the interlayer is as important as the thickness of the interlayer. This can be observed in the horizontal stress distributions summarized in Table 4.10. The tensile stress in the ACC layer generally increased with a stiffer interlayer. A 20% increase in thermal stresses in the ACC layer is observed within the given range of stiffness. However, the tensile stress in the PCC decreases as the interlayer becomes stiffer. These findings are already observed in the test sections R4, R5, and R6, where the stiffer interlayer experiences more reflection cracking than flexible base section R3. For ACC overlay design purposes, a less stiff material, e.g., flexible base, is better than other stiffer interlayers, such as asphalt binder material.

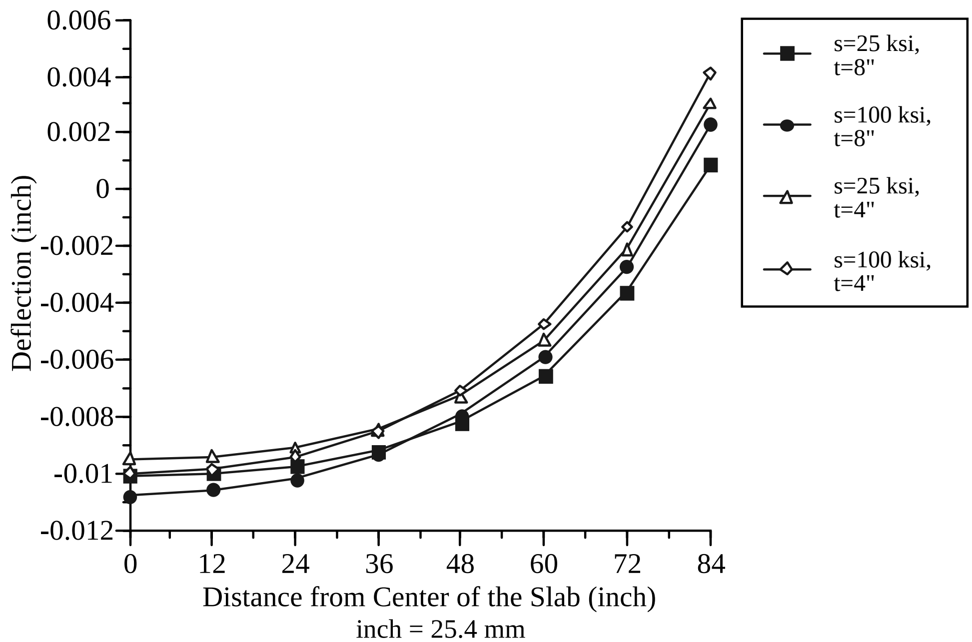

Figure 4.23. Deflection basin by changing thickness and stiffness of interlayer

Table 4.10. Extreme horizontal stress by different stiffness and thickness of interlayer (unit = psi)

Thickness of interlayer	*Stiffness of interlayer*	*PCC-max.*	*PCC-min.*	*ACC-max.*	*ACC-min.*
Int. = 8”	s=25000 psi	100.9	-154.5	426.8	114.6
	s=50000 psi	79.8	-245.0	458.0	109.4
	s=100000 psi	55.2	-382.3	494.6	126.5
	s=200000 psi	63.4	-533.4	532.9	170.6
Int. = 4”	s=25000 psi	149.2	-196.5	468.3	24.5
	s=50000 psi	133.9	-198.5	507.0	6.9
	s=100000 psi	118.3	-245.4	551.2	10.9
	s=200000 psi	101.5	-357.9	597.5	45.4

inch = 25.4 mm, psi = 6.897 kPa

Figure 4.24 shows horizontal stress variations generated by changing the stiffness of the 203 mm (8 in.) interlayer. As the stiffness of the interlayer increases, the compressive stress in the PCC and tensile stress in the ACC layer increases. The tensile stress on the ACC layer also increases as the stiffness of the interlayer increases. This fact can be used to explain the reflection cracking problem in the high stiffness interlayers constructed in the test sections. The Arkansas mix test section also developed slight reflection cracking on the surface. However, the flexible base layer never developed reflection cracking on the surface during 3 years of service. Both the mechanistic and field results suggest using low stiffness material to prevent reflection cracking.

A reasonable value for the thermal coefficient of the flexible interlayer could not be found, as mentioned above. Therefore, various thermal coefficient values are adopted to study the effect of the coefficient in the pavement structure. The deflection and horizontal stresses are not affected as shown in Tables 4.11 and 4.12. We observed no difference near the center of the slab, nor in the maximum and minimum slab stress. This means the thermal coefficient of the interlayer in the given ranges of stiffness has no significant effect on pavement response.

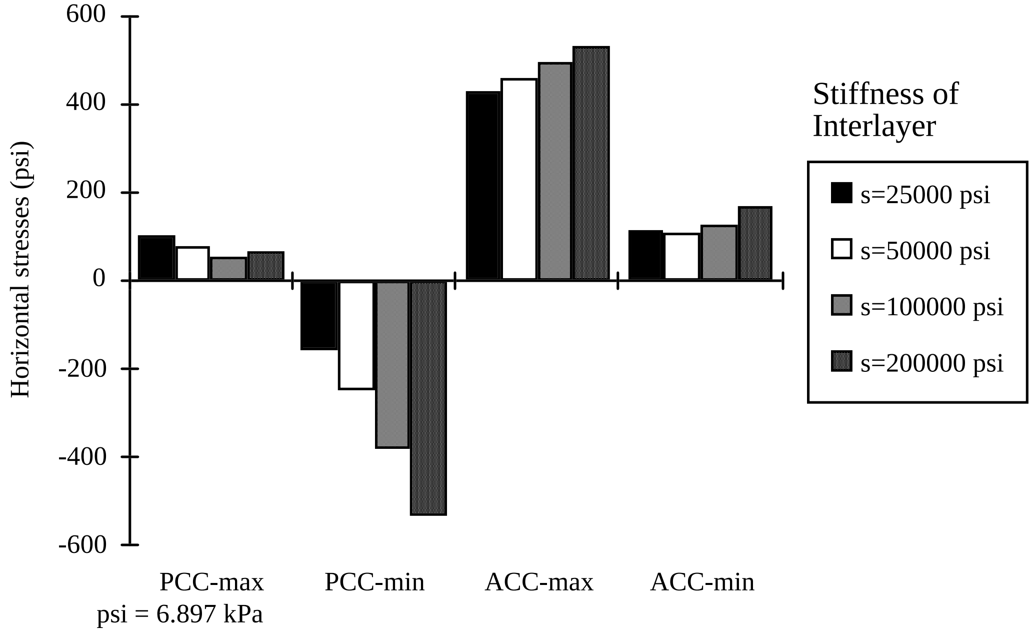

Figure 4.24. Horizontal stresses distribution by stiffness of interlayer

Table 4.11. Deflection basin variation by changing thermal coefficient of interlayer (in./in./°F)

Distance	*α= 1E-07*	*α=0*	*α= 1E-06*	*α= 1E-8*
0”	-1.01E-02	-1.01E-02	-1.01E-02	-1.01E-02
12”	-1.00E-02	-1.00E-02	-1.01E-02	-1.00E-02
24”	-9.75E-03	-9.75E-03	-9.79E-03	-9.75E-03
36”	-9.20E-03	-9.20E-03	-9.25E-03	-9.20E-03
48”	-8.22E-03	-8.22E-03	-8.26E-03	-8.22E-03
60”	-6.58E-03	-6.58E-03	-6.62E-03	-6.58E-03
72”	-3.61E-03	-3.61E-03	-3.66E-03	-3.61E-03
84”	8.75E-04	8.79E-04	8.31E-04	8.79E-04

inch = 25.4 mm
in./in./F = m/m/C °9/5

Table 4.12. Extreme horizontal stress by different thermal coefficient of interlayer at 203.2 mm (8 in.) of interlayer (unit = psi)

Thermal coefficient	*PCC-max.*	*PCC-min.*	*ACC-max.*	*ACC-min.*
α= 1E-07	100.9	-154.5	426.8	114.6
α= 0E-00	100.9	-154.5	426.8	114.6
α= 1E-06	100.9	-154.4	426.8	114.6
α= 1E-08	100.9	-154.5	426.8	114.6

in./in./°F = m/m/C °9/5
psi = 6.897 kPa

In summary, reducing the tensile stress in the ACC layer can be achieved by introducing a flexible layer having less stiffness. A thinner interlayer is also recommended to prevent traffic-related cracking problems. Reducing the thickness of the flexible base layer, say, to 101 mm (4 in.), can be recommended for this type of pavement structure.

Effect of Subgrade Reaction

The subgrade reaction varied, as shown in Figure 4.25. Two different thicknesses of interlayer are considered here to evaluate the combined effects. The deflection variation for the higher value of subgrade reaction does not differ substantially when compared with the deflection variation for the lower subgrade reaction. This shows that the effect of interlayer thickness is not as meaningful as the subgrade reaction. The subgrade reaction shifted pavement deflection up and down without changing the slope of the deflection basin. This means that the stress pattern in the pavement structure does not change, though the magnitude of stresses *does*, as shown in Figure 4.26.

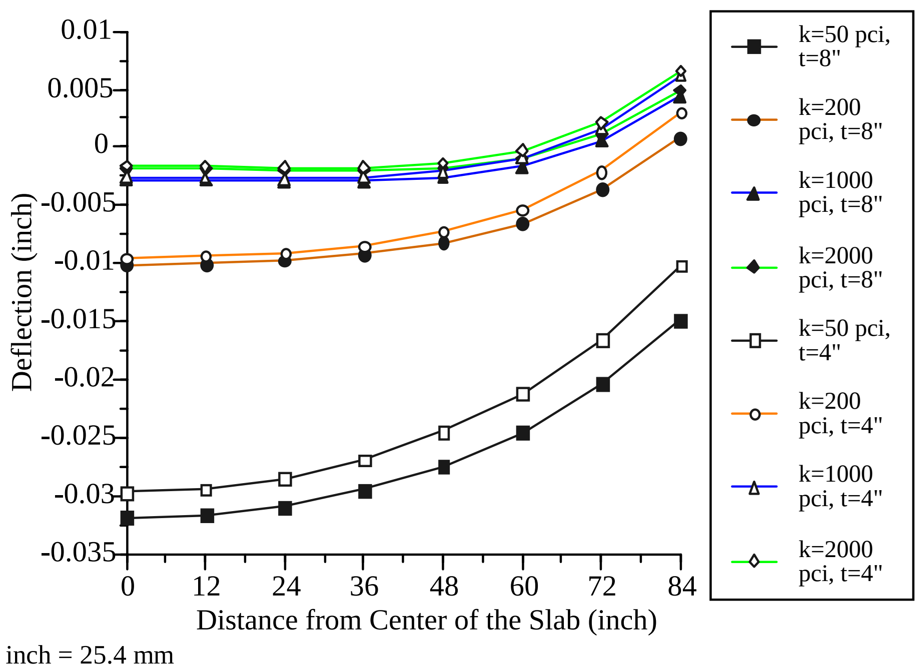

Figure 4.25. Deflection variation by different subgrade reaction of soil

The tensile stress and compressive stress in the PCC layer increase as the subgrade reaction increases, while the maximum tensile stress in the ACC layer decreases. This can be caused by the boundary condition of the ACC layer that is modeled without movement in the horizontal direction. The PCC layer becomes less vulnerable to deflections induced by temperature as the stiffness of the soil layer increases. However, its effect on the stress distribution becomes negligible over a 2,767 kg/m^3 (1,000 pci) value of soil reaction. Stresses in the PCC layer are not shifted when the pavement has a high value of subgrade reaction.

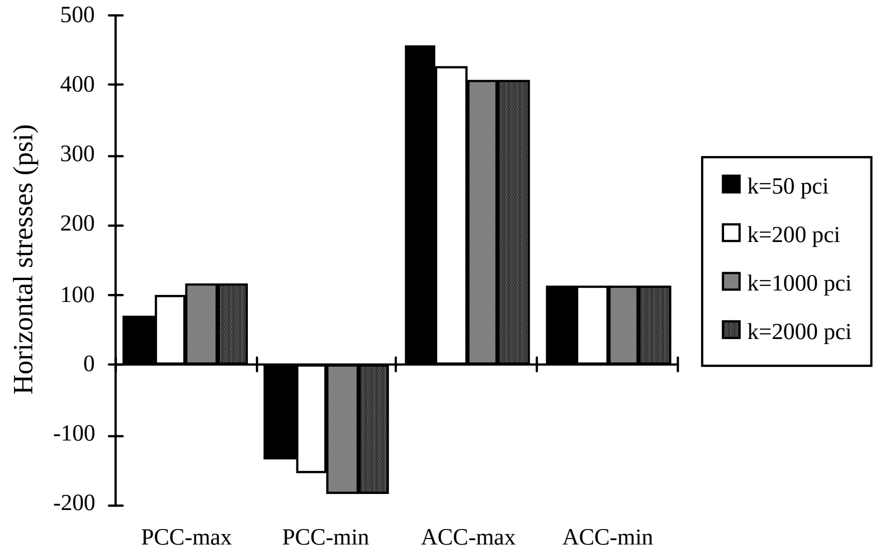

psi = 6.897 kPa, pci = 2.767 *10 ^{4} (kg/cm^3)

Figure 4.26. Horizontal stresses distribution by different subgrade reaction of soil

Effect of ACC Layer

The stiffness of the ACC layer, thickness, and thermal coefficient are investigated next to identify pavement behavior under thermal loadings. Figure 4.27 depicts deflections under different stiffnesses of the ACC layer, as well as different thicknesses of the ACC layer. The deflection for a 101-mm (4-in.) ACC layer presents deflections larger than those observed for a 203-mm (8-in.) ACC layer for a range of stiffnesses. As the stiffness of the ACC layer increases, the deflection basin changes, resulting in a smaller radius of curvature. This leads to a tensile stress concentration in the ACC layer right above the joint of an existing rigid pavement, which may eventually trigger a thermal crack on the surface of the ACC.

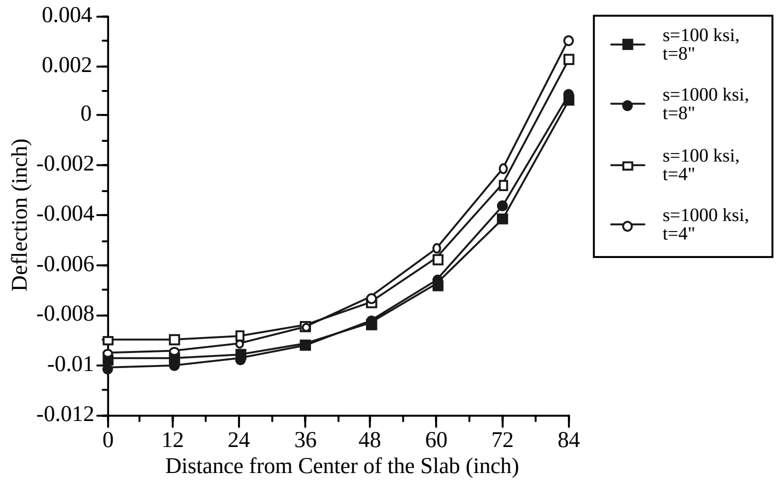

inch = 25.4 mm

Figure 4.27. Deflection variation by changing thickness of interlayer and stiffness of ACC

The effect of the stiffness of the ACC layer is summarized by the maximum stress development at different interlayer thicknesses, as shown in Table 4.13. The stress decreased to 2.8 MPa (420 psi) from 0.3 MPa (50 psi) when the stiffness of the ACC decreased from 6894 MPa (1000 ksi) to 689.4 MPa (100 ksi) for the 203 mm (8 in.) of flexible interlayer pavement. For the 101 mm (4 in.) of flexible interlayer, almost the same amount of ACC stress decrease is observed by changing the stiffness in the ACC. The effect of changing the interlayer thickness from 101 mm (4 in.) to 203 mm (8 in.) is not relevant, compared with the effect of the stiffness. The maximum horizontal stress in the 101-mm (4-in.) ACC layer is almost the same as that in the 203-mm (8-in.) flexible layer. This means that a 203-mm (8-in.) flexible layer is less efficient than a 101-mm (4-in.) flexible layer. By contrast, the thicker flexible base layer induces more rutting problems, so that the 203-mm (8-in.) flexible layer should be replaced with a thinner flexible layer.

Table 4.13. Extreme horizontal stress by stiffness of ACC (unit = psi)

Interlayer Thickness	Stiffness of ACC	PCC-max.	PCC-min.	ACC-max.	ACC-min.
Int. = 8"	s=100 ksi	116.1	-160.2	51.2	12.0
	s=350 ksi	107.2	-156.5	160.3	34.0
	s=600 ksi	103.7	-155.2	264.8	62.4
	s=1000 ksi	100.9	-154.5	426.8	24.5
Int. = 4"	s=100 ksi	172.1	-201.4	58.3	-2.0
	s=350 ksi	160.2	-198.5	179.6	-5.6
	s=600 ksi	154.3	-197.2	293.6	1.8
	s=1000 ksi	149.2	-196.5	468.3	24.5

inch = 25.4 mm, psi = 6.897 kPa

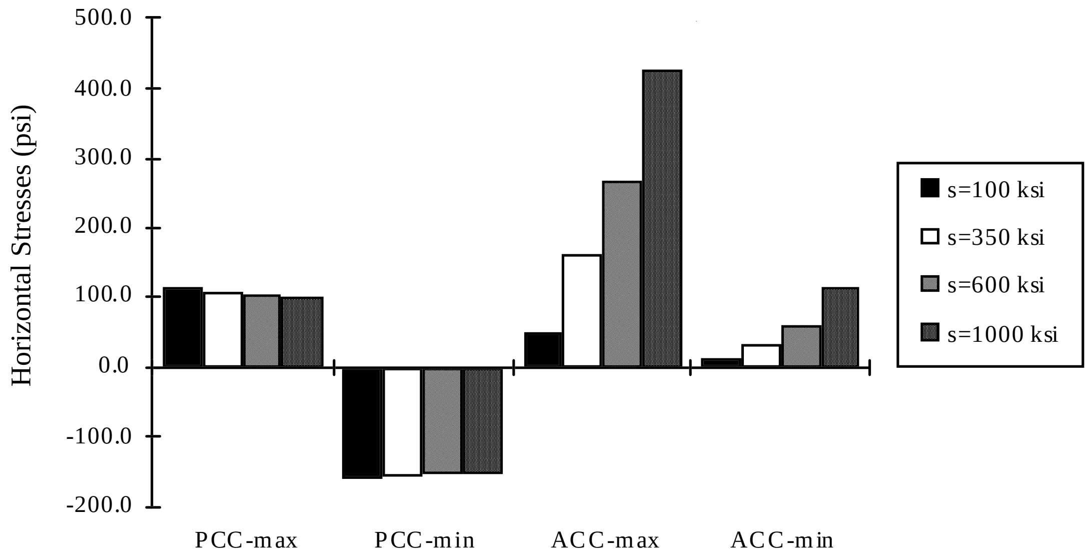

psi = 6.897 kPa, ksi = 6.897 MPa

Figure 4.28. Horizontal stresses distribution by different stiffness of ACC

The stress variation of each layer due to stiffness variation in the ACC layer is shown in Figure 4.28. The stress in the PCC layer does not vary much, but the stress in the ACC layer increases significantly as temperature differentials increase. This means that the effect of the stiffness of the ACC layer is critical for determining whether reflection cracks will occur or not. If the strength gain on that temperature is less than the stress gain at the lower temperature, the reflection cracks will become a predominant distress on this type of pavement.

The thickness effect of the ACC layer is shown in Table 4.14. For a given flexible layer thickness, a thicker ACC does not help reduce the thermal stress on the ACC layer itself. Stress reduction on the ACC layer is less than 5%, even when the thickness of the ACC layer is increased up to 229 mm (9 in.). This means that a thicker ACC layer can protect against reflection cracking.

Table 4.14. Extreme horizontal stress variation by thickness of ACC (unit = psi)

ACC	*PCC-max.*	*PCC-min.*	*ACC-max.*	*ACC-min.*
t=3 inch	100.9	-154.5	426.8	114.6
t=6 inch	70.0	-169.8	419.1	43.4
t=9 inch	44.7	-188.5	404.2	-1.2

inch = 25.4 mm, psi = 6.897 kPa

We next examine the thermal coefficient of the ACC layer in the presence of an interlayer. The thermal coefficient of the ACC is varied from 10 E-06 to 40 E-06, based on previous research. The stress variation as a function of the coefficient of the ACC layer is shown in Table 4.15 and Figure 4.29. The stress in the PCC layer is not affected, while the tensile stress on the ACC layer changed from about 2.4 MPa (350 psi) to 6.9 MPa (1,000 psi) for the same thicknesses of the interlayer. For the two representative coefficients, 14 E-06 and 40 E-06, the stress differences are more than 4.5 MPa (650 psi). This means that selecting correct thermal coefficients for the ACC layer is critical for AC overlay design on JCP.

Table 4.15. Horizontal stress variation by changing the thermal coefficient of ACC layer (unit = psi)

Thickness of interlayer	*Thermal coefficient of ACC*	*PCC-max.*	*PCC-min.*	*ACC-max.*	*ACC-min.*
Int. = 8"	α= 14E-06	100.9	-154.5	426.8	114.6
	α= 10E-06	100.9	-154.5	334.5	52.2
	α= 20E-06	100.9	-154.5	565.3	208.3
	α= 30E-06	100.9	-154.5	796.0	364.5
	α= 40E-06	100.9	-154.5	1027.0	520.6
Int. = 4"	α= 14E-06	149.2	-196.5	468.3	24.5
	α= 10E-06	149.2	-196.5	376.0	-27.9
	α= 20E-06	149.2	-196.5	606.8	103.1
	α= 30E-06	149.2	-196.5	837.5	234.2
	α= 40E-06	149.2	-196.5	1068.0	365.3

inch = 25.4 mm, psi = 6.897 kPa, in./in./ºF = m/m/ºC *9/5

Figure 4.29 also shows the stress variation in both the ACC and PCC layer by changing thermal coefficients of the ACC layer. Five different thermal coefficients are employed in this study. An almost linear relationship between the thermal coefficient and tensile stress indicates that selecting the aggregate that controls the coefficient of the ACC layer seems to be critical in the asphalt mix. It is desirable to have a low thermal coefficient aggregate, like limestone, in the ACC mix, because high thermal coefficients cause greater thermal stresses in the ACC layer.

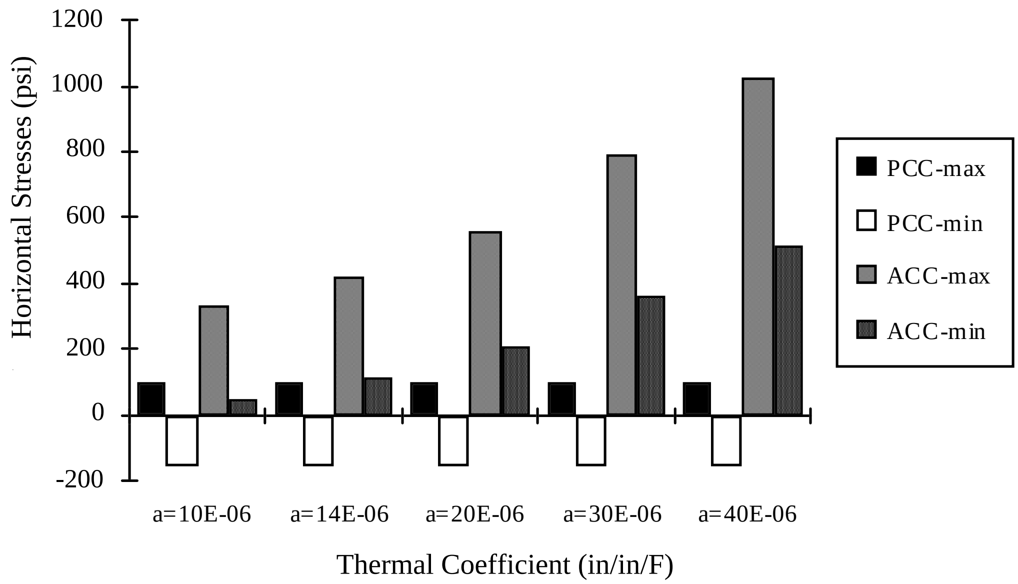

in./in./ºF = m/m/C °9/5
psi = 6.897 kPa

Figure 4.29. Horizontal stresses distribution by thermal coefficient of ACC

Effect of the PCC Layer

The thickness of the PCC layer is in the range of 203 mm (8 in.) to 406 mm (16 in.). As shown in Figure 4.30, the deflection at the center of the slab changed from 0.25 mm (10 mil) to 0.35 mm (14 mil), while no large difference is observed at the end of the slab. The thicker pavement shows more deflection than the thinner pavement.

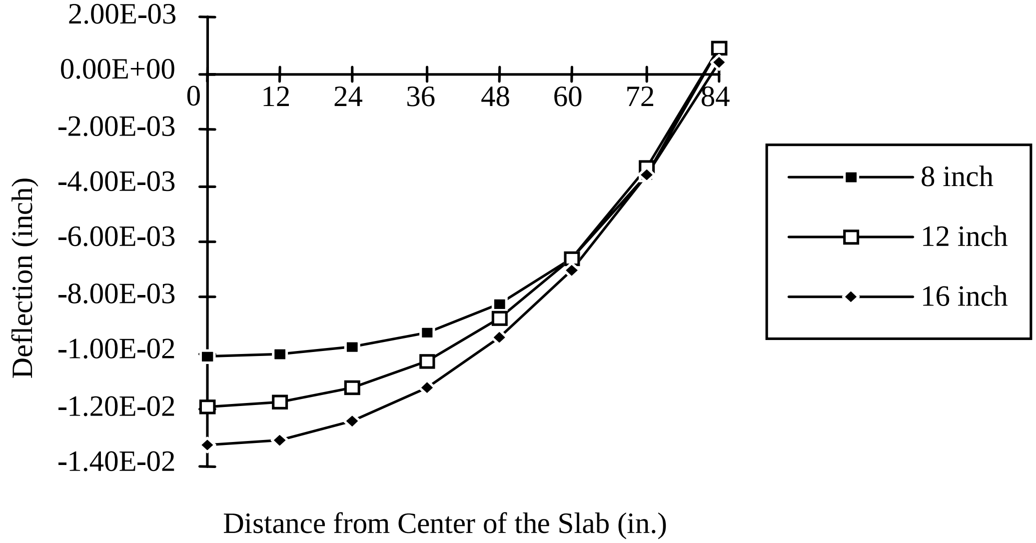

inch = 25.4 mm

Figure 4.30. Deflection variation by thickness of PCC layer

The horizontal stresses shown in Table 4.16 indicate that the maximum stress on both layers does not change as the thickness of the PCC layer varies. The maximum stresses in the ACC layer are not affected at all, while the minimum tensile stress in the ACC layer barely increases. This means that overall tensile stress in the ACC layer does not change as the thickness of the PCC layer increases. The maximum compressive stress on the PCC decreases as thickness increases, while the tensile stress maintains a unique value. This shows that the thickness of the PCC layer is not strongly related to the performance of the surface layer.

Table 4.16. Extreme horizontal stress variation by thickness of PCC layer (unit = psi)

Thickness of PCC	PCC-max.	PCC-min.	ACC-max.	ACC-min.
8 inch	100.9	-154.5	426.8	114.6
12 inch	118.3	-136.2	426.5	152.5
16 inch	110.9	-112.5	424.6	185.2

inch = 25.4 mm
psi = 6.897 kPa

We also investigated the stiffness effect of the PCC layer for two different thicknesses of interlayer, as shown in Table 4.17. The maximum tensile and compressive stresses in the PCC layer increases as the stiffness increases, while there is little variation of stress in the ACC layer. For example, the tensile stress in the PCC layer changes from 0.3 MPa (40 psi) to 1.4 MPa (200 psi), while it changes only from 2.85 MPa (414 psi) to 2.89 MPa (420 psi) in the ACC layer.

Table 4.17. Extreme horizontal stresses by stiffness of PCC layer (unit = psi)

Thickness of interlayer	*Stiffness of PCC*	*PCC-max.*	*PCC-min.*	*ACC-max.*	*ACC-min.*
Int. = 8”	s=2000 ksi	42.8	-128.1	414.4	121.7
	s=4000 ksi	100.9	-154.5	426.8	114.6
	s=6000 ksi	151.9	-203.2	435.3	112.0
	s=8000 ksi	196.3	-244.5	442.4	110.6
Int. = 4”	s=2000 ksi	68.6	-119.1	443.3	38.3
	s=4000 ksi	149.2	-196.5	468.3	24.5
	s=6000 ksi	218.0	-258.6	486.5	19.1
	s=8000 ksi	276.0	-309.6	501.7	16.2

inch = 25.4 mm
psi = 6.897 kPa, ksi = 6.897 MPa

The above result suggests that stiffness of the PCC layer does not affect stress distribution in the ACC layer. Furthermore, it indicates that the stiffness of the PCC layer does not affect the performance of asphalt overlays as long as the stiffness of the PCC layer is kept in the stiffness range given in this analysis.

Generally, the thickness and stiffness of the PCC layer are defined prior to the installation of the overlay. The nonassociation of stiffness and thickness of the PCC layer with stress in the ACC layer can help a designer select a thickness for the ACC layer based only on new material, not on the properties of the existing concrete pavement. However, the increase in tensile stresses in the PCC layer by thermal and traffic loadings can cause cracking at the center of the PCC slab, yielding opportunities for other reflection cracks to develop in the ACC layer. Therefore, the ranges of thickness and stiffness used for the PCC layer in the above analysis are required for this type of pavement structure.

The thermal coefficient of the PCC layer does affect the deflection or stress distribution as much as does the interlayer thickness. Three possible values of thermal coefficients shown in Figure 4.31 indicated that the coefficient of a PCC layer strongly influences maximum and minimum deflection, especially when a thinner interface layer is used. The radius of curvature of the deflection decreases as the coefficient of the PCC layer increases. Furthermore, it can be observed that the deflection difference at the end of the slab, which is a weak point for these types of pavement structures, is strongly affected by the coefficient of PCC layer.

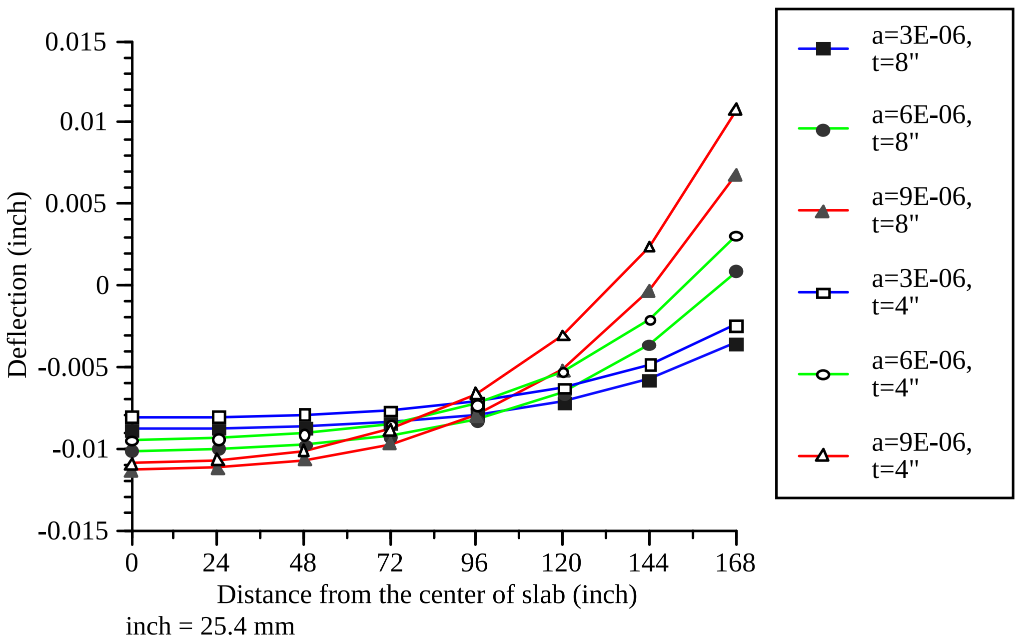

Figure 4.31. Deflection variation by thermal coefficient of PCC

The extreme values of the tensile stress in both layers are shown in Table 4.18 and Figure 4.32. We see that the coefficient of the PCC affects significantly the overall stress distribution in both layers. The tensile stress increases linearly as the coefficient increases in the PCC. For example, 200% of tensile stress increases as the coefficient increases 200% in the 203 mm (8 in.) of interlayer pavement. The tensile stress of the ACC layer increases as the coefficient of the PCC layer increases. Therefore, the existing JCP with siliceous river gravel may have a much higher tendency to develop reflection cracking problems than would the JCP with limestone. In addition, for the tensile stresses in the ACC layer, the thermal coefficient's effect is more critical for the pavement with thinner interlayer than for the pavement with the thicker interlayer.

Table 4.18. Extreme horizontal stresses by thermal coefficient of PCC (unit = psi)

Thickness of interlayer	Coefficient of PCC	PCC-max.	PCC-min.	ACC-max.	ACC-min.
Int. = 8”	a =3E-06	51.0	-78.8	373.8	166.7
	a =6E-06	100.9	-154.5	426.8	114.6
	a =9E-06	146.7	-220.7	490.0	60.9
Int. = 4”	a =3E-06	76.1	-102.4	390.5	105.0
	a =6E-06	149.2	-196.5	468.3	24.5
	a =9E-06	215.6	-275.8	562.7	-58.5

inch = 25.4 mm, psi = 6.897 kPa, in./in./ °F = m/m/°C *9/5

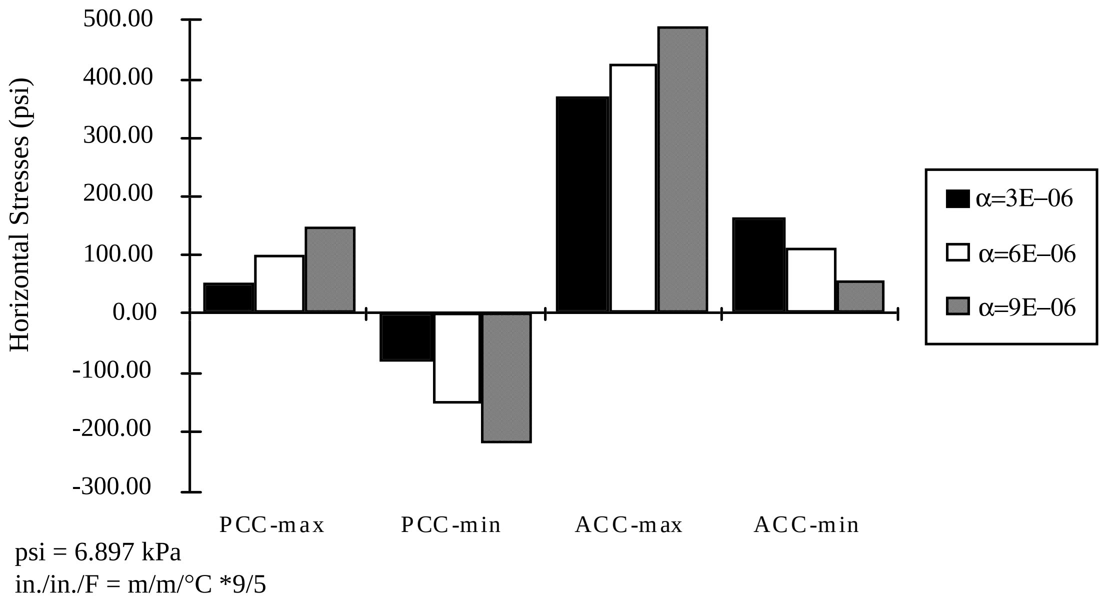

Figure 4.32. Horizontal stresses distribution by thermal coefficient of PCC in 203.2 mm (8 in.) of flexible interlayer

Summary of Sensitivity Analysis

The initial sensitivity analysis was performed to (1) test consistency of the mechanical model, (2) predict response of the pavement structure subjected to temperature variation, and (3) select the most important factor for overlay pavement design for further research. The results obtained form the models agree with observations. The calculated stresses and strains can be used for design purposes when combined with field experience. Furthermore, the initial sensitivity analysis provides significant results that can be used to develop a design equation using fractional factorial analysis.

Figure 4.33 shows the ranges of maximum and minimum horizontal stresses in the ACC layer from the above sensitivity analysis. Temperature differentials, thickness of interlayer, and stiffness and thermal coefficient of the ACC layer are important factors that control the horizontal stress in the ACC layer. Among these, the thermal coefficient and temperature differentials are the main factors in this pavement system. Furthermore, the insignificance of the thermal coefficient of the flexible interlayer, the thickness of the ACC and PCC layers, and the stiffness of the PCC have been demonstrated with examples.

The maximum horizontal tensile stress variation of the PCC layer is presented in Figure 4.34. Temperature and thickness of the flexible layer are dominant factors that control the stress. Unlike that in the ACC layer, the stiffness and thermal coefficient of the PCC layer appears to be governing factors for the PCC layer. Neither the coefficient of the interlayer nor the coefficient of the ACC nor the thickness of the PCC layer affects the stress response.

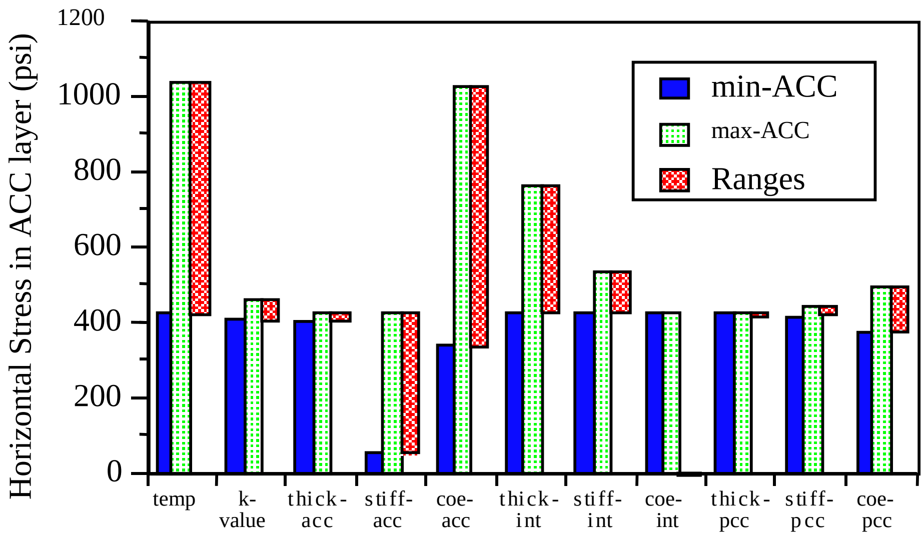

psi = 6.897 kPa

Figure 4.33. Comparisons of maximum horizontal stress in ACC layer

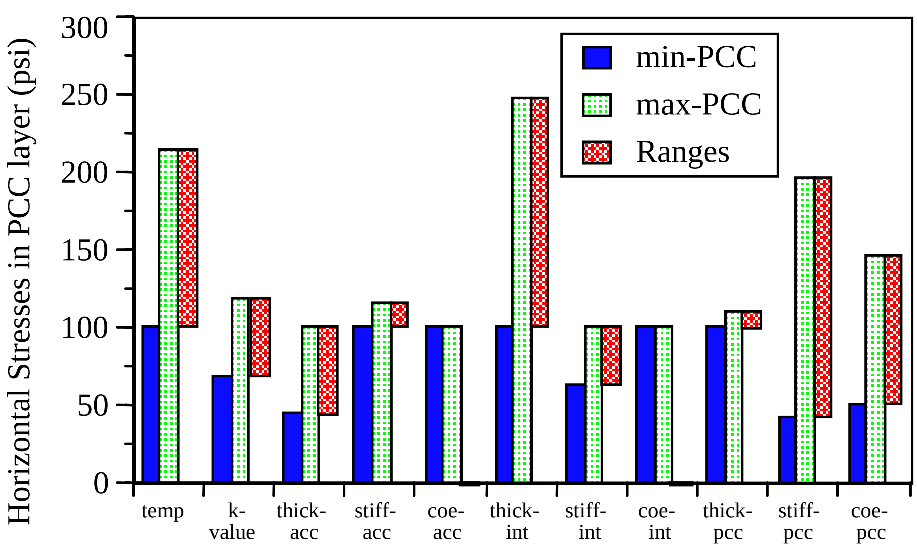

psi = 6.897 kPa

Figure 4.33. Comparisons of maximum horizontal stress in PCC layer

In summary, the thermal coefficient of the ACC layer, the thickness of the interlayer, and the temperature differential are all factors critical in estimating horizontal stresses in the pavement system. The nonrelevant factors are thermal coefficients of the flexible interlayer and thickness of the PCC. In addition, stiffness of the interlayer assigned by the above boundaries does not influence stress development in the pavement. However, these results are limited by sensitivity on single factors (not cross effects between multifactors).

FURTHER RESEARCH

The above thermal stress analysis was performed using simple assumptions that the pavement temperature distributes linearly by depth and that the warping force only acted on the pavement. However, the temperature distribution in the pavement may not be linear. In addition to the warping force, the frictional force between layers can also add tensile stresses in both ACC and PCC layers. Furthermore, the stiffness of the ACC is a function of temperature as well. All of these conditions should be addressed in designing pavements.

Materials Characteristic Variation of ACC by Temperature

The stiffness and strength of the ACC layer strongly depend on both loading time and temperature. Only the stiffness variation as a function of temperature is considered owing to the complexity of defining loading time. The maximum temperature variation observed in the test section was less than 2.8°C / hour (5°F / hour). The stiffness variation of the ACC mixture was investigated by Kennedy using the indirect tensile test (Kennedy 1983):

$$\begin{aligned} \text{Log } S_T = {} & 0.3202 + 0.9380\ A - 0.0116\ T - 0.0577\ A^2 - 0.0899\ GA \\ & + 0.0148\ GA^2 - 0.0003\ TA^2 \end{aligned} \tag{4.10}$$

$$\log E_s = 2.94 + 1.03 \log S_T \tag{4.11}$$

where

S_T = predicted indirect tensile strength, psi,

E_s = static modulus of elasticity, psi,

A = asphalt content, percent by weight of total mixture,

T = testing temperature, °F , and

G = coded value for aggregate (limestone = 0, gravel = 1).

Figures 4.35 and 4.36 show stiffness and tensile strength variation with temperature based on Kennedy's work with limestone aggregate. The stiffness for the low temperatures may have been estimated too high: 17,235 MPa (2.5 million psi) in -3.89° C (25°F) for 8% of asphalt contents. This may have been caused by an extrapolation error in the regression equation, for which the testing temperature boundary was 10°C (50°F) to 51.7°C (125°F).

The stiffness ranges from 1,378.8 MPa (200,000 psi) to 75.83 MPa (11,000 psi) for 4% asphalt content and 4,067.46 MPa (590,000 psi) to 75.83 MPa (11000 psi) for 6% asphalt content within the temperature boundary. Corresponding tensile strength is 0.86 MPa (125 psi) to 0.3 MPa (50 psi) for 4% and 3.8 MPa (560 psi) to 0.08 MPa (12 psi) for 8%. Relatively low tensile strength was observed in the high temperature: around 10 psi for the 6% and 8% asphalt content.

Using these material properties, we can calculate more precisely the thermal stresses on the pavement structure. The maximum temperature differential is fixed at 16.7°C (30°F) with linear variation by depth, as was done previously. The initial temperature in the pavement structure is fixed at 16.68°C (60°F). Then the temperature is assumed to be changed under two conditions. Temp1 is nighttime, with a lower temperature on the surface, in this case 8.34°C (45°F), and a hotter temperature on the bottom, in this case 23.9°C (75°F); Temp2 was the opposite, with the hotter temperature on the surface and the cooler at the bottom.

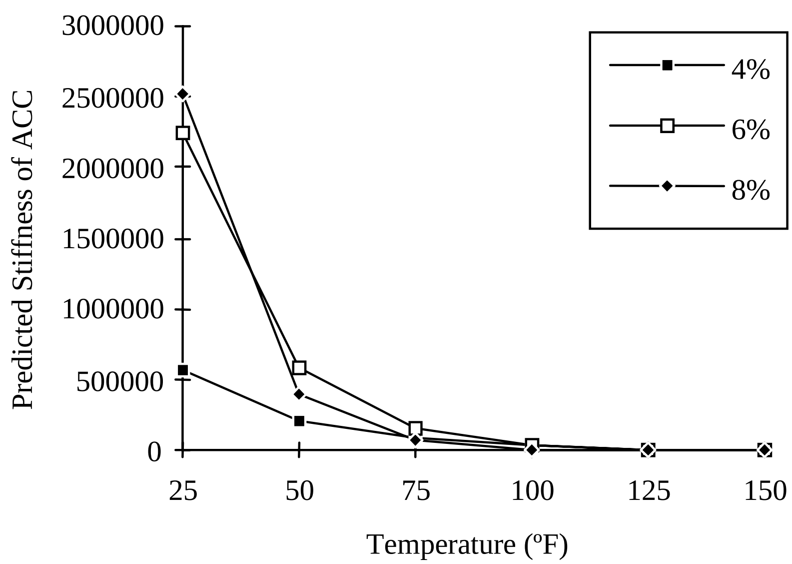

psi = 6.897 kPa, F = 9/5°C + 32

Figure 4.34. Stiffness variation of ACC by temperature

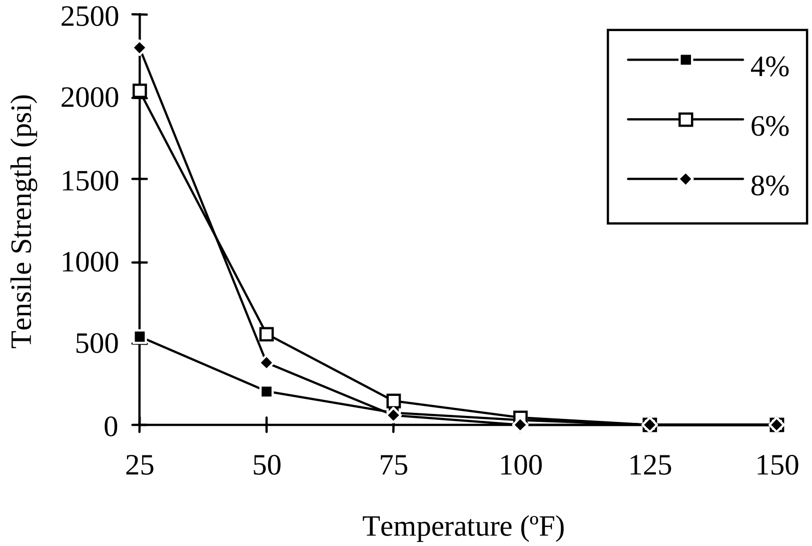

psi = 6.897 kPa, F = 9/5 °C + 32

Figure 4.35. Tensile strength variation of ACC by temperature

Under these two temperature conditions, two approaches to assign ACC layer stiffness are used and compared. CASE1 is fixed with an asphalt stiffness of 1,103.04 MPa (160,000 psi) for 4% of asphalt content, 1,551.15 MPa (255,000) psi for 8%, and 2,757.6 MPa (400,000 psi) for 6%, which are corresponding stiffnesses with the mean temperature at 16.7°C (60°F). In CASE2 the stiffness of the ACC layer is dynamically assigned for corresponding pavement temperatures. If they lead to approximately the same value of stress, then the material stiffness of the ACC layer can be treated as a unit value, as with CASE1. The 6.08 m (20 ft) of joint spacing is initially selected and the deflection and stresses are compared.

Deflections between CASE1 and CASE2 do not differ much at night; during the day, there exists some difference in deflection under daytime temperature distributions. Unlikely deflection, the horizontal stress variation shown in Table 4.20 for two cases of stiffness assigning methods, shows a significant difference, depending on the time of day. Little fluctuation is observed in the compressive stress, but variation of tensile stresses is insignificant. However, at night (Temp1), a greater difference in tensile stress in the ACC layer is observed. For the same amount of asphalt content, the stress difference reaches 1.4 MPa (200 psi). However, the thermal stress in the PCC layer does not present a large difference between the two cases. This shows that the dynamic allocation of stiffness of the ACC layer by the temperature has a large impact on stress development in the ACC layer, but not in the PCC layer.

Table 4.19. Horizontal stresses distribution under the different asphalt content and temperature distribution—6.1-m (20-ft) slab (unit = psi)

Temp.	Pavement Layer	CASE1 AC = 4%	CASE1 AC = 6%	CASE1 AC =8%	CASE2 AC = 4%	CASE2 AC = 6%	CASE2 AC =8%
Temp1	PCC-max	112.7	106.7	109.8	109.8	102.2	103.5
	PCC-min	-212.2	-206.4	-209.3	-209.4	-202.7	-203.9
	ACC-max	71.6	171.5	111.2	124.4	379.6	339.4
	ACC-min	2.8	14.5	5.8	4.1	33.8	17.8
Temp2	PCC-max	238.6	233.7	236.2	240.9	237.5	240.8
	PCC-min	-109.4	-102.7	-106.1	-112.6	-107.9	-112.4
	ACC-max	1.8	-13.1	-1.9	1.9	-0.2	2.0
	ACC-min	-61.8	-148.8	-96.9	-32.5	-67.7	-37.7

psi = 6.897 kPa

Figure 4.37 clearly shows that the ACC layer experiences thermal stresses between 0.8 MPa (120 psi) and 2.3 MPa (340 psi), depending on asphalt content, during the night. However, during the day, smaller differences of thermal stress are observed, such that tensile stresses are below 0.03 MPa (5 psi). When modeling the stiffness of an ACC layer, CASE1, a similar variation of tensile stress is observed in the ACC layer even though the absolute magnitude of the tensile stresses is about one-third that of CASE2.

This may be caused by the stiffness difference existing between the two analysis cases that consider high sensitivity of the stiffness of the ACC layer to the thermal stress in ACC layer shown previously. While the stiffness of the ACC layer goes up to 4,067.4 MPa (590 ksi) for 6% and 2,757.6 MPa (400 ksi) for 8% in CASE2 at 25°C (45°F), the average stiffness chosen for CASE 1 is 2,757.6 MPa (400 ksi) for 6% and 1,757.9 MPa (255 ksi) for 8% asphalt content. This suggests another procedure in which the stiffest value of the ACC layer under the lowest temperature can replace dynamic stiffness allocation procedures (CASE 2).

CONCLUSION

The sensitivity of thermal stresses was investigated for a multilayer pavement structure. A test designed to obtain precise temperature distribution in the pavement was developed with a heat transfer model using the FDM. The solution obtained from numerical results was calibrated by field measurements, with the calibrated results matching field temperature measurements.

An FEM that consists of three layers of an linear elastic element and a nontensile resistance spring foundation was proposed to model behavior of the pavement structures subjected to temperature changes. The nonlinear spring was introduced to avoid limitations of Winkler’s foundation element, which is valid only as long as the slab and soil act together without debonding. Throughout the sensitivity analysis, the maximum temperature differential is shown as a primary factor that affects stress distribution of both layers — ACC and PCC — among the various factors. The thickness of the interlayer and the stiffness and thermal coefficient of the ACC layer can be chosen as secondary significant factors for the

ACC layer, while the stiffness and thermal coefficient of the PCC layer seem to be governing factors for a PCC layer. The insignificant factors are the thermal coefficient of the flexible interlayer and the thickness of the PCC. However, these results were obtained in a sensitivity study of a single factor — that is, in the absence of any interaction effect among the factors.

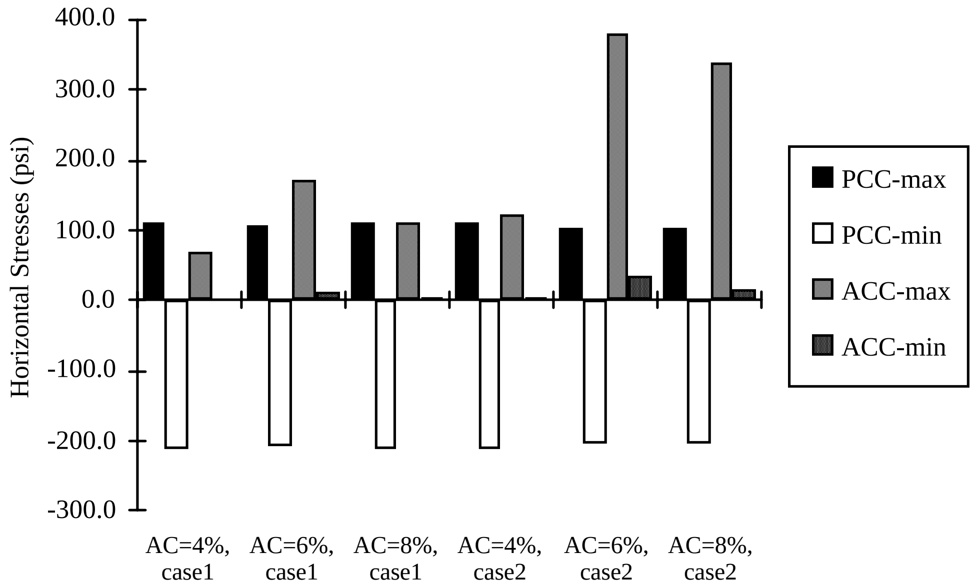

psi = 6.897 kPa

Figure 4.39. Extreme value of horizontal stress between two different stiffness allocation methods at nighttime temperature

Table 4.20. Horizontal stress variation by coefficient of friction between subgrade and PCC layer (unit = psi)

Coefficient of friction	S11-PCC		S11-INT		S11-ACC	
	Maximum	Minimum	Maximum	Minimum	Maximum	Minimum
0.1	404.3	-4369	-5.8	-38.0	119.7	68.4
0.4	403.6	-4362	-5.6	-38.0	119.6	68.4
0.7	403.2	-4357	-5.5	-38.0	119.6	68.4
1.1	402.9	-4354	-5.4	-38.0	119.6	68.4
3	402.2	-4346	-5.3	-38.0	119.5	68.4

psi = 6.897 kPa

CHAPTER 5. PERFORMANCE PREDICTION AND DESIGN MODELS

INTRODUCTION

An asphalt overlay can possess various geometric and material properties. The distress pattern depends on the design and quality of its construction. The following is assumed in developing the distress prediction model: The primary distresses considered in this analysis are rutting, fatigue cracking, and reflection cracking (the dominant distresses observed from the test section). It is assumed that linear elastic modeling results could be used to predict these distresses (using predefined empirical damage equations).

The FEM mechanistic model for pavement structures takes into account material properties, loads, and pavement geometry. Pavement geometry includes physical information for all layers (e.g., the thickness of each layer). Traffic loading considers type of axle, loading position, and load magnitudes. As in other design methods, pavement stress can be caused by wheel loads and/or temperature variation.

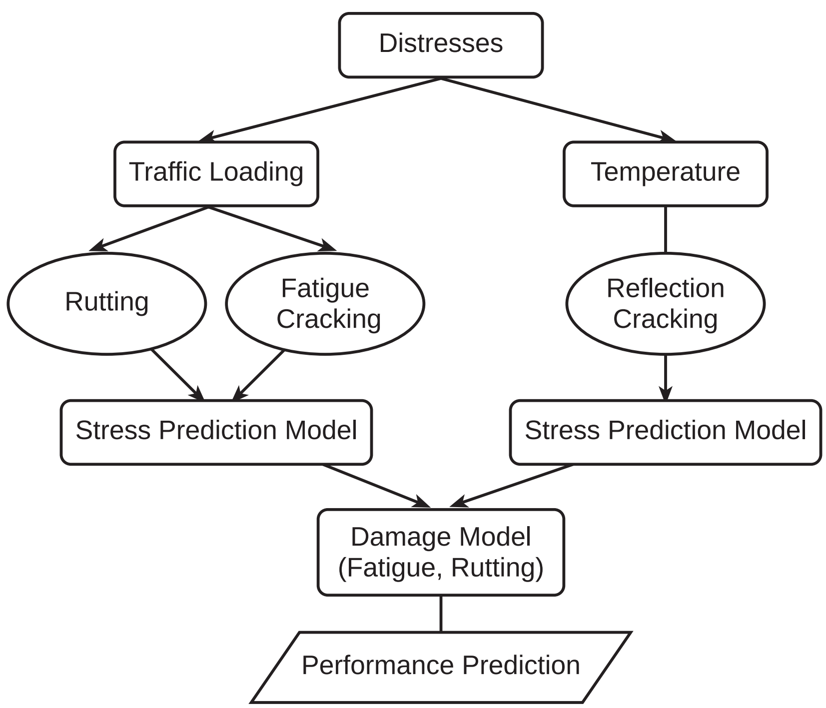

Figure 5.1. Flow chart used to predict pavement distress on ACC overlay on PCC

Considerable research has been carried out in an effort to develop a stress prediction model for flexible or rigid pavement subject to heavy traffic loading (Viljoen and McCullough 1985; von Metzinger and McCullough 1991). Our primary focus is an exploration of the pavement structure having an interlayer between the ACC and PCC layer.

Table 5.1 shows possible pavement overlay structure combinations used for traffic loading. A total of ten factors are selected according to their significance in the stress distribution. Each factor has three levels for investigating nonlinear trends. All combinations of these ten factors at three levels per factor yield a total of 3^{10} possible combinations. While it may be impossible to consider all these combinations, that total can be reduced to 243 combinations by the fractional factorial design method (McLean and Anderson 1984). A total of 27 blocks, or 243 sets (shown in Appendix C), can be used to examine both the effects of the factors and all two-factor interactions involving the stress or strain.

The axisymmetric finite element model assumed that single traffic wheel loading was applied to the center of the pavement structure. Therefore, traffic loading is modeled as a single wheel loading. The overall structural thicknesses and the stiffness information are derived from previous research (Kennedy 1983, and Viljeon and McCullough 1985). Other factors, such as Poisson's ratio and discontinuity in traffic, are not considered here.

Table 5.1. Ten factors and three levels used in the fractional factorial design for traffic loading

	Factor	Level 1	Level 2	Level 3
Single Wheel (lbf)		6000	9000	15000
Thickness (inch)	Overlay	3	6	9
	Interlayer	2	4	8
	Existing pavement	8	12	16
	Subbase	0	6	8
Stiffness (psi)	Overlay	200,000	600,000	1,000,000
	Interlayer	25,000	50,000	100,000
	Existing pavement	3,500,000	5,500,000	7,500,000
	Subbase	50,000	500,000	1,000,000
	Subgrade	5,000	20,000	40,000

inch = 25.4 mm, psi = 6.897 kPa, lbf = 453.5 g

DESIGN OF PARTIAL FACTORIAL FOR TEMPERATURE LOADING

Thermal stress is clearly affected by maximum temperature differentials as well as by temperature distribution between the layers. The assumption that thermal stress is a function of maximum temperature differential by depth can be used for developing the design equation. Only the warping stress caused by the temperature change with depth is considered in this experiment.

This experimental design for thermal stress can have many factors and levels, given the large variation of material property and material parameters. The thickness of the PCC layer, the thermal coefficient of the flexible interlayer, and the stiffness of interlayer, are set at 203.2 mm, $6*10^{-7}$, and 344.7 MPa (50,000 psi), respectively. Since the numerical calculation is time consuming, we develop a simple FORTRAN program to obtain input files for the ABAQUS environment (see Appendix D). ABAQUS results were stored in the database in order to perform both ANOVA and regression analyses.

Table 5.2. Factors and their level considered in the experimental design for thermal stress

	Factor	Level 1	Level 2	Level 3
Thickness (inches)	Overlay	3	6	9
	Interlayer	0	4	8
Stiffness	Overlay (psi)	200,000	600,000	1,000,000
	Interlayer (psi)	20,000	80,000	140,000
	Existing Layer (psi)	3,500,000	5,500,000	7,500,000
	Road Bed (pci)	400	800	1200
Thermal coefficient	Overlay	$15*10^{-6}$	$30*10^{-6}$	$45*10^{-6}$
(in/in/ºF)	Existing Layer	$4*10^{-6}$	$6*10^{-6}$	$8*10^{-6}$
Temperature Differentials (ºF/Day)		30	50	70

inch = 25.4 mm, psi = 6.897 kPa, pci = $2.767*10^{4}$ kg/m^{3}, lbf = 453.5 g

Database

The output from ABAQUS can relate to both deflections and stress/strains at various points in the structure. However, because such information is neither necessary nor significant, the extreme values, either maximum or minimum stress/strain, and the deflections at the position corresponding to the geophone arrangement of the FWD, are stored in the database; the geophone positions and plotted in Figure 5.2 (the deflection from the temperature loading is not included).

After completing the computational works, we constructed the database (see Appendix C) to include the basic data required to create the stress prediction model and to provide basic information for further research. The stress prediction model can be developed through the regression approach using tensile stress in both the PC and the ACC layers as independent variables. These stress/strain equations can be used to predict the rutting model in the interlayered pavement system, as well as reflection cracking in the AC layer, by applying a damage model. In addition, the deflection database under traffic is developed with the FWD sensor spacing used in Texas. It can be used to develop a so-called backcalculation model by statistical analysis. Furthermore, the stress distribution under different magnitudes of wheel loading can explain the heavy loading effect in the composite structure.

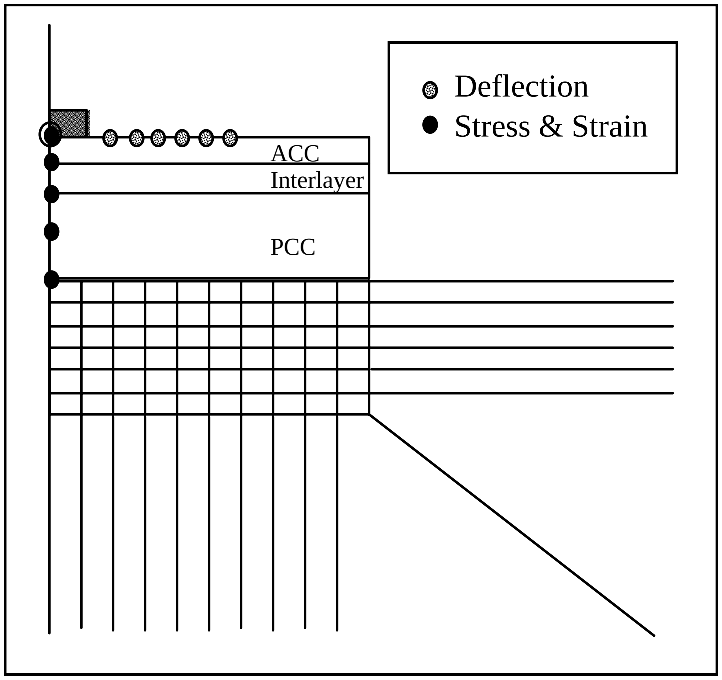

Figure 5.2. Independent variables to be collected from traffic loading analysis

ANOVA

The Statistical Analysis System (SAS) package is used to perform an analysis of variance (ANOVA), which is applied to select the most significant factors affecting the development of stress in both layers. Separate statistical procedures are developed for the traffic and thermal loading.

Table 5.3 shows the results of the traffic ANOVA, in which the tensile stress of the ACC layer was considered a dependent variable and the other ten factors were considered independent variables. Using this linear model, about 76.4% of the dependent variable can be explained by the independent variables. It also had a coefficient of variation of only 3%. F-test results also showed that this model is acceptable at a 1% significance level. As shown in Table 5.3, the overlay thickness (over-thick), interlayer thickness (int.-thick), overlay stiffness (over-E), interlayer stiffness (int.-E), and traffic loading were selected as factors that significantly affect tensile stress within the ACC layer.

A similar ANOVA table is constructed for tensile stress on the PCC layer under traffic loading. Almost 90% of the tensile stress of this model can be explained (r^2=0.90), with 5% of coefficient of variation for the estimation. The model is acceptable according to the F-test. All independent factors are shown to be significant except for the stiffness of the interlayer.

Table 5.3. ANOVA for tensile stress in the ACC layer under traffic loading

Source	DF	Sum of Squares	Mean Square	F Value	Pr > F
Model	20	22.23	1.11	35.96	0.0001
Error	222	6.86	0.03		
Corrected Total	242	29.10			
Over-thick	2	0.43	0.21	6.89	0.0012
int.-thick	2	18.65	9.32	301.59	0.0001
PCC-thick	2	0.00	0.00	0.07	0.9306
Sub.-thick	2	0.00	0.00	0.01	0.9937
Over-E	2	1.58	0.79	25.54	0.0001
int.-E	2	1.28	0.64	20.63	0.0001
PCC - E	2	0.00	0.00	0.01	0.9884
Subbase-E	2	0.00	0.00	0.01	0.9936
Subgrade-E	2	0.01	0.00	0.11	0.8978
Traffic	2	0.29	0.15	4.74	0.0096

Table 5.4. ANOVA for tensile stress in the PCC layer under traffic loading

Source	DF	Sum of Squares	Mean Square	F Value	Pr > F
Model	20	83.69	4.18	104.51	0.0001
Error	222	8.89	0.04		
Corrected Total	242	92.58			
Over-thick	2	4.97	2.48	62.01	0.0001
int.-thick	2	3.11	1.56	38.88	0.0001
PCC-thick	2	24.66	12.33	307.92	0.0001
Sub.-thick	2	5.59	2.80	69.82	0.0001
Over-E	2	0.40	0.20	5.03	0.0073
int.-E	2	0.03	0.02	0.42	0.657
PCC - E	2	3.95	1.97	49.26	0.0001
Subbase-E	2	5.45	2.73	68.12	0.0001
Subgrade-E	2	4.35	2.18	54.34	0.0001
Traffic	2	31.17	15.59	389.29	0.0001

Similarly, the results in Table 5.5 are summarized for the tensile stress in the ACC layer as a function of temperature. This model presents a coefficient of determination (=r^2) of 0.875, while the coefficient of variation of the mean is only 2.3% for the estimated tensile stress in the ACC layer. The F-test shows that this model is acceptable at a significance level of $\alpha = 0.01$. Among the ten factors, the thickness of the ACC layer, the stiffness of the PCC layer, and the soil subgrade reaction are shown to be insignificant.

Table 5.5. ANOVA for tensile stress in the ACC layer under thermal loading

Source	DF	Sum of Squares	Mean Square	F Value	Pr > F
Model	20	43.39	2.17	77.74	0.0001
Error	222	6.19	0.03		
Corrected Total	242	49.58			
Joint Spacing	2	0.58	0.29	10.46	0.0001
ACC-thick	2	0.25	0.13	4.49	0.0122
Int.-thick	2	1.05	0.52	18.81	0.0001
ACC-E	2	22.43	11.21	401.87	0.0001
INT.-E	2	0.59	0.30	10.64	0.0001
PCC-E	2	0.18	0.09	3.31	0.0384
Soil-K	2	0.00	0.00	0.09	0.9181
ACC-alpha	2	6.98	3.49	125.03	0.0001
PCC-alpha	2	0.96	0.48	17.24	0.0001
Temp	2	10.35	5.18	185.5	0.0001

The tensile stress in the PCC layer is analyzed using a similar process, with the results shown in Table 5.6. About 87.5% of the tensile stress in the PCC layer can be explained by the linear combination of independent variables considered. The F-test results indicate the acceptability of this linear model. The stiffness of the interlayer, the soil subgrade reaction, and the thermal coefficient of the ACC layer are shown to be insignificant. This information can be applied to develop a regression equation for further analysis.

Table 5.6. ANOVA for tensile stress in the PCC layer under thermal loading

Source	DF	Sum of Squares	Mean Square	F Value	Pr > F
Model	20	90.19	4.51	78.18	0.0001
Error	222	12.81	0.06		
Corrected Total	242	103.00			
Joint Spacing	2	18.46	9.23	159.98	0.0001
ACC-thick	2	4.03	2.02	34.94	0.0001
Int.-thick	2	7.66	3.83	66.38	0.0001
ACC-E	2	0.14	0.07	1.24	0.2914
INT.-E	2	0.15	0.08	1.31	0.2713
PCC-E	2	19.64	9.82	170.27	0.0001
Soil-K	2	0.01	0.00	0.09	0.9183
ACC-alpha	2	0.08	0.04	0.7	0.4953
PCC-alpha	2	15.26	7.63	132.25	0.0001
Temp	2	24.76	12.38	214.64	0.0001

Regression Analysis

Stress/strain Prediction Model under Traffic Loading: After selecting the dominant factors that affect pavement behavior, we performed the multiregression analysis using the "stepwise" routines (instead of the factors selected from the initial ANOVA). Stepwise regression begins with no variables and adds a significant variable step by step to the model; variables already in the model do not necessarily remain (SAS, Ver. 6.3). The following models are selected based on both engineering judgment and statistical analysis.

Equation 5.1 shows the tensile stress prediction model for the ACC layer. As expected, the tensile stress in the ACC layer is a function of overlay and interlayer, as well as of traffic loading. The tensile stress decreases as the overlay thickness increases and as the thickness of the interlayer decreases. Stress increases with increasing traffic loading. The tensile strain of the ACC layer can be predicted by Equation 5.2. Increasing the thickness and stiffness of the ACC and the interlayer reduces the tensile stain of the ACC layer. Equation 5.3 can be used to predict tensile stress in the PCC layer. The tensile stress in the PCC layer is also a function of the thickness of the PCC layer, as well as of the stiffness of the layer below the PCC layer. This indicates that the tensile stress in the PCC layer decreases with the increased thickness of all layers and with decreased traffic loading.

$$\begin{aligned} \mathrm{LN}\ (\mathrm{S11\ acc}) = {} & 5.3737 - 0.03116513\ (\mathrm{OVERT}) + 0.02969417\ (\mathrm{INTT}) \\ & + 0.00000036\ (\mathrm{OVERE}) - 0.00000323\ (\mathrm{INTE}) \\ & + 0.00002369\ (\mathrm{TLOAD})\ (r^2 = 0.81) \end{aligned} \tag{5.1}$$

$$\begin{aligned} \mathrm{LN}\ (\mathrm{E11\ acc}) = {} & -8.56364689 - 0.13271718(\mathrm{OVERT}) + 0.07007914(\mathrm{INTT}) \\ & - 0.00000106(\mathrm{OVERE}) - 0.00000867(\mathrm{INTE}) \\ & + 0.00009949(\mathrm{TLOAD})\ (r^2 = 0.95) \end{aligned} \tag{5.2}$$

$$\begin{aligned} \mathrm{LN}\ (\mathrm{S11\ pcc}) = {} & 4.63229673 - 0.20279632\ (\mathrm{OVERT}) - 0.04280466\ (\mathrm{INTT}) \\ & - 0.09656849\ (\mathrm{PCCT}) - 0.00000010\ (\mathrm{OVERE}) + 0.00000007\ (\mathrm{PCCE}) \\ & - 0.00000060\ (\mathrm{SUBE}) - 0.00000894\ (\mathrm{SOILE}) \\ & + 0.00009449\ (\mathrm{TLOAD})\ (r^2 = 0.92) \end{aligned} \tag{5.3}$$

where

S11 = tensile stress (psi),

E11 = tensile strain,

OVERT = ACC layer thickness (inch),

INTT = flexible base layer thickness (inch),

PCCT = PCC layer thickness (inch),

OVERE = stiffness of ACC layer (psi),

INTE	=	stiffness of flexible interlayer (psi),
PCCE	=	stiffness of PCC layer (psi),
SUBE	=	stiffness of subbase layer (psi),
soile	=	stiffness of soil layer (psi), and
TLOAD	=	traffic load (LB).

Figures 5.3 through 5.5 compare the plots of the independent variables and predicted values from Equations 5.1 through 5.3. The estimated values are plotted versus the observed values of the independent variables. There is good correlation of the tensile strain in the ACC and of stress in the PCC layer in the above regression equations. Therefore, they can be confidently used to calculate pavement response under traffic loading. However, the tensile stress in the ACC layer shows that the estimation tends to be lower than the observed values and varies over a wider range.

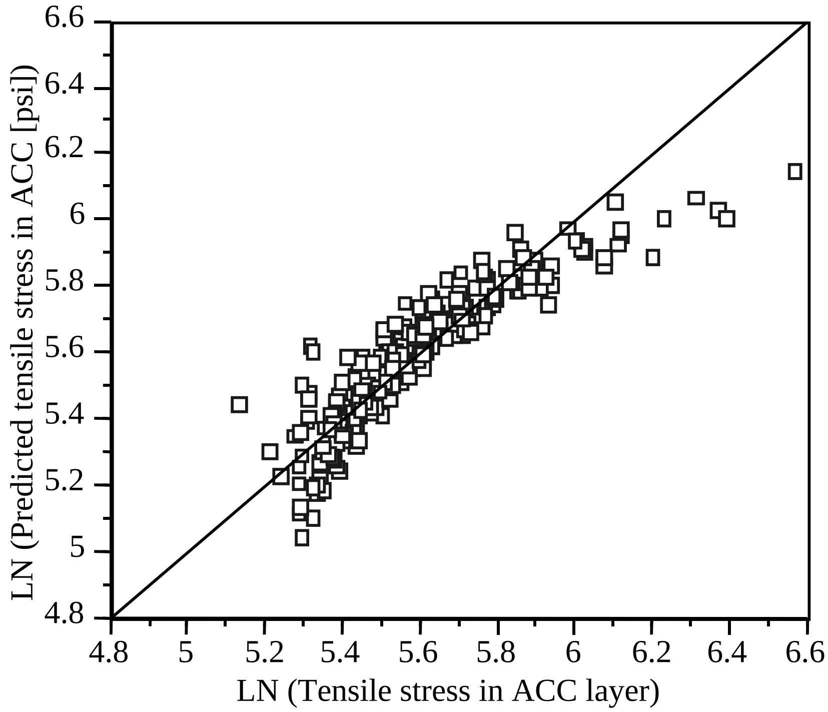

Figure 5.3. The calculated and predicted values from the regression model — tensile stress in ACC layer

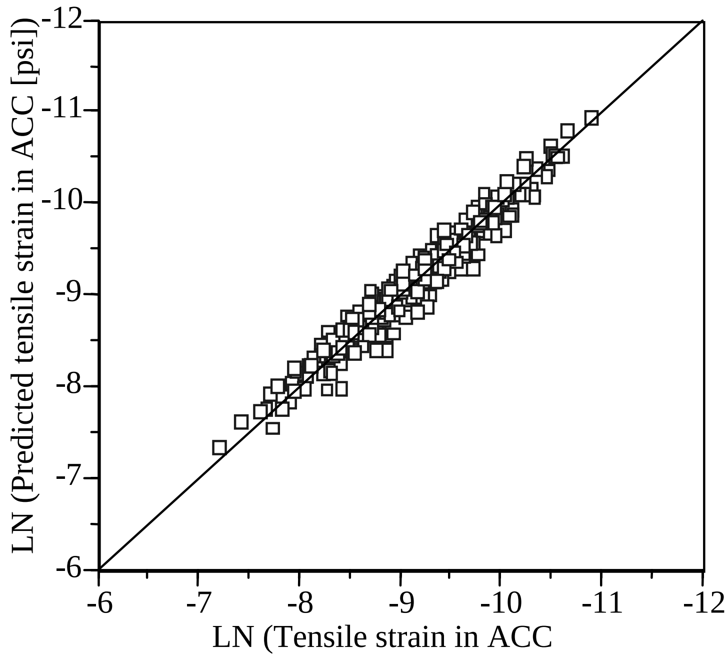

Figure 5.4. The calculated and predicted values from the regression model — tensile strain in ACC layer

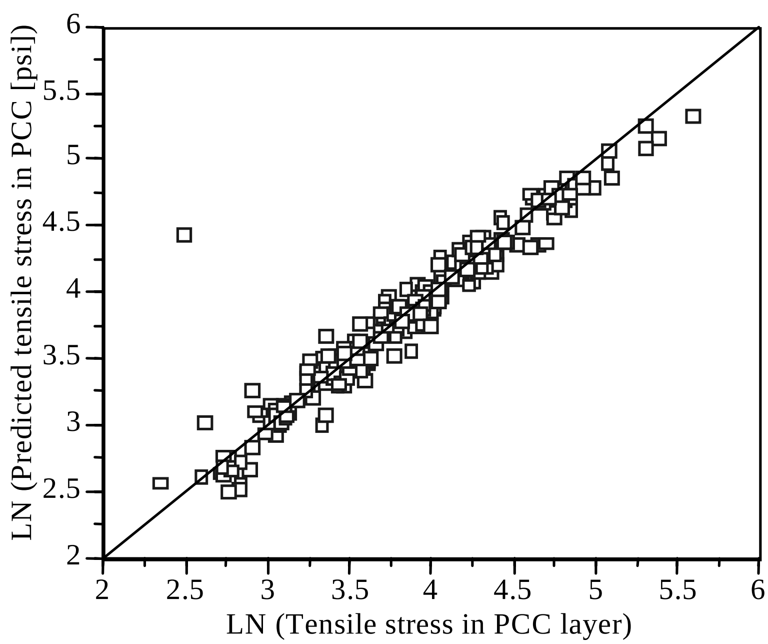

Figure 5.5. The calculated and predicted values from the regression model — tensile stress in the PCC layer

In addition to the tensile stresses of both layers, the vertical compressive stress and strain on the flexible interlayer are given by the following equations. As shown in Equation 5.4, the compressive stress at the top of the flexible base interlayer depends on the thickness of both the overlay and the flexible base layer. The compressive stress decreases as the thickness of the ACC and flexible interlayer increases. However, this stress definitely increases as the weight of the traffic load increases. Equation 5.5 can be used to predict compressive strain at the top of the flexible base interlayer. Figures 5.6 and 5.7 display the relationship between independent variables and predicted values. They support the feasibility of these regression models.

$$
\begin{aligned}
\text{LN (S22 int.)} = \;& 4.08694771 - 0.17349215\ (\text{OVERT}) - 0.06825335\ (\text{INTT}) \\
& - 0.00000056\ (\text{OVERE})\ \ 0.00000469\ (\text{INTE}) \\
& + 0.00009946\ (\text{TLOAD})\ (\ r^2 = 0.97)
\end{aligned}
\tag{5.4}
$$

$$
\begin{aligned}
\text{LN (E22 int.)} = \;& -6.32905920 - 0.16251076\ (\text{OVERT}) - 0.03088967\ (\text{INTT}) \\
& - 0.00000072\ (\text{OVERE}) - 0.00001186\ (\text{INTE}) \\
& + 0.00009937\ (\text{TLOAD})\ (\ r^2 = 0.95)
\end{aligned}
\tag{5.5}
$$

where

S22 = vertical compression stress (psi), and

E22 = vertical compression strain.

We also developed the regression model for the surface curvature index (SCI), which can be related to the rut depth appearing in the ACC layer with the flexible interlayer on JCP (Cho and McCullough, CTR Report 987-4). The SCI can be predicted by linear combinations of independent variables, such as overlay, flexible base thickness, and stiffness, and the weight of traffic loads. The SCI increases with the increasing thickness of the interlayer. This agrees with the filed observations to some extent.

$$
\begin{aligned}
\text{LN (SCI)} = \;& -5.54678965 - 0.12142416\ (\text{OVERT}) + 0.07532402\ (\text{INTT}) \\
& - 0.00000118\ (\text{OVERE}) - 0.00000651\ (\text{INTE}) \\
& + 0.00009923\ (\text{TLOAD})\ (\ r^2 = 0.90)
\end{aligned}
\tag{5.6}
$$

However, the above stress prediction models might not be used for pavements that have an ACC layer directly on the PCC layer. Therefore, another factorial set with an extra eighty-one sets of combinations is required, as shown in Table 5.7. The only difference between Table 5.1 and Table 5.7 is the level of the thickness of the ACC layer. Figure 5.8 shows the tensile stress distribution in the ACC layer as a function of interlayer thickness for all combinations. It shows that the ACC would develop compression only when no interlayer is used in the design. The regression model for predicting the tensile stress on top of the PCC is suggested as:

$$\begin{aligned} LN\ (s11\ pcc) = \ & 4.59308409 - 0.05820957\ (OVERT) - 0.03465072\ (INTT) \\ & - 0.09722697\ (PCCT) - 0.00000012\ (OVERE) + 0.00000008\ (PCCE) \\ & - 0.00000059\ (SUBE) - 0.00000900\ (SOILE) \\ & + 0.00009479\ (TLOAD)\ (r2= 0.92) \end{aligned} \tag{5.7}$$

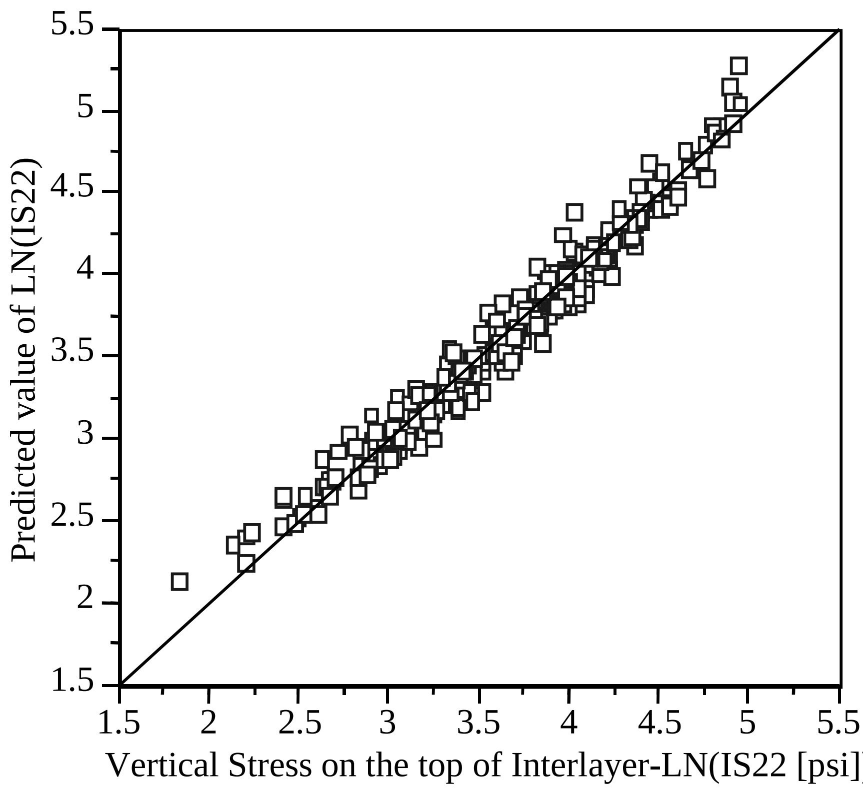

Figure 5.6. The calculated and predicted values from the regression model — vertical compressive stress at the top of interlayer

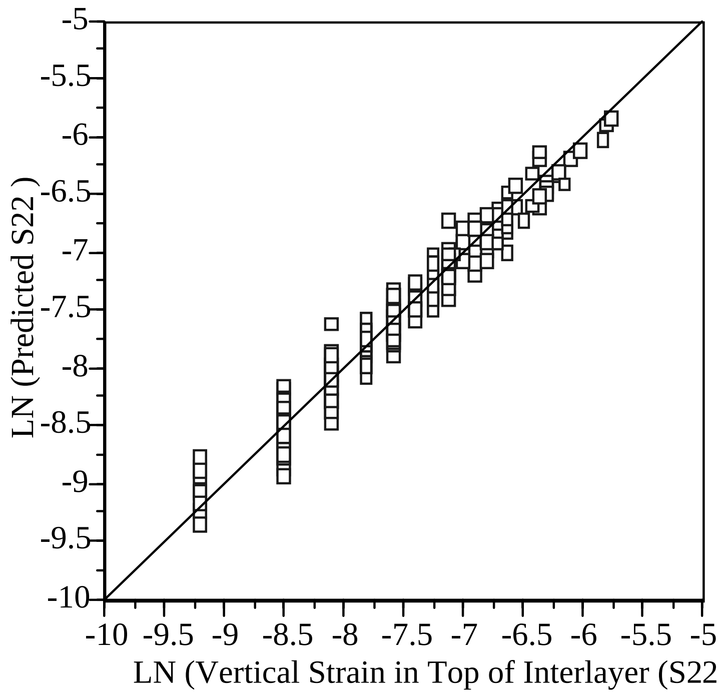

Figure 5.7. The calculated and predicted values from the regression model — vertical compressive strain at the top of interlayer

Table 5.7. Ten factors and three levels in the fractional factorial design under traffic loading

	Factor	Level 1	Level 2	Level 3
Single wheel (lbf)		6000	9000	15000
Thickness (inch)	Overlay	3	6	9
	Interlayer	0	4	8
	Existing pavement	8	12	16
	Subbase	0	6	8
Stiffness (psi)	Overlay	200,000	600,000	1,000,000
	Interlayer	25,000	50,000	100,000
	Existing pavement	3,500,000	5,500,000	7,500,000
	Subbase	50,000	500,000	1,000,000
	Subgrade	5,000	20,000	40,000

1 inch = 25.4 mm, 1 psi = 6.897 kPa, 1 pci = 2.767*10^4 kg/m, 1 lb = 4.45 N

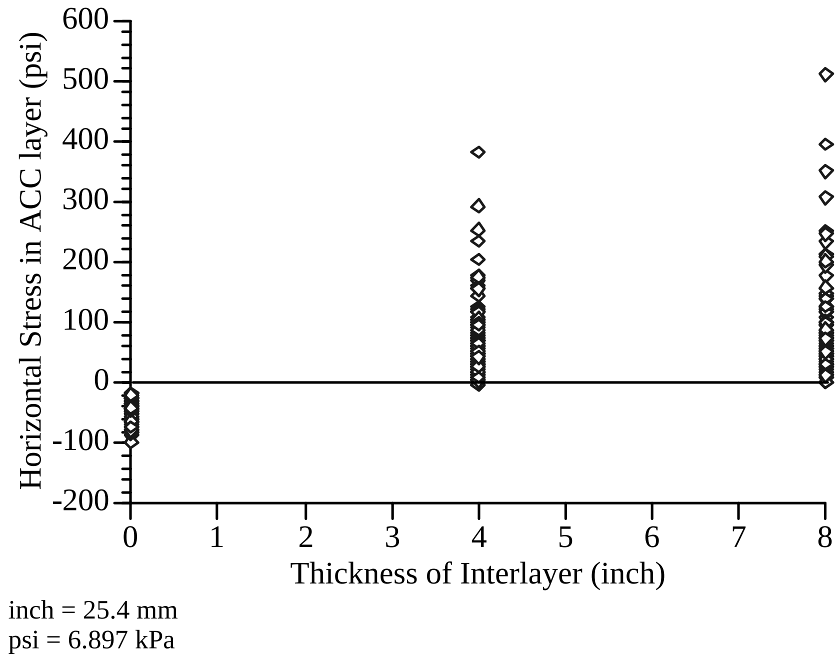

Figure 5.8. Tensile stress variation in ACC layer by changing the thickness of interlayer

Stress/strain Prediction Model under Thermal Loading: The same regression approaches are taken to obtain the equation for the tensile stress in both the ACC and PCC layer. The developed model, Equation 5.8, indicates that the tensile stress increases with increases in joints or crack spacing. In addition, the thickness of both the ACC and flexible base layer inversely affects stress development. The equation is consistent with engineering judgment, even though the predicted values do not match very well with the observed values, shown in Figure 5.9. Equation 5.9 shows the tensile stress prediction model for the PCC layer. It shows a fairly good linear relation between the selected variable and the observed value (see Figure 5.10).

$$
\begin{aligned}
LN\ (s11\ acc) = \ & 6.24917801 + 0.00595422\ (JOINTL) - 0.01311287\ (OVERT) \\
& - 0.08367148\ (INTT) + 0.00000062\ (OVERE) + 0.00000096\ (INTE) \\
& + 0.00476727\ (ACCA) + 0.03851593\ (PCCA) \\
& + 0.01256709\ (TEMP)\ \ (r2 = 0.49)
\end{aligned}
\tag{5.8}
$$

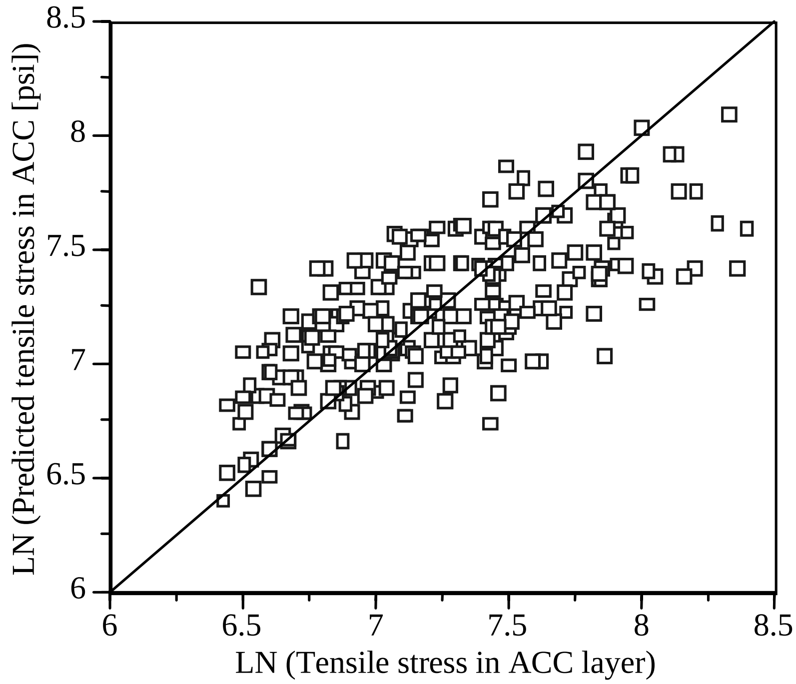

Figure 5.9. The calculated and predicted values from the regression model — tensile stress in ACC layer by thermal loading (psi = 6.897 kPa)

$$\begin{aligned} \text{LN (s11 pcc)} = {} & 2.45190285 + 0.03277117\ (\text{JOINTL}) + 0.04949690\ (\text{OVERT}) \\ & + 0.05425837\ (\text{INTT}) + 0.00000017\ (\text{PCCE}) + 0.15333618\ (\text{PCCA}) \\ & + 0.01934426\ (\text{TEMP})\quad (r2= 0.85) \end{aligned} \tag{5.9}$$

where

JOINTL	=	spacing of contraction joint or crack (ft, 1 ft = 0.304 m),
OVERT	=	ACC layer thickness (inch, inch = 25.4 mm),
INTT	=	flexible base layer thickness(inch, inch = 25.4 mm),
OVERE	=	stiffness of ACC layer (psi, psi = 6.897 kPa),
INTE	=	stiffness of flexible base layer (psi, psi = 6.897 kPa),
ACCA	=	thermal coefficient of ACC layer (in./in./F, °F= 9/5 °C+32),
PCCA	=	thermal coefficient of PCC layer (in./in./F, °F= 9/5 °C+32), and
TEMP	=	maximum temperature differentials (F/Day, °F= 9/5 °C+32).

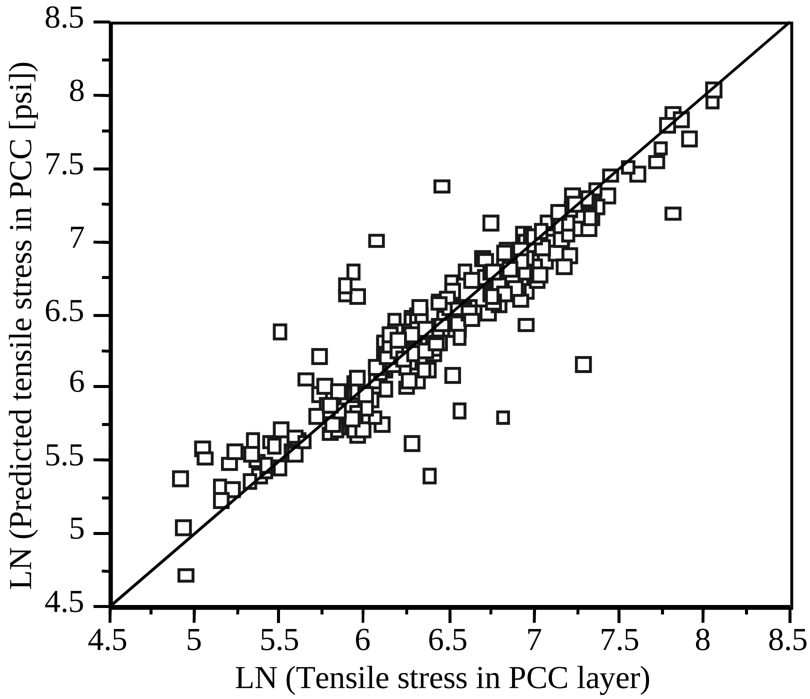

Figure 5.10. The calculated and predicted values from the regression model — tensile stress in PCC layer by thermal loading

CALIBRATION OF DEVELOPED MODEL FROM THE FIELD RESULTS

In previous sections, we discussed the regression models for predicting pavement rutting, fatigue cracking, and reflection cracking. The maximum compressive criterion may be imposed to restrain the rut depth development in the interlayer. The maximum compressive strain at the top of the subgrade was required to be less than $1.05*10^{-3}$ mm/mm by Monismith, $6.0*10^{-4}$ mm/mm by Saraf and Finn, and $1.06 * 10^{-3}$ mm/mm by Dorman and Metcalf. Empirical results suggested by Monismith and Dorman-Metcalf shown in Figure 5.11 are applied to estimate the rut depth using Equation 5.5.

Fatigue cracking can be predicted using the fatigue models for the ACC and PCC. The reflection cracking can be predicted using Equation 5.8. The test section consisted of various thickness combinations with different stiffnesses. The stiffness of each layer is backcalculated from the procedure explained in Report 987-4 (Cho and McCullough 1994). For example, the stiffness of the ACC layer is estimated as 2,757.6 MPa (400,000 psi), 344.7 MPa (50,000 psi) for the flexible base, and 17,235 MPa (2,500,000 psi) for the JCP in section R3. The stiffness of the ACC during the winter goes up to 5,515.2 MPa (800,000 psi). The thermal coefficient of the JCP is assumed to be $2.22*10^{-6}$ m/m/C ($4*10^{-6}$ in./in./°F), owing to the aggregate mixed in the JCP. The thermal coefficient of the ACC is given as $7.78*10^{-6}$ m/m/°C ($14*10^{-6}$ in./in./°F). The maximum daily temperature differential is reported as 16.67°C (30/°F). The total accumulated traffic occurring over 1.5 years on the right lane is about 900,000 ESALs.

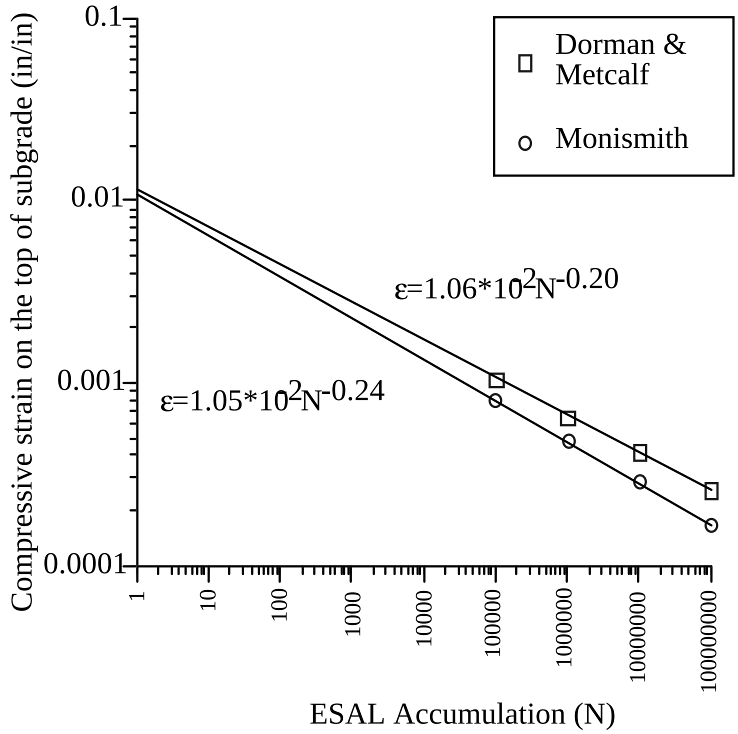

Figure 5.11. Maximum compressive strain criteria for the rut depth prediction

Table 5.8 shows the approximation of stress/strain for each layer for the 7.44 metric ton (8.2 ton, or 18,000 lb) single axle traffic load. For example, in test section R3, the maximum tensile stress is calculated as 2088.8 kPa (303 psi) for the ACC and 455.0 kPa (66 psi) for the PCC, respectively. The compressive strain was estimated as $8.67*10^{-4}$ m/m, with 408.81 kPa (59.3 psi) of vertical stress at the top of the subgrade. The distresses for each section can be predicted by the damage model based on the calculated stress and strain.

Table 5.8. Stress/strain prediction of test sections in US 59 under traffic loading

	Thickness (inch)			Stiffness (psi)					Pavement Behavior Models			
	ACC	Int.	PCC	ACC	INT.	PCC	SUBBASE	SOIL	S11-ACC (psi)	E11-ACC (in/in, m/m)	S11-PCC (psi)	E22-INT. (in/in)
R1	4	0	7	400000	0	3425	0	12000	0	*	79.60	
R2A	4	0	7	400000	0	430	0	12000	0	*	79.58	
R2B	5.5	0	7	400000	0	513	0	12000	0	*	72.93	
R3	3	8	7	400000	50000	2165	0	12000	303	2.33E-04	65.88	8.67E-4
R4	1.5	13	7	400000	450000	3934	0	12000	101	1.26E-05	57.88	
R5	3	8.5	7	400000	450000	4133	0	12000	84	7.53E-06	64.48	
R6	3	7	7	400000	450000	2704	0	12000	81	6.78E-06	68.76	
R0	1.5	7	7	400000	450000	2980	0	12000	85	8.28E-06	74.83	

1 inch = 25.4 mm, 1 psi = 6.897 kPa

The rutting on test section R3 can then be obtained. The estimated ESAL application for a limit of 10 mm of rutting (0.39 in.) is given as 2.54E+05 using Monismith's equation. Next, an ESAL of 7.10E+04 can be applied according to Dorman's equation. The rutting development for test section R3 versus ESAL is shown in Figure 5.12; it can be inferred from the graph that at the beginning of the loading application, rut depth increases rapidly and then maintains a steady state of development after initial rutting. However, the estimates derived from both Monismith's and Dorman's model can be interpreted as relatively conservative, though actually they are quite accurate (since theirs is a regression type equation). The shift factor *c* for the rutting can be assumed to be approximately 2.0 when calibrating the model with the results from test section R3.

Fatigue crack development is a function of tensile stress/strain at the bottom of the ACC layer and the PCC layer. The tensile stress of the ACC layer is estimated using Equation 5.1; the number of traffic loads required to cause fatigue cracking can then be predicted. The tensile strain in the ACC can also be estimated using Equation 5.2, and its fatigue life can be predicted using fatigue equations (shown in Table 5.9). The fatigue life based on the tensile strain suggested by Kennedy is shorter than the fatigue life predicted using Finn's equation. Finn's prediction works rather well, although it underestimates the field performance: Fatigue cracking appeared on the test section after about 0.53 million ESALs. The shift factor from this single test section is c=1.8 when using Finn's equation.

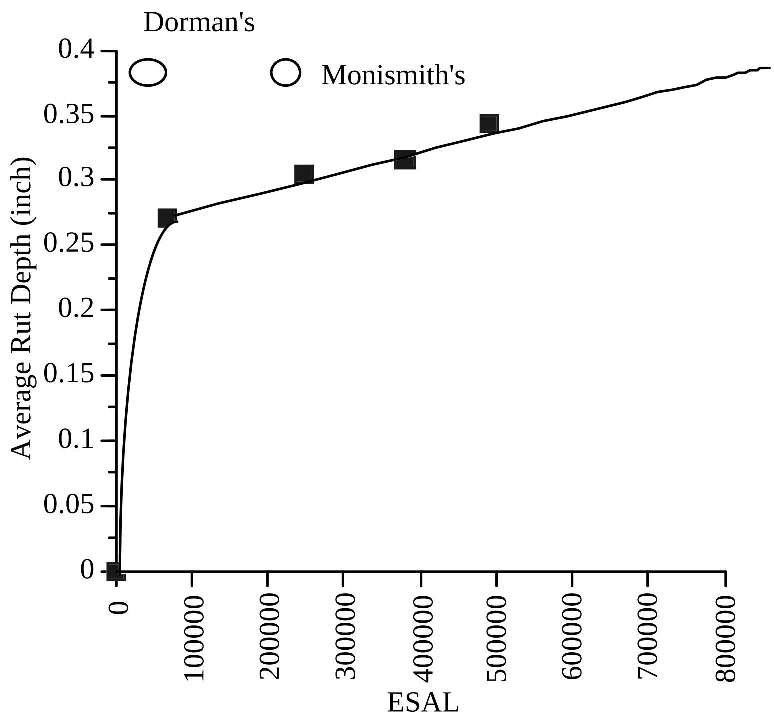

inch = 25.4 mm

Figure 5.12. Rut depth development under the traffic loading in section R3

Table 5.9. Calibration of distress in the test section R3

	Tensile Stress (psi)	*Fatigue Life*	*Tensile Strain (in./in.)*	*Fatigue Life*		*Tensile Stress(psi)*	*Fatigue Life*
	ACC	*Kennedy*	*ACC*	*Kennedy*	*Finn*	*S11-PCC*	*Texas*
R3	302.92	8	2.33E-04	9.93E+02	303482	65.88	2.01E+07

1 inch = 25.4 mm, 1 psi = 6.897 kPa

Reflection cracks are predicted based on the tensile stress of the ACC layer from Equation 5.8. Table 5.10 and Figure 5.13 show the estimated tensile stress for the ACC layer. These tables show that the predicted tensile stress is higher than the estimated tensile strength of the ACC layer, except for sections R3 and R4. These two sections are identified as the test sections that perform well against reflection cracking. They show that the tensile stress estimation model can be applied to predict reflection cracking at an earlier age.

Table 5.10. Stress/strain prediction of test sections constructed in US 59 under temperature

	Thickness (inch)				*Stiffness (psi)*			*Thermal coefficient (in./in./° F)*		*temp (°F)*	*Tensile Stress (psi)*	
	Joint	*ACC*	*Int.*	*PCC*	*ACC*	*INT.*	*PCC*	*ACC*	*PCC*		*ACC*	*PCC*
R1	15	4	0	7	600000	0	3425	1.50E-05	4.50E-06	30	1136	41.36
R2A	15	4	0	7	600000	0	430	1.50E-05	4.50E-06	30	1136	41.34
R2B	15	6	0	7	600000	0	513	1.50E-05	4.50E-06	30	1114	44.53
R3	15	3	8	7	600000	50000	2165	1.50E-05	4.50E-06	30	618	60.75
R4	15	2	13	7	600000	450000	3934	1.50E-05	4.50E-06	30	609	74.00
R5	15	3	9	7	600000	450000	4133	1.50E-05	4.50E-06	30	870	62.44
R6	15	3	7	7	600000	450000	2704	1.50E-05	4.50E-06	30	987	57.54
R0	15	2	7	7	600000	450000	2980	1.50E-05	4.50E-06	30	1006	53.43

1 inch = 25.4 mm, 1 psi = 6.897 kPa, 1 °F= 9/5 °C+32

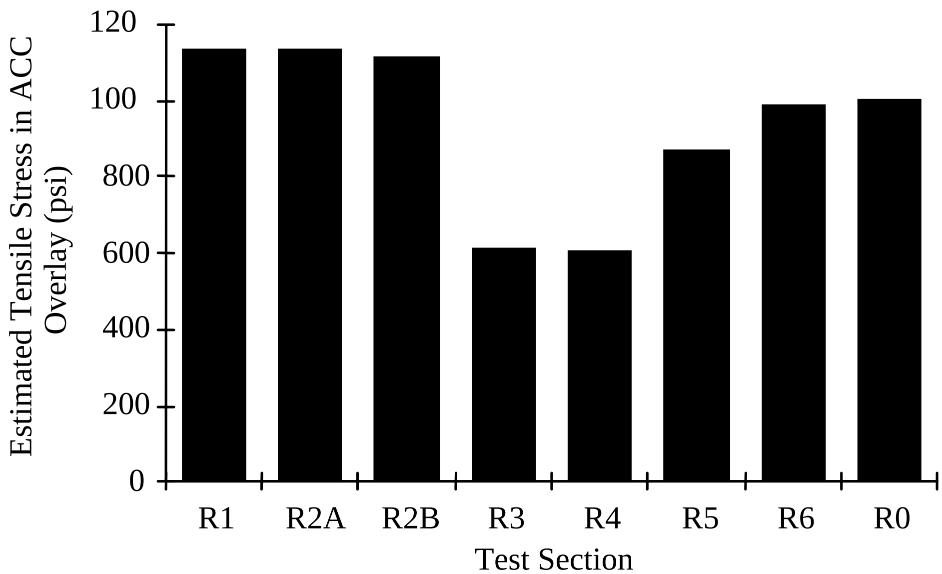

inch = 25.4 mm
psi = 6.897 kPa

Figure 5.13. Predicted thermal tensile stress of the test section

DESIGN EXAMPLE

The application of the performance prediction model into pavement design is briefly illustrated using the following sample problem. The PCC pavement is a 254 mm (10 in.) thick JCP with contraction joint spacing of 4.56 m (15 ft). The resilient modulus of the PCC layer and the soil layer are assumed to be 27,576 MPa (4,000,000 psi) and 103.4 MPa (15000 psi), respectively. The flexural strength of the PCC is assumed to be 3447 kPa (500 psi). The tensile strength of the ACC for this example is 4481 kPa (650 psi) during the winter. The maximum temperature differential during the winter is assumed to be 16.67°C/day (30 °F/day). The design ESAL is given as 15,000,000 ESALs. The average unit price of the flexible base layer is estimated at $28.88/CY, and the ACC surface Type C is estimated at $75.09/CY (e.g., test section R3).

An interlayer having a thickness ranging from 0 to 203 mm (8 in.) is considered in this design. The desired ESAL and cost are the criteria in selecting the thickness of the ACC layer with/without an interlayer. Figure 5.14 shows the fatigue life of the ACC layer with a flexible interlayer. The example shows that the design ESAL increases as the thickness of the flexible layer decreases. For example, while the design ESAL for 50.8 mm (2 in.) of the interlayer is over 12 million ESALs, it is only 4 million ESALs when the ACC layer is 152.4 mm (6 in.) thick.

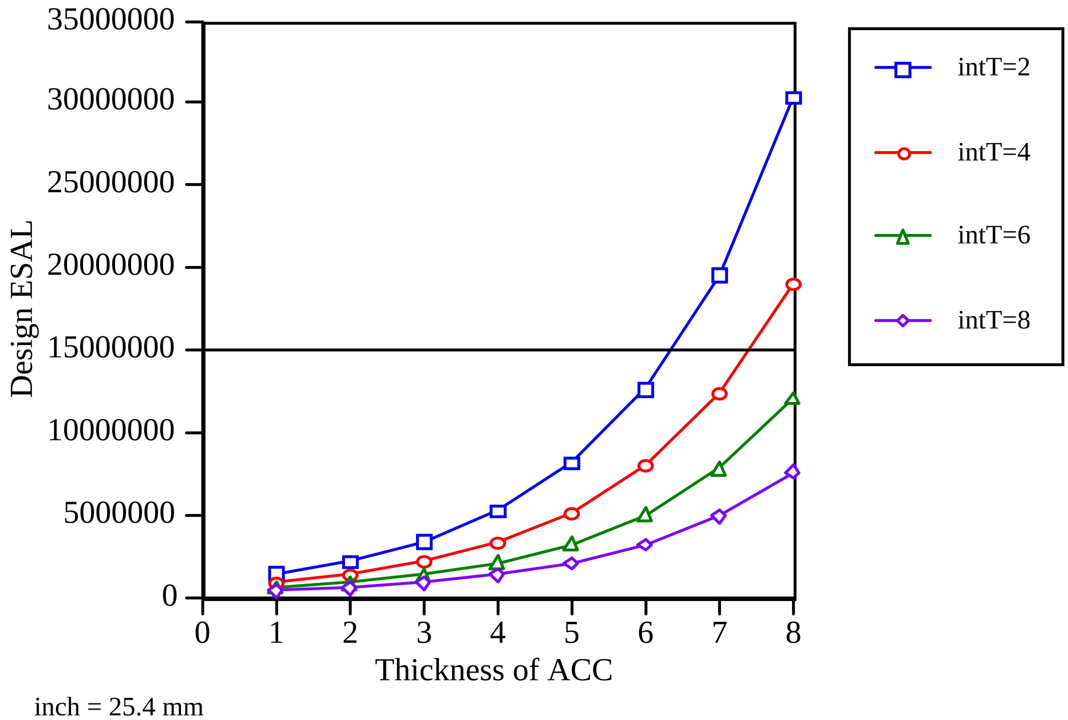

Figure 5.14. Design thickness from the ACC fatigue criteria for various interlayers and AC thickness

The rutting criterion is also applied to the overlay design as shown in Figure 5.15. Many combinations are generated, including a 165.1-mm (6.5-in.) ACC layer with a 203.2-

mm (8-in.) flexible base layer or a 190.5-mm (7.5-in.) ACC layer with a 111.6-mm (4-in.) flexible base layer. The thickness requirement ranges from 165 mm to 90 mm for the ACC layer, and from 110 to 200 mm for the flexible base. It was found that the combination of a 101.6-mm (4-in.) ACC layer and a 101.6 mm (4-in.) flexible base layer is the solution for this design.

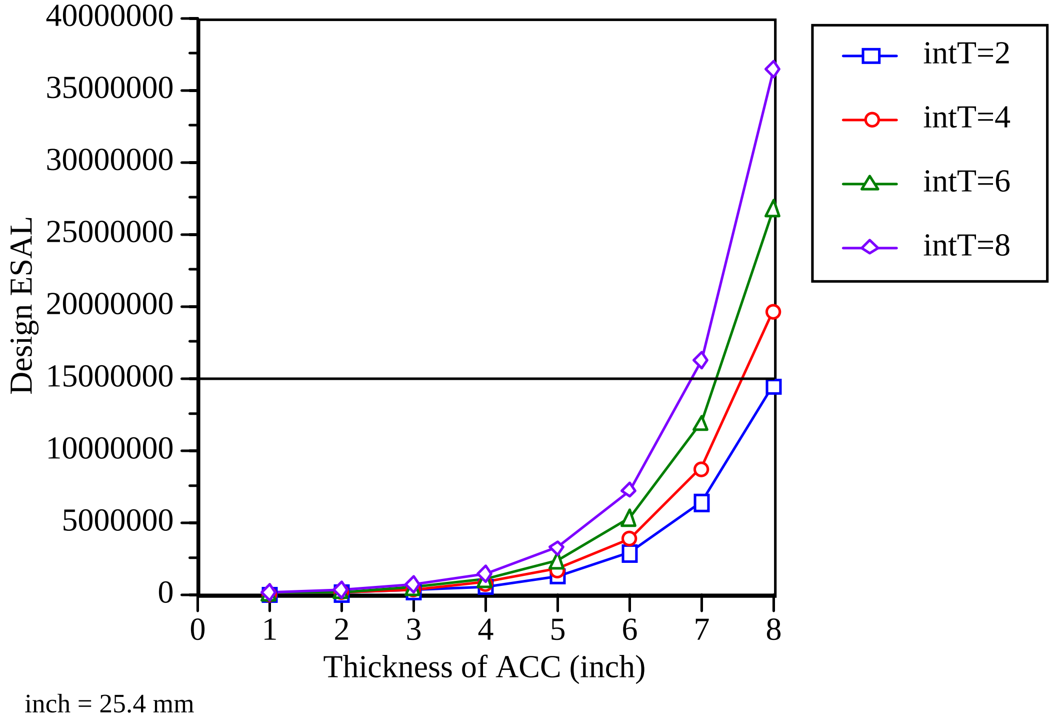

Figure 5.15. Design thickness from the rutting criteria for various interlayers and AC thickness

The reflection cracking is considered simply as a stress-and-strength relationship. The tensile strength of the ACC layer is estimated as 4480 kPa (650 psi). The estimated stresses for four different interlayers show that the reflection cracking in asphalt should not develop within the design limit for traffic loading when a flexible base of over 152.4 mm (6 in.) is used in the design, shown in Figure 5.16. Considering the reflection cracking criteria, the combination of a 152.4-mm (6-in.) flexible base 76.2 mm (3 in.) below the ACC layer, is suggested for the design.

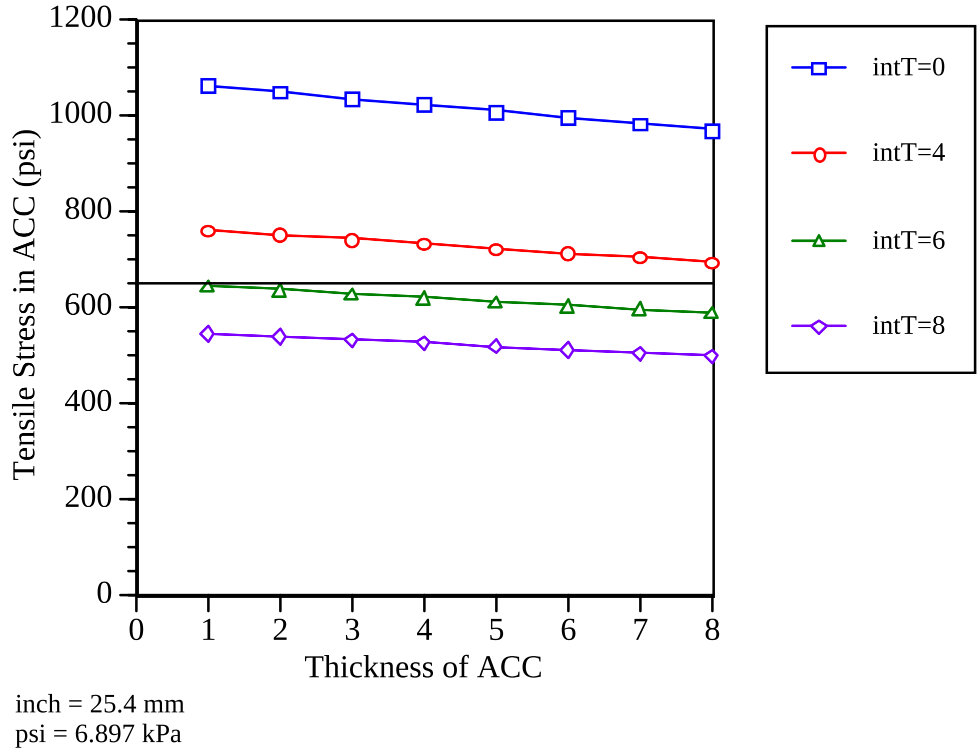

Figure 5.16. Tensile stress calculation of the example problem for various interlayers and AC thickness

Figure 5.17 shows the design ESAL versus the design thickness of the ACC layer for the decision criteria for the PCC layer. The prescribed thickness of the ACC is not affected by the fatigue life of the PCC layer, because only 25.4 or 50.8 mm (1 or 2 in.) of ACC overlay without flexible interlayer is used in those cases where the design ESAL is lower than the given ESAL. It is found that a 50.8-mm (2-in.) ACC and a 101.6-mm (4-in.) flexible base combination is the desirable recipe for the given PCC fatigue criteria.

FURTHER RESEARCH

We have described a method for the design of overlay thicknesses based on the developed performance prediction models. The traffic and temperature effects on the ACC overlay can be taken into account by the performance equation developed using statistical methods. Although this method can be applied to other asphalt overlay situations, it is recommended for ACC overlays supported by a flexible base interlayer. Pavement response resulting from traffic loading and temperature variation in the structure is considered separately owing to the limitations of the FEM approaches. Thus, we recommend further efforts be undertaken to better understand the response of pavements subjected to traffic loading and temperature variation. The damage models, serving as bridges linking theory and practice, can be improved by taking into account the material properties that characterize the pavement structures of highways in Texas.

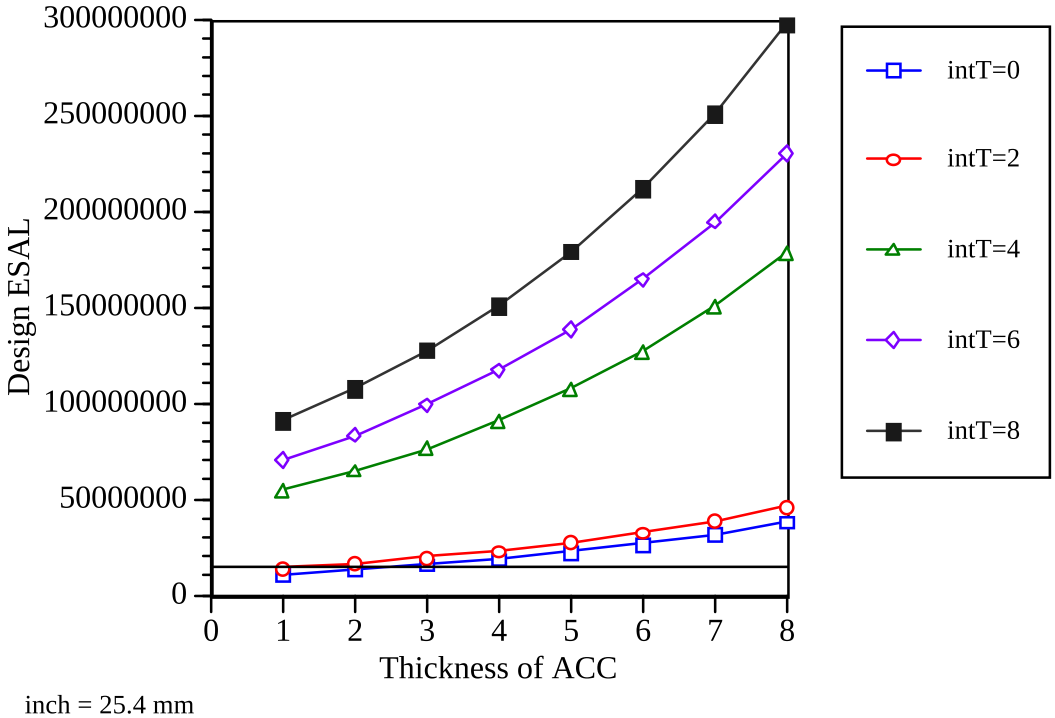

Figure 5.17. Design thickness from the PCC fatigue criteria

CHAPTER 6. CONCLUSIONS AND FURTHER RESEARCH

This report summarized the findings of a research project undertaken (1) to collect performance data on rehabilitation methods, (2) to seek an ACP overlay method that can prevent reflection cracking, and (3) to provide a design tool that can be used in developing a long-range rehabilitation plan not only for US 59 in the Lufkin District, but for other highways in Texas as well. In this report, we focused on structural performance by examining three distinct distresses of an ACC overlay, namely, fatigue cracking, reflective cracking, and rutting. Seven test sections (six alternative and one control section) were constructed on US 59 as an experimental study designed to observe pavement performance under mixed traffic and environmental conditions.

Theoretical modeling of the pavement structure (covering both traffic and temperature conditions) was developed using the finite element method (FEM). The FEM modeling of the pavement structure was initially reviewed using three different approaches: axisymmetric modeling, plane strain, and full three-dimensional modeling. Because three-dimensional modeling is time and labor intensive (and requires extensive computer memory), this study pursued a two-dimensional model that could replace a three-dimensional model. Axisymmetric modeling matched existing solutions well for traffic loadings, while the plane strain model was sufficiently accurate to replace the three-dimensional model for thermal loading analysis. This means that the modeling procedure must be carried out separately for traffic and temperature loadings.

PERFORMANCE EVALUATION OF EACH REHABILITATION ALTERNATIVE FOR THE TEST SECTIONS

The six alternative sections and one control section performed differently under the same traffic loadings and environmental conditions. While reflective cracking cannot be eliminated, it can be kept at acceptable levels by some of the rehabilitation alternatives studied. Table 6.1 summarizes the costs and performance of the rigid test sections for the different pavement attributes monitored throughout this study.

Table 6.1. Performance of summary for the test sections

	R1	R2A	R2B	R3	R4	R5	R6	R0
Cost ($/SY)	$32.89	$16.04	$17.64	$21.82	$22.05	$9.86	$7.35	$4.62
Deflection	G	B	B	B	G	G	N	N
Rutting	G	B	N	B	G	G	G	N
Condition	N	B	G	G	G	N	N	N
Profile	N	B	B	N	G	G	G	G
RC	B	B	N	G	N	N	B	B

*G=Good, N=Normal, B=Bad, RC=Reflective Cracking

Thicker asphalt pavement does not prevent reflection cracking (even pavements up to 28 m [11 in.] thick). The break and seat method does increase fatigue cracking on the surface by decreasing the stiffness of portland cement concrete (PCC). The crack-repaired section is not immune to reflection cracking. However, little reflection cracking occurred on the interlayered sections during the first 3-year observation period. The open-graded asphalt mix has shown that only light reflection cracking will occur on the surface for the first 2 years of service. Compared with the conventional construction recipe (i.e., overlay recipe R0), the insertion of a relief interlayer can retard reflection cracking.

Using the thicker flexible base layer and Arkansas mix might cause traffic-induced rutting. The flexible interlayered test sections experienced more severe rutting problems right after they were opened to traffic. Thus, there is a possible trade-off between rutting with the insertion of an interlayer and reflection cracking (without using an interlayer). We might draw the following conclusions for the test sections:

1. Section R1 with no sawcuts in its surface exhibits reflection cracks. The sawcut sections also exhibit reflective cracking when the sawcut line does not lie right above the existing joints. The preoverlay repair of the existing JCP strengthens the pavement structure, leading to a better overall performance of the section.
2. Section R2A exhibited both reflective cracks and fatigue cracks as a result of low structural strength caused by the crack and seat method. Along with the reduced stiffness, relatively large ruts are observed for this test section. The section also experienced pumping problems. These kinds of structural deficiencies led to unexpected early functional failure. Section R2B showed fewer problems than did section R2A; the thicker ACC overlay for section R2B may explain this finding.
3. Reflective cracking is not a problem in section R3; but relatively deeper rutting appears in the section. The deflection test results indicate a large surface curvature index associated with a shear mode of failure, such as rutting. This finding shows that there is a trade-off between retarding reflective cracks and reducing rut depth when applying recipe R3 to overlay rigid pavements. Considering the good performance in the left lane, we recommend this method for highways having relatively low traffic volumes.
4. Section R4 represents the best rehabilitation solution, based on condition survey results, rut depth measurements, deflections, and profile. Both rutting and reflection cracking do not appear to be noticeable; moreover, both low IRI and high serviceability index are observed for the section. However, constructing this section was costly. It can be selected as an alternative method for rigid pavements having high traffic loading.
5. Reflective cracking developed after the second winter in test section R5. This section presented the best surface condition during the first year, though it later deteriorated because of hairline cracking caused by reflective action. No rutting

problems were observed. Considering its relatively lower cost and better performance, it represents an option for highway rehabilitation.

6. Test section R6 (with Type C mix) is very resistant to reflective cracking; it definitely performs better than control section R0. Hairline cracks reflected after 2 years in test section R6. Deflections found in section R6 are lower than those found in other test sections; no rutting problem is observed. This section is still providing good serviceability.
7. Test section R0 developed 100% reflective cracks of 4.56-m (15-ft) crack spacing just after 2 years of temperature loading cycles. A rapid increase in deflection was observed, and its longitudinal surface roughness also increased with traffic loading. Fair serviceability and fair IRI were observed for the section; no rutting problem is present.

TRAFFIC LOADING EFFECT ON THE PERFORMANCE OF ACC OVERLAY ON RIGID PAVEMENTS

In this report, we have focused on explaining the effect of an interlayer on the performance of overlays using FEM modeling. To apply the FEM axisymmetric modeling, we identified and selected ten significant factors. In addition, we have found the following:

1. The ACC on the rigid pavement without flexible base layer does not experience any tensile stress under traffic loadings. This means fatigue cracking on the ACC layer is not expected. However, the ACC layer with flexible base layer experiences tensile stresses at the bottom, which may trigger fatigue cracking.
2. The estimated tensile stress is inversely affected by the thickness of the flexible base layer. The tensile stress in the surface layer increases as the thickness of the interlayer is increased.
3. The vertical strain on the top of the flexible layer, which is used as an indicator of permanent deformation, increases as the thickness of ACC and flexible base decreases.
4. The stiffness and thickness of the PCC layer does not strongly influence pavement response. In other words, the existing rigid pavement is not strongly related to the performance of the ACC layer under traffic loading.
5. The peak deflection basin found from dynamic analysis is the same as that found from static analysis; however, the tensile stress is not the same. The tensile stress within the AC layer generated by a high-speed vehicle is about 12% higher than that found in static loading, and about 20% lower at lower speeds. Comparing dynamic versus static analysis results, the static loading corresponds to a vehicle loading at about 30 mph.
6. Pavement behavior under tandem- and single-axle loads differs notably. The deflection of single- and tandem-axle loads do not vary significantly under light

loads; but the prediction obtained using dynamic analysis differs substantially from that obtained using static analysis for heavy loads. It is shown that tandem axles induced almost 50% less deflection than single axles under heavier traffic loading. In addition, tandem axle loads reduce stress in both ACC and PCC layers significantly, as compared with the equal weight of a single-axle load.

TEMPERATURE EFFECT ON THE ACC OVERLAY ON RIGID PAVEMENTS

The temperature prediction model, used with a multilayer pavement structure, was developed based on both weather information and on a heat transfer model. Because the predicted temperature is higher than the observed temperature, a calibration process is carried out so as to yield desirable results. Predictions using the model reveal that temperature variation in the upper layer is more significant than that in the lower layer.

The thermal stress prediction model was developed based on the plane strain model. The maximum tensile stress appears on the ACC layer surface, where the discontinuity of the rigid pavement exists. This model can explain reflection crack development by comparing the stress and strength relationships. The variation of deflection, as well as the maximum tensile stresses in both ACC and PCC layers, is used as an indicator of the sensitivity analyses. From the sensitivity analysis, the following conclusions were drawn:

1. The tensile stress of the ACC without an interlayer matches the strength of the ACC layer during the winter, while the tensile stress within the flexible base layer decreases dramatically as the thickness of the base layer increases. The tensile stress on the ACC layer also increases as the stiffness of the interlayer increases.
2. Using a thicker ACC overlay to retard reflection cracking is not as effective as inserting an interlayer. A thicker ACC layer is not necessary for thermal loading unless the traffic loading requires a thicker pavement. It was found that the stress magnitude in ACC in summer is 10% of that in ACC in winter. This means that the effect of stiffness on ACC performance is critical in determining how soon the reflection cracks will develop.
3. Neither the stiffness nor the PCC layer thickness strongly affects stress development within an ACC layer.
4. The thermal coefficient of both ACC and PCC layers significantly impacts the stress in each layer. Varying the thermal coefficient of ACC changes the tensile stress in the ACC layer substantially, but not in the PCC layer. Selecting the correct thermal coefficient of the ACC layer can be a critical factor for an ACC overlay design.

DEVELOPMENT OF THE DESIGN EQUATION

After the initial screening process, ten significant factors for both traffic and temperature loading were identified. A three-level experimental design was then used. As part of the fractional factorial design, a total of 243 sets of FEM results were generated. The results, input into a database designed to back up the extreme values of stress/strain, were used to identify the important factors through analysis of variance (ANOVA); design equations were then obtained using regression analysis. These design equations can work together with a damage model to explain the distress development within the pavement. These design equations can be applied directly to asphalt overlay designs.

FURTHER RESEARCH

This research has concentrated mainly on ACC overlays on rigid pavements. Future research could expand this work to include ACC overlays on flexible pavement. (Different mechanisms of distress may need to be considered.) However, the developed process for overlaying ACC over rigid pavement has the following limitations:

1. Separate models are adapted for traffic and thermal loading — even though actual highway pavements have two loadings at the same time. The moisture effect is also excluded from the mechanistic modeling.
2. Inelastic and visco-elastic material properties are not considered in the mechanistic models.
3. The predictions obtained from damage models in this research appear to be conservative. In addition, rutting on ACC layers under traffic is not considered in this research; it should be incorporated to explain rutting appearing in other sections.
4. Temperature effects on both pavement material and structural behavior should be combined with a temperature prediction model.
5. Finally, calibration of the developed mechanistic models with field results is necessary to produce an effective rehabilitation strategy.

REFERENCES

AASHTO, "AASHTO Guide for Design of Pavement Structures 1986," 1986.

AASHTO, "AASHTO Interim Guide for Design of Pavement Structures," 1972.

ABAQUS, "ABAQUS, Finite Element Computer Program," Version 5.3, Hibbitt, Karlsson & Sorensen, 1993.

Abdulaziz Ibrahim Al-Negheimish, "Bond Strength, Long-Term Performance and Temperature-Induced Stresses in Polymer Concrete — Portland Cement Concrete Composite Members," doctoral dissertation, The University of Texas at Austin, December 1988.

Adams, J. B., and L. E. Goesset, "Texas Regulations Governing the Size and Weight of Commercial Vehicles," Texas Department of Public Safety, 1984.

Allison, B. T., and B. F. McCullough, "Construction of Rehabilitation Test Sections on U.S. 59 in the Lufkin District," Research Report 987-3, Center for Transportation Research, The University of Texas at Austin, August 1994.

Allison, B. T., B. F. McCullough, and D. W. Fowler, "Feasibility Study for a Full-Scale Bonded Concrete Overlay on IH-10 in El Paso, Texas," Research Report 1957-1F, Center for Transportation Research, The University of Texas at Austin, January 1993.

Anderson, D. T., and C. K. Koskey, "Advances in Asphalt Overlay Design Procedures," Sixth International Conference, Structural Design of Asphalt Pavements, Volume I, Proceedings, University of Michigan, Ann Arbor, Michigan, July 1987, pp 748-761.

Anderson, M., "A Data Base Method for Backcalculation of Composite Pavement Layer Moduli," ASTP 1026, 1989.

ARE, "Overlay Design and Reflection Cracking Analysis for Rigid Pavements, Volume I — Development of New Design Criteria," FHWA Report No. FHWA-RD-77-66, Austin Research Engineers Inc, August 1977.

Asphalt Institute, "The Asphalt Handbook," 1989.

Asphalt Institute, "Asphalt Overlays for Highway and Street Rehabilitation," Manual Series No. 17, June 1983.

ASTM, "Standard Specification of Highway Weigh-in-Motion (WIM) Systems with User Requirements and Test Method," American Society for Testing and Materials, ASTM Designation: E 1318-90.

Barber, Edward S. “Calculation of Maximum Pavement Temperatures from Weather Reports,” Highway Research Board, 168, 1957, pp 1-8.

Bonse, R. P. H., and S. H. Kuhn, “Dynamic Forces Exerted by Moving Vehicles on a Road Surface,” Highway Research Board Bulletin No. 233, 1959.

Button, Joe W., Dario Perdomo, and Robert L. Lytton, “Influence of Aggregates on Rutting in Asphalt Concrete Pavements,” Transportation Research Record 1259, pp 141-152.

CALTRANS, Materials and Research Divisions, “Methods of Testing to Determine Overlay and Maintenance Requirements by Pavement Deflection Measurements,” Test Method No. Calif. 356-C, October 1972.

Carey, W. N., and P. E. Irick, “The Pavement Serviceability-Performance Concept,” HRB Bulletin 250, 1960.

Chao, Wei, and B. F. McCullough, “Development of Load Transfer Coefficients for Use with the AASHTO Guide for Design of Rigid Pavements Based on Field Measurements,” Research Project 1169-3, Center for Transportation Research, February 1992.

Cho, Yoon-Ho, and B. Frank McCullough, “Initial Performance of Asphalt Overlays on Overlaid Jointed Concrete Pavement (JCP) and on Flexible Pavements in Field Test Sections in Lufkin, Texas,” Research Report 987-4, Center for Transportation Research, The University of Texas at Austin, August 1994.

Cho, Yoon-Ho, “Sensitivity Analysis of AC Overlay on the PCC under Traffic Loading,” Term papers for CE 391P, The University of Texas at Austin, 1992.

Cho, Yoon-Ho, and B. F. McCullough, “Development of Reflection Cracking on US 59 in Lufkin, Texas,” 3rd International Workshop on the Design and the Evaluation of Concrete Pavements, October 1994.

Choubane, B., and Tia Mang, “Nonlinear Temperature Gradient Effect on Maximum Warping Stresses in Rigid Pavements,” TRR 1370, 1992.

Choubane, B., and Tia Mang, “Analysis and Verification of Thermal-Gradient Effects on Concrete Pavement,” *Journal of Transportation Engineering,* Vol. 121, No. 1, January/February 1995.

Claessen, A. I. M., and R. Ditmarsch, “Pavement Evaluation and Overlay Design: The Shell Method,” 4th International Conference, pp 649-662, Ann Arbor, Michigan, 1977.

Darte, Michael, Gerald F. Voigt, and Samuel H. Carpenter, “Rehabilitation of Concrete Pavements,” Volume II: Overlay Rehabilitation Techniques, Federal Highway Administration, FHWA-RD-88-072, July 1989.

de Beer, M. “Developments in the Failure Criteria of the South African Mechanistic Design Procedure for Asphalt Pavements,” 7th International Conference on Asphalt Pavements, South Africa, 1993.

DeCabooter, Philip H., “Wisconsin Truck Tire Pressure Study,” FHWA/WI-88/1, Wisconsin Department of Transportation, Madison, Wisconsin, January 1988.

Drucker, D. C., and W. Prager, “Soil Mechanics and Plastic Analysis of Limit Design,” *Quarterly of Applied Mathematics*, Vol. 10, pp 157-165, 1952.

Easa, Said M., “Extension of AASHTO Remaining Life Methodology of Overlay Design,” *Transportation Research Record 1272*, 1990.

Echmann, B., “Rut Depth Prediction: A Practical Verification,” Sixth International Conference, Structural Design of Asphalt Pavements, Volume I, Proceedings, University of Michigan, July 1987, Ann Arbor, Michigan, pp 209-219.

Eisemann, J., and A. Hilmar, “Influence of Wheel Load and Inflation Pressure on the Rutting Effect on Asphalt Pavement — Experiments and Theoretical Investigations,” Sixth International Conference, Structural Design of Asphalt Pavements, Volume I, Proceedings, University of Michigan, Ann Arbor, Michigan, July 1987, pp 392-403.

Elliot, R. P., R. P. Selvam, and L. K Mun, “Effect of Truck Tire Contact Pressure — Final Report,” Arkansas State Highway and Transportation, February 1991.

Elliott, Robert P., “An Examination of the AASHTO Remaining Life Factor,” *Transportation Research Record 1215*, 1989.

Elmore, William E., Thomas W. Kennedy, Mansour Solaimanian, and Pablo Bolzan, “Long-Term Performance Evaluation of Polymer-Modified Asphalt Concrete Pavements,” Research Report 1306-1F, Center for Transportation Research, The University of Texas at Austin, November 1993.

Elton, R. Brown, “Evaluation of Fatigue Properties of Recycled Asphalt Concrete,” Sixth International Conference, Structural Design of Asphalt Pavements, Volume I, Proceedings, University of Michigan, Ann Arbor, Michigan, July 1987, pp 305-323.

Freeme, C. R., J. H. Maree, and A. W. Viljoen, “Mechanistic Design for Asphalt Pavements and Verification Using the Heavy Vehicle Simulator,” Proceedings of the 5th International Conference on the Structural Design of Asphalt Pavements, Vol. 1, Delft, Holland, August 1982.

Haas, Ralph, and W. R. Hudson, *Pavement Management Systems*, McGraw Hill, 1986.

Hall, Kathleen T., and Alaeddin Mohseni, “Backcalculation of Asphalt Concrete-Overlaid Portland Cement Concrete Pavement Layer Moduli,” *Transportation Research Record 1293,* 1991.

Hansen, R. W., Carl Bertrand, K. M. Marshek, and W. R. Hudson, “Truck Tire Pavement Contact Pressure Distribution Characteristics for Super Single 18-22.5 and Smooth 11R24.5 Tires,” Research Report 1190-1, Center for Transportation Research, The University of Texas at Austin, 1989.

Hegmon, Rudolph R., “A Close Look at the Road Surface,” *Public Roads,* summer 1993.

Heukelom, W., and A. J. G. Klomp, “Consideration of Calculated Strains at Various Depths in Connection with the Stability of Asphalt Pavements,” Proceedings, Second International Conference on the Structural Design of Asphalt Pavements, University of Michigan, 1967, pp 107-123.

Hoskins, B. E., B. F. McCullough, and D. W. Fowler, “The Development of a Long-Range Rehabilitation Plan for US-59 in District 11 — Preliminary Report,” Research Report 987-1, Center for Transportation Research, The University of Texas at Austin, 1991.

Hossain, Mustaque, and Larry A. Schofield, “Interpretation of Backcalculated Layer Moduli Crack-and-Seat Pavement from Falling Weight Deflectometer Data,” *Transportation Research Record 1377,* 1992.

HRB, “AASHO Road Test Report 7 — Summary Report,” Special Report 61G, Highway Research Board, 1962.

HRB, “The AASHO Road Test — Report 5 Pavement Research,” Highway Research Board, Special Report 61E, National Academy of Sciences, Washington, D.C., 1962.

Huang, Yang H., *Pavement Analysis and Design,* Prentice Hall, 1993.

Hugo, F., B. F. McCullough, and Barry van der Walt, “The Development of a Strategy for the Implementation of Full-Scale Accelerated Pavement Testing for the Texas Highway Department,” Research Report 1246-2F, Center for Transportation Research, The University of Texas at Austin, November 1990.

Huhtala, Matti, Jari Pihlajamaki, and Markku Pienimaki, “Effect of Tires and Tire Pressures on Road Pavements,” *Transportation Research Record 1227,* pp 107-114.

Ioannides, A. M., and J. P. Donnelly, “Three-Dimensional Analysis of Slab on Stress-Dependent Foundation,” *Transportation Research Record 1196,* pp 72-84.

Janet M. Brunton, Stephen F. Brown, and Peter S. Pell, “Developments to the Nottingham Analytical Design Method for Asphalt Pavements,” Sixth International Conference, Structural Design of Asphalt Pavements, Volume I, Proceedings, University of Michigan, Ann Arbor, Michigan, July 1987, pp 366-377.

Janoff, M. S., J. B. Nick, P. S. Davit, and G. F. Hayhoe, “Pavement Roughness and Rideability,” NCHRP Report 275, TRB, 1985.

Jayawickrama, P. W., and R. L. Lytten, “Methodology for Predicting Asphalt Concrete Overlay Life Against Reflection Cracking,” The 6th International Conference on Structural Design of Asphalt Pavements, Ann Arbor, Michigan, September 1987.

Kamy, Sepehrnoori, “Numerical Methods in Petroleum Engineering,” Class Notes from PEN 382L, Fall 1992.

Kennedy, T. W., “Tensile Characterization of Highway Pavement Materials,” Research Report 183-15F, Center for Transportation Research, The University of Texas at Austin, July 1983.

Kennedy, T. W., “Forensic Engineering in HMAC,” Class Notes in CE 397, The University of Texas at Austin, summer 1994.

Kennedy, T. W., and C. E Cowher, “Cumulative Damage of Asphalt Materials Under Repeated-Load Indirect Tension,” Research Report 183-13, Center for Transportation Research, The University of Texas at Austin, January 1975.

Ko-young Shao, “Dynamic Interpretation of Dynaflect, Falling Weight Deflectometer, and Spectral Analysis of Surface Wave Tests on Pavement System,” doctoral dissertation, The University of Texas at Austin, December 1985.

Koesmo, Koestomo, and B. Frank McCullough, “Evaluation of the Performance of the Bonded Concrete Overlay on Interstate Highway 610 North, Houston, Texas,” Research Report 920-2, Center for Transportation Research, The University of Texas at Austin, 1987.

Lee, Clyde E., and Safry Kamal Ahmad, “Effect of Work Zone Detours on Rural Highway Traffic Operations,” Research Project 987-2, Center for Transportation Research, The University of Texas at Austin, May 1993.

Lytton, Robert L., Jacob Uzan, Emmanuel G. Fernando, Dennis Hiltunen, and Shelly M. Stoffels, “Development and Validation of Performance Prediction Models and Specifications for Asphalt Binders and Paving Mixes,” Strategic Highway Research Program, SHRP-A-357, Washington, D.C., 1993.

Lytton, Robert L., Uzan, Jacob, Fernando, Emmanuel G., Reynaldo, Dennis Hiltunen, and Stoffels, Shelly M., “Development and Validation of Performance Prediction Models and Specifications for Asphalt Binders and Paving Mixes,” Strategic Highway Research Program, SHRP-A-357, Washington, D.C., 1993.

Mahboub, Kamyar, and Dallas Little, “Improved Asphalt Concrete Mixture Design Procedure,” FHWA/TX-87/474-1F, Texas Transportation Institute, The Texas A&M University System, College Station, Texas, 1988.

Majidzadeh, K., F. Bayomy, and S. Khedr, “Rutting Evaluation of Subgrade Soils in Ohio,” *Transportation Research Record 671,* 1979.

Majidzadeh, K., S. Cheddar, and H. Guirguis, “Laboratory Verification of a Mechanistic Subgrade Rutting Model,” *Transportation Research Record 616,* 1976.

McCullough, B. F., “Review and Critique of WES Rigid Pavement Research,” submitted to U.S. Army Corps of Engineers, Waterways Experiment Station, March 1993.

McCullough, B. F., “A Pavement Overlay Design System Considering Wheel Loads, Temperature Changes, and Performances,” Graduate Report, ITTE, University of California, Berkeley, 1970.

McCullough, B. F., Jose Weissmann, Terry Dossey, and Yoon-Ho Cho, “A Case Study of Overlay Performance on Rigid Pavement on IH-30 Bowie County, Texas,” Research Report 1342-1, Center for Transportation Research, The University of Texas at Austin, February 1994.

McCullough, B. F., and Piti Yimprasert, “Fatigue and Stress Analysis Concepts for Modifying the Rigid Pavement Design System,” Research Report 123-16, Center for Transportation Research, The University of Texas at Austin, January 1973.

McCullough, B. F., and K. J. Boedecker, “Use of Linear-Elastic Theory for the Design of CRCP Overlays,” Proceeding of the 48th Annual Meeting of Transportation Research Board.

McDaniel, Mark, “Accelerated Trafficking with model MLS,” Paper submitted in the First Annual CTR and TTI student seminar, April 1993.

McDowell, Chester, “Wheel Load Stress Computations Related to the Texas Highway Department Triaxial Method of Flexible Pavement Design,” from educational material for TxDOT engineers, 1961.

McDowell, Chester, “Road Test Findings Utilized in Analysis of Texas Triaxial Methods of Pavement Design,” Prepared for presentation at Conference on the AASHO Road test, May 1962.

Mendoza Diaz, Alberto, and B. F. McCullough, “Design Charts for the Design of HMAC Overlays on Pavements to Prevent Reflection Cracklings,” Research Report 249-6, Center for Transportation Research, The University of Texas at Austin, November 1983.

Michael J. Markow, J. Karl Hedrick, Brian D. Brademeyer, and Edward Abbo, "Analyzing the Interactions between Dynamic Vehicle Loads and Highway Pavements," *Transportation Research Record 1196.*

Michael, L., S. Alden, Stilson and Associates, K. Majidzadeh, and Chang Che-Wei, "Mechanistic Investigation of Reflection Cracking of Asphalt Overlays," *Transportation Research Record 572*, Transportation Research Board, 1976.

Mohamed, Y. Shahin, and B. Frank McCullough, "Prediction of Low-Temperature and Thermal-Fatigue Cracking in Flexible Pavements," Research Report 123-14, Center for Transportation Research, The University of Texas at Austin, 1973.

Monismith, C. L., J. A. Epps, and F. N. Finn, "Improved Asphalt Mix Design," AAPT, Vol. 54, 1985, pp 347-406.

Moore, Raymond K., "Wide-Base Truck Tire Effects on Pavement Performance and Vehicle Regulatory Legislation," Kansas Department of Transportation, June 1992.

Nam, Dongho, "Effect of Slab Flexibility on the Vertical Stiffness of Circular Foundations," master's thesis, The University of Texas at Austin, August 1994.

NCHRP 1-26, "Calibrated Mechanistic Structural Analysis Procedure for Pavements," Final Report, Volume II — Appendix, National Cooperative Highway Research Program Project I-26, TRB, Washington, D.C., March 1990.

Neville, A. M., *Properties of Concrete,* 3rd edition, Pitman, 1981.

Paterson, W. D. O., "International Roughness Index: Relationship to Other Measures of Roughness and Riding Quality," *Transportation Research Record 1084.*

Paterson, W. D. O., "Prediction of Road Deterioration and Maintenance Effects: Theory and Quantification," Highway Design and Maintenance Standard Study, Vol III, Transportation Department, World Bank, 1987.

PCA, "Thicknesses Design for Concrete Highway and Street Pavements," Portland Cement Association, 1984.

Ponniah, J., R. Haas, W. A. Phang, and L. Rothenburg, "Low Temperature Cracking through Asphalt Overlays," The 6th International Conference on Structural Design of Asphalt Pavements, Ann Arbor, Michigan, September 1987.

Ramsamooj, D. V., K. Majidzadeh, and E. M. Kauffmann, "The Design and Analysis of the Flexibility of Pavements," The 3rd International Conference on Structural Design of Asphalt Pavements, London, September 1972.

Ramsamooj, D.V., “Prediction of Reflection Cracking in Pavement Overlays,” Highway Research Record 434, Highway Research Board, 1973.

Rauhut, J. Brent, John C. O’Quin, and W. R. Hudson, “Sensitivity Analysis of FHWA Structural Model VESYS II,” Vol. I, Report No. FA 1/1, Austin Research Engineers, Inc., Austin, Texas, November 1975.

Reilley, K., C. Saraf, B. F. McCullough, and D. W. Fowler, “A Laboratory Study of the Fatigue of Bonded PCC Overlays,” Research Report 457-2, Center for Transportation Research, The University of Texas at Austin, September 1986.

Rhode, G. T., and T. Scullion, “Modulus 4.0: Expansion and Validation of the Modulus Backcalculation System,” Research Report 1123-3, Texas Transportation Institute, Texas A&M University, November 1990.

Ricci, Eduardo A., and A. H. Meyer, “Falling Weight Deflectometer for Nondestructive Evaluation of Rigid Pavements,” Research Report 387-3F, Center for Transportation Research, The University of Texas at Austin, November 1985.

Roberts, F. L., et al., “The Effect of Tire Pressures on Flexible Pavements,” Research Report TTI 372-1F, Texas Transportation Institute, Texas A&M University, August 1986.

Roberts, Freddy L., Prithvi S. Kandhal, E. Ray Brown, Dah-Yinn Lee, and Thomas W. Kennedy, “Hot Mix Asphalt Materials, Mixture Design, and Construction,” NAPA Education Foundation, 1991.

Rodriguez, Manuel, and T. W. Kennedy, “The Resilient and Fatigue Characteristics of Asphalt Mixtures Processed by the Dryer-drum Mixer,” Research Report 183-8, Center for Transportation Research, The University of Texas at Austin, December 1976.

Romain, J. E., “Rut Depth Prediction in Asphalt Pavements,” Proceedings, Third International Conference on Structural Design of Asphalt Pavements, University of Michigan, 1972.

Roque, R., M. Tia, and B. Ruth, “Asphalt Rheology to Define the Properties of Asphalt Concrete Mixtures and Performance of Pavements,” Asphalt Rheology: Relationship to Mixtures, ASTM STP 941, American Society for Testing Materials, Philadelphia, 1987, pp 3-27.

Saraf, C. L., B. F. McCullough, and M. F. Aslam, “Rutting of ACP Overlays on CRCP in the State of Texas,” TRR 1109, January 1987.

Sayers, Michael W., Thomas D. Gillespie, and Caesar A. V. Queiroz, “The International Road Roughness Experiment: Establishing Correlation and a Calibration Standard for Measurement,” World Bank, 1986.

Sebaaly, P., and Nader Tabatabaee, "Effect of Tire Pressure and Type on Response of Flexible Pavement," *Transportation Research Record 1227,* pp 115-127.

Seed, H. B., C. K. Chan, and C. E. Lee, "Resilient Characteristics of Subgrade Soils and their Relation to Fatigue Failure in Asphalt Pavements," First International Conference, Structural Design of Asphalt Pavements, Proceedings, University of Michigan, Ann Arbor, Michigan, July 1962.

Seeds, S., B. F. McCullough, and W. R. Hudson, "A Design System for Rigid Pavement Rehabilitation," Research Report 249-2, Center for Transportation Research, The University of Texas at Austin, November 1981.

Sherman, George, "Minimizing Reflection Cracking of Pavement Overlays," National Cooperative Research Program Synthesis of Highway Practice 92, September 1982.

SHRP, "Manual for FWD Testing in the Long-Term Pavement Performance Program," SHRP-P-661, 1993.

Steven, C. Chapra, and Raymond P. Canale, *Numerical Methods for Engineers,* McGraw-Hill, 1989.

Stokoe, K. H., William M. Isenhower, and J. R. Hsu, "Dynamic Properties of Offshore Silty Samples," Offshore Technology Conference, 1980.

Suh, Young-Chan, K. Hankins, and B. F. McCullough, "Early-age Behavior of Continuously Reinforced Concrete Pavement and Calibration of the Failure Prediction Model in the CRCP-7 Program," Research Report 1244-3, Center for Transportation Research, The University of Texas at Austin, March 1992.

Taute, A. McCullough, B. F., and Hudson, W. R., "Improvements to the Materials Characterization and Fatigue Life Prediction Method of the Texas Rigid Pavement Overlay Design Procedure," Research Report 249-1, Center for Transportation Research, The University of Texas at Austin, November, 1981

Tayabji, S. D., and P. A. Okamato, "Thickness Design of Concrete Resurfacing," Third International conference on Concrete Pavement Design and Rehabilitation, Purdue University, West Lafayette, Indiana, 1985

Thompson, M. R., "ILLI-PAVE, Users Manual," Transportation Facilities Group, Department of Civil Engineering, University of Illinois, Urbana, Illinois, 1982.

Treybig, Harvey J., B. F. McCullough, Phil Smith, and Harold von Quintus, "Overlay Design and Reflection Cracking Analysis for Rigid Pavement," Austin Research Engineers, August 1977.

TxDOT, “Standard Specifications for Construction of Highways, Streets and Bridges,” Texas Department of Transportation, March 1, 1993.

TxDOT, “Texas Highway Department Plan Preparation,” Book II, Prepared by the Road Design Division and the Traffic Series Division of the Texas Highway Department for the Instructor School, Austin, Texas, December 1952.

Van Vuuren, D. J., “Tire Pressure and Its Effect on Pavement Design and Performance,” *Civil Engineering in South Africa,* Vol. 16, No. 8, August 1974.

van Metzinger, Willem A., B. F. McCullough, and D. W. Fowler, “An Empirical-Mechanistic Design Methods Using Bonded Concrete Overlays for the Rehabilitation of Pavements,” Research Report 1205-3, Center for Transportation Research, The University of Texas at Austin, January 1991.

Viljeon, Adrianus W., and B. F. McCullough, “Implementation of a Comprehensive Rigid Pavement Overlay Design System into a Condensed Overlay Design Manual,” Research Report 388-4, Center for Transportation Research, The University of Texas at Austin, May 1985.

von Metzinger, Willem A., and B. F. McCullough, “An Empirical-Mechanistic Design Method Using Bonded Concrete Overlays for the Rehabilitation of Pavements,” Research Report 1205-1, Center for Transportation Research, The University of Texas at Austin, January 1991.

WA-RD 65.1 “State-of-the-Art on Pavement Overlay Procedures, Vol. I, State-of-the-Art Review and Research Plan,” Washington State Department of Transportation, December 1983.

Walton, C. M., Chien-pei Yu, and Paul Ng, “Truck Weight Shifting Methodology for Predicting Highway Loads,” Research Report 241-5, Center for Transportation Research, The University of Texas at Austin, April 1983.

Westergaard, H. M., “Analysis of Stresses in Concrete Pavement Due to Variations of Temperature,” Proceedings of the Sixth Annual Meeting of the Highway Research Board, Washington, D.C., December 2-3, 1926, pp 201-214.

Westergaard, H. M., “Stresses in Concrete Runways of Airports,” *Proceedings of the Nineteenth Annual Meeting of the Highway Research Board,* Washington, D.C, 1939.

Won., M., K. Hankins, and B. F. McCullough, “Mechanistic Analysis of Continuously Reinforced Concrete Pavements Considering Material Characteristics, Variability, and Fatigue,” Research Report 1169-2, Center for Transportation Research, The University of Texas at Austin, April 1990.

Yoder and Witczak, *Principles of Pavement Design*, 2nd edition, John Wiley & Sons, Inc., 1975.

Zaghloul, S. M., T. D. White, V. P. Drnevich, and B. Coree, "Dynamic Analysis of FWD Loading and Pavement Response Using a Three-Dimensional Finite Element Program," *Nondestructive Testing of Pavements and Backcalculation of Moduli* (2nd Volume), ASTM STP 1198, 1994.

Zaghloul, Sameh M., T. D. White, Vincent P. Drenvich, and Drian Coree, "Dynamic Analysis of FWD and Pavement Response Using a Three-Dimensional Dynamic Finite Element Program," *Nondestructive Testing of Pavements and Backcalculation of Moduli* (2nd Volume), ASTM STP 1198, American Society for Testing and Materials, Philadelphia, 1994.

Zaghloul, Sameh, and T. D. White, "Non-Linear Dynamic Analysis of Concrete Pavements," Submitted for Presentation at the 5th International Conference on Concrete Pavement Design and Rehabilitation, Purdue University, Indiana, April, 1993.

Zekoski, J., "Impact of Truck Tire Selection on Contact Pressers," FHWA Load Equivalence Workshop sponsored by the Federal Highway Administration Pavement Division, Turner-Fairbanks Highway Research Center, McLean, Virginia, September 1988.

APPENDIX A

TEMPERATURE PREDICTION MODEL: FDM MODELING

FDM Modeling

The governing partial differential equation can be solved by the following approaches, using the so-called finite difference method (FDM):

The governing equation can be first simplified as:

$$\frac{\partial^2 T}{\partial x^2} = \frac{1}{\alpha}\frac{\partial \mathrm{T}}{\partial \mathrm{t}} = \frac{\rho \mathrm{c}}{\mathrm{k}}\frac{\partial \mathrm{T}}{\partial \mathrm{t}} = o\frac{\partial \mathrm{T}}{\partial \mathrm{t}} \quad \text{...(1)}$$

Applying Crank-Nicolson method and simplifying it gives:

$$\frac{1}{2}\left(\frac{T_{i+1}^{n+1} - 2T_i^{n+1} + T_{i-1}^{n+1}}{\Delta x^2} + \frac{T_{i+1}^{n} - 2T_i^{n} + T_{i-1}^{n}}{\Delta x^2}\right) = o\frac{T_i^{n+1} - T_i^n}{\Delta t} \quad \text{...................(2)}$$

Let $R = \dfrac{\Delta \mathrm{t}}{\Delta \mathrm{x}^2}$ and $o = \dfrac{\rho \mathrm{c}}{\mathrm{k}}$ and then

$$\frac{R}{2}(T_{i+1}^{n+1} - 2T_i^{n+1} + T_{i-1}^{n+1} + T_{i+1}^{n+1} - 2T_i^{n+1} + T_{i-1}^{n+1}) = o\,(T_i^{n+1} - T_i^n) \quad \text{......(3)}$$

the boundary condition and initial value are also incorporated. The contact surface between each layer was given by equation (4).

$$k_a\frac{\partial \mathrm{T}}{\partial \mathrm{x}} = k_b\frac{\partial \mathrm{T}}{\partial \mathrm{x}} \quad \text{...(4)}$$

Applying central difference, the following relationship will be given

$$k_a\frac{T_{i+1}^n - T_{i-1}^n}{2\Delta x} = k_b\frac{T_{i+1}^n - T_{i-1}^n}{2\Delta x} \quad \text{..(5)}$$

$$(k_a - k_b)T_{i+1}^n = (k_a - k_b)T_{i-1}^n \quad \text{..(6)}$$

$$T_{i+1}^n = T_{i-1}^n \quad \text{...(7)}$$

The boundary condition at the end of pavement depth considered here was given equation (8) and its finite difference could be expressed by equation (10).

$$k_c\frac{\partial \mathrm{T}}{\partial \mathrm{x}} = 0 \quad \text{...(8)}$$

$$k_c \frac{T^n_{i+1} - T^n_{i-1}}{2\Delta x} = 0 \quad \text{...(9)}$$

$$T^n_{i+1} = T^n_{i-1} \quad \text{...(10)}$$

The configuration of time and space generation will have advantages that make the program easier to operate. The following arrange and node expressions were used to solve the problem:

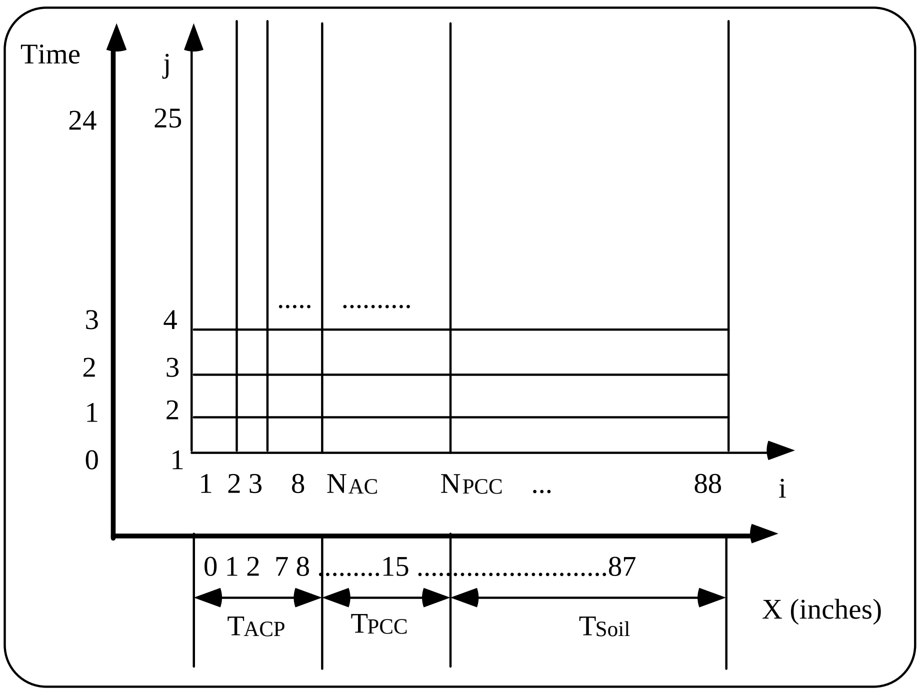

Figure A-1. Configuration of time and space node in the model

A linear system was constructed based on above equation and on a mesh arrangement as followings:

From Equation (3) and initial and boundary conditions, the linear equation at initial space, j = 2,25 and i = 2, can be expressed:

$$\frac{R}{2}(T_3^{n+1} - 2T_2^{n+1} + T_1^{n+1} + T_3^{n+1} - 2T_2^{n+1} + T_1^{n+1}) = o\,(T_2^{n+1} - T_2^{n}) \text{..............11)}$$

Because initial temperature was given, Equation (4) become to the following simple equation.

$$\frac{R}{2}T_3^{n+1} + (R - o)T_2^{n+1} = (\text{-o} + \text{R})T_2^{n} - \frac{R}{2}T_1^{n} + \frac{R}{2}T_3^{n} + \frac{R}{2}T_1^{n+1} \text{..................12)}$$

Intermediate space condition, j= 2,25 and i=3, m-1, can also be expressed as:

$$\frac{R}{2}T_{i+1}^{n+1} + (-R-o)T_i^{n+1} + \frac{R}{2}T_{i-1}^{n+1} \; = \; (\text{-}o + R)T_i^n \; \text{-}\frac{R}{2}T_{i+1}^n - \frac{R}{2}T_{i-1}^n \ldots\ldots\ldots\ldots\ldots 13)$$

The bottom boundary, j=2,25 and i=m, can have the following linear equation:

$$(-R-o)T_m^{n+1} \; + \; RT_{m-1}^{n+1} \; = \; (\text{-}o + R)T_m^n \; - \; RT_m^n \ldots\ldots\ldots\ldots\ldots\ldots\ldots\ldots\ldots\ldots\ldots\ldots 14)$$

However, the boundary condition at the contact surface, e.g., the surface between ACC and PCC or j = 2,25 and i = N_{AC} and N_{PCC}, required changing some of equations expressed in linear Equation (13). From Equation (7) and the mesh configuration, the following equation could be drawn:

$$(-R-o)T_{NAC}^{n+1} \; + \; RT_{NAC-1}^{n+1} \; = \; (\text{-}o + R)T_{NAC}^n \; - \; RT_{NAC-1}^n \ldots\ldots\ldots\ldots\ldots\ldots\ldots\ldots 15)$$

Based on the above equations, the following linear tridiagonal system was drawn. This tridiagonal system can be solved easily using the Thomas algorithm.

$$
\begin{bmatrix}
(-R-O) & R/2 & & & & & & & & & & \\
R/2 & (-R-O) & R/2 & & & & & & & & & \\
 & & . & . & . & & & & & & & \\
 & & . & . & . & & & & & & & \\
 & & & R/2 & (-R-O) & R/2 & & & & & & \\
 & & & & R & (-R-O) & 0 & & & & & \\
 & & & & & R/2 & (-R-O) & R/2 & & & & \\
 & & & & & & . & . & . & & & \\
 & & & & & & R/2 & (-R-O) & R/2 & & & \\
 & & & & & & & R & (-R-O) & 0 & & \\
 & & & & & & & & R/2 & (-R-O) & R/2 & \\
 & & & & & & & & . & . & . & \\
 & & & & & & & & & . & . & . \\
 & & & & & & & & & R/2 & (-R-O) & R/2 \\
 & & & & & & & & & & R & (-R-O)
\end{bmatrix}
\begin{vmatrix}
T_2^{n+1} \\
T_3^{n+1} \\
. \\
. \\
T_{NAC-1}^{n+1} \\
T_{NAC}^{n+1} \\
. \\
. \\
T_{NPC-1}^{n+1} \\
T_{NPC}^{n+1} \\
T_{NPC+1}^{n+1} \\
. \\
. \\
T_{M-1}^{n+1} \\
T_M^{n+1}
\end{vmatrix}
$$

$$=$$

$$
\begin{bmatrix}
(-O+R)\ T2 - R/2\ T3^{*} - R/2\ T1 - R/2\ T_1^{n+1} \\
(-O+R)\ T3 - R/2\ T4 - R/2\ T2 \\
. \\
. \\
(-O+R)\ (Tnac-1) - R/2\ (Tnac-2) - R/2\ (Tnac) \\
(-O+R)\ (Tnac) - R\ (Tnac-1) \\
(-O+R)\ (Tnac+1) - R/2\ (Tnac+1) - R/2\ (Tnac-1) \\
. \\
(-O+R)\ (Tnpc-1) - R/2\ (Tnpc-2) - R/2\ (Tnpc) \\
(-O+R)\ (Tnpc) - R\ (Tnpc-1) \\
(-O+R)\ (Tnpc+1) - R/2\ (Tnpc+1) - R/2\ (Tnpc-1) \\
. \\
. \\
(-O+R)\ (Tm-1) - R/2\ (Tm-1) - R/2\ (Tm+1) \\
(-O+R)\ (Tm) - R\ (Tm-1)
\end{bmatrix}
$$

*: nth time step, T_i^n , i= 2,m

APPENDIX B

TEMPERATURE PREDICTION MODEL: FORTRAN PROGRAMMING

FORTRAN Programming

Input Data file - Heat.DAT

```
7.    7.    1.    1.    4.
140.  150.  120.
0.7   0.9   0.6
0.22  0.20  0.18
20    0.95  526
69    28
1.0
```

Program List

```
C
C   A PROGRAM WHICH CAN PREDICT TEMPERATURE DISTRIBUTION OF
C   COMPOSITE PAVEMENTS
C
C   INPUT VARIABLES
C       PAVEMENT  : TACC    : THICKNESS OF ACC (INCH)
C                   TPCC    : THICKNESS OF PCC (INCH)
C                           tsoil1: thickness of soil 1 (FT)
C                           tsoil2: thickness of soil 2 (FT)
C                           tsoil3: thickness of soil 3 (FT)
C                           tsoil : finite thickness assumed to be effected
C                                   by air temp. (=tsoil1+tsoil2+tsoil3)
C
C       COEFFICIENT OF THERMAL CONDUCTIVITY
C           WACC : UNIT WEIGHT OF ACC
C           WPCC : UNIT WEIGHT OF PCC
C           WPSOIL    : UNIT WEIGHT OF SOIL
C           CONACC    : CONDUCTIVITY OF ACC
C           CONPCC    : CONDUCTIVITY OF PCC
C           CONSOIL   : CONDUCTIVITY OF SOIL
C           SHACC     : SPECIFIC HEAT OF ACC
C           SHPCC     : SPECIFIC HEAT OF PCC
C           SHSOIL    : SPECIFIC HEAT OF SOIL
C
C       AIR TEMPERATURE
C           WINDVEL   : WIND VELOCITY
C           SUNCOE    : SURFACE COEFFICIENT
C           ABSORB    : SURFACE ABSORBITIVITY
C           ANETLOSS  : AVERAGE NET LOSS
C           SLANG     : SOLAR LONGLEYS PER DAY
C           TEMPA     : MEAN AIR TEMPERATURE
C           TEMPR     : DAILY AIR TEMPERATURE RANGE
C
C           TIME CONSTRAINT
C                   DELT      : TIME INCREASE BY USER
C
C       OUTPUT
C           TEMPSOL(TIME,TEMP)
C           Programmer : Yoon-Ho Cho, U.T. at Austin, May in 1994
C
            IMPLICIT REAL*8 (A-H,O-Z)
      PARAMETER (N=200)
      DIMENSION TVALUE(N), SPACE(N),TEMPSOL(60,N),SOL(N)
      DIMENSION SUPERD(N),SUBD(N),DMAIN(N),RHS(N)
      OPEN(5,FILE='heat0.dat',STATUS='OLD')
      OPEN(6,FILE='heat0.out',STATUS='NEW')
C
C ----    READ INPUT FILE
C
      READ(5,*) TACC, TPCC, tsoil1,tsoil2,tsoil3
```

```
      READ(5,*) WACC,WPCC,WSOIL
      READ(5,*) CONACC, CONPCC,CONSOIL
      READ(5,*) SHACC,SHPCC,SHSOIL
      READ(5,*) WINDSPD, ABSORB,SOLANG
      READ(5,*) TEMPA, TEMPR
C
      READ(5,*) DELT
c
c----        initialize the array
c
             do 1 i=1,n
               superd(i) = 0.0
               dmain(i) = 0.0
               subd(i) = 0.0
               tvalue(i) = 0.0
               space(i) = 0.0
1            continue
             WRITE(6,311)
C
C*** CALCULATE AH = SURFACE COEFFICIENT
C
        AH = 1.3 + .62*WINDSPD**.75
        H = AH / CONACC
              WRITE(6,312) H
C
C*** CALCULATE AC = DIFFUSIVITY IN SQ.FT./HR.
C
        AC = CONACC / ( SHACC * WACC )
        C = ( .131 / AC ) ** .5
             WRITE(6,313) C
C
C*** CALCULATE R = AVERAGE CONTRIBUTION TO EFFECTIVE AIR TEMPERATURE
C             BY SOLAR RADIATION
C
        R = .67 * ABSORB * 3.69 * SOLANG / ( 24. * AH )
             WRITE(6,314) R
C
C*** CALCULATE TM = MEAN EFFEVTIVE AIR TEMPERATURE, DEG.F AND
C       TV = THE HALF-AMPLITUDE OF THE EFFECTIVE AIR TEMPERATURE, DEG.F
C
C           TEMPV = .5 * TEMPR + 3. * R
          TEMPV = .5 * TEMPR
          TEMPM = TEMPA + R
             WRITE(6,315) TEMPV, TEMPM
C***********************************************************************
C   ROUTINE TO SOLVE THE PDE WITH BOUNDARY CONDITION
C***********************************************************************
C
C-----       DELX1,DELX2,DELX3 = INCHES UNITS
C
      DELX1 = 0.5
      DELX2 = 3.0
      DELX3 = 12.
      TIME1 = 0.0
      TIMEF = 24.0
             ITIME = 0
      TEMPMAX = 999.
C
C-----
C
      NNACC = INT(TACC/delx1)
      NNPCC = INT(TPCC/delx1)
             TFSOIL1=TSOIL1*12.
             TFSOIL2=TSOIL2*12.
             TFSOIL3=TSOIL3*12.
             nsoil1 =int(tFsoil1/delx1)
             nsoil2 =int(tFsoil2/delx2)
             nsoil3 =int(tFsoil3/delx3)
      NNACC = NNACC + 1
      NPAV1 = NNACC + NNPCC
      NPAV2 = NPAV1 + nsoil1
      NPAV3 = NPAV2 + nsoil2
      NPAV4 = NPAV3 + nsoil3
      NROW  = NPAV4-1
C            WRITE(6,411) npav4, nrow
C
```

```
C--- SET THE COORDINATE OF NODE
C
C              DELX1,DELX2,DELX3 = FT UNITS HERE
C
     SPACE(1) = 0.0
     DO 110 I=2,NPAV2
        SPACE(I) = SPACE(I-1) + DELX1/12.
 110  CONTINUE
     DO 120 I=NPAV2+1, NPAV3
        SPACE(I) = SPACE(I-1) + DELX2/12.
 120  CONTINUE
     DO 130 I=NPAV3+1, NPAV4
        SPACE(I) = SPACE(I-1) + DELX3/12.
 130  CONTINUE
C
C-----    SET THE INITIAL VALUE TO RHS ( TIME = 0)
C
              WRITE(6,412)
     DO 140 I=1,NROW
              DIST = SPACE(I)
       TVALUE(I) = TIMEINI(TIME1,TEMPM,TEMPV,H,C,DIST)
              WRITE(6,413) SPACE(I),TVALUE(I)
 140  CONTINUE
C
C----     LOOP START
C               YOU NEED TO CHANGE DEL1,DEL2,DEL3 INTO FT
C
     IFLAG = 1
     ITER1 = 0
     MAXITE = 10000
     ALPHA1 = (SHACC*WACC)/CONACC
     ALPHA2 = (SHPCC*WPCC)/CONPCC
     ALPHA3 = (SHSOIL*WSOIL)/CONSOIL
C
     RAMDA1 = DELT/((DELX1/12.)**2)
     RAMDA2 = DELT/((DELX1/12.)**2)
     RAMDA3 = DELT/((DELX1/12.)**2)
     RAMDA4 = DELT/((DELX2/12.)**2)
     RAMDA5 = DELT/((DELX3/12.)**2)
c
c----          PRINT THE TITLE
C
     DO WHILE(TIME1.LE.24)
               IF(IFLAG.EQ.0) GO TO 8888
               IF(ITER1.GE.MAXITE) GO TO 8888
        IFLAG = 1
        ITER1 = ITER1 + 1
C
C----- MAKE TRIDIGONAL MATRIX USING THE CRACK-NICOLSON METHOD
C     FIRST SET THE DIGONAL MATRIX,
C
C----- ASPHALT LAYER
C
     DMAIN(1) = (-RAMDA1-ALPHA1)
     SUPERD(1) = RAMDA1/2.
     DO 200 I=2,NNACC-2,1
        DMAIN (I) = (-RAMDA1-ALPHA1)
        SUPERD(I) =  RAMDA1/2.
        SUBD(I)   =  RAMDA1/2.
 200    CONTINUE
     DMAIN(NNACC-1) = (-RAMDA1-ALPHA1)
     SUBD(NNACC-1)  = RAMDA1
     SUPERD(NNACC-1) = 0.0
C
C-----    PCC LAYER
C
     DO 210 I=NNACC,NPAV1-2
        DMAIN (I) = (-RAMDA2-ALPHA2)
        SUPERD(I) =  RAMDA2/2.
        SUBD(I)   =  RAMDA2/2.
 210    CONTINUE
     DMAIN(NPAV1-1) = (-RAMDA2-ALPHA2)
     SUBD(NPAV1-1)  = RAMDA2
     SUPERD(NPAV1-1) = 0.0
C
C----- NOW WE HAVE SOIL LAYER. TO IMPROVE SPEED AND EFFICIENCY,
```

```
C      THREE LAYERS WITH DIFFERENT THICKNESS WILL BE CONSIDERED.
C
      DO 220 I=NPAV1, NPAV2-1
         DMAIN (I) = (-RAMDA3-ALPHA3)
         SUPERD(I) =  RAMDA3/2.
         SUBD(I)   =  RAMDA3/2.
220   CONTINUE
      DO 230 I=NPAV2, NPAV3-1
         DMAIN (I) = (-RAMDA4-ALPHA3)
         SUPERD(I) =  RAMDA4/2.
         SUBD(I)   =  RAMDA4/2.
230     CONTINUE
      DO 240 I=NPAV3, NPAV4-2
         DMAIN (I) = (-RAMDA5-ALPHA3)
         SUPERD(I) =  RAMDA5/2.
         SUBD(I)   =  RAMDA5/2.
240   CONTINUE
      DMAIN (NPAV4-1) = (-RAMDA5-ALPHA3)
      SUBD(NPAV4-1)   = RAMDA5
      SUPERD(NPAV4-1) = 0.0
C
C----     SET THE RIGHT HAND SIDE : RHS
C
      TIME1 = TIME1 + DELT
C
C ------  RHS IN THE ASPHALT
C
      DIST = SPACE(1)
      RHS(1) = (-ALPHA1+RAMDA1)*TVALUE(2)-(RAMDA1/2.)*TVALUE(3) -
     *                          (RAMDA1/2.)*TVALUE(1) -
     *                          RAMDA1/2.*TIMEINI(TIME1,TEMPM,TEMPV,H,C,DIST)
C
      DO 241 I=3,NNACC-1
         RHS(I-1) = -(RAMDA1/2.)*TVALUE(I-1)+(-ALPHA1+RAMDA1)*TVALUE(I)
     *                          -(RAMDA1/2.)*TVALUE(I+1)
241   CONTINUE
      RHS(NNACC-1)=-RAMDA1*TVALUE(NNACC-2)+
     *                            (-ALPHA1+RAMDA1)*TVALUE(NNACC-1)
C
C ------  RHS IN THE PCC
C
      DO 242 I=NNACC, NPAV1-2
                IF(I.EQ.NNACC) THEN
          RHS(I) = -RAMDA1/2.*TVALUE(I-1) + (-ALPHA2+RAMDA2)*TVALUE(I)
     *                          -RAMDA2/2.*TVALUE(I+1)
                ELSE
          RHS(I) = -RAMDA2/2.*TVALUE(I-1) + (-ALPHA2+RAMDA2)*TVALUE(I)
     *                          -RAMDA2/2.*TVALUE(I+1)
                ENDIF
242   CONTINUE
      RHS(NPAV1-1)=-RAMDA2*TVALUE(NPAV1-2)+
     *                            (-ALPHA2+RAMDA2)*TVALUE(NPAV1-1)
C
C ------  RHS IN THE SOIL WITH 1 INCHES MESH
C
      DO 243 I=NPAV1, NPAV2-1
                IF(I.EQ.NPAV1) THEN
          RHS(I) = -RAMDA2/2.*TVALUE(I-1) + (-ALPHA3+RAMDA3)*TVALUE(I)
     *                          -RAMDA3/2.*TVALUE(I+1)
                ELSE
          RHS(I) = -RAMDA3/2.*TVALUE(I-1) + (-ALPHA3+RAMDA3)*TVALUE(I)
     *                          -RAMDA3/2.*TVALUE(I+1)
                ENDIF
243     CONTINUE
C
C ------  RHS IN THE SOIL WITH 3 INCHES MESH
C
      DO 244 I=NPAV2, NPAV3-1
          RHS(I) = -RAMDA4/2.*TVALUE(I-1) + (-ALPHA3+RAMDA4)*TVALUE(I)
     *                          -RAMDA4/2.*TVALUE(I+1)
244     CONTINUE
C
C ------  RHS IN THE SOIL WITH 12 INCHES MESH
C
      DO 245 I=NPAV3, NPAV4-2
          RHS(I) = -RAMDA5/2.*TVALUE(I-1) + (-ALPHA3+RAMDA5)*TVALUE(I)
```

```
    *                       -RAMDA5/2.*TVALUE(I+1)
245    CONTINUE
C
    RHS(NPAV4-1)=-RAMDA5*TVALUE(NPAV4-2)+(-ALPHA3+RAMDA5)
    *                         *TVALUE(NPAV4-1)
C
C---         ECHO PRINT
C
C            IF(ITER1.LE.1) THEN
C              DO 410 I=1,NPAV4-1
C                WRITE(6,415) I,DMAIN(I),SUPERD(I),SUBD(I),RHS(I)
C410           CONTINUE
C            ENDIF
C
C----        CALL SUBROUTINE WHICH CALCULATE A SOLUTION OF THREE DIAGONAL MATRIX
C
    CALL THOMAS(DMAIN,SUPERD,SUBD,RHS,SOL,NROW)
C
C----        CHANGE THE TEMPERATURE AND FIND OUTPUT
C
    DO 250 I=1,NROW
       TVALUE(I+1) = SOL(I)
250    CONTINUE
    DO 255 I=1,NROW
       IF(TVALUE(I).GE.TEMPMAX) THEN
         IFLAG = 0
                WRITE(*,*) ' ERROR, NO CONVERGENCE !'
                WRITE(*,*) ' TIME =',TIME1
       IF(ITER1.LE.1) WRITE(*,*) I,TVALUE(I)
       ENDIF
         TEMPSOL(ITER1,I+1) = SOL(I)
255   CONTINUE
C
C----        SET NEW INITIAL VALUE
C
             TVALUE(1) = TIMEINI(TIME1,TEMPM,TEMPV,H,C,DIST)
             TEMPSOL(ITER1,1) = TIMEINI(TIME1,TEMPM,TEMPV,H,C,DIST)
C
C------   LOOP END
C
    ENDDO
C
C------
C
             GO TO 8887
8888         CONTINUE
             WRITE(*,*) 'ERROR EITHER OVERRUN OR NO CONVERGENCE'
             GO TO 8889
C
C-----      OUPUT MODULUS TO SOLVE
C
8887         CONTINUE
    WRITE(6,1001)
    DO 1000 J=1,NPAV4-1
              DEPTH = SPACE(J) *12.
       WRITE(6,1002) DEPTH, (TEMPSOL(I,J),I=1,ITER1)
1000  CONTINUE
C
C
C
311          FORMAT(4X,'INFORMATION RELATED WITH TEMPERATURE',/)
312          FORMAT(6X,'SURFACE COEFFICIENT       =',F8.4)
313          FORMAT(6X,'DIFFUSIVITY IN SQ.FT./HR. =',F8.4)
314          FORMAT(6X,'AVERAGE CONTRIBUTION (R)  =',F8.4)
315          FORMAT(6X,'THE  HALF-AMPLITUDE OF THE',
    *             1X,'EFFECTIVE AIR TEMPERATURE =',F8.4,/,
    *             6X,'DAILY RANGE IN AIR TEMP.  =',F8.4/)
411          format(4x,' Total Node considered in the running =  ',i3,
    *                   /,4X,' Total Number of Unknown             =  ',i3,/)
412          FORMAT(4x,'Initial Temperature Distribution at Time = 0.0',/,
    *             4x,'Depth(ft)      Temperature(F)            ',/,
    *             4x,60('='))
413          FORMAT(8x,F9.2,7x,F11.2)
415   FORMAT(4X,I4,1X,4(F10.2,1X))
1001  FORMAT(//,4X,'TEMPERATURE DISTRIBUTION OF COMPOSITE PAVEMENT',/,
    *                       4X,'DEPTH (INCHES)',1X,'TIME 1 2 3 4....',/,4X,77('='))
```

```
1002  FORMAT(1X,F8.2,2X,10(F6.1,1X),/,((11X,10(F6.1,1X))))
C
C
C
8889        CONTINUE
     STOP
     END

C
C***********************************************************
***********
C    SUBROUTINE TO SOLVE LINEAR SYSTEM PROBLEM, SPECIAALY FOR
C    TRIDIGONAL MATRIX OF HWIHC ELEMENTS CONSIST OF ZERO EXCEP
C    THREE DIAGONAL PARTS: MAIN, SUPER, AND SUB DIGONAL ELEMENTS
C    Ax = b
C        WHERE :   A = TRIDIGONAL MATRIX
C                  b =  RHS
C                  x = unknown to be solved
C
     SUBROUTINE THOMAS (A,B,C,D,X,IT)
            IMPLICIT REAL*8 (A-H,O-Z)
     DIMENSION A(1),B(1),C(1),D(1),X(1),Q(200),G(200)
     WI = A(1)
     G(1) = D(1)/WI
     DO 10 I=2,IT
       Q(I-1) = B(I-1)/WI
       WI = A(I) - C(I) *Q(I-1)
       G(I) = (D(I) - C(I)*G(I-1))/WI
10     CONTINUE
     X(IT) = G(IT)
     DO 20 I=2,IT
       J = IT - I +1
       X(J) = G(J) - Q(J)*X(J+1)
20     CONTINUE
     RETURN
     END
C
C----        FUNCTION TO CALCULATE INITIAL CONDITION OF TEMPERATURE AT TIME=TIME1
C
            FUNCTION TIMEINI(TIME1,TEMPM,TEMPV,H,C,DIST)
            IMPLICIT REAL*8 (A-H,O-Z)
            F1 = H/SQRT((H+C)**2+C**2)
            G1 = EXP(-DIST*C)
            H1 = DSIN(0.261799388*TIME1-DIST*C-DATAN(C/(H+C)))
            TIMEINI= TEMPM+TEMPV*F1*G1*H1
C
            RETURN
            END
```

OUTPUT List

```
 INFORMATION RELATED WITH TEMPERATURE

     SURFACE COEFFICIENT       =  8.6080
     DIFFUSIVITY IN SQ.FT./HR. =  2.4008
     AVERAGE CONTRIBUTION (R)  = 10.5566
     THE  HALF-AMPLITUDE OF THE EFFECTIVE AIR TEMPERATURE = 16.0000
     DAILY RANGE IN AIR TEMP.  = 56.5566

   Initial Temperature Distribution at Time = 0.0
   Depth(ft)      Temperature(F)
   ============================================================
         0.00          53.95
         0.04          53.13
         0.08          52.52
         0.13          52.10
         0.17          51.83
         0.21          51.70
         0.25          51.68
         0.29          51.75
         0.33          51.89
         0.38          52.10
         0.42          52.34
```

0.46	52.62
0.50	52.92
0.54	53.23
0.58	53.55
0.62	53.86
0.67	54.16
0.71	54.46
0.75	54.73
0.79	54.99
0.83	55.24
0.87	55.46
0.92	55.66
0.96	55.84
1.00	56.00
1.04	56.14
1.08	56.27
1.12	56.37
1.17	56.46
1.21	56.54
1.25	56.60
1.29	56.65
1.33	56.69
1.38	56.72
1.42	56.74
1.46	56.76
1.50	56.76
1.54	56.77
1.58	56.77
1.63	56.76
1.67	56.75
1.71	56.74
1.75	56.73
1.79	56.72
1.83	56.71
1.88	56.69
1.92	56.68
1.96	56.67
2.00	56.65
2.04	56.64
2.08	56.63
2.13	56.62
2.17	56.61
2.21	56.60
2.25	56.59
2.29	56.58
2.33	56.58
2.38	56.57
2.42	56.57
2.46	56.56
2.50	56.56
2.54	56.56
2.58	56.55
2.83	56.55
3.08	56.55
3.33	56.55
3.58	56.56
4.58	56.56
5.58	56.56
6.58	56.56

TEMPERATURE DISTRIBUTION OF COMPOSITE PAVEMENT
DEPTH (INCHES) TIME 1 2 3 4....
==

```
0.00    57.1   60.3   63.2   65.6   67.4   68.5   68.8   68.2   66.8   64.8
        62.2   59.2   56.0   52.8   50.0   47.5   45.7   44.6   44.3   44.9
        46.3   48.3   50.9   54.0   57.1
 0.50    56.0   58.8   61.6   63.9   65.8   67.0   67.6   67.3   66.4   64.7
        62.6   60.0   57.2   54.3   51.6   49.2   47.4   46.1   45.6   45.8
        46.8   48.4   50.6   53.2   56.0
 1.00    55.0   57.6   60.2   62.4   64.3   65.6   66.3   66.4   65.8   64.6
```

62.8 60.6 58.1 55.5 53.0 50.8 48.9 47.6 46.8 46.8
47.4 48.6 50.4 52.6 55.0
1.50 54.3 56.6 58.9 61.1 62.9 64.3 65.2 65.5 65.2 64.3
62.9 61.0 58.9 56.6 54.3 52.2 50.3 48.9 48.0 47.7
48.0 48.9 50.3 52.2 54.3
2.00 53.7 55.8 57.9 59.9 61.6 63.1 64.0 64.5 64.5 63.9
62.8 61.3 59.5 57.5 55.4 53.4 51.6 50.2 49.2 48.7
48.8 49.3 50.4 51.9 53.7
2.50 53.3 55.1 57.0 58.8 60.5 61.9 63.0 63.6 63.8 63.4
62.6 61.4 59.9 58.2 56.3 54.5 52.8 51.4 50.3 49.7
49.5 49.8 50.6 51.8 53.3
3.00 53.0 54.6 56.3 57.9 59.5 60.9 62.0 62.7 63.0 62.9
62.4 61.5 60.2 58.7 57.1 55.4 53.8 52.5 51.3 50.6
50.2 50.3 50.8 51.8 53.0
3.50 52.9 54.2 55.6 57.1 58.6 59.9 61.0 61.9 62.3 62.4
62.1 61.4 60.4 59.2 57.8 56.3 54.8 53.4 52.3 51.5
51.0 50.9 51.2 51.8 52.8
4.00 52.8 53.9 55.1 56.5 57.8 59.1 60.2 61.1 61.6 61.9
61.8 61.3 60.6 59.5 58.3 57.0 55.6 54.3 53.2 52.3
51.7 51.4 51.5 52.0 52.7
4.50 52.8 53.7 54.7 55.9 57.1 58.3 59.4 60.3 61.0 61.4
61.4 61.2 60.6 59.8 58.8 57.6 56.3 55.1 54.0 53.1
52.4 52.0 51.9 52.1 52.7
5.00 52.9 53.6 54.4 55.4 56.5 57.6 58.7 59.6 60.4 60.9
61.1 61.0 60.6 60.0 59.1 58.1 57.0 55.8 54.7 53.8
53.0 52.5 52.3 52.3 52.7
5.50 53.0 53.5 54.2 55.0 56.0 57.0 58.1 59.0 59.8 60.4
60.7 60.8 60.6 60.1 59.4 58.5 57.5 56.4 55.4 54.4
53.6 53.0 52.6 52.5 52.7
6.00 53.1 53.5 54.0 54.7 55.6 56.5 57.5 58.4 59.3 59.9
60.4 60.6 60.5 60.2 59.6 58.9 58.0 57.0 55.9 55.0
54.1 53.5 53.0 52.8 52.8
6.50 53.3 53.5 53.8 54.4 55.2 56.1 57.0 58.0 58.8 59.5
60.1 60.4 60.4 60.2 59.8 59.1 58.3 57.4 56.4 55.5
54.6 53.9 53.3 53.0 52.9
7.00 53.5 53.5 53.7 54.2 54.9 55.7 56.6 57.5 58.4 59.2
59.8 60.2 60.3 60.2 59.9 59.4 58.7 57.8 56.9 55.9
55.0 54.2 53.6 53.2 53.0
7.50 53.7 53.5 53.7 54.1 54.7 55.4 56.3 57.2 58.1 58.9
59.5 60.0 60.2 60.2 60.0 59.6 58.9 58.1 57.2 56.3
55.4 54.5 53.9 53.4 53.1
8.00 53.8 53.5 53.6 54.0 54.5 55.2 56.0 56.9 57.8 58.6
59.3 59.9 60.2 60.2 60.1 59.7 59.1 58.4 57.5 56.6
55.6 54.8 54.1 53.5 53.2
8.50 54.0 53.5 53.6 53.9 54.3 55.0 55.8 56.7 57.6 58.5
59.2 59.7 60.1 60.2 60.1 59.8 59.3 58.5 57.7 56.8
55.8 55.0 54.2 53.6 53.3
9.00 54.0 53.5 53.6 53.8 54.3 54.9 55.7 56.6 57.5 58.3
59.1 59.7 60.1 60.2 60.2 59.9 59.3 58.7 57.8 56.9
56.0 55.1 54.3 53.7 53.3
9.50 54.0 53.5 53.7 53.7 54.3 54.8 55.6 56.5 57.4 58.3
59.0 59.6 60.0 60.2 60.2 59.9 59.4 58.7 57.9 57.0
56.1 55.2 54.4 53.8 53.3

10.00 53.8 53.6 53.6 53.7 54.3 54.8 55.7 56.5 57.4 58.3
59.0 59.6 60.0 60.2 60.2 59.9 59.4 58.7 57.9 57.0
56.1 55.2 54.4 53.7 53.3
10.50 54.3 54.2 54.0 53.9 54.3 54.7 55.4 56.0 56.8 57.6
58.3 58.9 59.4 59.7 59.8 59.7 59.4 58.9 58.2 57.5
56.7 55.9 55.1 54.5 54.0
11.00 54.7 54.3 53.8 53.9 54.2 54.6 55.2 55.9 56.7 57.5
58.3 58.9 59.4 59.8 59.9 59.8 59.5 59.0 58.3 57.6
56.8 55.9 55.2 54.5 54.0
11.50 55.0 54.5 54.2 54.3 54.4 54.7 55.2 55.7 56.4 57.0
57.7 58.3 58.8 59.2 59.4 59.4 59.2 58.9 58.4 57.8
57.2 56.4 55.8 55.1 54.6
12.00 55.3 54.7 54.4 54.3 54.2 54.5 54.9 55.5 56.2 56.9
57.6 58.3 58.8 59.2 59.5 59.6 59.4 59.1 58.7 58.1
57.4 56.6 55.9 55.2 54.6
12.50 55.5 54.9 54.6 54.4 54.4 54.7 55.0 55.5 56.0 56.6
57.2 57.8 58.3 58.7 59.0 59.1 59.1 58.9 58.6 58.1
57.5 56.9 56.3 55.7 55.1
13.00 55.7 55.1 54.8 54.5 54.5 54.6 54.7 55.2 55.7 56.3
57.0 57.6 58.2 58.7 59.1 59.3 59.3 59.2 58.8 58.4
57.8 57.2 56.5 55.8 55.2
13.50 55.9 55.3 55.0 54.7 54.6 54.6 54.8 55.3 55.7 56.2
56.8 57.4 57.9 58.3 58.7 58.9 59.0 58.9 58.7 58.3
57.8 57.3 56.7 56.1 55.6
14.00 56.0 55.5 55.1 54.8 54.7 54.7 54.8 55.1 55.4 55.9
56.5 57.1 57.7 58.2 58.6 58.9 59.1 59.1 58.9 58.6
58.2 57.6 57.0 56.4 55.8
14.50 56.2 55.7 55.3 55.0 54.8 54.7 54.8 55.0 55.4 55.9
56.5 57.0 57.5 58.0 58.4 58.7 58.8 58.8 58.7 58.5
58.1 57.6 57.1 56.5 56.0
15.00 56.3 55.8 55.4 55.1 54.9 54.8 54.8 55.0 55.3 55.7
56.1 56.6 57.2 57.7 58.2 58.6 58.8 59.0 58.9 58.7
58.4 58.0 57.4 56.9 56.3
15.50 56.4 56.0 55.5 55.2 54.9 54.8 54.8 54.9 55.2 55.6
56.1 56.6 57.2 57.7 58.1 58.4 58.7 58.8 58.8 58.6
58.3 57.9 57.4 56.9 56.3
16.00 56.4 56.1 55.7 55.3 55.0 54.9 54.8 54.9 55.1 55.5
55.9 56.4 56.9 57.4 57.9 58.3 58.6 58.8 58.9 58.8
58.5 58.2 57.7 57.2 56.7
16.50 56.5 56.2 55.8 55.4 55.1 54.9 54.8 54.9 55.1 55.4
55.8 56.3 56.8 57.4 57.9 58.3 58.6 58.7 58.8 58.7
58.5 58.1 57.7 57.2 56.6
17.00 56.6 56.2 55.9 55.5 55.2 54.9 54.8 54.9 55.0 55.3
55.7 56.2 56.7 57.2 57.6 58.1 58.4 58.7 58.8 58.8
58.6 58.3 57.9 57.4 56.9
17.50 56.6 56.3 55.9 55.5 55.2 55.0 54.8 54.9 55.0 55.3
55.6 56.1 56.6 57.1 57.6 58.1 58.5 58.7 58.8 58.8
58.6 58.3 57.9 57.4 56.8
18.00 56.6 56.3 56.0 55.6 55.2 55.0 54.9 54.8 55.0 55.2
55.6 56.0 56.5 57.1 57.6 58.0 58.3 58.6 58.7 58.8
58.6 58.4 58.0 57.6 57.0
18.50 56.6 56.4 56.0 55.6 55.3 55.0 54.9 54.8 55.0 55.2
55.6 56.0 56.5 57.0 57.5 58.0 58.4 58.7 58.8 58.8

58.7 58.4 58.0 57.5 57.0
19.00 56.6 56.4 56.0 55.6 55.3 55.0 54.9 54.8 55.0 55.2
55.6 56.0 56.5 57.0 57.5 58.0 58.4 58.6 58.7 58.7
58.6 58.4 58.0 57.5 57.0
19.50 56.7 56.5 56.2 55.8 55.5 55.3 55.1 55.0 55.1 55.2
55.5 55.8 56.3 56.7 57.2 57.6 58.0 58.3 58.5 58.6
58.5 58.4 58.1 57.7 57.2
20.00 56.7 56.5 56.2 55.9 55.6 55.3 55.1 55.0 55.0 55.2
55.4 55.8 56.2 56.7 57.1 57.6 58.0 58.3 58.5 58.6
58.5 58.3 58.1 57.7 57.3
20.50 56.7 56.5 56.3 56.0 55.7 55.5 55.3 55.2 55.2 55.3
55.5 55.7 56.1 56.5 56.9 57.3 57.6 57.9 58.1 58.3
58.3 58.3 58.1 57.8 57.4
21.00 56.7 56.6 56.4 56.1 55.8 55.6 55.3 55.2 55.1 55.2
55.4 55.6 56.0 56.3 56.8 57.2 57.6 57.9 58.2 58.3
58.4 58.3 58.1 57.8 57.5
21.50 56.7 56.6 56.4 56.2 55.9 55.7 55.5 55.4 55.3 55.4
55.5 55.7 55.9 56.3 56.6 57.0 57.3 57.6 57.9 58.0
58.1 58.1 58.0 57.8 57.5
22.00 56.7 56.6 56.5 56.3 56.0 55.8 55.6 55.4 55.3 55.3
55.4 55.6 55.8 56.1 56.5 56.8 57.2 57.5 57.8 58.0
58.1 58.2 58.1 57.9 57.6
22.50 56.7 56.6 56.5 56.3 56.1 55.9 55.7 55.5 55.4 55.4
55.5 55.6 55.9 56.1 56.4 56.7 57.1 57.3 57.6 57.8
57.9 57.9 57.9 57.8 57.6
23.00 56.7 56.6 56.5 56.4 56.2 56.0 55.8 55.6 55.5 55.4
55.5 55.6 55.7 56.0 56.3 56.6 56.9 57.2 57.5 57.7
57.9 58.0 58.0 57.9 57.7
23.50 56.7 56.6 56.6 56.4 56.3 56.1 55.9 55.7 55.6 55.5
55.5 55.6 55.8 56.0 56.3 56.5 56.8 57.1 57.4 57.6
57.7 57.8 57.8 57.7 57.6
24.00 56.7 56.6 56.6 56.5 56.3 56.1 55.9 55.8 55.7 55.6
55.6 55.6 55.7 55.9 56.1 56.4 56.7 57.0 57.2 57.5
57.6 57.8 57.8 57.8 57.7
24.50 56.7 56.6 56.6 56.5 56.4 56.2 56.0 55.9 55.7 55.7
55.6 55.7 55.8 55.9 56.1 56.4 56.6 56.9 57.1 57.4
57.5 57.6 57.7 57.6 57.5
25.00 56.6 56.6 56.6 56.5 56.4 56.3 56.1 55.9 55.8 55.7
55.7 55.7 55.8 55.9 56.0 56.3 56.5 56.7 57.0 57.2
57.4 57.5 57.6 57.6 57.6
25.50 56.6 56.6 56.6 56.5 56.4 56.3 56.2 56.0 55.9 55.8
55.7 55.7 55.8 55.9 56.1 56.3 56.5 56.7 56.9 57.1
57.3 57.4 57.5 57.5 57.5
26.00 56.6 56.6 56.6 56.6 56.5 56.3 56.2 56.1 55.9 55.8
55.8 55.8 55.8 55.9 56.0 56.2 56.4 56.6 56.8 57.0
57.2 57.3 57.4 57.5 57.5
26.50 56.6 56.6 56.6 56.6 56.5 56.4 56.3 56.1 56.0 55.9
55.8 55.8 55.8 55.9 56.0 56.2 56.4 56.6 56.8 57.0
57.1 57.3 57.4 57.4 57.4
27.00 56.6 56.6 56.6 56.6 56.5 56.4 56.3 56.2 56.1 56.0
55.9 55.9 55.9 55.9 56.0 56.1 56.3 56.5 56.6 56.8
57.0 57.1 57.2 57.3 57.3
27.50 56.6 56.6 56.6 56.6 56.5 56.4 56.3 56.2 56.1 56.0

56.0 55.9 55.9 55.9 56.0 56.1 56.3 56.4 56.6 56.8
56.9 57.1 57.2 57.3 57.3
28.00 56.6 56.6 56.6 56.6 56.5 56.5 56.4 56.3 56.2 56.1
56.0 56.0 56.0 56.0 56.0 56.1 56.2 56.4 56.5 56.7
56.8 56.9 57.0 57.1 57.2
28.50 56.6 56.6 56.6 56.6 56.6 56.5 56.4 56.3 56.2 56.1
56.1 56.0 56.0 56.0 56.0 56.1 56.2 56.3 56.5 56.6
56.8 56.9 57.0 57.1 57.1
29.00 56.6 56.6 56.6 56.6 56.6 56.5 56.4 56.4 56.3 56.2
56.1 56.1 56.0 56.0 56.1 56.1 56.2 56.3 56.4 56.5
56.7 56.8 56.9 57.0 57.0
29.50 56.6 56.6 56.6 56.6 56.6 56.5 56.5 56.4 56.3 56.3
56.2 56.1 56.1 56.1 56.1 56.1 56.2 56.3 56.4 56.5
56.6 56.7 56.8 56.9 57.0
30.00 56.6 56.6 56.6 56.6 56.6 56.5 56.5 56.4 56.4 56.3
56.2 56.2 56.1 56.1 56.1 56.1 56.2 56.2 56.3 56.4
56.5 56.6 56.7 56.8 56.9
30.50 56.6 56.6 56.6 56.6 56.6 56.6 56.5 56.5 56.4 56.4
56.3 56.2 56.2 56.2 56.1 56.1 56.2 56.2 56.3 56.4
56.4 56.5 56.6 56.7 56.8
31.00 56.6 56.6 56.6 56.6 56.6 56.6 56.5 56.5 56.5 56.4
56.3 56.3 56.2 56.2 56.2 56.2 56.2 56.2 56.2 56.3
56.4 56.5 56.5 56.6 56.7
34.00 56.6 56.6 56.6 56.6 56.6 56.6 56.6 56.5 56.5 56.5
56.4 56.3 56.3 56.2 56.2 56.2 56.2 56.2 56.2 56.2
56.3 56.4 56.5 56.5 56.6
37.00 56.5 56.6 56.6 56.6 56.6 56.6 56.6 56.6 56.5 56.5
56.5 56.4 56.3 56.3 56.2 56.2 56.2 56.2 56.2 56.2
56.2 56.3 56.4 56.5 56.5
40.00 56.6 56.6 56.6 56.6 56.6 56.6 56.6 56.6 56.6 56.5
56.5 56.4 56.4 56.3 56.3 56.2 56.2 56.2 56.2 56.2
56.2 56.3 56.3 56.4 56.5
43.00 56.6 56.6 56.6 56.6 56.6 56.6 56.6 56.6 56.6 56.5
56.5 56.5 56.4 56.4 56.3 56.3 56.3 56.2 56.2 56.2
56.2 56.2 56.3 56.3 56.4
55.00 56.6 56.6 56.6 56.6 56.6 56.6 56.6 56.6 56.6 56.6
56.5 56.5 56.5 56.4 56.4 56.3 56.3 56.3 56.2 56.2
56.2 56.2 56.2 56.3 56.3
67.00 56.6 56.6 56.6 56.6 56.6 56.6 56.6 56.6 56.6 56.6
56.6 56.5 56.5 56.5 56.4 56.4 56.3 56.3 56.3 56.2
56.2 56.2 56.2 56.2 56.3
79.00 56.6 56.6 56.6 56.6 56.6 56.6 56.6 56.6 56.6 56.6
56.6 56.6 56.5 56.5 56.5 56.4 56.4 56.3 56.3 56.3
56.2 56.2 56.2 56.2 56.2

APPENDIX C

DATABASE FROM THE ABAQUS FOR THE STATISTICAL ANALYSIS

1. INPUTS OF FEM ANALYSIS

2. FEM ANALYSIS RESULTS UNDER TRAFFIC LOADING

3. FEM ANALYSIS RESULTS UNDER TEMPERATURE LOADING

1. Inputs of FEM Analysis

1.1 Input variable for FEM Analysis Results under Traffic Loading

Col.		Layer	1	2	3
1	Single wheel (lbf)		6000	9000	15000
2	Thickness (inch)	Overlay	3	6	9
3		Interlayer	0	4	8
4		Existing pavement	8	12	16
5		Subbase	0	6	8
6	Stiffness (psi)	Overlay	200,000	600,000	1,000,000
7		Interlayer	25,000	50,000	100,000
8		Existing pavement	3,500,000	5,500,000	7,500,000
9		Subbase	50,000	500,000	1,000,000
10		Subgrade	5,000	20,000	40,000

1.2 Input Variable FEM Analysis Results under Temperature Loading

Col.		Layer	1	2	3
1	Thickness (inches)	Overlay	3	6	9
2		Interlayer	0	4	8
3	Stiffness	Overlay (psi)	200,000	600,000	1,000,000
4		Interlayer (psi)	20,000	80,000	140,000
5		Existing Layer (psi)	3,500,000	5,500,000	7,500,000
6		Road Bed (pci)	400	800	1200
7	Thermal coefficient	Overlay	$15*10^{-6}$	$30*10^{-6}$	$45*10^{-6}$
8	(in/in/F)	Existing Layer	$4*10^{-6}$	$6*10^{-6}$	$8*10^{-6}$
9	Temperature Differentials (F/Day)		30	50	70
10		Subgrade	5,000	20,000	40,000

2. FEM analysis Results under Traffic Loading

										Deflection						
1										w1 (r=0")	w2 (r=12")	w3 (r=24")	w4 (r=36")	w5 (r=48")	w6 (r=60")	w7 (r=72")
0	0	0	0	0	0	0	0	0	0	-1.20E-02	-8.53E-03	-7.84E-03	-6.99E-03	-6.14E-03	-5.36E-03	-4.65E-03
2	1	2	0	0	1	2	0	2	0	-3.39E-03	-1.13E-03	-7.89E-04	-7.33E-04	-6.67E-04	-5.95E-04	-5.28E-04
1	2	1	0	0	2	1	0	1	0	-4.34E-03	-1.92E-03	-1.58E-03	-1.47E-03	-1.33E-03	-1.19E-03	-1.06E-03
0	1	1	2	1	1	0	2	1	2	-9.86E-03	-4.18E-03	-3.81E-03	-3.49E-03	-3.16E-03	-2.83E-03	-2.52E-03
2	2	0	2	1	2	2	2	0	2	-1.18E-02	-9.45E-03	-8.54E-03	-8.11E-03	-7.71E-03	-7.29E-03	-6.86E-03
1	0	2	2	1	0	1	2	2	2	-5.49E-03	-2.41E-03	-1.76E-03	-1.65E-03	-1.50E-03	-1.35E-03	-1.21E-03
0	2	2	1	2	2	0	1	2	1	-4.14E-03	-1.51E-03	-1.16E-03	-1.09E-03	-9.81E-04	-8.72E-04	-7.72E-04
2	0	1	1	2	0	2	1	1	1	-3.45E-03	-2.51E-03	-2.09E-03	-1.89E-03	-1.72E-03	-1.56E-03	-1.41E-03
1	1	0	1	2	1	1	1	0	1	-9.17E-03	-7.68E-03	-6.94E-03	-6.46E-03	-5.97E-03	-5.49E-03	-5.02E-03
2																
0	0	0	2	1	1	2	0	2	0	-3.01E-03	-1.54E-03	-1.32E-03	-1.08E-03	-8.82E-04	-7.21E-04	-5.95E-04
2	1	2	2	1	2	1	0	1	0	-2.19E-03	-1.36E-03	-1.17E-03	-1.09E-03	-1.02E-03	-9.36E-04	-8.56E-04
1	2	1	2	1	0	0	0	0	0	-7.52E-03	-5.51E-03	-4.41E-03	-4.06E-03	-3.80E-03	-3.52E-03	-3.24E-03
0	1	1	1	2	2	2	2	0	2	-1.19E-02	-8.83E-03	-8.54E-03	-8.19E-03	-7.79E-03	-7.38E-03	-6.95E-03
2	2	0	1	2	0	1	2	2	2	-6.52E-03	-4.50E-03	-3.07E-03	-2.31E-03	-1.89E-03	-1.61E-03	-1.39E-03
1	0	2	1	2	1	0	2	1	2	-5.37E-03	-3.55E-03	-3.09E-03	-2.88E-03	-2.65E-03	-2.43E-03	-2.21E-03
0	2	2	0	0	0	2	1	1	1	-1.37E-02	-2.57E-03	-1.67E-03	-1.73E-03	-1.61E-03	-1.48E-03	-1.35E-03
2	0	1	0	0	1	1	1	0	1	-9.91E-03	-6.81E-03	-6.34E-03	-6.02E-03	-5.65E-03	-5.26E-03	-4.86E-03
1	1	0	0	0	2	0	1	2	1	-5.76E-03	-2.54E-03	-2.04E-03	-1.66E-03	-1.34E-03	-1.08E-03	-8.83E-04
3																
0	0	0	1	2	2	1	0	1	0	-3.46E-03	-2.57E-03	-2.26E-03	-1.94E-03	-1.65E-03	-1.39E-03	-1.18E-03
2	1	2	1	2	0	0	0	0	0	-4.54E-03	-3.82E-03	-3.40E-03	-3.18E-03	-3.02E-03	-2.86E-03	-2.69E-03
1	2	1	1	2	1	2	0	2	0	-2.58E-03	-1.45E-03	-9.06E-04	-7.79E-04	-7.04E-04	-6.20E-04	-5.41E-04
0	1	1	0	0	0	1	2	2	2	-1.57E-02	-2.97E-03	-2.72E-03	-2.38E-03	-2.05E-03	-1.75E-03	-1.49E-03
2	2	0	0	0	1	0	2	1	2	-1.38E-02	-7.32E-03	-5.33E-03	-4.53E-03	-3.88E-03	-3.31E-03	-2.82E-03
1	0	2	0	0	2	2	2	0	2	-1.22E-02	-7.89E-03	-7.69E-03	-7.45E-03	-7.16E-03	-6.84E-03	-6.50E-03
0	2	2	2	1	1	1	1	0	1	-9.88E-03	-5.00E-03	-4.37E-03	-4.33E-03	-4.16E-03	-3.98E-03	-3.80E-03
2	0	1	2	1	2	0	1	2	1	-2.71E-03	-1.58E-03	-1.33E-03	-1.19E-03	-1.05E-03	-9.23E-04	-8.08E-04
1	1	0	2	1	0	2	1	1	1	-6.11E-03	-3.67E-03	-2.72E-03	-2.42E-03	-2.14E-03	-1.87E-03	-1.63E-03
4																
0	1	0	1	0	1	0	0	2	2	-1.27E-02	-4.38E-03	-3.66E-03	-2.88E-03	-2.25E-03	-1.78E-03	-1.44E-03
2	2	2	1	0	2	2	0	1	2	-9.10E-03	-3.60E-03	-2.73E-03	-2.60E-03	-2.45E-03	-2.28E-03	-2.09E-03
1	0	1	1	0	0	1	0	0	2	-1.83E-02	-1.19E-02	-1.10E-02	-1.04E-02	-9.73E-03	-9.02E-03	-8.30E-03
0	2	1	0	1	2	0	2	0	1	-1.03E-02	-7.15E-03	-6.65E-03	-6.29E-03	-5.86E-03	-5.42E-03	-4.98E-03
2	0	0	0	1	0	2	2	2	1	-3.88E-03	-2.42E-03	-1.82E-03	-1.51E-03	-1.25E-03	-1.04E-03	-8.70E-04
1	1	2	0	1	1	1	2	1	1	-4.27E-03	-2.36E-03	-1.91E-03	-1.80E-03	-1.66E-03	-1.52E-03	-1.37E-03
0	0	2	2	2	0	0	1	1	0	-3.33E-03	-1.54E-03	-1.36E-03	-1.26E-03	-1.15E-03	-1.04E-03	-9.41E-04
2	1	1	2	2	1	2	1	0	0	-4.07E-03	-3.43E-03	-3.14E-03	-2.99E-03	-2.86E-03	-2.73E-03	-2.59E-03
1	2	0	2	2	2	1	1	2	0	-2.27E-03	-1.35E-03	-9.70E-04	-8.40E-04	-7.29E-04	-6.27E-04	-5.41E-04
5																
0	1	0	0	1	2	2	0	1	2	-9.84E-03	-6.05E-03	-5.44E-03	-4.74E-03	-4.07E-03	-3.48E-03	-2.98E-03

	Stress/Strain						
	ACC		ACC		Interlayer		PCC
	Vertical		Horizontal		Vertical		Horizontal
	Stress	Strain	Stress	Strain	Stress	Strain	Stress
	-53.16	-6.26E-05	18.55	1.52E-04	-53.47	-1.20E-03	102.20
	-53.33	-9.91E-05	14.20	8.27E-05	-21.28	-3.09E-04	19.31
	-53.45	-9.03E-05	10.87	9.10E-05	-32.11	-2.71E-04	30.83
	-135.90	6.77E-05	177.90	2.53E-04	-106.90	-1.34E-03	40.62
	-133.70	-4.27E-05	64.82	9.06E-05	-36.49	-2.91E-04	64.98
	-134.80	-1.79E-05	121.20	1.65E-04	-62.19	-1.38E-03	35.80
	-82.21	4.76E-05	128.30	1.03E-04	-56.81	-4.02E-04	19.94
	-80.32	-1.13E-05	56.45	4.29E-05	-19.07	-4.13E-04	41.65
	-81.20	1.82E-05	93.97	7.03E-05	-28.75	-3.62E-04	70.94
	-53.50	-7.57E-06	35.80	6.78E-05	-50.85	-5.65E-04	79.47
	-53.42	-2.68E-05	19.59	3.18E-05	-18.70	-1.30E-04	19.88
	-54.34	3.49E-05	83.89	9.80E-05	-13.79	-3.88E-04	31.85
	-135.50	3.06E-05	146.00	1.33E-04	-111.00	-6.95E-04	89.90
	-134.20	8.91E-06	145.40	9.93E-05	-16.04	-4.32E-04	36.62
	-134.70	-9.34E-06	110.50	9.31E-05	-64.35	-7.25E-04	33.42
	-81.82	1.47E-04	107.30	4.51E-04	-60.09	-1.72E-03	38.60
	-79.93	-1.60E-04	9.08	9.48E-05	-38.14	-4.82E-04	67.58
	-80.00	-1.55E-04	8.26	1.20E-04	-54.04	-4.13E-04	68.98
	-53.41	-8.57E-07	25.46	3.41E-05	-51.27	-2.85E-04	77.68
	-53.62	-1.08E-06	47.69	3.38E-05	-9.05	-2.14E-04	20.30
	-54.29	1.61E-05	78.85	5.59E-05	-14.95	-2.14E-04	27.28
	-134.80	8.43E-06	124.80	6.04E-04	-116.10	-2.97E-03	95.34
	-133.60	-1.79E-04	49.58	2.33E-04	-41.98	-7.02E-04	93.18
	-132.90	-3.35E-04	-4.83	1.64E-04	-103.90	-7.03E-04	81.31
	-82.58	9.67E-05	148.80	1.92E-04	-54.47	-7.64E-04	32.15
	-80.02	-4.63E-05	17.80	3.84E-05	-33.68	-2.08E-04	24.22
	-81.26	2.16E-05	101.80	1.25E-04	-27.58	-6.81E-04	63.79
	-133.40	-1.70E-04	45.84	3.68E-04	-126.30	-1.67E-03	144.90
	-133.30	-2.55E-04	21.69	1.62E-04	-52.95	-4.63E-04	50.27
	-133.90	-2.04E-04	56.38	3.27E-04	-84.72	-2.02E-03	126.10
	-81.36	3.89E-05	71.52	1.14E-04	-63.32	-4.47E-04	56.14
	-80.25	-2.57E-05	47.76	6.42E-05	-22.62	-5.08E-04	76.39
	-80.92	-6.62E-06	72.56	9.82E-05	-35.47	-4.62E-04	35.60
	-54.89	3.35E-05	101.30	7.89E-05	-39.76	-8.47E-04	18.08
	-53.56	-6.32E-06	37.33	2.82E-05	-12.15	-1.51E-04	28.49
	-54.07	6.62E-06	57.47	4.37E-05	-19.40	-1.49E-04	24.37
	-134.20	-5.21E-06	81.12	1.57E-04	-120.30	-7.70E-04	199.20

2	2	2	0	1	0	1	0	0	2	-1.29E-02	-9.83E-03	-8.11E-03	-7.41E-03	-7.06E-03	-6.76E-03	-6.44E-03
1	0	1	0	1	1	0	0	2	2	-5.98E-03	-3.39E-03	-2.77E-03	-2.39E-03	-2.03E-03	-1.72E-03	-1.46E-03
0	2	1	2	2	0	2	2	2	1	-8.33E-03	-2.61E-03	-1.04E-03	-1.10E-03	-1.01E-03	-8.93E-04	-7.87E-04
2	0	0	2	2	1	1	2	1	1	-3.54E-03	-2.67E-03	-2.31E-03	-2.08E-03	-1.87E-03	-1.67E-03	-1.48E-03
1	1	2	2	2	2	0	2	0	1	-5.64E-03	-4.54E-03	-4.25E-03	-4.12E-03	-3.98E-03	-3.82E-03	-3.65E-03
0	0	2	1	0	1	2	1	0	0	-5.02E-03	-3.04E-03	-3.00E-03	-2.91E-03	-2.80E-03	-2.68E-03	-2.55E-03
2	1	1	1	0	2	1	1	2	0	-3.16E-03	-1.13E-03	-8.95E-04	-8.16E-04	-7.25E-04	-6.37E-04	-5.56E-04
1	2	0	1	0	0	0	1	1	0	-7.40E-03	-3.28E-03	-2.00E-03	-1.77E-03	-1.55E-03	-1.33E-03	-1.13E-03
6																
0	1	0	2	2	0	1	0	0	2	-2.39E-02	-1.67E-02	-1.48E-02	-1.36E-02	-1.23E-02	-1.10E-02	-9.82E-03
2	2	2	2	2	1	0	0	2	2	-4.98E-03	-3.20E-03	-2.22E-03	-1.81E-03	-1.60E-03	-1.43E-03	-1.27E-03
1	0	1	2	2	2	2	0	1	2	-5.47E-03	-4.01E-03	-3.64E-03	-3.35E-03	-3.05E-03	-2.75E-03	-2.46E-03
0	2	1	1	0	1	1	2	1	1	-9.50E-03	-2.59E-03	-2.18E-03	-2.07E-03	-1.89E-03	-1.70E-03	-1.52E-03
2	0	0	1	0	2	0	2	0	1	-1.08E-02	-7.92E-03	-7.42E-03	-6.95E-03	-6.44E-03	-5.90E-03	-5.37E-03
1	1	2	1	0	0	2	2	2	1	-6.51E-03	-1.67E-03	-9.87E-04	-9.78E-04	-8.98E-04	-8.12E-04	-7.30E-04
0	0	2	0	1	2	1	1	2	0	-1.83E-03	-9.23E-04	-8.65E-04	-7.83E-04	-7.00E-04	-6.20E-04	-5.46E-04
2	1	1	0	1	0	0	1	1	0	-3.45E-03	-2.36E-03	-1.82E-03	-1.57E-03	-1.39E-03	-1.22E-03	-1.07E-03
1	2	0	0	1	1	2	1	0	0	-7.21E-03	-5.56E-03	-4.79E-03	-4.45E-03	-4.11E-03	-3.76E-03	-3.43E-03
7																
0	2	0	2	0	2	0	0	1	1	-8.31E-03	-3.95E-03	-3.39E-03	-2.92E-03	-2.47E-03	-2.08E-03	-1.76E-03
2	0	2	2	0	0	2	0	0	1	-8.32E-03	-4.96E-03	-4.46E-03	-4.34E-03	-4.18E-03	-4.00E-03	-3.81E-03
1	1	1	2	0	1	1	0	2	1	-5.79E-03	-1.94E-03	-1.52E-03	-1.37E-03	-1.18E-03	-1.02E-03	-8.76E-04
0	0	1	1	1	0	0	2	2	0	-3.35E-03	-1.17E-03	-1.02E-03	-8.94E-04	-7.74E-04	-6.67E-04	-5.74E-04
2	1	0	1	1	1	2	2	1	0	-2.99E-03	-2.02E-03	-1.65E-03	-1.48E-03	-1.32E-03	-1.17E-03	-1.03E-03
1	2	2	1	1	2	1	2	0	0	-4.30E-03	-3.07E-03	-2.75E-03	-2.69E-03	-2.60E-03	-2.51E-03	-2.40E-03
0	1	2	0	2	1	0	1	0	2	-1.45E-02	-9.79E-03	-9.21E-03	-8.81E-03	-8.32E-03	-7.82E-03	-7.32E-03
2	2	1	0	2	2	2	1	2	2	-4.32E-03	-2.76E-03	-2.07E-03	-1.79E-03	-1.61E-03	-1.43E-03	-1.27E-03
1	0	0	0	2	0	1	1	1	2	-9.31E-03	-6.83E-03	-5.53E-03	-4.72E-03	-3.99E-03	-3.38E-03	-2.87E-03
8																
0	2	0	1	1	0	2	0	0	1	-1.73E-02	-9.87E-03	-8.04E-03	-7.61E-03	-6.95E-03	-6.28E-03	-5.65E-03
2	0	2	1	1	1	1	0	2	1	-2.68E-03	-1.45E-03	-1.17E-03	-1.07E-03	-9.64E-04	-8.62E-04	-7.66E-04
1	1	1	1	1	2	0	0	1	1	-4.52E-03	-2.95E-03	-2.56E-03	-2.31E-03	-2.06E-03	-1.82E-03	-1.60E-03
0	0	1	0	2	1	2	2	1	0	-2.95E-03	-1.77E-03	-1.64E-03	-1.49E-03	-1.34E-03	-1.20E-03	-1.06E-03
2	1	0	0	2	2	1	2	0	0	-5.18E-03	-4.56E-03	-4.21E-03	-3.93E-03	-3.66E-03	-3.39E-03	-3.13E-03
1	2	2	0	2	0	0	2	2	0	-3.21E-03	-1.84E-03	-9.96E-04	-7.65E-04	-6.92E-04	-6.21E-04	-5.45E-04
0	1	2	2	0	2	2	1	2	2	-6.84E-03	-1.83E-03	-1.81E-03	-1.68E-03	-1.53E-03	-1.38E-03	-1.24E-03
2	2	1	2	0	0	1	1	1	2	-1.36E-02	-6.27E-03	-3.75E-03	-3.21E-03	-2.99E-03	-2.73E-03	-2.45E-03
1	0	0	2	0	1	0	1	0	2	-2.00E-02	-1.46E-02	-1.36E-02	-1.26E-02	-1.16E-02	-1.05E-02	-9.49E-03
9																
0	2	0	0	2	1	1	0	2	1	-6.87E-03	-2.78E-03	-1.81E-03	-1.56E-03	-1.27E-03	-1.04E-03	-8.62E-04
2	0	2	0	2	2	0	0	1	1	-2.89E-03	-2.13E-03	-1.91E-03	-1.77E-03	-1.62E-03	-1.48E-03	-1.34E-03
1	1	1	0	2	0	2	0	0	1	-8.22E-03	-6.51E-03	-5.65E-03	-5.34E-03	-5.06E-03	-4.74E-03	-4.43E-03
0	0	1	2	0	2	1	2	0	0	-5.13E-03	-3.74E-03	-3.64E-03	-3.48E-03	-3.29E-03	-3.10E-03	-2.90E-03
2	1	0	2	0	0	0	2	2	0	-4.29E-03	-1.70E-03	-1.06E-03	-9.05E-04	-7.84E-04	-6.69E-04	-5.71E-04
1	2	2	2	0	1	2	2	1	0	-4.62E-03	-1.52E-03	-9.72E-04	-9.67E-04	-9.22E-04	-8.59E-04	-7.95E-04
0	1	2	1	1	0	1	1	1	2	-1.23E-02	-3.82E-03	-3.13E-03	-2.99E-03	-2.75E-03	-2.51E-03	-2.27E-03
2	2	1	1	1	1	0	1	0	2	-1.31E-02	-1.04E-02	-9.05E-03	-8.44E-03	-7.99E-03	-7.52E-03	-7.05E-03

	-134.10	-6.46E-06	121.90	1.43E-04	-20.90	-5.81E-04	55.66
	-134.30	-3.99E-05	81.18	1.30E-04	-74.51	-8.68E-04	75.69
	-84.92	1.52E-04	307.00	2.11E-04	-37.26	-9.77E-04	30.60
	-80.23	-1.48E-05	43.60	3.62E-05	-23.63	-2.69E-04	32.58
	-80.84	-3.93E-06	64.40	5.41E-05	-36.95	-2.45E-04	18.53
	-52.77	-1.40E-04	1.76	1.03E-04	-56.29	-6.63E-04	30.80
	-53.28	-1.12E-04	4.76	5.79E-05	-24.51	-1.92E-04	21.77
	-53.98	2.12E-06	50.43	1.99E-04	-21.40	-6.65E-04	26.99
	-139.80	1.88E-04	382.20	2.73E-04	-77.62	-1.81E-03	216.00
	-134.00	-6.57E-06	116.90	8.30E-05	-22.31	-3.19E-04	31.11
	-134.10	-2.68E-05	67.88	7.05E-05	-78.45	-4.60E-04	98.44
	-80.75	-2.06E-05	46.25	2.68E-04	-67.93	-9.91E-04	34.00
	-79.84	-1.66E-04	-2.71	6.16E-05	-40.77	-2.72E-04	38.82
	-80.69	-7.39E-05	57.64	2.56E-04	-40.65	-1.10E-03	26.64
	-52.99	-3.39E-05	11.71	4.42E-05	-54.69	-3.14E-04	25.20
	-53.57	-9.32E-06	41.07	5.05E-05	-11.17	-2.76E-04	25.84
	-54.13	1.89E-05	61.81	7.68E-05	-18.17	-2.72E-04	67.83
	-80.07	-1.15E-04	2.16	1.34E-04	-72.85	-5.19E-04	71.95
	-80.04	-1.49E-04	22.41	1.30E-04	-33.53	-7.99E-04	44.98
	-80.32	-1.26E-04	31.81	1.86E-04	-48.38	-7.00E-04	48.61
	-54.25	2.25E-05	71.04	1.02E-04	-44.97	-9.76E-04	19.17
	-53.50	-1.74E-05	30.60	4.12E-05	-14.65	-1.92E-04	31.51
	-53.87	-5.83E-06	40.58	5.72E-05	-23.68	-1.87E-04	16.83
	-137.60	9.73E-05	254.10	1.96E-04	-94.75	-1.15E-03	72.95
	-133.90	-1.91E-05	88.58	6.74E-05	-29.96	-2.30E-04	57.08
	-135.30	2.69E-05	163.40	1.22E-04	-49.67	-1.09E-03	157.00
	-83.96	1.92E-04	233.10	2.76E-04	-44.33	-1.20E-03	125.50
	-80.12	-4.16E-05	30.79	4.98E-05	-29.33	-3.40E-04	29.53
	-80.57	-2.14E-05	45.09	7.29E-05	-42.72	-2.97E-04	44.20
	-54.03	9.40E-06	59.51	5.45E-05	-46.69	-5.08E-04	48.57
	-53.50	-4.60E-06	28.85	2.35E-05	-14.32	-9.82E-05	50.24
	-54.46	2.76E-05	99.83	6.81E-05	-11.10	-2.98E-04	14.80
	-132.50	-3.33E-04	-1.18	2.27E-04	-132.50	-9.21E-04	51.16
	-133.80	-1.41E-04	78.91	3.12E-04	-33.57	-1.04E-03	50.31
	-133.40	-2.50E-04	21.04	2.30E-04	-94.69	-1.19E-03	97.87
	-83.61	1.01E-04	212.10	1.53E-04	-46.82	-6.41E-04	76.48
	-80.11	-2.19E-05	27.62	2.78E-05	-29.26	-1.74E-04	27.19
	-81.47	2.68E-05	121.20	8.58E-05	-22.62	-5.37E-04	67.60
	-52.69	-1.62E-04	-11.52	6.04E-05	-56.33	-3.43E-04	28.97
	-53.45	-7.70E-05	24.41	1.08E-04	-17.24	-4.66E-04	12.55
	-53.71	-5.51E-05	29.86	1.43E-04	-27.03	-4.43E-04	15.86
	-138.10	1.74E-04	292.10	3.66E-04	-90.88	-2.18E-03	55.70
	-133.90	-2.19E-05	94.92	1.18E-04	-27.73	-4.16E-04	48.06

1	0	0	1	1	2	2	1	2	2	-5.36E-03	-3.27E-03	-2.79E-03	-2.40E-03	-2.04E-03	-1.73E-03	-1.46E-03
10																
0	1	0	2	1	2	0	1	0	0	-7.09E-03	-5.53E-03	-5.22E-03	-4.84E-03	-4.45E-03	-4.06E-03	-3.68E-03
2	2	2	2	1	0	2	1	2	0	-2.69E-03	-1.49E-03	-8.40E-04	-6.18E-04	-5.53E-04	-5.14E-04	-4.71E-04
1	0	1	2	1	1	1	1	1	0	-2.68E-03	-1.68E-03	-1.48E-03	-1.36E-03	-1.23E-03	-1.11E-03	-9.91E-04
0	2	1	1	2	0	0	0	1	2	-1.69E-02	-7.22E-03	-4.30E-03	-4.06E-03	-3.61E-03	-3.14E-03	-2.73E-03
2	0	0	1	2	1	2	0	0	2	-1.33E-02	-1.18E-02	-1.09E-02	-1.02E-02	-9.46E-03	-8.74E-03	-8.04E-03
1	1	2	1	2	2	1	0	2	2	-4.16E-03	-2.34E-03	-1.91E-03	-1.76E-03	-1.59E-03	-1.42E-03	-1.27E-03
0	0	2	0	0	1	0	2	2	1	-4.64E-03	-1.58E-03	-1.49E-03	-1.32E-03	-1.16E-03	-1.00E-03	-8.68E-04
2	1	1	0	0	2	2	2	1	1	-5.68E-03	-2.62E-03	-2.25E-03	-2.10E-03	-1.91E-03	-1.72E-03	-1.54E-03
1	2	0	0	0	0	1	2	0	1	-1.72E-02	-1.10E-02	-8.82E-03	-8.14E-03	-7.42E-03	-6.66E-03	-5.95E-03
11																
0	1	0	1	2	0	2	1	2	0	-4.40E-03	-1.65E-03	-1.15E-03	-1.00E-03	-8.32E-04	-6.93E-04	-5.81E-04
2	2	2	1	2	1	1	1	1	0	-2.27E-03	-1.56E-03	-1.18E-03	-1.03E-03	-9.54E-04	-8.88E-04	-8.19E-04
1	0	1	1	2	2	0	1	0	0	-4.67E-03	-4.04E-03	-3.83E-03	-3.64E-03	-3.42E-03	-3.21E-03	-2.99E-03
0	2	1	0	0	1	2	0	0	2	-2.22E-02	-1.07E-02	-9.85E-03	-9.50E-03	-8.95E-03	-8.37E-03	-7.78E-03
2	0	0	0	0	2	1	0	2	2	-8.67E-03	-3.84E-03	-3.15E-03	-2.65E-03	-2.18E-03	-1.80E-03	-1.50E-03
1	1	2	0	0	0	0	0	1	2	-1.32E-02	-5.08E-03	-3.76E-03	-3.55E-03	-3.22E-03	-2.89E-03	-2.57E-03
0	0	2	2	1	2	2	2	1	1	-3.01E-03	-1.69E-03	-1.63E-03	-1.54E-03	-1.44E-03	-1.33E-03	-1.23E-03
2	1	1	2	1	0	1	2	0	1	-7.30E-03	-5.68E-03	-4.97E-03	-4.68E-03	-4.47E-03	-4.25E-03	-4.01E-03
1	2	0	2	1	1	0	2	2	1	-4.84E-03	-2.44E-03	-1.49E-03	-1.28E-03	-1.13E-03	-9.67E-04	-8.30E-04
12																
0	1	0	0	0	1	1	1	1	0	-6.03E-03	-2.71E-03	-2.43E-03	-2.06E-03	-1.73E-03	-1.45E-03	-1.21E-03
2	2	2	0	0	2	0	1	0	0	-5.98E-03	-3.75E-03	-3.35E-03	-3.23E-03	-3.09E-03	-2.93E-03	-2.76E-03
1	0	1	0	0	0	2	1	2	0	-3.75E-03	-1.23E-03	-9.89E-04	-8.91E-04	-7.79E-04	-6.75E-04	-5.84E-04
0	2	1	2	1	2	1	0	2	2	-8.14E-03	-2.94E-03	-2.40E-03	-2.18E-03	-1.90E-03	-1.65E-03	-1.43E-03
2	0	0	2	1	0	0	0	1	2	-9.27E-03	-6.69E-03	-5.40E-03	-4.55E-03	-3.85E-03	-3.26E-03	-2.78E-03
1	1	2	2	1	1	2	0	0	2	-1.11E-02	-7.99E-03	-7.25E-03	-7.06E-03	-6.81E-03	-6.52E-03	-6.23E-03
0	0	2	1	2	0	1	2	0	1	-7.43E-03	-4.78E-03	-4.54E-03	-4.39E-03	-4.21E-03	-4.03E-03	-3.83E-03
2	1	1	1	2	1	0	2	2	1	-2.72E-03	-1.77E-03	-1.34E-03	-1.15E-03	-1.02E-03	-8.95E-04	-7.84E-04
1	2	0	1	2	2	2	2	1	1	-4.24E-03	-2.86E-03	-2.29E-03	-2.07E-03	-1.87E-03	-1.67E-03	-1.48E-03
13																
0	2	0	0	1	0	0	1	2	2	-0.01865	-0.00619	-0.00320	-0.00278	-0.00219	-0.00173	-0.00141
2	0	2	0	1	1	2	1	1	2	-5.35E-03	-3.31E-03	-2.85E-03	-2.68E-03	-2.50E-03	-2.31E-03	-2.12E-03
1	1	1	0	1	2	1	1	0	2	-0.01306	-0.01047	-0.00982	-0.00935	-0.00879	-0.00822	-0.00765
0	0	1	2	2	1	0	0	0	1	-9.49E-03	-7.58E-03	-7.17E-03	-6.69E-03	-6.20E-03	-5.69E-03	-5.20E-03
2	1	0	2	2	2	2	0	2	1	-0.00282	-0.00194	-0.00156	-0.00133	-0.00114	-0.00097	-0.00083
1	2	2	2	2	0	1	0	1	1	-0.00534	-0.00329	-0.00204	-0.00171	-0.00160	-0.00148	-0.00135
0	1	2	1	0	2	0	2	1	0	-0.00345	-0.00141	-0.00136	-0.00127	-0.00116	-0.00106	-0.00095
2	2	1	1	0	0	2	2	0	0	-0.00736	-0.00444	-0.00343	-0.00319	-0.00307	-0.00292	-0.00276
1	0	0	1	0	1	1	2	2	0	-3.44E-03	-1.36E-03	-1.15E-03	-9.87E-04	-8.33E-04	-7.02E-04	-5.92E-04
14																
0	2	0	2	2	1	2	1	1	2	-0.01245	-0.00571	-0.00424	-0.00394	-0.00348	-0.00305	-0.00267
2	0	2	2	2	2	1	1	0	2	-8.35E-03	-7.13E-03	-6.80E-03	-6.61E-03	-6.39E-03	-6.16E-03	-5.92E-03
1	1	1	2	2	0	0	1	2	2	-0.00664	-0.00380	-0.00245	-0.00208	-0.00183	-0.00159	-0.00137
0	0	1	1	0	2	2	0	2	1	-3.70E-03	-1.65E-03	-1.54E-03	-1.36E-03	-1.18E-03	-1.02E-03	-8.82E-04
2	1	0	1	0	0	1	0	1	1	-0.00835	-0.00439	-0.00324	-0.00278	-0.00238	-0.00202	-0.00172

	-133.70	-6.69E-05	42.17	9.53E-05	-87.49	-5.35E-04	121.3
	-53.71	2.91E-06	30.47	6.04E-05	-47.84	-3.04E-04	39.6
	-53.62	-4.58E-06	48.91	5.74E-05	-8.42	-2.34E-04	13.8
	-53.70	-1.80E-05	31.75	5.13E-05	-30.27	-3.51E-04	28.2
	-141.50	2.61E-04	510.50	3.51E-04	-61.93	-1.62E-03	75.6
	-133.70	-1.33E-05	74.43	6.10E-05	-38.17	-4.38E-04	158.9
	-134.70	-1.04E-05	109.30	9.17E-05	-62.10	-4.12E-04	49.7
	-79.19	-2.05E-04	2.61	1.54E-04	-84.10	-9.90E-04	34.7
	-79.92	-1.67E-04	6.85	8.60E-05	-36.84	-2.87E-04	52.5
	-80.97	1.46E-05	74.34	2.95E-04	-32.04	-9.91E-04	108.1
	-55.90	6.80E-05	155.50	1.11E-04	-31.20	-7.30E-04	51.07
	-53.61	-2.91E-06	46.27	3.29E-05	-9.02	-1.28E-04	14.21
	-53.67	-6.75E-06	26.62	2.76E-05	-30.48	-1.79E-04	27.49
	-134.60	-2.68E-05	75.32	4.41E-04	-113.20	-1.64E-03	122.50
	-133.10	-2.89E-04	-2.81	1.08E-04	-68.03	-4.62E-04	125.70
	-134.50	-1.14E-04	95.49	4.23E-04	-67.43	-1.82E-03	56.42
	-79.45	-5.33E-05	17.88	6.67E-05	-82.31	-4.73E-04	31.21
	-80.36	-1.64E-05	59.74	7.40E-05	-17.17	-4.19E-04	29.25
	-81.19	1.92E-05	94.85	1.18E-04	-27.43	-4.13E-04	17.12
	-53.35	-6.91E-05	18.07	1.46E-04	-50.63	-6.68E-04	78.19
	-53.33	-9.74E-05	8.07	6.26E-05	-21.04	-1.82E-04	20.38
	-53.54	-8.74E-05	23.19	1.33E-04	-34.00	-8.12E-04	39.33
	-135.60	4.84E-05	128.60	2.00E-04	-105.80	-7.60E-04	73.91
	-133.80	-3.06E-05	83.86	1.10E-04	-35.72	-8.14E-04	103.90
	-134.90	-1.09E-05	119.90	1.63E-04	-59.31	-7.70E-04	73.14
	-82.31	4.92E-05	150.30	1.17E-04	-59.90	-1.27E-03	34.89
	-80.34	-1.06E-05	57.59	4.33E-05	-17.93	-2.25E-04	17.16
	-81.10	1.05E-05	85.03	6.48E-05	-29.22	-2.23E-04	44.64
	-139.90	3.14E-04	395.60	4.68E-04	-73.70	-2.00E-03	113.50
	-133.50	-6.97E-05	50.57	8.24E-05	-49.27	-5.70E-04	60.58
	-134.20	-3.44E-05	72.29	1.19E-04	-71.86	-4.94E-04	106.50
	-81.12	2.38E-05	85.78	7.91E-05	-69.27	-7.52E-04	70.80
	-80.19	-1.40E-05	43.63	3.58E-05	-22.32	-1.52E-04	61.82
	-81.65	4.12E-05	149.00	1.02E-04	-16.70	-4.47E-04	28.86
	-53.00	-1.29E-04	-1.01	8.88E-05	-52.82	-3.65E-04	14.27
	-53.48	-5.54E-05	31.32	1.24E-04	-13.44	-4.16E-04	27.46
	-53.33	-1.11E-04	9.44	9.62E-05	-38.26	-4.85E-04	32.90
	-139.30	1.66E-04	351.30	2.54E-04	-78.20	-1.07E-03	107.50
	-133.50	-3.86E-05	43.76	4.54E-05	-50.32	-2.95E-04	47.65
	-135.70	4.13E-05	205.10	1.45E-04	-37.45	-8.92E-04	39.65
	-79.03	-2.46E-04	-16.72	9.26E-05	-84.60	-5.18E-04	63.57
	-80.14	-1.07E-04	36.79	1.63E-04	-25.56	-6.94E-04	80.02

1	2	2	1	0	1	0	0	0	1	-0.01091	-0.00621	-0.00527	-0.00511	-0.00487	-0.00459	-0.00431
0	1	2	0	1	0	2	2	0	0	-0.00671	-0.00333	-0.00305	-0.00298	-0.00286	-0.00273	-0.00259
2	2	1	0	1	1	1	2	2	0	-0.00254	-0.00146	-0.00098	-0.00080	-0.00071	-0.00062	-0.00054
1	0	0	0	1	2	0	2	1	0	-3.59E-03	-2.65E-03	-2.28E-03	-1.95E-03	-1.65E-03	-1.40E-03	-1.19E-03
15																
0	2	0	1	0	2	1	1	0	2	-2.12E-02	-1.40E-02	-1.31E-02	-1.23E-02	-1.13E-02	-1.03E-02	-9.34E-03
2	0	2	1	0	0	0	1	2	2	-8.57E-03	-2.93E-03	-2.09E-03	-1.91E-03	-1.72E-03	-1.52E-03	-1.34E-03
1	1	1	1	0	1	2	1	1	2	-0.01071	-0.00432	-0.00366	-0.00343	-0.00312	-0.00281	-0.00252
0	0	1	0	1	0	1	0	1	1	-6.28E-03	-3.01E-03	-2.73E-03	-2.45E-03	-2.18E-03	-1.92E-03	-1.68E-03
2	1	0	0	1	1	0	0	0	1	-1.02E-02	-8.66E-03	-7.78E-03	-7.11E-03	-6.48E-03	-5.88E-03	-5.33E-03
1	2	2	0	1	2	2	0	2	1	-3.32E-03	-1.48E-03	-1.03E-03	-9.70E-04	-8.97E-04	-8.11E-04	-7.28E-04
0	1	2	2	2	1	1	2	2	0	-2.69E-03	-8.47E-04	-7.10E-04	-6.64E-04	-6.02E-04	-5.43E-04	-4.87E-04
2	2	1	2	2	2	0	2	1	0	-2.12E-03	-1.49E-03	-1.21E-03	-1.09E-03	-1.01E-03	-9.25E-04	-8.45E-04
1	0	0	2	2	0	2	2	0	0	-5.42E-03	-4.48E-03	-4.08E-03	-3.85E-03	-3.61E-03	-3.36E-03	-3.11E-03
16																
0	0	0	1	1	1	0	1	1	1	-6.11E-03	-3.81E-03	-3.35E-03	-2.87E-03	-2.45E-03	-2.07E-03	-1.76E-03
2	1	2	1	1	2	2	1	0	1	-0.00556	-0.00433	-0.00404	-0.00394	-0.00382	-0.00368	-0.00354
1	2	1	1	1	0	1	1	2	1	-0.00587	-0.00292	-0.00145	-0.00117	-0.00108	-0.00095	-0.00083
0	1	1	0	2	2	0	0	2	0	-0.00255	-0.00128	-0.00111	-0.00096	-0.00081	-0.00069	-0.00059
2	2	0	0	2	0	2	0	1	0	-0.00354	-0.00271	-0.00208	-0.00170	-0.00145	-0.00125	-0.00108
1	0	2	0	2	1	1	0	0	0	-4.05E-03	-3.32E-03	-3.13E-03	-3.02E-03	-2.89E-03	-2.75E-03	-2.62E-03
0	2	2	2	0	0	0	2	0	2	-0.02775	-0.00911	-0.00753	-0.00755	-0.00724	-0.00691	-0.00656
2	0	1	2	0	1	2	2	2	2	-7.57E-03	-2.51E-03	-2.01E-03	-1.86E-03	-1.67E-03	-1.49E-03	-1.32E-03
1	1	0	2	0	2	1	2	1	2	-0.01004	-0.00486	-0.00434	-0.00394	-0.00352	-0.00311	-0.00273
17																
0	0	0	0	2	2	2	1	0	1	-1.06E-02	-9.22E-03	-8.67E-03	-8.00E-03	-7.30E-03	-6.60E-03	-5.93E-03
2	1	2	0	2	0	1	1	2	1	-0.00291	-0.00185	-0.00130	-0.00108	-0.00096	-0.00087	-0.00077
1	2	1	0	2	1	0	1	1	1	-0.00518	-0.00344	-0.00253	-0.00221	-0.00198	-0.00175	-0.00154
0	1	1	2	0	0	2	0	1	0	-0.00682	-0.00173	-0.00164	-0.00150	-0.00135	-0.00120	-0.00106
2	2	0	2	0	1	1	0	0	0	-0.00845	-0.00584	-0.00502	-0.00464	-0.00428	-0.00390	-0.00355
1	0	2	2	0	2	0	0	2	0	-2.77E-03	-1.04E-03	-9.38E-04	-8.43E-04	-7.44E-04	-6.51E-04	-5.67E-04
0	2	2	1	1	1	2	2	2	2	-0.01061	-0.00251	-0.00156	-0.00160	-0.00147	-0.00133	-0.00120
2	0	1	1	1	2	1	2	1	2	-5.61E-03	-3.74E-03	-3.36E-03	-3.12E-03	-2.86E-03	-2.60E-03	-2.34E-03
1	1	0	1	1	0	0	2	0	2	-0.01831	-0.01413	-0.01227	-0.01140	-0.01051	-0.00961	-0.00874
18																
0	0	0	2	0	0	1	1	2	1	-6.78E-03	-2.04E-03	-1.82E-03	-1.52E-03	-1.27E-03	-1.05E-03	-8.81E-04
2	1	2	2	0	1	0	1	1	1	-5.84E-03	-2.44E-03	-1.90E-03	-1.79E-03	-1.66E-03	-1.51E-03	-1.37E-03
1	2	1	2	0	2	2	1	0	1	-9.12E-03	-5.50E-03	-5.02E-03	-4.87E-03	-4.65E-03	-4.41E-03	-4.16E-03
0	1	1	1	1	1	1	0	0	0	-6.81E-03	-4.52E-03	-4.30E-03	-4.07E-03	-3.80E-03	-3.53E-03	-3.25E-03
2	2	0	1	1	2	0	0	2	0	-2.48E-03	-1.51E-03	-1.11E-03	-9.10E-04	-7.66E-04	-6.47E-04	-5.51E-04
1	0	2	1	1	0	2	0	1	0	-2.69E-03	-1.46E-03	-1.19E-03	-1.13E-03	-1.04E-03	-9.58E-04	-8.74E-04
0	2	2	0	2	2	1	2	1	2	-8.01E-03	-3.62E-03	-3.06E-03	-2.93E-03	-2.70E-03	-2.47E-03	-2.24E-03
2	0	1	0	2	0	0	2	0	2	-1.30E-02	-1.13E-02	-1.03E-02	-9.66E-03	-9.01E-03	-8.36E-03	-7.74E-03
1	1	0	0	2	1	2	2	2	2	-6.42E-03	-4.02E-03	-2.98E-03	-2.49E-03	-2.07E-03	-1.72E-03	-1.44E-03
19																
0	2	0	1	2	1	0	2	0	0	-8.03E-03	-5.29E-03	-4.61E-03	-4.36E-03	-4.03E-03	-3.70E-03	-3.38E-03
2	0	2	1	2	2	2	2	2	0	-1.22E-03	-7.40E-04	-6.35E-04	-5.91E-04	-5.44E-04	-4.97E-04	-4.51E-04

-80.52	-7.44E-05	43.59	2.11E-04	-40.39	-6.58E-04	34.74
-55.21	6.99E-05	116.20	1.46E-04	-36.36	-8.73E-04	34.00
-53.53	-1.16E-05	38.52	4.78E-05	-11.19	-1.68E-04	21.90
-53.52	-1.77E-05	16.84	3.72E-05	-33.45	-2.06E-04	55.78
-133.40	-1.93E-04	3.02	2.22E-04	-121.60	-8.64E-04	129.10
-133.40	-2.49E-04	38.16	2.18E-04	-55.40	-1.32E-03	35.55
-133.90	-2.12E-04	52.86	3.10E-04	-80.83	-1.17E-03	11.00
-81.35	3.44E-05	105.00	1.52E-04	-67.64	-1.46E-03	69.87
-80.27	-1.13E-05	48.18	6.34E-05	-20.31	-2.74E-04	73.81
-80.80	-1.10E-05	62.01	8.71E-05	-35.57	-2.82E-04	28.85
-55.02	3.47E-05	104.30	8.04E-05	-38.06	-4.62E-04	14.94
-53.54	-7.10E-06	35.28	2.68E-05	-11.90	-9.13E-05	9.33
-54.11	8.08E-06	61.79	4.67E-05	-20.44	-4.44E-04	39.52
-80.31	-3.96E-06	52.95	1.00E-04	-75.62	-8.40E-04	66.57
-80.12	-4.03E-05	28.92	4.73E-05	-28.27	-1.95E-04	33.73
-81.50	4.54E-05	126.60	1.48E-04	-20.86	-5.87E-04	30.00
-54.22	1.39E-05	59.69	5.37E-05	-44.00	-2.77E-04	31.47
-53.67	5.42E-06	59.45	4.05E-05	-6.27	-1.71E-04	38.72
-53.88	-3.25E-06	43.01	3.66E-05	-26.01	-2.91E-04	29.25
-136.40	2.52E-04	177.90	7.48E-04	-100.10	-2.87E-03	33.35
-133.20	-2.86E-04	16.78	1.65E-04	-64.23	-8.19E-04	53.48
-133.30	-2.76E-04	14.71	2.06E-04	-91.31	-7.01E-04	66.95
-80.07	1.62E-06	33.13	4.81E-05	-77.35	-4.25E-04	160.60
-80.42	-5.02E-06	71.20	5.06E-05	-13.82	-3.25E-04	25.17
-81.44	2.75E-05	118.60	8.40E-05	-22.15	-3.19E-04	37.29
-53.92	2.98E-06	49.80	2.41E-04	-46.45	-1.19E-03	45.22
-53.43	-6.86E-05	19.15	9.10E-05	-16.91	-2.79E-04	53.79
-53.16	-1.32E-04	-1.77	6.54E-05	-41.15	-2.79E-04	19.72
-137.60	1.56E-04	251.00	3.22E-04	-90.84	-1.28E-03	42.09
-133.30	-7.82E-05	28.13	6.30E-05	-57.37	-3.52E-04	52.53
-135.50	4.75E-05	168.50	2.07E-04	-45.49	-1.12E-03	62.62
-79.70	-1.28E-04	32.07	2.43E-04	-80.63	-1.83E-03	72.59
-80.04	-1.47E-04	21.17	1.23E-04	-31.79	-4.61E-04	20.50
-80.17	-1.36E-04	16.21	1.36E-04	-48.26	-4.07E-04	47.31
-54.39	2.98E-05	69.19	9.91E-05	-42.85	-5.32E-04	50.30
-53.49	-1.64E-05	27.49	3.76E-05	-14.07	-1.16E-04	25.14
-53.93	-6.76E-06	48.15	6.58E-05	-24.94	-5.53E-04	26.99
-137.10	7.95E-05	212.30	1.70E-04	-94.87	-6.69E-04	56.03
-133.90	-7.46E-06	98.17	7.36E-05	-30.16	-6.61E-04	81.88
-135.30	2.13E-05	160.60	1.20E-04	-48.19	-6.10E-04	134.70
-55.74	7.02E-05	137.80	9.96E-05	-31.21	-4.24E-04	25.23
-53.39	-1.72E-05	18.03	1.86E-05	-20.44	-1.20E-04	15.84

1	1	1	1	2	0	1	2	1	0	-3.12E-03	-1.99E-03	-1.46E-03	-1.32E-03	-1.21E-03	-1.09E-03	-9.73E-04
0	0	1	0	0	2	0	1	1	2	-9.27E-03	-5.64E-03	-5.16E-03	-4.56E-03	-3.97E-03	-3.43E-03	-2.95E-03
2	1	0	0	0	0	2	1	0	2	-2.24E-02	-1.58E-02	-1.37E-02	-1.27E-02	-1.16E-02	-1.05E-02	-9.49E-03
1	2	2	0	0	1	1	1	2	2	-1.11E-02	-3.27E-03	-1.87E-03	-1.81E-03	-1.67E-03	-1.49E-03	-1.32E-03
0	1	2	2	1	0	0	0	2	1	-6.96E-03	-1.85E-03	-1.39E-03	-1.28E-03	-1.12E-03	-9.71E-04	-8.43E-04
2	2	1	2	1	1	2	0	1	1	-4.47E-03	-2.87E-03	-2.14E-03	-1.88E-03	-1.72E-03	-1.56E-03	-1.41E-03
1	0	0	2	1	2	1	0	0	1	-1.01E-02	-8.73E-03	-8.15E-03	-7.54E-03	-6.90E-03	-6.26E-03	-5.65E-03
20																
0	2	0	0	0	2	2	2	2	0	-0.00430	-0.00145	-0.00121	-0.00104	-0.00087	-0.00072	-0.00060
2	0	2	0	0	0	1	2	1	0	-3.90E-03	-1.65E-03	-1.32E-03	-1.24E-03	-1.14E-03	-1.04E-03	-9.42E-04
1	1	1	0	0	1	0	2	0	0	-0.00798	-0.00535	-0.00493	-0.00464	-0.00429	-0.00394	-0.00358
0	0	1	2	1	0	2	1	0	2	-1.49E-02	-9.51E-03	-9.12E-03	-8.71E-03	-8.25E-03	-7.76E-03	-7.26E-03
2	1	0	2	1	1	1	1	2	2	-0.00596	-0.00354	-0.00262	-0.00222	-0.00190	-0.00162	-0.00139
1	2	2	2	1	2	0	1	1	2	-0.00683	-0.00375	-0.00292	-0.00276	-0.00257	-0.00236	-0.00215
0	1	2	1	2	1	2	0	1	1	-0.00477	-0.00201	-0.00179	-0.00170	-0.00157	-0.00144	-0.00131
2	2	1	1	2	2	1	0	0	1	-0.00622	-0.00526	-0.00479	-0.00454	-0.00433	-0.00411	-0.00389
1	0	0	1	2	0	0	0	2	1	-4.34E-03	-2.84E-03	-2.06E-03	-1.62E-03	-1.29E-03	-1.04E-03	-8.50E-04
21																
0	2	0	2	1	0	1	2	1	0	-7.57E-03	-2.65E-03	-1.61E-03	-1.57E-03	-1.40E-03	-1.23E-03	-1.08E-03
2	0	2	2	1	1	0	2	0	0	-3.91E-03	-3.08E-03	-2.88E-03	-2.78E-03	-2.68E-03	-2.57E-03	-2.46E-03
1	1	1	2	1	2	2	2	2	0	-1.95E-03	-9.48E-04	-7.86E-04	-7.25E-04	-6.52E-04	-5.82E-04	-5.16E-04
0	0	1	1	2	1	1	1	2	2	-5.74E-03	-2.76E-03	-2.47E-03	-2.17E-03	-1.89E-03	-1.64E-03	-1.42E-03
2	1	0	1	2	2	0	1	1	2	-6.38E-03	-4.88E-03	-4.16E-03	-3.68E-03	-3.26E-03	-2.88E-03	-2.54E-03
1	2	2	1	2	0	2	1	0	2	-1.27E-02	-9.29E-03	-7.22E-03	-6.67E-03	-6.49E-03	-6.28E-03	-6.02E-03
0	1	2	0	0	2	1	0	0	1	-8.26E-03	-5.21E-03	-5.11E-03	-4.92E-03	-4.69E-03	-4.44E-03	-4.19E-03
2	2	1	0	0	0	0	0	2	1	-7.65E-03	-3.26E-03	-1.70E-03	-1.33E-03	-1.17E-03	-1.01E-03	-8.60E-04
1	0	0	0	0	1	2	0	1	1	-6.99E-03	-3.80E-03	-3.34E-03	-2.91E-03	-2.49E-03	-2.12E-03	-1.81E-03
22																
0	0	0	2	2	2	0	2	2	2	-5.29E-03	-3.17E-03	-2.76E-03	-2.37E-03	-2.02E-03	-1.71E-03	-1.46E-03
2	1	2	2	2	0	2	2	1	2	-5.34E-03	-3.60E-03	-2.71E-03	-2.39E-03	-2.23E-03	-2.09E-03	-1.94E-03
1	2	1	2	2	1	1	2	0	2	-1.21E-02	-9.27E-03	-7.87E-03	-7.48E-03	-7.20E-03	-6.86E-03	-6.50E-03
0	1	1	1	0	0	0	1	0	1	-1.50E-02	-7.23E-03	-6.93E-03	-6.52E-03	-6.07E-03	-5.60E-03	-5.13E-03
2	2	0	1	0	1	2	1	2	1	-6.39E-03	-2.56E-03	-1.57E-03	-1.34E-03	-1.17E-03	-9.98E-04	-8.51E-04
1	0	2	1	0	2	1	1	1	1	-4.58E-03	-2.01E-03	-1.90E-03	-1.78E-03	-1.65E-03	-1.51E-03	-1.37E-03
0	2	2	0	1	1	0	0	1	0	-5.13E-03	-1.86E-03	-1.42E-03	-1.36E-03	-1.24E-03	-1.11E-03	-9.95E-04
2	0	1	0	1	2	2	0	0	0	-4.44E-03	-3.69E-03	-3.50E-03	-3.35E-03	-3.19E-03	-3.01E-03	-2.83E-03
1	1	0	0	1	0	1	0	2	0	-3.67E-03	-2.01E-03	-1.31E-03	-1.06E-03	-8.65E-04	-7.00E-04	-5.76E-04
23																
0	0	0	1	0	0	2	2	1	2	-1.31E-02	-5.28E-03	-4.92E-03	-4.37E-03	-3.83E-03	-3.33E-03	-2.88E-03
2	1	2	1	0	1	1	2	0	2	-1.38E-02	-8.15E-03	-7.27E-03	-7.09E-03	-6.85E-03	-6.57E-03	-6.27E-03
1	2	1	1	0	2	0	2	2	2	-9.00E-03	-2.98E-03	-2.20E-03	-2.03E-03	-1.81E-03	-1.59E-03	-1.38E-03
0	1	1	0	1	1	2	1	2	1	-5.05E-03	-1.68E-03	-1.49E-03	-1.33E-03	-1.16E-03	-1.00E-03	-8.69E-04
2	2	0	0	1	2	1	1	1	1	-4.67E-03	-3.21E-03	-2.60E-03	-2.27E-03	-2.01E-03	-1.76E-03	-1.55E-03
1	0	2	0	1	0	0	1	0	1	-7.94E-03	-6.03E-03	-5.51E-03	-5.26E-03	-4.98E-03	-4.68E-03	-4.37E-03
0	2	2	2	2	2	2	0	0	0	-4.80E-03	-3.05E-03	-2.83E-03	-2.78E-03	-2.68E-03	-2.57E-03	-2.46E-03
2	0	1	2	2	0	1	0	2	0	-1.92E-03	-1.28E-03	-9.89E-04	-8.46E-04	-7.36E-04	-6.38E-04	-5.52E-04
1	1	0	2	2	1	0	0	1	0	-3.68E-03	-2.66E-03	-2.12E-03	-1.80E-03	-1.52E-03	-1.29E-03	-1.10E-03

-54.32	1.63E-05	81.30	5.75E-05	-15.09	-3.58E-04	21.08
-131.80	-3.89E-04	-30.66	1.44E-04	-140.20	-8.46E-04	102.60
-133.60	-1.68E-04	59.94	2.67E-04	-42.77	-1.15E-03	198.20
-134.30	-1.36E-04	74.55	3.57E-04	-67.50	-1.11E-03	46.52
-82.87	1.06E-04	175.70	2.20E-04	-54.42	-1.31E-03	31.98
-80.34	-1.71E-05	57.36	7.13E-05	-16.86	-2.52E-04	41.34
-80.24	-2.56E-05	22.16	5.31E-05	-51.38	-3.11E-04	113.60
-53.38	-8.47E-05	2.90	9.45E-05	-48.68	-3.53E-04	56.71
-53.36	-9.95E-05	15.08	8.68E-05	-22.28	-5.32E-04	24.18
-53.55	-7.49E-05	20.06	1.20E-04	-32.06	-4.59E-04	42.79
-135.60	5.53E-05	173.70	2.51E-04	-113.00	-2.44E-03	111.60
-133.80	-4.44E-05	77.74	1.04E-04	-36.28	-4.78E-04	64.06
-134.70	-1.46E-05	102.40	1.44E-04	-58.98	-4.67E-04	30.87
-82.52	5.25E-05	155.40	1.20E-04	-57.15	-6.93E-04	41.86
-80.32	-8.03E-06	52.13	3.97E-05	-17.74	-1.36E-04	40.34
-81.21	1.63E-05	100.50	7.47E-05	-29.27	-6.46E-04	66.93
-55.97	1.23E-04	157.60	1.86E-04	-29.59	-8.01E-04	24.77
-53.42	-2.60E-05	20.17	3.27E-05	-19.33	-2.24E-04	12.27
-53.70	-1.93E-05	30.71	4.96E-05	-29.04	-2.02E-04	21.41
-135.10	2.28E-05	151.50	1.38E-04	-116.40	-1.27E-03	78.60
-133.70	-1.92E-05	73.60	5.98E-05	-36.12	-2.48E-04	55.81
-136.20	6.90E-05	247.10	1.69E-04	-27.90	-7.46E-04	55.48
-79.53	-1.94E-04	-1.94	1.32E-04	-79.41	-5.47E-04	48.07
-80.27	-8.31E-05	47.63	1.88E-04	-20.03	-6.25E-04	31.10
-80.00	-1.60E-04	13.45	1.42E-04	-57.31	-7.24E-04	119.30
-133.60	-1.17E-05	71.75	9.05E-05	-127.80	-7.17E-04	55.42
-134.00	-9.41E-06	117.40	8.36E-05	-23.25	-5.46E-04	36.21
-135.70	4.31E-05	194.50	1.38E-04	-37.35	-5.33E-04	47.10
-80.90	1.42E-05	73.34	3.57E-04	-69.56	-1.77E-03	50.31
-80.14	-1.18E-04	29.99	1.41E-04	-25.71	-4.28E-04	47.64
-79.73	-2.01E-04	-2.63	9.88E-05	-62.15	-4.22E-04	31.59
-55.06	6.52E-05	99.31	1.28E-04	-36.27	-5.09E-04	20.98
-53.34	-2.93E-05	10.53	2.45E-05	-23.02	-1.40E-04	42.58
-54.18	1.59E-05	69.03	8.45E-05	-18.18	-4.52E-04	50.55
-132.80	-2.15E-04	52.93	4.04E-04	-134.60	-3.05E-03	135.10
-133.40	-2.45E-04	34.91	2.04E-04	-53.26	-7.70E-04	46.58
-133.60	-2.30E-04	28.06	2.30E-04	-80.23	-6.82E-04	31.13
-81.57	3.78E-05	107.20	1.52E-04	-64.40	-8.04E-04	59.89
-80.23	-2.36E-05	40.36	5.56E-05	-21.31	-1.74E-04	55.12
-80.91	-3.97E-06	71.66	9.79E-05	-36.91	-8.20E-04	42.33
-54.82	3.20E-05	84.37	6.76E-05	-37.98	-2.67E-04	27.72
-53.55	-7.20E-06	38.44	2.90E-05	-12.52	-2.72E-04	26.32
-54.15	1.27E-05	65.88	4.88E-05	-18.66	-2.39E-04	44.35

24																
0	0	0	0	1	1	1	2	0	2	-2.16E-02	-1.77E-02	-1.64E-02	-1.50E-02	-1.35E-02	-1.20E-02	-1.07E-02
2	1	2	0	1	2	0	2	2	2	-4.66E-03	-2.57E-03	-2.05E-03	-1.85E-03	-1.66E-03	-1.48E-03	-1.30E-03
1	2	1	0	1	0	2	2	1	2	-1.13E-02	-6.42E-03	-3.94E-03	-3.41E-03	-3.16E-03	-2.86E-03	-2.55E-03
0	1	1	2	2	2	1	1	1	1	-4.26E-03	-2.41E-03	-2.23E-03	-2.05E-03	-1.86E-03	-1.67E-03	-1.49E-03
2	2	0	2	2	0	0	1	0	1	-9.02E-03	-7.75E-03	-6.75E-03	-6.09E-03	-5.59E-03	-5.15E-03	-4.74E-03
1	0	2	2	2	1	2	1	2	1	-2.31E-03	-1.25E-03	-1.03E-03	-9.56E-04	-8.73E-04	-7.90E-04	-7.11E-04
0	2	2	1	0	0	1	0	2	0	-8.77E-03	-1.32E-03	-7.19E-04	-7.64E-04	-6.86E-04	-6.09E-04	-5.38E-04
2	0	1	1	0	1	0	0	1	0	-4.19E-03	-2.12E-03	-1.81E-03	-1.64E-03	-1.45E-03	-1.27E-03	-1.11E-03
1	1	0	1	0	2	2	0	0	0	-8.06E-03	-5.92E-03	-5.55E-03	-5.16E-03	-4.73E-03	-4.29E-03	-3.86E-03
25																
0	1	0	0	2	0	0	2	1	1	-9.25E-03	-4.91E-03	-3.75E-03	-3.13E-03	-2.55E-03	-2.09E-03	-1.74E-03
2	2	2	0	2	1	2	2	0	1	-5.82E-03	-4.76E-03	-4.18E-03	-3.94E-03	-3.80E-03	-3.66E-03	-3.52E-03
1	0	1	0	2	2	1	2	2	1	-2.59E-03	-1.69E-03	-1.46E-03	-1.30E-03	-1.13E-03	-9.84E-04	-8.52E-04
0	2	1	2	0	1	0	1	2	0	-5.84E-03	-1.22E-03	-9.32E-04	-8.65E-04	-7.55E-04	-6.55E-04	-5.66E-04
2	0	0	2	0	2	2	1	1	0	-3.93E-03	-2.02E-03	-1.79E-03	-1.62E-03	-1.44E-03	-1.26E-03	-1.11E-03
1	1	2	2	0	0	1	1	0	0	-6.75E-03	-3.51E-03	-3.02E-03	-2.96E-03	-2.84E-03	-2.71E-03	-2.58E-03
0	0	2	1	1	2	0	0	0	2	-1.22E-02	-9.84E-03	-9.50E-03	-9.05E-03	-8.54E-03	-8.01E-03	-7.47E-03
2	1	1	1	1	0	2	0	2	2	-6.27E-03	-3.60E-03	-2.45E-03	-2.05E-03	-1.81E-03	-1.59E-03	-1.38E-03
1	2	0	1	1	1	1	0	1	2	-1.09E-02	-6.75E-03	-4.92E-03	-4.26E-03	-3.70E-03	-3.17E-03	-2.73E-03
26																
0	1	0	2	0	1	2	2	0	1	-1.18E-02	-6.96E-03	-6.74E-03	-6.35E-03	-5.92E-03	-5.47E-03	-5.03E-03
2	2	2	2	0	2	1	2	2	1	-4.77E-03	-1.47E-03	-9.62E-04	-9.03E-04	-8.45E-04	-7.73E-04	-7.00E-04
1	0	1	2	0	0	0	2	1	1	-6.51E-03	-2.69E-03	-2.29E-03	-2.12E-03	-1.91E-03	-1.72E-03	-1.53E-03
0	2	1	1	1	2	2	1	1	0	-3.66E-03	-1.59E-03	-1.39E-03	-1.31E-03	-1.20E-03	-1.08E-03	-9.72E-04
2	0	0	1	1	0	1	1	0	0	-6.22E-03	-5.21E-03	-4.73E-03	-4.39E-03	-4.06E-03	-3.72E-03	-3.40E-03
1	1	2	1	1	1	0	1	2	0	-2.39E-03	-1.12E-03	-8.13E-04	-7.48E-04	-6.70E-04	-5.93E-04	-5.23E-04
0	0	2	0	2	0	2	0	2	2	-6.68E-03	-2.31E-03	-1.97E-03	-1.81E-03	-1.63E-03	-1.46E-03	-1.30E-03
2	1	1	0	2	1	1	0	1	2	-6.15E-03	-4.54E-03	-3.77E-03	-3.37E-03	-3.04E-03	-2.73E-03	-2.44E-03
1	2	0	0	2	2	0	0	0	2	-1.53E-02	-1.28E-02	-1.14E-02	-1.06E-02	-9.73E-03	-8.93E-03	-8.18E-03
27																
0	1	0	1	1	2	1	2	2	1	-4.15E-03	-1.93E-03	-1.71E-03	-1.46E-03	-1.24E-03	-1.04E-03	-8.82E-04
2	2	2	1	1	0	0	2	1	1	-4.91E-03	-3.11E-03	-2.10E-03	-1.71E-03	-1.56E-03	-1.44E-03	-1.32E-03
1	0	1	1	1	1	2	2	0	1	-6.89E-03	-5.40E-03	-5.10E-03	-4.90E-03	-4.66E-03	-4.42E-03	-4.16E-03
0	2	1	0	2	0	1	1	0	0	-9.09E-03	-5.24E-03	-4.07E-03	-3.96E-03	-3.72E-03	-3.45E-03	-3.18E-03
2	0	0	0	2	1	0	1	2	0	-2.16E-03	-1.54E-03	-1.21E-03	-9.91E-04	-8.16E-04	-6.78E-04	-5.70E-04
1	1	2	0	2	2	2	1	1	0	-2.01E-03	-1.29E-03	-1.12E-03	-1.06E-03	-9.88E-04	-9.13E-04	-8.38E-04
0	0	2	2	0	1	1	0	1	2	-8.59E-03	-3.59E-03	-3.48E-03	-3.23E-03	-2.95E-03	-2.68E-03	-2.41E-03
2	1	1	2	0	2	0	0	0	2	-1.69E-02	-1.17E-02	-1.09E-02	-1.03E-02	-9.64E-03	-8.93E-03	-8.22E-03
1	2	0	2	0	0	2	0	2	2	-1.61E-02	-5.90E-03	-2.87E-03	-2.48E-03	-2.12E-03	-1.75E-03	-1.45E-03

-133.80	7.02E-06	79.55	1.58E-04	-126.50	-1.39E-03	263.80
-133.50	-6.58E-05	49.89	8.01E-05	-46.12	-3.22E-04	38.77
-135.80	7.74E-05	210.50	2.46E-04	-34.77	-9.77E-04	82.59
-81.29	1.80E-05	89.23	8.05E-05	-66.40	-4.17E-04	43.81
-80.50	1.06E-05	89.27	6.08E-05	[redacted]	-2.55E-04	27.42
-80.81	-8.63E-06	65.93	5.59E-05	-39.35	-4.42E-04	29.58
-54.55	9.83E-05	71.61	3.01E-04	-40.05	-1.15E-03	20.83
-53.29	-1.08E-04	6.47	6.41E-05	-25.17	-3.20E-04	30.53
-53.32	-1.01E-04	4.57	7.79E-05	-36.42	-2.74E-04	84.42
-83.85	1.11E-04	234.60	1.67E-04	-46.32	-1.09E-03	97.71
-80.37	-3.60E-06	68.73	4.90E-05	-13.54	-1.92E-04	33.48
-80.48	-1.57E-05	41.88	4.29E-05	-46.57	-2.75E-04	49.16
-53.81	-1.34E-05	30.89	1.79E-04	-45.24	-6.61E-04	17.45
-53.22	-1.18E-04	-1.16	4.40E-05	-27.64	-1.88E-04	43.59
-53.77	-4.67E-05	38.08	1.69E-04	-27.04	-7.30E-04	22.82
-132.50	-7.12E-05	24.36	1.05E-04	-135.80	-7.73E-04	75.67
-133.90	-3.07E-05	100.80	1.25E-04	-28.63	-7.01E-04	70.04
-135.30	4.09E-05	157.90	1.96E-04	-45.30	-6.84E-04	116.50
-80.01	-1.12E-04	27.95	2.23E-04	-76.13	-1.01E-03	72.20
-79.99	-1.54E-04	13.23	9.79E-05	-31.76	-2.79E-04	15.68
-80.32	-1.28E-04	34.75	1.99E-04	-50.72	-1.21E-03	24.10
-54.23	1.90E-05	51.32	7.98E-05	-42.35	-3.04E-04	30.72
-53.50	-1.28E-05	31.37	4.22E-05	-14.93	-3.35E-04	45.40
-53.95	-4.39E-06	48.83	6.59E-05	-23.53	-3.07E-04	14.06
-137.20	7.82E-05	252.80	1.97E-04	-100.00	-2.13E-03	68.28
-133.90	-1.52E-05	95.86	7.20E-05	-29.86	-3.75E-04	70.28
-135.20	3.46E-05	140.40	1.07E-04	-47.08	-3.62E-04	109.90
-80.48	-8.35E-06	51.32	9.70E-05	-72.14	-4.66E-04	50.09
-80.40	-5.23E-06	73.49	8.62E-05	-12.53	-3.49E-04	14.64
-80.54	-2.67E-05	46.56	7.60E-05	-45.69	-5.28E-04	52.50
-56.59	1.05E-04	202.40	1.39E-04	-24.79	-6.48E-04	44.26
-53.51	-6.80E-06	32.52	2.59E-05	-14.40	-1.69E-04	33.99
-53.86	-4.29E-06	43.25	3.64E-05	-24.96	-1.65E-04	24.38
-131.90	-3.47E-04	4.40	2.58E-04	-140.5	-1.66E-03	70.75
-133.10	-2.59E-04	9.57	1.36E-04	-60.46	-4.63E-04	82.93
-134.90	-2.54E-06	126.60	5.01E-04	-53.63	-1.67E-03	125.00

3. FEM analysis Results under Temperature Load												
Joint	Thick		Stiffness				a				Horizontal Stress	
Spacin	ACC	INT	ACC	INT	PCC	K	AC(	PCC			PCC	ACC
10	3	0	200000	0	3500000	400	0	4	30		139	126
30	6	8	200000	20000	5500000	1200	15	8	30		968	184
20	9	4	200000	20000	7500000	800	15	6	30		743	155
10	6	4	1000000	80000	5500000	400	45	6	70		771	2906
30	9	0	1000000	0	7500000	1200	0	4	70		1171	3131
20	3	8	1000000	80000	3500000	800	45	8	70		1160	3159
10	9	8	600000	140000	7500000	400	30	8	50		1378	953
30	3	4	600000	140000	3500000	1200	30	6	50		581	1127
20	6	0	600000	0	5500000	800	0	4	50		401	1028
10	3	0	1000000	0	5500000	1200	0	8	30		383	898
30	6	8	1000000	80000	7500000	800	15	6	30		1059	632
20	9	4	1000000	80000	3500000	400	15	4	30		261	450
10	6	4	600000	140000	7500000	1200	45	4	70		674	1725
30	9	0	600000	0	3500000	800	0	8	70		1019	2195
20	3	8	600000	140000	5500000	400	45	6	70		1339	1987
10	9	8	200000	20000	3500000	1200	30	6	50		455	287
30	3	4	200000	20000	5500000	800	30	4	50		527	350
20	6	0	200000	0	7500000	400	0	8	50		805	624
10	3	0	600000	0	7500000	800	0	6	30		377	498
30	6	8	600000	140000	3500000	400	15	4	30		307	498
20	9	4	600000	140000	5500000	1200	15	8	30		833	444
10	6	4	200000	20000	3500000	800	45	8	70		531	656
30	9	0	200000	0	5500000	400	0	6	70		1407	853
20	3	8	200000	20000	7500000	1200	45	4	70		927	622
10	9	8	1000000	80000	5500000	800	30	4	50		526	1290
30	3	4	1000000	80000	7500000	400	30	8	50		1536	2330
20	6	0	1000000	0	3500000	1200	0	6	50		333	1738
10	6	0	600000	0	5500000	400	0	8	70		616	1217
30	9	8	600000	20000	7500000	1200	15	6	70		2454	948
20	3	4	600000	20000	3500000	800	15	4	70		379	732
10	9	4	200000	80000	7500000	400	45	4	50		528	422
30	3	0	200000	0	3500000	1200	0	8	50		508	758
20	6	8	200000	80000	5500000	800	45	6	50		1036	493
10	3	8	1000000	140000	3500000	400	30	6	30		243	848
30	6	4	1000000	140000	5500000	1200	30	4	30		432	883
20	9	0	1000000	0	7500000	800	0	8	30		844	1221
10	6	0	200000	0	7500000	1200	0	6	70		359	404
30	9	8	200000	80000	3500000	800	15	4	70		817	261
20	3	4	200000	80000	5500000	400	15	8	70		1035	630
10	9	4	1000000	140000	3500000	1200	45	8	50		601	2050
30	3	0	1000000	0	5500000	800	0	6	50		563	3004
20	6	8	1000000	140000	7500000	400	45	4	50		987	2030
10	3	8	600000	20000	5500000	1200	30	4	30		212	468

30	6	4	600000	20000	7500000	800	30	8	30	1070	750
20	9	0	600000	0	3500000	400	0	6	30	269	592
10	6	0	1000000	0	3500000	800	0	4	70	207	1229
30	9	8	1000000	140000	5500000	400	15	8	70	2579	1557
20	3	4	1000000	140000	7500000	1200	15	6	70	1279	1913
10	9	4	600000	20000	5500000	800	45	6	50	599	1206
30	3	0	600000	0	7500000	400	0	4	50	549	1644
20	6	8	600000	20000	3500000	1200	45	8	50	869	1316
10	3	8	200000	80000	7500000	800	30	8	30	531	234
30	6	4	200000	80000	3500000	400	30	6	30	426	231
20	9	0	200000	0	5500000	1200	0	4	30	328	201
10	9	0	1000000	0	7500000	400	0	6	50	692	1056
30	3	8	1000000	20000	3500000	1200	15	4	50	486	779
20	6	4	1000000	20000	5500000	800	15	8	50	1071	1173
10	3	4	600000	80000	3500000	400	45	8	30	205	815
30	6	0	600000	0	5500000	1200	0	6	30	453	969
20	9	8	600000	80000	7500000	800	45	4	30	636	718
10	6	8	200000	140000	5500000	400	30	4	70	616	418
30	9	4	200000	140000	7500000	1200	30	8	70	3102	801
20	3	0	200000	0	3500000	800	0	6	70	587	677
10	9	0	600000	0	3500000	1200	0	4	50	587	297
30	3	8	600000	80000	5500000	800	15	8	50	1536	381
20	6	4	600000	80000	7500000	400	15	6	50	376	206
10	3	4	200000	140000	5500000	1200	45	6	30	154	1148
30	6	0	200000	0	7500000	800	0	4	30	308	1544
20	9	8	200000	140000	3500000	400	45	8	30	686	1180
10	6	8	1000000	20000	7500000	1200	30	8	70	633	1196
30	9	4	1000000	20000	3500000	800	30	6	70	1176	1289
20	3	0	1000000	0	5500000	400	0	4	70	1446	2632
10	9	0	200000	0	5500000	800	0	8	50	616	1217
30	3	8	200000	140000	7500000	400	15	6	50	2454	948
20	6	4	200000	140000	3500000	1200	15	4	50	379	732
10	3	4	1000000	20000	7500000	800	45	4	30	528	422
30	6	0	1000000	0	3500000	400	0	8	30	508	758
20	9	8	1000000	20000	5500000	1200	45	6	30	1036	493
10	6	8	600000	80000	3500000	800	30	6	70	243	848
30	9	4	600000	80000	5500000	400	30	4	70	432	883
20	3	0	600000	0	7500000	1200	0	8	70	844	1221
10	6	0	1000000	0	7500000	400	0	4	30	189	925
30	9	8	1000000	80000	3500000	1200	30	8	30	667	886
20	3	4	1000000	80000	5500000	800	30	6	30	417	1003
10	9	4	600000	140000	3500000	400	15	6	70	623	743
30	3	0	600000	0	5500000	1200	0	4	70	544	1278
20	6	8	600000	140000	7500000	800	15	8	70	2723	1199
10	3	8	200000	20000	5500000	400	45	8	50	560	458
30	6	4	200000	20000	7500000	1200	45	6	50	1260	571

20	9	0	200000	0	3500000	800	0	4	50		347	441
10	6	0	600000	0	3500000	1200	0	8	30		180	661
30	9	8	600000	140000	5500000	800	30	6	30		811	561
20	3	4	600000	140000	7500000	400	30	4	30		376	595
10	9	4	200000	20000	5500000	1200	15	4	70		516	243
30	3	0	200000	0	7500000	800	0	8	70		1701	976
20	6	8	200000	20000	3500000	400	15	6	70		884	314
10	3	8	1000000	80000	7500000	1200	45	6	50		721	2048
30	6	4	1000000	80000	3500000	800	45	4	50		449	1989
20	9	0	1000000	0	5500000	400	0	8	50		981	2535
10	6	0	200000	0	5500000	800	0	6	30		156	226
30	9	8	200000	20000	7500000	400	30	4	30		723	190
20	3	4	200000	20000	3500000	1200	30	8	30		328	237
10	9	4	1000000	80000	7500000	800	15	8	70		1678	1407
30	3	0	1000000	0	3500000	400	0	6	70		477	2322
20	6	8	1000000	80000	5500000	1200	15	4	70		1007	1160
10	3	8	600000	140000	3500000	800	45	4	50		266	1163
30	6	4	600000	140000	5500000	400	45	8	50		1503	1674
20	9	0	600000	0	7500000	1200	0	6	50		1111	1536
10	9	0	200000	0	3500000	400	0	8	70		571	549
30	3	8	200000	80000	5500000	1200	30	6	70		1578	645
20	6	4	200000	80000	7500000	800	30	4	70		1004	523
10	3	4	1000000	140000	5500000	400	15	4	50		267	854
30	6	0	1000000	0	7500000	1200	0	8	50		1405	2069
20	9	8	1000000	140000	3500000	800	15	6	50		704	821
10	6	8	600000	20000	7500000	400	45	6	30		448	719
30	9	4	600000	20000	3500000	1200	45	4	30		321	691
20	3	0	600000	0	5500000	800	0	8	30		510	1161
10	9	0	1000000	0	5500000	1200	0	6	70		694	2213
30	3	8	1000000	140000	7500000	800	30	4	70		1513	2213
20	6	4	1000000	140000	3500000	400	30	8	70		1091	2467
10	3	4	600000	20000	7500000	1200	15	8	50		384	642
30	6	0	600000	0	3500000	800	0	6	50		450	838
20	9	8	600000	20000	5500000	400	15	4	50		743	476
10	6	8	200000	80000	3500000	1200	45	4	30		184	234
30	9	4	200000	80000	5500000	800	45	8	30		1000	-349
20	3	0	200000	0	7500000	400	0	6	30		546	371
10	9	0	600000	0	7500000	800	0	4	70		636	1280
30	3	8	600000	20000	3500000	400	30	8	70		1299	1528
20	6	4	600000	20000	5500000	1200	30	6	70		1087	1438
10	3	4	200000	80000	3500000	800	15	6	50		228	235
30	6	0	200000	0	5500000	400	0	4	50		496	297
20	9	8	200000	80000	7500000	1200	15	8	50		1991	325
10	6	8	1000000	140000	5500000	800	45	8	30		573	1251
30	9	4	1000000	140000	7500000	400	45	6	30		1021	1348
20	3	0	1000000	0	3500000	1200	0	4	30		138	1306

10	3	0	600000	0	5500000	400	0	6	50	442	1164
30	6	8	600000	80000	7500000	1200	30	4	50	1175	933
20	9	4	600000	80000	3500000	800	30	8	50	888	1017
10	6	4	200000	140000	7500000	400	15	8	30	506	181
30	9	0	200000	0	3500000	1200	0	6	30	382	166
20	3	8	200000	140000	5500000	800	15	4	30	382	127
10	9	8	1000000	20000	3500000	400	45	4	70	451	2552
30	3	4	1000000	20000	5500000	1200	45	8	70	1358	3647
20	6	0	1000000	0	7500000	800	0	6	70	1165	3774
10	3	0	200000	0	7500000	1200	0	4	50	905	352
30	6	8	200000	140000	3500000	800	30	8	50	1066	420
20	9	4	200000	140000	5500000	400	30	6	50	1005	392
10	6	4	1000000	20000	3500000	1200	15	6	30	215	466
30	9	0	1000000	0	5500000	800	0	4	30	317	555
20	3	8	1000000	20000	7500000	400	15	8	30	842	661
10	9	8	600000	80000	5500000	1200	45	8	70	1415	1765
30	3	4	600000	80000	7500000	800	45	6	70	1559	2377
20	6	0	600000	0	3500000	400	0	4	70	344	1853
10	3	0	1000000	0	3500000	800	0	8	50	398	1989
30	6	8	1000000	20000	5500000	400	30	6	50	1224	1563
20	9	4	1000000	20000	7500000	1200	30	4	50	892	1400
10	6	4	600000	80000	5500000	800	15	4	30	224	296
30	9	0	600000	0	7500000	400	0	8	30	1087	656
20	3	8	600000	80000	3500000	1200	15	6	30	373	339
10	9	8	200000	140000	7500000	800	45	6	70	1352	623
30	3	4	200000	140000	3500000	400	45	4	70	527	695
20	6	0	200000	0	5500000	1200	0	8	70	917	999
10	9	0	600000	0	5500000	400	0	4	30	204	737
30	3	8	600000	140000	7500000	1200	45	8	30	1284	999
20	6	4	600000	140000	3500000	800	45	6	30	340	782
10	3	4	200000	20000	7500000	400	30	6	70	358	477
30	6	0	200000	0	3500000	1200	0	4	70	458	540
20	9	8	200000	20000	5500000	800	30	8	70	1894	564
10	6	8	1000000	80000	3500000	400	15	8	50	613	870
30	9	4	1000000	80000	5500000	1200	15	6	50	1244	1019
20	3	0	1000000	0	7500000	800	0	4	50	570	1318
10	9	0	200000	0	7500000	1200	0	8	30	452	322
30	3	8	200000	20000	3500000	800	45	6	30	444	272
20	6	4	200000	20000	5500000	400	45	4	30	334	257
10	3	4	1000000	80000	3500000	1200	30	4	70	246	1922
30	6	0	1000000	0	5500000	800	0	8	70	1386	3457
20	9	8	1000000	80000	7500000	400	30	6	70	2226	2177
10	6	8	600000	140000	5500000	1200	15	6	50	701	545
30	9	4	600000	140000	7500000	800	15	4	50	1145	610
20	3	0	600000	0	3500000	400	0	8	50	522	1175
10	9	0	1000000	0	3500000	800	0	6	30	171	1235

30	3	8	1000000	80000	5500000	400	45	4	30	474	1203
20	6	4	1000000	80000	7500000	1200	45	8	30	960	1489
10	3	4	600000	140000	5500000	800	30	8	70	677	1575
30	6	0	600000	0	7500000	400	0	6	70	1488	2121
20	9	8	600000	140000	3500000	1200	30	4	70	660	1136
10	6	8	200000	20000	7500000	800	15	4	50	481	168
30	9	4	200000	20000	3500000	400	15	8	50	1042	304
20	3	0	200000	0	5500000	1200	0	6	50	670	389
10	3	0	1000000	0	7500000	400	0	8	70	1028	3914
30	6	8	1000000	140000	3500000	1200	45	6	70	1087	2913
20	9	4	1000000	140000	5500000	800	45	4	70	977	2804
10	6	4	600000	20000	3500000	400	30	4	50	224	799
30	9	0	600000	0	5500000	1200	0	8	50	1280	1362
20	3	8	600000	20000	7500000	800	30	6	50	1015	989
10	9	8	200000	80000	5500000	400	15	6	30	441	117
30	3	4	200000	80000	7500000	1200	15	4	30	464	165
20	6	0	200000	0	3500000	800	0	8	30	302	217
10	3	0	600000	0	3500000	1200	0	6	70	427	2045
30	6	8	600000	20000	5500000	800	45	4	70	1136	1729
20	9	4	600000	20000	7500000	400	45	8	70	2297	2108
10	6	4	200000	80000	5500000	1200	30	8	50	630	396
30	9	0	200000	0	7500000	800	0	6	50	1331	519
20	3	8	200000	80000	3500000	400	30	4	50	407	313
10	9	8	1000000	140000	7500000	1200	15	4	30	432	440
30	3	4	1000000	140000	3500000	800	15	8	30	457	783
20	6	0	1000000	0	5500000	400	0	6	30	346	772
10	3	0	200000	0	5500000	800	0	4	70	700	651
30	6	8	200000	80000	7500000	400	45	8	70	3143	936
20	9	4	200000	80000	3500000	1200	45	6	70	918	666
10	6	4	1000000	140000	7500000	800	30	6	50	753	1556
30	9	0	1000000	0	3500000	400	0	4	50	283	1437
20	3	8	1000000	140000	5500000	1200	30	8	50	1296	1812
10	9	8	600000	20000	3500000	800	15	8	30	385	289
30	3	4	600000	20000	5500000	400	15	6	30	484	417
20	6	0	600000	0	7500000	1200	0	4	30	328	417
10	6	0	200000	0	3500000	400	0	6	50	187	484
30	9	8	200000	140000	5500000	1200	45	4	50	914	434
20	3	4	200000	140000	7500000	800	45	8	50	1000	724
10	9	4	1000000	20000	5500000	400	30	8	30	503	865
30	3	0	1000000	0	7500000	1200	0	6	30	468	1482
20	6	8	1000000	20000	3500000	800	30	4	30	281	773
10	3	8	600000	80000	7500000	400	15	4	70	654	706
30	6	4	600000	80000	3500000	1200	15	8	70	1330	1184
20	9	0	600000	0	5500000	800	0	6	70	1120	1109
10	6	0	1000000	0	5500000	1200	0	4	50	236	2080
30	9	8	1000000	20000	7500000	800	45	8	50	2383	2300

20	3	4	1000000	20000	3500000	400	45	6	50	404	2113
10	9	4	600000	80000	7500000	1200	30	6	30	533	548
30	3	0	600000	0	3500000	800	0	4	30	135	632
20	6	8	600000	80000	5500000	400	30	8	30	859	637
10	3	8	200000	140000	3500000	1200	15	8	70	691	364
30	6	4	200000	140000	5500000	800	15	6	70	1512	514
20	9	0	200000	0	7500000	400	0	4	70	946	380
10	6	0	600000	0	7500000	800	0	8	50	554	1601
30	9	8	600000	80000	3500000	400	45	6	50	858	1240
20	3	4	600000	80000	5500000	1200	45	4	50	455	1296
10	9	4	200000	140000	3500000	800	30	4	30	172	169
30	3	0	200000	0	5500000	400	0	8	30	491	399
20	6	8	200000	140000	7500000	1200	30	6	30	850	234
10	3	8	1000000	20000	5500000	800	15	6	70	622	1124
30	6	4	1000000	20000	7500000	400	15	4	70	1257	1359
20	9	0	1000000	0	3500000	1200	0	8	70	753	1684

APPENDIX D

FORTRAN PROGRAM TO GENERATE ABAQUS INPUT FILES

1. INPUT DATA FILES
2. GENERATION PROGRAM
3. GENERATED ABAQUS INPUT FILE

1. Input Data files

SOURCE.DAT

```
0	0	0	1	2	2	1	0	1	0
2	1	2	1	2	0	0	0	0	0
1	2	1	1	2	1	2	0	2	0
0	1	1	0	0	0	1	2	2	2
2	2	0	0	0	1	0	2	1	2
1	0	2	0	0	2	2	2	0	2
0	2	2	2	1	1	1	1	0	1
2	0	1	2	1	2	0	1	2	1
1	1	0	2	1	0	2	1	1	1
```

TABLE.DAT

```
10.	20.	30.
3.	6.	9.
0.	4.	8.
200000.		600000.		1000000.
20000. 80000. 140000.
3500000. 5500000. 7500000.
400.	800.	1200.
15E-6	30E-6	45E-6
4E-6	6E-6	8E-6
30.	50.	70.
```

CHAR.DAT

```
CONC1		FLE1	ASP1
CONC2		FLE2	ASP2
CONC3		FLE3	ASP3
CONC4		FLE4	ASP4
CONC5		FLE5	ASP5
CONC6		FLE6	ASP6
CONC7		FLE7	ASP7
CONC8		FLE8	ASP8
CONC9		FLE9	ASP9
CONC10		FLE10 ASP10
CONC11		FLE11 ASP11
CONC12		FLE12 ASP12
CONC13		FLE13 ASP13
CONC14		FLE14 ASP14
CONC15		FLE15 ASP15
CONC16		FLE16 ASP16
CONC17		FLE17 ASP17
CONC18		FLE18 ASP18
CONC19		FLE19 ASP19
CONC20		FLE20 ASP20
```

2. Generation Program

```
C
C PROGRAM TO GENERATE THE INPUT FOR THE PARTIAL FACTORIAL
C
      DIMENSION IPARTF(9,10), ITABLE(10,3), IINC(4), TB(4),IT1(4),IT(4)
      DIMENSION POISSON(5),IN(4),INDT(4)
      CHARACTER*8 ICHAR1(5),ICHAR2(5),ICHAR3(5),ICHAR4(5),ATABLE(20,4)
      OPEN(10,FILE='SOURCE.DAT',STATUS='OLD')
      OPEN(7,FILE='TABLE.DAT',STATUS='OLD')
      OPEN(8,FILE='CHAR.DAT',STATUS='OLD')
      DO 100 I=1,9
            READ(10,*) (IPARTF(I,J),J=1,10)
100   CONTINUE
      DO 200 I=1,10
            READ(7,*) (ITABLE(I,J),J=1,3)
200   CONTINUE
      DO 50 I=1,9
            DO 55 J=1,10
              IPARTF(I,J) = IPARTF(I,J) +1
55          CONTINUE
50    CONTINUE
      DO 30 I=1,20
        READ(8,33) (ATABLE(I,J),J=1,4)
30    CONTINUE
33    FORMAT(A5,1X,A6,1X,A5,1X,A6)
      CLOSE(10)
      CLOSE(7)
      CLOSE(8)
C
C
C
      DO 10000 ILOOP=1,1
C
C
C
      OPEN(6,FILE='CFILE',STATUS='NEW')
C
C
      DO 20 I=1,5
            ICHAR2(I)=' '
20    CONTINUE
C
C
C
      WRITE(6,1001)
1001  FORMAT('*HEADING')
      WRITE(6,1002)
1002  FORMAT('*PREPRINT,ECHO=NO,HISTORY=NO,MODEL=NO')
      WRITE(6,1003)
1003  FORMAT('*NODE')
      WRITE(6,1004)
1004  FORMAT('1,0.0,0.0')
      WRITE(6,1005)
1005  FORMAT('181,90.0,0.0')
      WRITE(6,1006)
1006  FORMAT('500001,0,-90')
      WRITE(6,1007)
1007  FORMAT('500181,90,-90')
      WRITE(6,1008)
1008  FORMAT('197,180,0.0')
      WRITE(6,1009)
1009  FORMAT('500197,180.0,-90')
      WRITE(6,1010)
1010  FORMAT('*NGEN, NSET=BOT1')
      WRITE(6,1011)
1011  FORMAT('1,181,1')
      WRITE(6,1012)
1012  FORMAT('*NGEN, NSET=BOIT')
      WRITE(6,1013)
1013  FORMAT('500001,500181')
      WRITE(6,1014)
1014  FORMAT('*NSET,NSET=BBOT')
      WRITE(6,1015)
1015  FORMAT('BOT1,197')
```

```
            WRITE(6,12)
12          FORMAT('*NCOPY,CHANGE NUMBER=78000,OLD SET=BBOT,SHIFT,NEW SET=BOT2',/,
     *'0.,78.0',/,'0.,0.,0.,0.,0.,0.,0.',/,'*NFILL,NSET=NSUBB',/,
     *'BBOT,BOT2,156,500')
            WRITE(6,4001)
C
C
C
                  ITBASIC=78
                  IT(1) = ITBASIC + ITABLE(4,IPARTF(ILOOP,4))
                  IT(2) = IT(1) + ITABLE(3,IPARTF(ILOOP,3))
                  IT(3) = IT(2) + ITABLE(2,IPARTF(ILOOP,2))
                  IT(4) = IT(3) + ITABLE(1,IPARTF(ILOOP,1))
                  INDT(1) = ITABLE(4,IPARTF(ILOOP,4))
                  INDT(2) = ITABLE(3,IPARTF(ILOOP,3))
                  INDT(3) = ITABLE(2,IPARTF(ILOOP,2))
                  INDT(4) = ITABLE(1,IPARTF(ILOOP,1))
                  DO 300 N=1,4
                        IN(N) =1
300               CONTINUE
                  DO 310 N=1,4
                  IF(ITABLE(N,IPARTF(ILOOP,N)).EQ.0) IN(5-N)=0
310               CONTINUE
C
C
C
                  ICHAR1(1) ='BOT2'
                  ICHAR1(2) ='BASE1'
                  ICHAR1(3) ='CON1'
                  ICHAR1(4) ='FLEX'
                  ICHAR1(5) ='ASP1'
                  IINC(1) = ITABLE(4,IPARTF(ILOOP,4))*2
                  IINC(2) = ITABLE(3,IPARTF(ILOOP,3))*2
                  IINC(3) = ITABLE(2,IPARTF(ILOOP,2))*2
                  IINC(4) = ITABLE(1,IPARTF(ILOOP,1))*2
                  DO 350 I=1,4
                        TB(I) = FLOAT(IT(I))
                        IT1(I) =IT(I) * 1000
350               CONTINUE
C
C
C
                  J=1
                  DO 400 I=1,4
                        IF(IN(I).NE.0) THEN
                              WRITE(6,201) IT1(I), ICHAR1(I+1)
                              WRITE(6,202) TB(I)
                              WRITE(6,203) ICHAR1(J), ICHAR1(I+1), IINC(I)
                              J=I+1
                        ELSE
                              J=I
                        ENDIF
400               CONTINUE
C
201         FORMAT('*NCOPY,CHANGE NUMBER=',I6,',',
     *'OLD SET=BBOT,SHIFT,NEW SET=',A6)
202         FORMAT('0.,',F5.1,/,'0.,0.,0.,0.,0.,0.,0.',/,'*NFILL,NSET=NBASE')
203         FORMAT(A6,',',A6,',',I2,',500')
C
C
C
                  ITEMP1=IT1(4) +1
                  WRITE(6,2001)
                  WRITE(6,204) ITEMP1
204               FORMAT('1,',I6,',500')
                  WRITE(6,2002)
                  WRITE(6,2051)
C
2001        FORMAT('*NSET,NSET=CENTER1,GENERATE')
2002        FORMAT('*NSET,NSE=CENTER')
2051        FORMAT('CENTER1,500001')
C
C
            WRITE(6,4001)
                  WRITE(6,2003)
                  WRITE(6,2004)
                  WRITE(6,2005)
                  WRITE(6,2006)
```

```
            WRITE(6,2007)
            WRITE(6,2008)
            WRITE(6,2009)
            WRITE(6,2010)
            WRITE(6,2011)
            WRITE(6,2012)
            WRITE(6,2013)
            WRITE(6,2014)
            WRITE(6,2015)
            WRITE(6,2016)
            WRITE(6,2017)
            WRITE(6,2018)
            WRITE(6,2019)
            WRITE(6,2020)
            WRITE(6,2021)
            WRITE(6,2022)
            WRITE(6,2023)
            WRITE(6,2024)
            WRITE(6,2025)
            WRITE(6,2026)
            WRITE(6,2027)
            WRITE(6,2028)
            WRITE(6,2029)
2003     FORMAT('*** Element generation for soil**********')
2004     FORMAT('*ELEMENT, TYPE=CAX8')
2005     FORMAT('1,1,3,1003,1001,2,503,1002,501')
2006     FORMAT('*ELGEN, ELSET=BASE1')
2007     FORMAT('1,90,2,1,78,1000,100')
2008     FORMAT('*ELEMENT,TYPE=CINAX5R')
2009     FORMAT('20001,3,1,500001,500003,2')
2010     FORMAT('20191,2181,1181,1197,2197,1681')
2011     FORMAT('*ELGEN,ELSET=BASE2')
2012     FORMAT('20001,89,2,1')
2013     FORMAT('*ELEMENT,TYPE=CINAX5R')
2014     FORMAT('20090,181,179,500179,500197,180')
2015     FORMAT('20091,1181,181,500197,1197,681')
2016     FORMAT('*ELGEN,ELSET=BASE3')
2017     FORMAT('20191,77,1000,100')
2018     FORMAT('*ELSET,ELSET=BASE')
2019     FORMAT('20090,20091,BASE1,BASE2,BASE3')
2020     FORMAT('*** Element generation for Concrete ')
2021     FORMAT('*ELEMENT, TYPE=CAX8')
2022     FORMAT('7901,78001,78003,79003,79001,78002,78503,79002,78501')
2023     FORMAT('*ELGEN,ELSET=CCONC1')
2024     FORMAT('7901,90,2,1')
2025     FORMAT('*ELEMENT,TYPE=CINAX5R')
2026     FORMAT('27991,79181,78181,78197,79197,78681')
2027     FORMAT('*ELSET,ELSET=BASIC1')
2028     FORMAT('CCONC1,27991')
2029     FORMAT('**************************************************')
C
C ********************************************************
C
            J=0
            L=0
            DO 450 I=1,4
                  IF(IN(I).EQ.0) THEN
                        L=L+1
                  ELSE
                   J=J+1
                   IF(J.EQ.1) THEN
                        ICHAR2(I)='BASIC1'
                        ITEMP=I
                        IORDER=INDT(I) -1
                   ELSE
                     ICHAR2(I) = ATABLE(IORDER,ITEMP)
                         ITEMP=I
                         IORDER=INDT(I)
               ENDIF
              ENDIF
450         CONTINUE
C
C@@@@@@@@@@@@@@@@@@@@@@@@@@@@@@@@@@@@@@@@@@@@@@@@@@@@@@@@@@@@@@@@@@@@@@@@@@@@
@
C
            L=0
            DO 500 I=1,4
              IF(IN(I).NE.0) THEN
```

```
                    L=L+1
                    IF(L.EQ.1) THEN
                      WRITE(6,501) ICHAR2(I),ATABLE(1,I)
                      ITEMP1=INDT(I)-2
                      DO 520 K=1,ITEMP1
                         WRITE(6,501) ATABLE(K,I), ATABLE(K+1,I)
520                   CONTINUE
                    ELSEIF(L.EQ.2) THEN
                      ITEMP1=INDT(L)-1
                      WRITE(6,501) ICHAR2(I),ATABLE(1,I)
                      DO 540 K=1,INDT(I)-1
                         WRITE(6,501) ATABLE(K,I), ATABLE(K+1,I)
540                   CONTINUE
                    ELSE
                      WRITE(6,501) ICHAR2(I),ATABLE(1,I)
                      ITEMP1=INDT(I)-1
                      DO 560 K=1,ITEMP1
                         WRITE(6,501) ATABLE(K,I), ATABLE(K+1,I)
560                   CONTINUE
                    ENDIF
                    MKEY = I
                   ENDIF
500           CONTINUE
501           FORMAT('*ELCOPY,OLD SET=',A7,',NEW SET=',A7,
     *',ELEMENT SHIFT =100,SHIFT NODES=1000')
C
C
C
          WRITE(6,4001)
              J=0
              ICHAR3(1)='AGGBASE'
              ICHAR3(2)='PCON'
              ICHAR3(3)='FLEXIBLE'
              ICHAR3(4)='ASP'
              ICHAR3(5)='BASE'
              DO 600 I=1,4
                   IF(IN(I).EQ.0) THEN
                    GO TO 600
                   ELSE
                    J=J+1
                    IF(J.EQ.1) THEN
                      WRITE(6,601) ICHAR3(I)
                      WRITE(6,602) (ATABLE(JL,I), JL=1,INDT(I)-1)
                    ELSE
                WRITE(6,601) ICHAR3(I)
                      WRITE(6,603) (ATABLE(JL,I), JL=1,INDT(I))
               ENDIF
              ENDIF
600           CONTINUE
C
601           FORMAT('*ELSET, ELSET=',A8)
602           FORMAT('BASIC1,'2X,9(A6,','))
603           FORMAT(10(A6,','))
C
C
C
          WRITE(6,4001)
              WRITE(6,691)
691       FORMAT('*ELSET,ELSET=LAD')
              WRITE(6,701) (IT(4),I=1,6)
701           FORMAT(I3,'01,',I3,'02,',I3,'03,',I3,'04,',I3,'05,',I3,'06,')
C
C***  Node and Element  for Output ***************************
C
              WRITE(6,692)
692           FORMAT('*NSET, NSET=OUTNODE,GENERATE')
              WRITE(6,702) IT(4), IT(4)
702           FORMAT(I3,'001,',I3,'145',',24')
C
C
C
              WRITE(6,693)
693           FORMAT('*ELSET, ELSET=OUTELE')
              WRITE(6,694)
694           FORMAT('7801',/,'7901')
              DO 800 I=1,4
                   IF(IN(I).NE.0) THEN
                         IELE = IT(I)*100 +1
```

```
                    WRITE(6,801) IELE
                    IOPUT= IELE+100
                    IF(I.NE.4) THEN
                          WRITE(6,801) IOPUT
                    ENDIF
              ENDIF
800         CONTINUE
C
801         FORMAT(I5)
C
C
      WRITE(6,4001)
            ICHAR3(1)='AGGBASE'
            ICHAR3(2)='PCON'
            ICHAR3(3)='FLEXIBLE'
            ICHAR3(4)='ASP'
            ICHAR3(5)='BASE'
            ICHAR4(1)='MAT1'
            ICHAR4(2)='MAT2'
            ICHAR4(3)='MAT3'
            ICHAR4(4)='MAT4'
            ICHAR4(5)='MAT5'
            POISSON(1) = 0.40
            POISSON(2) = 0.15
            POISSON(3) = 0.40
            POISSON(4) = 0.35
            POISSON(5) = 0.40
C
              IF(ITABLE(8,IPARTF(ILOOP,8)).GT.300000) THEN
                POISSON(1) = 0.35
              ELSEIF (ITABLE(8,IPARTF(ILOOP,8)).GT.500000) THEN
                POISSON(1) = 0.2
              ENDIF
C
            DO 900 I=1,4
              IF(IN(I).NE.0) THEN
                    WRITE(6,901) ICHAR3(I),ICHAR4(I),ICHAR4(I)
                    WRITE(6,902) ITABLE(9-I,IPARTF(ILOOP,9-I)),POISSON(I)
              ENDIF
900         CONTINUE
C
C
C
            WRITE(6,901) ICHAR3(5),ICHAR4(5),ICHAR4(5)
            WRITE(6,902) ITABLE(9,IPARTF(ILOOP,9)),POISSON(5)
901         FORMAT('*SOLID SECTION, ELSET=',A8,', MATERIAL=',A4,/,
     *'*MATERIAL, NAME=',A4,/,'*ELASTIC')
902         FORMAT(I7,',',F4.2)
C
C
C
            WRITE(6,3001)
            WRITE(6,3002)
            WRITE(6,3003)
            WRITE(6,3004)
            WRITE(6,3005)
            WRITE(6,3006)
            WRITE(6,3007)
            WRITE(6,3008)
3001      FORMAT('*BOUNDARY')
3002      FORMAT('CENTER,XSYMM')
3003      FORMAT('*AMPLITUDE,NAME=TRUCK1')
3004      FORMAT('0.,0.,1.,1.')
3005      FORMAT('*STEP,INC=100')
3006      FORMAT('*STATIC')
3007      FORMAT('0.0,1.0')
3008      FORMAT('*DLOAD,AMP=TRUCK1')
C
C
C
            PLOAD = ITABLE(10,IPARTF(ILOOP,10))/(3.14*6*6)
            WRITE(6,903) PLOAD
903       FORMAT('LAD,P3,',F8.3)
C
C
C
      WRITE(6,4001)
      WRITE(6,3011)
```

```
          WRITE(6,3012)
          WRITE(6,3013)

          WRITE(6,3014)
          WRITE(6,3015)
          CLOSE(6)
10000  CONTINUE
C
C
C
3011      FORMAT('*NODE PRINT,NSET=OUTNODE,FREQUENCY=1')
3012      FORMAT('U2')
3013      FORMAT('*EL PRINT,ELSET=OUTELE,POSITION=AVERAGED AT NODES')
3014      FORMAT('S11,S22,E22')
3015      FORMAT('*END STEP')
4001      FORMAT(80('*'))
C
C
C
                    STOP

                    END
```

3. Generated ABAQUS INPUT FILE

```
*HEADING
*PREPRINT,ECHO=NO,HISTORY=NO,MODEL=NO
*NODE
1,0.0,0.0
181,90.0,0.0
500001,0,-90
500181,90,-90
197,180,0.0
500197,180.0,-90
*NGEN, NSET=BOT1
1,181,1
*NGEN, NSET=BOIT
500001,500181
*NSET,NSET=BBOT
BOT1,197
*NCOPY,CHANGE NUMBER=78000,OLD SET=BBOT,SHIFT,NEW SET=BOT2
0.,78.0
0.,0.,0.,0.,0.,0.,0.
*NFILL,NSET=NSUBB
BBOT,BOT2,156,500
*********************************************************************************
*NCOPY,CHANGE NUMBER= 84000,OLD SET=BBOT,SHIFT,NEW SET=BASE1
0., 84.0
0.,0.,0.,0.,0.,0.,0.
*NFILL,NSET=NBASE
BOT2  ,BASE1 ,12,500
*NCOPY,CHANGE NUMBER= 92000,OLD SET=BBOT,SHIFT,NEW SET=CON1
0., 92.0
0.,0.,0.,0.,0.,0.,0.
*NFILL,NSET=NBASE
BASE1 ,CON1  ,16,500
*NCOPY,CHANGE NUMBER= 94000,OLD SET=BBOT,SHIFT,NEW SET=FLEX
0., 94.0
0.,0.,0.,0.,0.,0.,0.
*NFILL,NSET=NBASE
CON1  ,FLEX  , 4,500
*NCOPY,CHANGE NUMBER= 97000,OLD SET=BBOT,SHIFT,NEW SET=ASP1
0., 97.0
0.,0.,0.,0.,0.,0.,0.
*NFILL,NSET=NBASE
FLEX  ,ASP1  , 6,500
*NSET,NSET=CENTER1,GENERATE
1, 97001,500
*NSET,NSE=CENTER
CENTER1,500001
*********************************************************************************
*** Element generation for soil**********
*ELEMENT, TYPE=CAX8
1,1,3,1003,1001,2,503,1002,501
*ELGEN, ELSET=BASE1
1,90,2,1,78,1000,100
*ELEMENT,TYPE=CINAX5R
20001,3,1,500001,500003,2
20191,2181,1181,1197,2197,1681
*ELGEN,ELSET=BASE2
20001,89,2,1
*ELEMENT,TYPE=CINAX5R
20090,181,179,500179,500197,180
20091,1181,181,500197,1197,681
*ELGEN,ELSET=BASE3
20191,77,1000,100
*ELSET,ELSET=BASE
20090,20091,BASE1,BASE2,BASE3
*** Element generation for Concrete
*ELEMENT, TYPE=CAX8
7901,78001,78003,79003,79001,78002,78503,79002,78501
*ELGEN,ELSET=CCONC1
7901,90,2,1
*ELEMENT,TYPE=CINAX5R
27991,79181,78181,78197,79197,78681
*ELSET,ELSET=BASIC1
CCONC1,27991
*************************************************
*ELCOPY,OLD SET=BASIC1 ,NEW SET= AGG1  ,ELEMENT SHIFT =100,SHIFT NODES=1000
*ELCOPY,OLD SET= AGG1  ,NEW SET= AGG2  ,ELEMENT SHIFT =100,SHIFT NODES=1000
```

```
*ELCOPY,OLD SET= AGG2  ,NEW SET= AGG3  ,ELEMENT SHIFT =100,SHIFT NODES=1000
*ELCOPY,OLD SET= AGG3  ,NEW SET= AGG4  ,ELEMENT SHIFT =100,SHIFT NODES=1000
*ELCOPY,OLD SET= AGG4  ,NEW SET= AGG5  ,ELEMENT SHIFT =100,SHIFT NODES=1000
*ELCOPY,OLD SET= AGG5  ,NEW SET= CONC1 ,ELEMENT SHIFT =100,SHIFT NODES=1000
*ELCOPY,OLD SET= CONC1 ,NEW SET= CONC2 ,ELEMENT SHIFT =100,SHIFT NODES=1000
*ELCOPY,OLD SET= CONC2 ,NEW SET= CONC3 ,ELEMENT SHIFT =100,SHIFT NODES=1000
*ELCOPY,OLD SET= CONC3 ,NEW SET= CONC4 ,ELEMENT SHIFT =100,SHIFT NODES=1000
*ELCOPY,OLD SET= CONC4 ,NEW SET= CONC5 ,ELEMENT SHIFT =100,SHIFT NODES=1000
*ELCOPY,OLD SET= CONC5 ,NEW SET= CONC6 ,ELEMENT SHIFT =100,SHIFT NODES=1000
*ELCOPY,OLD SET= CONC6 ,NEW SET= CONC7 ,ELEMENT SHIFT =100,SHIFT NODES=1000
*ELCOPY,OLD SET= CONC7 ,NEW SET= CONC8 ,ELEMENT SHIFT =100,SHIFT NODES=1000
*ELCOPY,OLD SET= CONC8 ,NEW SET= FLE1  ,ELEMENT SHIFT =100,SHIFT NODES=1000
*ELCOPY,OLD SET= FLE1  ,NEW SET= FLE2  ,ELEMENT SHIFT =100,SHIFT NODES=1000
*ELCOPY,OLD SET= FLE2  ,NEW SET= ASP1  ,ELEMENT SHIFT =100,SHIFT NODES=1000
*ELCOPY,OLD SET= ASP1  ,NEW SET= ASP2  ,ELEMENT SHIFT =100,SHIFT NODES=1000
*ELCOPY,OLD SET= ASP2  ,NEW SET= ASP3  ,ELEMENT SHIFT =100,SHIFT NODES=1000
*********************************************************************************
*ELSET, ELSET=AGGBASE
BASIC1,   AGG1 , AGG2 , AGG3 , AGG4 , AGG5 ,
*ELSET, ELSET=PCON
 CONC1, CONC2, CONC3, CONC4, CONC5, CONC6, CONC7, CONC8,
*ELSET, ELSET=FLEXIBLE
 FLE1 , FLE2 ,
*ELSET, ELSET=ASP
 ASP1 , ASP2 , ASP3 ,
*********************************************************************************
*ELSET,ELSET=LAD
 9701, 9702, 9703, 9704, 9705, 9706
*NSET, NSET=OUTNODE,GENERATE
 97001, 97145,24
*ELSET, ELSET=OUTELE
7801
7901
 8401
 8501
 9201
 9301
 9401
 9501
 9701
*********************************************************************************
*SOLID SECTION, ELSET=AGGBASE , MATERIAL=MAT1
*MATERIAL, NAME=MAT1
*ELASTIC
  50000,0.40
*SOLID SECTION, ELSET=PCON    , MATERIAL=MAT2
*MATERIAL, NAME=MAT2
*ELASTIC
5500000,0.15
*SOLID SECTION, ELSET=FLEXIBLE, MATERIAL=MAT3
*MATERIAL, NAME=MAT3
*ELASTIC
 100000,0.40
*SOLID SECTION, ELSET=ASP     , MATERIAL=MAT4
*MATERIAL, NAME=MAT4
*ELASTIC
1000000,0.35
*SOLID SECTION, ELSET=BASE    , MATERIAL=MAT5
*MATERIAL, NAME=MAT5
*ELASTIC
  20000,0.40
*BOUNDARY
CENTER,XSYMM
*AMPLITUDE,NAME=TRUCK1
0.,0.,1.,1.
*STEP,INC=100
*STATIC
0.0,1.0
*DLOAD,AMP=TRUCK1
LAD,P3,  53.079
*********************************************************************************
*NODE PRINT,NSET=OUTNODE,FREQUENCY=1
U2
*EL PRINT,ELSET=OUTELE,POSITION=AVERAGED AT NODES
S11,S12,S22,E11,E22,E12
*END STEP
```